europhysics
conference
abstracts

Abstracts

43rd Conference of the European Group for Atomic Systems (EGAS)

University of Fribourg

Fribourg, Switzerland

June 28 – July 2, 2011

Published by: European Physical Society
Series Editor: Prof. O. Scholten, Groningen
Managing Editor: P. Helfenstein, Mulhouse
Editors: A. Weis, Fribourg
J.-Cl. Dousse, Fribourg
M. Allan, Fribourg
P. Knowles, Fribourg

Online Version
20110629

Colophon
This book has been assembled from the LaTeX source files submitted by the contributing authors. Layout, editing, and customized TeX & LaTeX macros used to typeset the book were developed by P. Knowles.

This online version has been updated for all changes until June 29, and differs from the printed book in that:

- The ISBN number has been removed.
- CT–018 is presented by G. Krois, not W. E. Ernst, and has an associated poster in the CAM section.
- CAM–007 is presented by S. Willitsch, not F. Hall.
- FPT–401 D. A. Glazov post-deadline abstract added.
- QOI–001 D. Aghamalyan marked as withdrawn.
- CT–040 has associated poster in AAP section.
- BPB error with CT talk schedule of Wed. 29 fixed.

Copyright and cataloging information

Europhysics Conference Abstracts, **35C: Online Version**
43rd Conference of the European Group for Atomic Systems: EGAS–43.
Fribourg, Switzerland, June 28–July 2, 2011.

The Local organizing committee of the 43rd EGAS Conference gratefully acknowledges the support of the following sponsors.

University of Fribourg
Av. Europe 20
CH-1700 Fribourg
Switzerland

Department of Physics
University of Fribourg
Chemin du Musée 3
CH-1700 Fribourg, Switzerland

Department of Chemistry
University of Fribourg
Chemin du Musée 9
CH-1700 Fribourg, Switzerland

Swiss National Science Foundation
Wildhainweg 3
PO-Box 8232
CH-3001 Bern, Switzerland

Swiss Academy of Sciences
Schwarztorstrasse 9
CH-3007 Bern, Switzerland

Swiss Chemical Society
Schweizerische Chemische Gesellschaft (SCG)
Schwarztorstrasse 9
CH-3007 Bern, Switzerland

KontaktGruppe für Forschungsfragen
Contact Group for Research Matters

EGAS–43 is supported by the member companies of the Kontaktgruppe für Forschungsfragen (KGF), BASF, Novartis, Syngenta, Merck Serono, and F. Hoffmann-La Roche.

Swiss International Air Lines
Official Carrier of EGAS–43
P.O. Box
CH-4002, Basel, Switzerland

The European Physical Journal
Springer-Verlag GmbH
Tiergartenstrasse 17
69121 Heidelberg, Germany

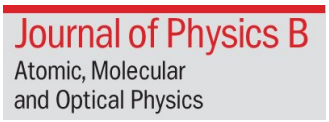

Journal of Physics B
IOP Publishing Ltd.
Dirac House, Temple Back
Bristol, BS1 6BE, United Kingdom

GMP SA Laser & Photonics
Av. des Baumettes 17
CH-1020 Renens
Lausanne, Switzerland

Newport Spectra-Physics GmbH
Guerickeweg 7
64291 Darmstadt
Germany

Thorlabs GmbH
Hans-Boeckler-Str. 6
85221 Dachau
Munich, Germany

TOPTICA Photonics AG
Lochhamer Schlag 19
82166 Graefelfing
Munich, Germany

Zurich Instruments AG
Technoparkstrasse 1
CH-8005 Zurich
Switzerland

Local organizing committee

Prof. Antoine Weis
Conference Chair
Department of Physics
University of Fribourg
Chemin du Musée 3
CH-1700 Fribourg
Switzerland
tel: +41 (0)26 300 90 30
fax: +41 (0)26 300 96 31
antoine.weis@unifr.ch

Prof. Jean-Claude Dousse
Department of Physics
University of Fribourg
Chemin du Musée 3
CH-1700 Fribourg
Switzerland
tel: +41 (0)26 300 90 73
fax: +41 (0)26 300 97 47
jean-claude.dousse@unifr.ch

Prof. Michael Allan
Department of Chemistry
University of Fribourg
Chemin du Musée 9
CH-1700 Fribourg
Switzerland
tel: +41 (0)26 300 87 04
fax: +41 (0)26 300 97 38
michael.allan@unifr.ch

Dr. Paul Knowles
Department of Physics
University of Fribourg
Chemin du Musée 3
CH-1700 Fribourg
Switzerland
tel: +41 (0)26 300 90 64
fax: +41 (0)26 300 96 31
paul.knowles@unifr.ch

Conference logistics and organization

art&fact
congress and events management

Artefact Management, Sàrl
Fabien Stauffacher
Grand–Fontaine 7
CH–1700 Fribourg
Switzerland
tel: +41 26 321 31 09
fax: +41 26 321 31 10
contact@artefactmanagement.com

Art&Fact builds high qualitative exchange platforms in the fields of arts and sciences, contributing to the development of our society and our knowledge in a sustainable and responsible manner. For you, we create a positive focal point: the one allowing you to reach the summit of your skills, the one bringing people together and supporting them in their collaboration; the one which will be fixed in your memories.

EGAS Board members, 2011

The EGAS Board typically consists of 15 members, including a chair and secretary. The Board meetings may also be attended by members of the local organizing committee of EGAS Conferences, outside experts, and EPS representatives. The Board members are elected by the General Assembly for a three year term (renewable once) and represent the different countries of Europe. The Board meets three times a year, twice during the annual conference and once in November/December. It is bound by decisions made at the General Assembly (which is held once a year, during the Conference).

Prof. Eva Lindroth (05, 08) Chair
Atomic Physics, Fysikum
Stockholm University
AlbaNova University Centre
SE-106 91 Stockholm, Sweden
tel: +46 8 5537 8616
fax: +46 8 5537 8601
lindroth@physto.se

Prof. Peter Barker (09)
University College London
Department of Physics and Astronomy
Gower Street
London–WC1E 6BT, UK
tel: +44 20 7679 7331
fax: +44 20 7679 7145
p.barker@ucl.ac.uk

Prof. Mike Charlton (03, 06) (09 Webmaster)
Department of Physics
University of Wales, Swansea
Singleton Park
Swansea–SA2 8PP, UK
tel: +44 17 9229 5372
fax: +44 17 9229 5324
M.Charlton@swansea.ac.uk

Prof. Michael Drewsen (06, 09)
Department of Physics and Astronomy
University of Aarhus
NY Munkegade, BYG.520
DK-8000 Aarhus, Denmark
tel: +45 89 42 3752
fax: +45 86 12 0740
drewsen@phys.au.dk

Prof. Jürgen Eschner (05, 08)
Experimentalphysik – Quantum Photonics
Universität des Saarlandes
Campus E2 6, 66123 Saarbrücken,
Germany
tel: +49 681 302 5016/58017
fax: +49 681 302 58018
juergen.eschner@physik.uni-saarland.de

Dr. Gleb Gribakin (10)
Department of Applied Mathematics
and Theoretical Physics
Room DBB 0G.012
Queen's University Belfast
University Road
Belfast BT7 1NN, UK
tel: +44 28 9097 6056
fax: +44 28 9097 6061
g.gribakin@qub.ac.uk

Prof. Nikolay Kabachnik (07)
Institute of Nuclear Physics
Moscow State University
Leninskie Gory
Moscow 119992, Russia
tel: +7 495 939 3605
fax: +7 495 939 0896
nkabach@mail.ru

Prof. Krzysztof Pachucki (05, 08)
Institute of Theoretical Physics
Warsaw University
Ul. Hoza 69
PL-00-681 Warsaw, Poland
tel: +48 22 553 2246
fax: +48 22 621 9475
Krzysztof.Pachucki@fuw.edu.pl

Prof. Tilman Pfau (08)
Universität Stuttgart
5. Physikalisches Institut
Pfaffenwaldring 57, Room 4.162
D-70550 Stuttgart, Germany
tel: +49 711 685 68025
fax: +49 711 685 63810
t.pfau@physik.uni-stuttgart.de

Prof. Laurence Pruvost (09)
Laboratoire Aimé Cotton, (UPR 3321)
Université de Paris-Sud
Campus d'Orsay
F-91405 Orsay, France
tel: +33 1 69 35 2101
fax: +33 1 69 41 0156
Laurence.Pruvost@lac.u-psud.fr

Prof. Guglielmo M. L. Tino (08)
Dipartimento di Fisica and LENS
Laboratory
Università di Firenze, INFN (Firenze)
Polo Scientifico — Via Sansone 1
I-50019 Sesto Fiorentino (Firenze), Italy
tel: +39 055 457 2034/2462
fax: +39 055 457 2451
guglielmo.tino@fi.infn.it

Prof. Xavier Urbain (10)
Institute of Condensed Matter and
Nanosciences
Université Catholique de Louvain, PAMO
Chemin du Cyclotron 2
B-1348 Louvain-la-Neuve, Belgium
tel: +32 10 47 32 47
fax: +32 10 47 29 99
xavier.urbain@uclouvain.be

Prof. Nikolay V. Vitanov (06, 09)
Department of Physics
Sofia University
James Bourchier 5 Blvd.
1164 Sofia, Bulgaria
tel: +359 2 8161 652
fax: +359 2 9625 276
vitanov@phys.uni-sofia.bg

Prof. Marc J. J. Vrakking (06, 09)
Institute for Atomic and Molecular Physics
Kruislaan 407
1098 SJ Amsterdam, The Netherlands
tel: +31 20 7547100
fax: +31 20 6684106
vrakking@amolf.nl

Prof. Antoine Weis (10)
Department of Physics
University of Fribourg
Chemin du Musée 3
1700 Fribourg
Switzerland
tel: +41 26 300 90 30
fax: +41 26 300 96 31
antoine.weis@unifr.ch

Internet access and wireless connections

For the duration of the conference, wifi internet access will be available for participants with their own computers. The access should work throughout the Pérolles II site.

SSID: public-unifr
Username: egas43
Password: Sm6Xe7Fr

Public terminals are also available on the first floor. The same username and password as for the wifi access should permit you to login to the terminals and access a browser.

In addition to the dedicated wifi system 'public-unifr', UniFR is also member of the 'eduroam' network, so if you are a regular user of that system, you can simply use it instead of the wifi instructions above.

This information is correct as of the time this book went to press. Changes will, of course, be communicated to you during the conference should anything change in the meantime.

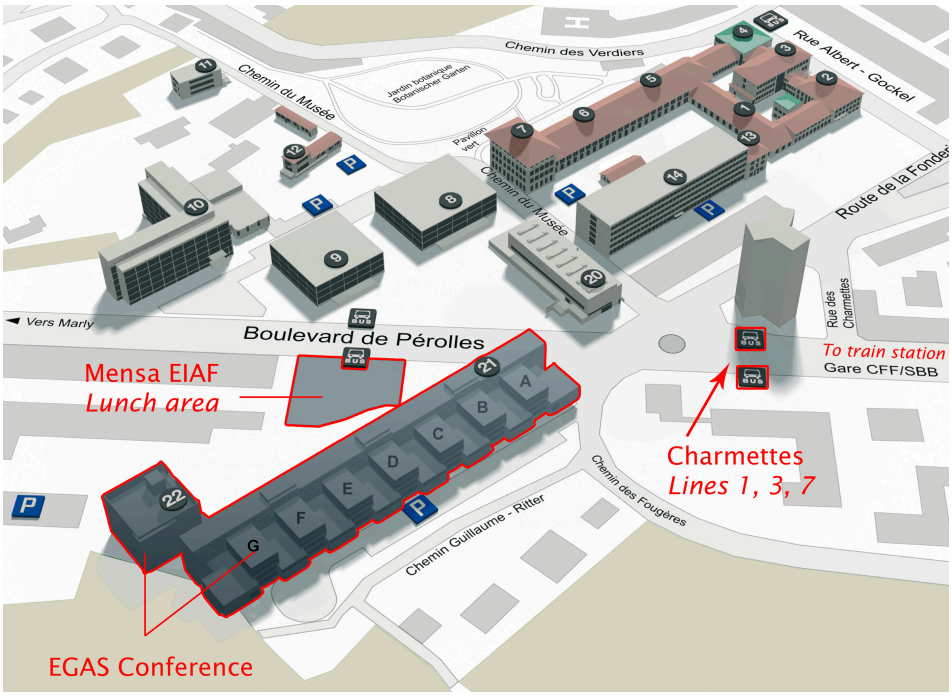

Pérolles II encompasses buildings 21 and 22 on the above diagram.
Auditorium J. Deiss is contained in block 22.
Auditorium G140 is on the first floor of block G in building 21.
The Physics Department is in building 8.

Time	Auditorium J. Deiss	Auditorium G140	Ground & First Floor	
16:00–19:00			Poster Setup Ground floor & First floor	Registration Welcome Drinks Ground floor (Block 22)

20:00–21:00			EGAS Board Meeting (F130, 1st floor, Pérolles II)

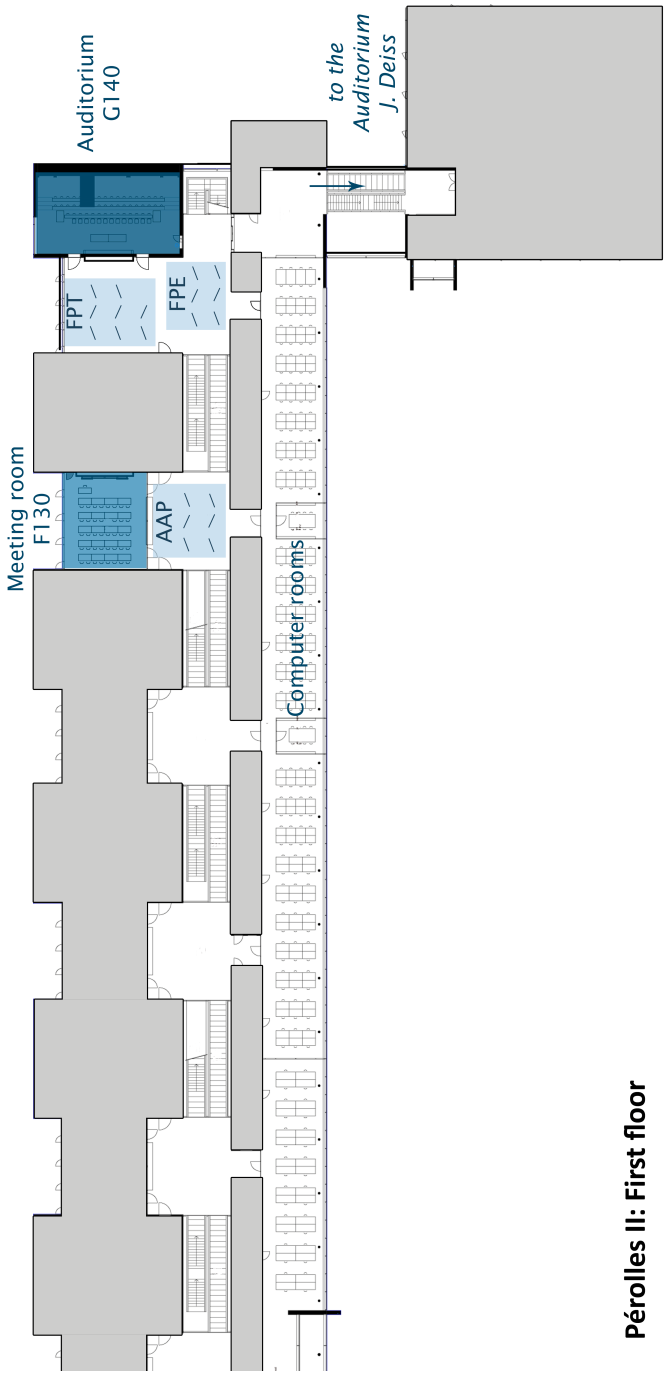
Auditorium
G140
to the
Auditorium
J. Deiss
FPT
FPE
Meeting room
F130
AAP
Computer rooms
Pérolles II: First floor

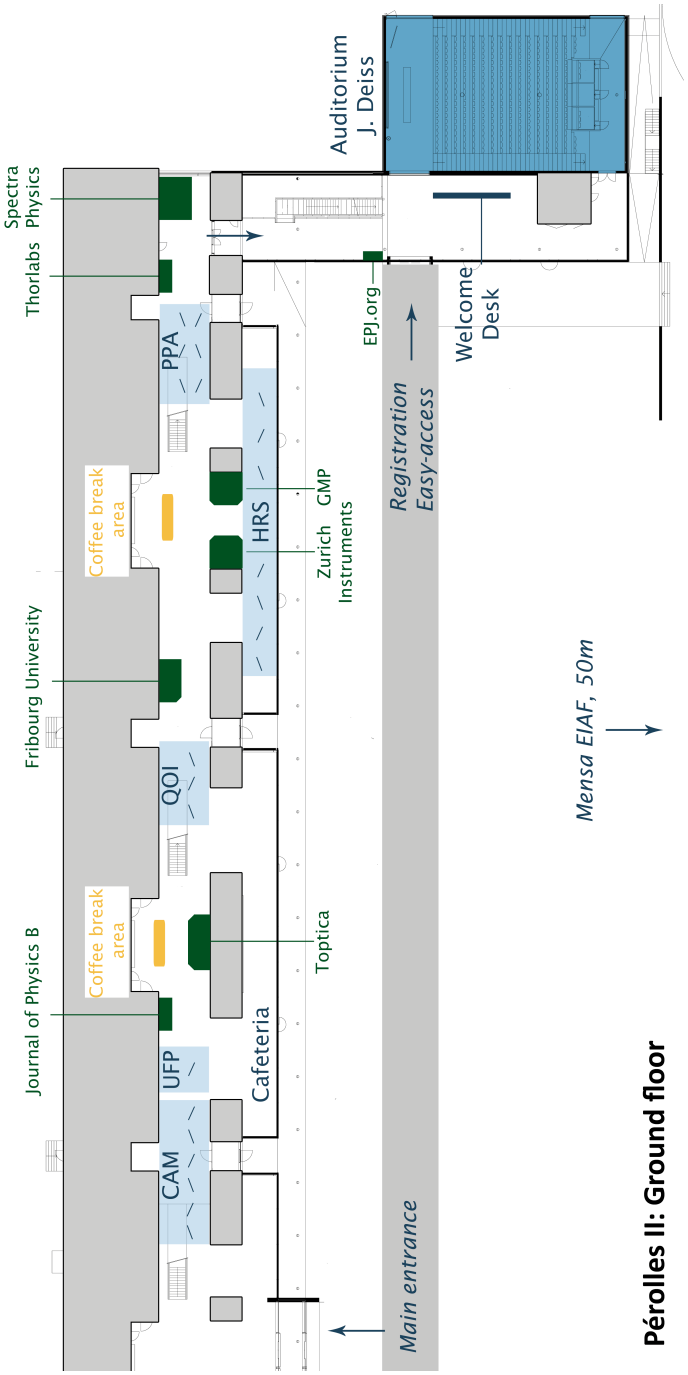
Auditorium
J. Deiss
Spectra Physics
Thorlabs
PPA
EPJ.org
Welcome Desk
Registration
Easy-access
Coffee break area
HRS
GMP
Zurich Instruments
Fribourg University
QOI
Mensa EIAF, 50m
Coffee break area
Journal of Physics B
Toptica
Cafeteria
UFP
CAM
Main entrance
Pérolles II: Ground floor

Time	Auditorium J. Deiss	Auditorium G140	Halls
08:30	**EGAS–43 Opening**		
08:45	Chair: E. Lindroth		
08:45–09:30	PL–001: J. Ye		
09:30–10:15	PL–002: A. Imamoglu		
10:15–10:45	Coffee break Commercial exhibition		
10:45	**Fundamental Physics I** Chair: K. Pachucki	**Cold Atoms I** Chair: L. Pruvost	
10:45–11:15	PR–001: M. Prevedelli	PR–002: J. C. Garreau	
11:15–11:30	CT–001: H. Kracke	CT–002: E. Maréchal	
11:30–11:45	CT–003: D. Lindenfels	CT–004: J. S. Krauser	
11:45–12:00	CT–005: A. Wagner	CT–006: M. Fink	
12:00–12:15	CT–007: J. Repp	CT–008: P. Böhi	
12:15–12:30	CT–009: S. Streubel	CT–010: D. Sukachev	
12:30–12:45	CT–011: P. Moroshkin	CT–012: A. Avdeenkov	
12:45–14:30	Commercial exhibition Lunch at the Engineering School (EIAF) Mensa		
14:30	Chair: P. Barker		
14:30–15:15	PL–003: C. Salomon		
15:15–16:00	PL–004: M. Fleischhauer		
16:00–18:00	Poster session I Odd numbered posters		
18:00–20:00	Welcome reception		
20:00–21:00	PEL–005: R. R. Ernst, Nobel Prize 1991 (Chemistry) Title: Raman Spectroscopy for Exploring Cultural Heritage Chair: F. Merkt		

Time	Auditorium J. Deiss	Auditorium G140	Halls
08:30	Chair: H. Hotop		
08:30–09:15	PL–006: I. Bloch		
09:15–10:00	PL–007: T. Oka		
10:00–10:45	Coffee break Commercial exhibition		
10:45	**Fundamental Physics II** Chair: X. Urbain	**Cold Atoms II** **HiRes Spectroscopy** Chair: D. Hanstorp	
10:45–11:15	PR–003: J. Komasa	PR–004: F. Ferlaino	
11:15–11:30	CT–013: A. Antognini	CT–014: A. K. Hansen	
11:30–11:45	CT–015: V. A. Yerokhin	CT–016: R. Le Targat	
11:45–12:00	CT–017: M. G. Kozlov	CT–018: G. Krois	
12:00–12:15	CT–019: D. G. Green	CT–020: A. J. Krmpot	
12:15–12:30	CT–021: Ph. V. Demekhin	CT–022: D. Sarkisyan	
12:30–12:45	CT–023: B. Botermann	CT–024: J. Hoszowska	
12:45–18:30	Excursion to Gruyères Castle (inscription required) Buses will be waiting at Pérolles II at 12:50. Bag lunch will be distributed at the bus. **Buses will leave at 13:15. (Swiss timing!)** Buses will return at about 18:00.		
19:30–22:00	Conference dinner Salle Grenette of the restaurant Punkt, Place de Notre–Dame 4 (Near the traffic circle by the cathedral)		

Time	Auditorium J. Deiss	Auditorium G140	Halls
08:30	Chair: M. Drewsen		
08:30–09:15	PL–008: T. Kippenberg		
09:15–10:00	PL–009: F. Martín		
10:00–10:45	Coffee break Commercial exhibition		
10:45	**AMO Applications** Chair: N. Kabachnik	**Clocks / Metrology** Chair: H. Bachau	
10:45–11:15	PR–005: I. I. Ryabtsev	PR–006: T. Ban	
11:15–11:30	CT–025: S. Nic Chormaic	CT–026: L. Devenoges	
11:30–11:45	CT–027: P. Roncin	CT–028: J.–L. Robyr	
11:45–12:00	CT–029: M. Chevrollier	CT–030: O. Kozlova	
12:00–12:15	CT–031: M. Oriá	CT–032: M. D. De Vizia	
12:30–12:45	EGAS General Assembly		Commercial exhibition Lunch at the Engineering School (EIAF) Mensa
12:45–13:00			
13:00–13:15		EGAS Board Meeting (A06, EIAF)	
13:15–13:30			
13:30–13:45			
13:45–14:00			
14:00–14:15			
14:15–14:30			
14:30	**Photo-Ionization** **Photo-Detachment** Chair: G. Gribakin	**Quantum Optics** **Electron Scattering** Chair: N. Vitanov	
14:30–15:00	PR–007: A. Surzhykov	PR–008: C. P. Koch	
15:00–15:15	CT–033: T. Carette	CT–034: Th. Busch	
15:15–15:30	CT–035: A. Dimitriou	CT–036: M. Albert	
15:30–15:45	CT–037: J. Lecointre	CT–038: O. Plekan	
15:45–16:00	CT–039: A. O. Lindahl	CT–040: M. Pajek	
16:00–18:00	Poster session II Even numbered posters		

Mini-Symposium on Atomic Magnetometry

Time	Auditorium J. Deiss	Auditorium G140	Halls
08:30	Chair: A. Weis		
08:30–09:15	PL–010: E. B. Alexandrov		
09:15–10:00	PL–011: M. Romalis		
10:00–10:45	Coffee break Commercial exhibition		
10:45	Chair: G. Tino		
10:45–11:15	PR–009: W. Heil		
11:15–11:45	PR–010: G. Bison		
11:45–12:00	EGAS–43 Closing		

This book contains all abstracts accepted as of June 29, 2011. Note that abstracts have been edited for style uniformity. The abstracts representing talks are indicated by PL, PR, and CT, followed by the contribution number. Poster abstracts are sorted by category (see abbreviation table below) and alphabetically within each section by corresponding author. In cases where the presenting author is different from the corresponding author, the presenting author is indicated by a note at the bottom of the abstract page. **All posters will be on display for the entire conference.** The contribution number for posters is used to determine the corresponding poster session where the presenting author is expected to be available close to the poster: odd numbered posters are on Wednesday, even numbered posters are on Friday.

PL	Plenary Lectures
PEL	Public Evening Lecture
PR	Progress Reports
CT	Contributed Talks
AAP	AMO Physics at Large Facilities
CAM	Cold Atoms/Molecules, Ions, and Quantum Gases
FPE	Fundamental Physics: Experiment
FPT	Fundamental Physics: Theory
HRS	High-Resolution Spectroscopy
PPA	Photoionization, Photodetachment, Anions
QOI	Quantum Optics and Information
UFP	Ultrafast Processes

Contents

Sponsors and Exhibitors **I**

Local organizing committee **III**

Conference logistics **IV**

EGAS Board **V**

Internet access **VIII**

Program and Maps **IX**

PL: Plenary Lectures **1**

PL–001 **J. Ye**
Quantum metrology with ultracold atoms — a strongly interacting optical lattice clock 2

PL–002 **A. Imamoglu**
Observation of Kondo correlations in optical absorption 3

PL–003 **C. Salomon**
Quantum sensors on earth and in space 4

PL–004 **M. Fleischhauer**
Slow-light and Rydberg polaritons 5

PEL–005 **R. R. Ernst**
Raman spectroscopy for exploring cultural heritage 6

PL–006 **I. Bloch**
Controlling and imaging quantum gases at the single atom level . . 7

PL–007 **T. Oka**
Infrared spectrum of H_3^+ from the laboratory to the galactic center 8

PL–008 **T. J. Kippenberg**
Cavity optomechanics: back-action cooling of mechanical oscillators 9

PL–009 **F. Martín**
XUV/x-ray lasers for ultrafast electronic control in simple molecules 10

PL–010 **E. B. Alexandrov**
Half a century of optically pumped magnetometers 11

PL–011 **M. Romalis**
Recent progress in high-density alkali-metal magnetometers 12

PR: Progress Reports **13**

PR–001 **M. Prevedelli**
Measuring the gravitational constant G with an atom interferometer 14

PR–002 **J. C. Garreau**
Quantum simulators: the Anderson transition case 15

PR–003 **J. Komasa**
High precision theoretical spectra of the hydrogen molecule 16
PR–004 **F. Ferlaino**
New results on Efimov physics and the creation RbCs molecules . 17
PR–005 **I. I. Ryabtsev**
Stark-tuned Förster resonance and dipole blockade between few Rydberg atoms: experiment and theory 18
PR–006 **T. Ban**
Direct frequency comb spectroscopy: time and frequency domain approach 19
PR–007 **A. Surzhykov**
Heavy–ion collisions: from formation of quasi–molecules to relativistic regime 20
PR–008 **C. P. Koch**
Optimal two-qubit gates for trapped neutral atoms at the quantum speed limit 21
PR–009 **W. Heil**
Test of fundamental symmetries in ^{3}He/^{129}Xe clock comparison experiments 22
PR–010 **G. Bison**
Optically pumped magnetometers in life science and fundamental research 23

CT: Contributed Talks **24**
CT–001 **H. Kracke**
First observation of spin flips of a single trapped proton 25
CT–002 **E. Maréchal**
Magnetization dynamics of a dipolar BEC at ultralow magnetic field 26
CT–003 **D. Lindenfels**
Bound electron g-factor measurement by double-resonance spectroscopy on a fine-structure transition 27
CT–004 **J. S. Krauser**
Probing ultracold fermions in optical lattices 28
CT–005 **A. Wagner**
The g-factor of hydrogen-like silicon $^{28}Si^{13+}$ 29
CT–006 **M. Fink**
Scattering of ultracold atoms by an absorbing nanowire 30
CT–007 **J. Repp**
High-precision mass measurements of stored and cooled highly charged ions for fundamental studies at PENTATRAP 31
CT–008 **P. Böhi**
Imaging of microwave fields using ultracold atoms 32

CT–009 **S. Streubel**
First mass measurements with THe-Trap 33
CT–010 **D. Sukachev**
Sub-Doppler laser cooling and magnetic trapping of thulium atoms 34
CT–011 **P. Moroshkin**
Spectroscopy of alkali metal atoms in dense supercritical helium at low temperature 35
CT–012 **A. Avdeenkov**
Temporal evolution of ultracold polar molecules in a circularly polarized microwave field 36
CT–013 **A. Antognini**
The proton radius puzzle 37
CT–014 **A. K. Hansen**
Single ion recycling reaction experiments 38
CT–015 **V. A. Yerokhin**
QED theory of the nuclear magnetic shielding in hydrogen-like ions 39
CT–016 **R. Le Targat**
Quantum simulation of frustrated classical magnetism in triangular optical lattices 40
CT–017 **M. G. Kozlov**
Using microwave and submillimeter molecular transitions to search for variation of the fundamental constants 41
CT–018 **W. E. Ernst**
Ionization of Rb (Cs) atoms and Rb_n (Cs_n) clusters on He droplets 42
CT–019 **D. G. Green**
Enhancement of positron annihilation on core electrons 43
CT–020 **A. J. Krmpot**
Atomic dark state evolution in the constant laser field 44
CT–021 **Ph. V. Demekhin**
Strong interference effects in the resonant Auger decay of atoms induced by intense x-ray laser fields 45
CT–022 **D. Sarkisyan**
High contrast sub-natural resonance of increased absorption formed in cell filled with Rb and buffer gas 46
CT–023 **B. Botermann**
A fundamental test of Lorentz invariance using relativistic $^7Li^+$ ion beams 47
CT–024 **J. Hoszowska**
Two-electron one-photon transitions of Mg, Al, and Si in K-shell double photoionization 48
CT–025 **S. Nic Chormaic**
Dark and light optical nanofibre probes for cold atoms 49

CT–026 **L. Devenoges**
Time and frequency metrology with laser cooled atoms: evaluation of the Swiss continuous atomic fountain clock 50

CT–027 **P. Roncin**
Atomic diffraction to reveal the atomic structure of surfaces, surfaces to construct atomic interferometers 51

CT–028 **J.–L. Robyr**
Atomic beam measurement of the DC Stark shift of the Cs clock transition frequency 52

CT–029 **M. Chevrollier**
Selective reflection probing of thin film deposition 53

CT–030 **O. Kozlova**
Cs cell Ramsey clock based on coherent population trapping: current status 54

CT–031 **M. Oriá**
Nonlinearly-generated atomic signal for robust laser locking 55

CT–032 **L. Gianfrani**
A novel approach to Doppler-width thermometry: Implications for an improved determination of the Boltzmann constant 56

CT–033 **T. Carette**
Isotope effects in atomic negative ions: promises and challenges . . 57

CT–034 **Th. Busch**
Coupling a single quantum bit to an ultra-cold Fermi sea 58

CT–035 **A. Dimitriou**
Strong laser-induced-coupling between autoionizing states in the vicinity of four-photon excitation of Mg $3p^2\ ^1S_0$ resonance 59

CT–036 **M. Albert**
Cavity electromagnetically induced transparency and all-optical switching with cold ion Coulomb crystals 60

CT–037 **J. Lecointre**
Photodissociation of HeH^+ in the ground state: comparison with experiment 61

CT–038 **O. Plekan**
New ferroelectric materials studied by cold electron scattering . . . 62

CT–039 **D. Hanstorp**
Threshold behaviour in photodetachment of K^- 63

CT–040 **M. Pajek**
Enhanced radiative recombination of U^{92+} ions with electrons in cold magnetized plasma 64

POST: Contributed Posters **65**

AAP: AMO Physics at Large Facilities **66**

AAP–001 **M. Bouledroua**
Theoretical investigation of the lithium 2s-2p line broadened by ground hydrogen . . . 67

AAP–002 **N. Bucalovic**
Er:Yb:Glass oscillator (ERGO): a low-noise optical frequency comb for frequency metrology . . . 68

AAP–003 **N. Castagna**
Spatially resolved magneto-relaxation of magnetic nanoparticles using atomic magnetometry . . . 69

AAP–004 **M. Chevrollier**
Laser-induced cesium lithography . . . 70

AAP–005 **V. Dolgovskiy**
All-optical low-noise microwave generation from a 1.5 μm ultra-stable laser . . . 71

AAP–006 **M. Ellmeier**
Investigation on a coupled dark state magnetometer . . . 72

AAP–007 **M. Fertl**
Improvements of the Hg cohabiting magnetometer for the nEDM experiment at PSI . . . 73

AAP–008 **C. L. Garrido Alzar**
High-sensitivity large-area cold atom gyroscope . . . 74

AAP–009 **H. Hartman**
A setup for investigation of VUV transitions of iron group elements for astrophysical applications using synchrotron radiation at MAX-lab, Sweden . . . 75

AAP–010 **M. Kasprzak**
Scalar and vector Cs magnetometer for an nEDM experiment . . . 76

AAP–011 **Y. Kayser**
Depth profiling of low energy P, In, and Sb implants using synchrotron radiation based high-resolution micro-GEXRF . . . 77

AAP–012 **P.–J. Nacher**
Optical techniques for measuring the nuclear polarization of ^{3}He gas 78

AAP–013 **S. Nic Chormaic**
Thermo-optical effects on the transduction of mechanical motion of a microspherical pendulum . . . 79

AAP–014 **S. H. Nowak**
Effects of the sample surface roughness in grazing emission x-ray fluorescence measurements . . . 80

AAP–015 **Ş. Osmanoğlu**
Identification of gamma radiation treatment of anticancer drug 5-fluorouracyl by electron paramagnetic resonance 81
AAP–016 **A. Papoyan**
High-spatial-resolution monitoring of strong magnetic field using Rb nano-thin cell 82
AAP–017 **G. Pichler**
Atomic spectra of high-pressure Cs and Na light sources and their energy applications 83
AAP–018 **O. Plekan**
Cyclic dipeptide immobilization on Au (111) and Cu (110) surfaces 84
AAP–019 **M. Polasik**
Modelling of benchmark x-ray spectra from tungsten ions with charge 44+ to 46+ in the 3.5–8.0 Å range 85
AAP–020 **P. Quinet**
Spectroscopic parameters for neutral tungsten lines of interest for fusion plasma research 86
AAP–021 **T. Scholtes**
Stretched-state optically pumped magnetometer with miniaturized Cs cell 87
AAP–022 **S. Woetzel**
Integrated array of optically pumped magnetometers 88

CAM: Cold Atoms/Molecules, Ions, and Quantum Gases **89**
CAM–001 **Th. Busch**
Vortex lattices in anisotropic traps 90
CAM–002 **P. Cheinet**
Observation of resonant 4-body process with cold Rydberg atoms . 91
CAM–003 **V. M. Entin**
Microwave spectroscopy and Förster resonance between a few Rydberg atoms reveal an ultracold plasma formation at laser excitation 92
CAM–004 **E. Gazazyan**
Laser assisted Feshbach resonances 93
CAM–005 **M. Germann**
Production of ultracold, internally state-selected molecular ions in ion traps 94
CAM–006 **A. Grochola**
Spectroscopic investigation of the states dissociating to the Li(2s) +Cs(5d) asymptote of LiCs molecule 95
CAM–007 **F. Hall**
A new experiment to study cold molecular ion – atom reactions . . 96

CAM–008 **Z. Jędrzejewski-Szmek**
Deperturbation of the $3^1\Pi_u$, $4^1\Pi_u$ states in Li_2 and the $c^3\Sigma^+$, $B^1\Pi$ states in NaCs . . . 97
CAM–009 **S. Kotochigova**
Strong anisotropy in the interaction between ultracold Dy atoms . 98
CAM–010 **G. Krois**
Excitation and ionization of highly excited Cs atoms on helium nanodroplets . . . 99
CAM–011 **C. Maher–McWilliams**
Chirped optical Stark acceleration and deceleration . . . 100
CAM–012 **E. A. Pazyuk**
Prospects of the $a^3\Sigma^+ \rightarrow E^1\Sigma^+ \rightarrow X^1\Sigma^+$ optical cycle for ultracold KCs molecule production . . . 101
CAM–013 **J. Pedregosa-Gutierrez**
Ion dynamics in linear RF traps . . . 102
CAM–014 **J. Poms**
Electron spin resonance of ^{87}Rb monomers on superfluid helium nanodroplets: optical pumping scheme and line shape analysis . . . 103
CAM–015 **L. Pruvost**
Cold atoms in Laguerre-Gaussian laser beams . . . 104
CAM–016 **L. Pruvost**
Vibrational quantum defect to analyze photoassociation spectra of Rb_2 and Cs_2 and to detect coupled states . . . 105
CAM–017 **I. I. Ryabtsev**
Counterintuitive behavior of nonsymmetric Penning ionization cross-section for two Rydberg atoms . . . 106
CAM–018 **J. Szczepkowski**
Spin domain formation in an expanding anti-ferromagnetic quantum gas . . . 107
CAM–019 **E. Tiesinga**
Study of the Bose-Hubbard model by collapse and revival measurements . . . 108

FPE: Fundamental Physics: Experiment **109**
FPE–001 **B. Arcimowicz**
Analysis of the odd parity configurations of tantalum atom–revisited 110
FPE–002 **D. Banaś**
The status of the Kielce EBIS facility for the studies of ion-matter interactions . . . 111
FPE–003 **D. Barredo**
A versatile setup to study Rydberg atom – surface interactions . . 112

FPE–004 **Gö. Başar**
Hyperfine structure measurements in the $3d^3 4s4p\ {}^6G_J$ levels of atomic vanadium with Fourier transform spectroscopy 113

FPE–005 **É. Biémont**
Lifetime measurements and calculations in Y^+ and Y^{2+} ions . . . 114

FPE–006 **B. Furmann**
Experimental verification isotope shift of some levels even parity in neutral Eu 115

FPE–007 **F. Güzelçimen**
Hyperfine structure measurements and determination of new energy levels of atomic lanthanum by laser induced fluorescence spectroscopy 116

FPE–008 **K. Katsonis**
Measurement and evaluation of transitions probabilities of Ar I to III 117

FPE–009 **S. Khan**
Investigation of the hyperfine structure of Pr I lines involving levels having J= 7/2 118

FPE–010 **A. Knie**
Interference between differently localized electrons in N_2O 119

FPE–011 **V. Lebedev**
Impurity-phonon coupling in liquid and solid helium 120

FPE–012 **Š. Masys**
Electronic structure of semi-core states in $BiFeO_3$ thin films: an experimental and *ab initio* study 121

FPE–013 **P.–J. Nacher**
Experimental determination of collisional broadening for the 1083 nm 2^3S–2^3P transition of helium 122

FPE–014 **I. I. Ryabtsev**
Particularities of Doppler profile for supersonic beams with circular, square, and arbitrary collimating apertures 123

FPE–015 **I. Siddiqui**
Hyperfine structure investigations of singly ionized praseodymium and discovery of new Pr II levels 124

FPE–016 **S. Tanweer I.**
New odd-parity energy levels in neutral praseodymium 125

FPE–017 **G. Tastevin**
Rotational spectra and time dynamics of metastable He dimers probed by light absorption at 465 nm 126

FPE–018 **U. Zaheer**
New levels of the Pr atom with almost similar energies 127

FPT: Fundamental Physics: Theory **128**

FPT–001 **P. Bhowmik**
Correlation between ionization potential and dipole polarizability of metastable species 129

FPT–002 **M. Bouamoud**
Higher order effects in the electron impact ionization of water molecule 130

FPT–003 **N. Bouloufa**
Optimal trapping wavelengths of Cs_2 and RbCs molecules in an optical lattice 131

FPT–004 **N. Bouloufa**
Hyperfine structure of Cs_2 and RbCs excited molecules 132

FPT–005 **C. Daul**
Molecular magnets: symmetry constrained manybody theory and the calculation of the parameters of the effective Heisenberg–Van Vleck–Dirac Hamiltonian 133

FPT–006 **J. Dembczyński**
Critical analysis of the methods of interpretation in the hyperfine structure of free atoms and ions. Case of the extended configuration system of the lanthanum atom 134

FPT–007 **Ph. V. Demekhin**
Resonant Auger decay of the core-excited C^*O molecule in intense x-ray laser fields 135

FPT–008 **L. Glowacki**
New approach to generation of spin orbitals in relativistic CI calculations for many electron atoms 136

FPT–009 **A.–V. Glushkov**
Muon-gamma-nuclear spectroscopy of atoms: Cooperative muon-gamma-nuclear processes 137

FPT–010 **A.–V. Glushkov**
Electron-β -nuclear spectroscopy of atoms: bound β-decay and decay of isomeric states for ionized atoms 138

FPT–011 **G. F. Gribakin**
Dense spectrum of resonances and capture of particles in the field of a body with near-black-hole metric 139

FPT–012 **G. P. Gupta**
Calculated energy levels and lifetimes in Mg-like vanadium 140

FPT–013 **G. P. Gupta**
Excitation energies, oscillator strengths and lifetimes in Ni XV . . 141

FPT–014 **P. Jönsson**
Transition rates in the B-, C-, N-, O-, and Ne-like sequences from relativistic CI calculations 142

FPT–015 **O. Yu. Khetselius**
Nuclear moments and hyperfine structure parameters for heavy atoms within relativistic many-body theory 143
FPT–016 **O. Yu. Khetselius**
Parity nonconservation effect in heavy atoms and nuclei: nuclear-relativistic many-body theory 144
FPT–017 **J. G. Li**
Ab-initio multi-configuration Dirac-Hartree-Fock calculation on the lifetimes of levels in $2p^5 3s$ configuration of neutral neon 145
FPT–018 **T.–O. Müller**
Universal and specific properties of atomic interactions 146
FPT–019 **C. Nazé**
Relativistic calculations on isotope shifts in barium 147
FPT–020 **K. Rajchel**
Trigonometric unit circle and the stationary Schrödinger equation . 148
FPT–021 **P. Rynkun**
Peculiarities of spectroscopic properties of W^{8+} 149
FPT–022 **M. Selg**
Nonadiabatic state-independent potential for the hydrogen molecule in ground electronic state 150
FPT–023 **A. V. Stolyarov**
Spin-orbit coupling effect in the low-lying states of Rb_2, Cs_2 and RbCs molecules 151
FPT–024 **A. V. Stolyarov**
Adaptive mapping procedure for scattering length calculation . . . 152
FPT–025 **V. L. Sukhorukov**
Strong polarization of outer electron shells by inner vacancies in Ba 153
FPT–026 **J. Szczepkowski**
The $4^1\Sigma^+$ electronic state of LiCs molecule 154
FPT–027 **S. Verdebout**
Interaction of variational localized correlation functions for atomic properties 155
FPT–028 **S. Verdebout**
Atomic properties of neutral Ne using the LCFI method 156
FPT–029 **V. A. Yerokhin**
Polarization correlations in radiative recombination and bremsstrahlung157

HRS: High-Resolution Spectroscopy **158**
HRS–001 **N. Akhtar**
Doppler reduced investigation of hyperfine structures of Pr II lines using collinear laser ion beam spectroscopy 159
HRS–002 **C. Andreeva**
Interference of laser-dressed states in the Autler-Townes effect . . . 160

HRS–003 **N. Anjum**
High resolution spectroscopic study of La II by using collinear laser ion beam spectroscopy 161
HRS–004 **T. Bandi**
High-resolution double resonance spectroscopy of the clock transition in ^{87}Rb atomic vapour 162
HRS–005 **A. Berzins**
Magneto-optical resonances in D_2 excitation of atomic rubidium vapour confined in an extremely thin cell 163
HRS–006 **A. Berzins**
Influence of laser power density on bright and dark magneto-optical resonances 164
HRS–007 **I. Birzniece**
Fourier transform spectroscopy and potential construction for low vibrational levels of $B^1\Pi$ state in KCs 165
HRS–008 **E. Breschi**
Laser spectroscopy of optical transitions in Rb microfabricated-cells 166
HRS–009 **J.–Cl. Dousse**
High-resolution KMM radiative Auger x-ray spectra of calcium induced by synchrotron radiation 167
HRS–010 **A. Er**
Laser induced fluorescence spectroscopy of atomic niobium in the wavelength range of 560 nm to 620 nm 168
HRS–011 **T. Kirova**
Creation of dark states in the Autler-Townes spectrum of Na hyperfine levels 169
HRS–012 **O. Kozlova**
Precise measurement of the collisional shift of Cs clock frequency in presence of N_2, Ne, and Ar buffer gases 170
HRS–013 **O. Kozlova**
Laser-induced line narrowing of the coherent population trapping resonance: experiment and theory 171
HRS–014 **A. Kruzins**
Novel study of the $A^1\Sigma^+ \sim b^3\Pi$ complex in KCs and refinement of deperturbation analysis 172
HRS–015 **A. Krzykowski**
High resolution spectroscopy of chromium atom 173
HRS–016 **D. Miletic**
AC Stark-shift in double resonance and coherent population trapping in wall-coated cells for compact Rb atomic clocks 174
HRS–017 **J. Musielok**
Transition probability determination for some LS-forbidden lines in neutral sulfur by branching ratio measurements 175

HRS–018 **M. Pajek**
The x-ray satellites and hypersatellites excited in fast ion-atom collisions . . . 176
HRS–019 **Y. Pashayan–Leroy**
High-contrast dark-line atomic resonance of D_1 excitation in nanometric-thin cell filled with rubidium . . . 177
HRS–020 **M. Polasik**
Theoretical study on the influence of shake process accompanying β^- decay on the structures of x-ray spectra . . . 178
HRS–021 **V. Polischuk**
MatLab based modeling of nonlinear interaction of ^{87}Rb atoms with polarized radiation . . . 179
HRS–022 **A. Sargsyan**
Study of electromagnetically induced transparency in strong magnetic field using Rb nanometric-thin cell . . . 180
HRS–023 **K. Słabkowska**
Theoretical decomposition of the satellite $L\gamma$ x-ray lines spectra of thorium . . . 181
HRS–024 **K. Słabkowska**
Influence of open-shell effect on double K-shell hole states radiative de-excitation parameters . . . 182

PPA: Photoionization, Photodetachment, Anions **183**
PPA–001 **M. Allan**
Electron scattering from krypton: high-resolution electron scattering experiments and B-spline R-matrix calculations . . . 184
PPA–002 **M. Allan**
Electron scattering in $Pt(PF_3)_4$: elastic scattering, vibrational and electronic excitation . . . 185
PPA–003 **M. Allan**
Absolute angle-differential vibrational excitation cross sections for electron collisions with diacetylene . . . 186
PPA–004 **P. Andersson**
Effects of laser light in a negative ion sputter ion source — sulphur vs. chlorine production . . . 187
PPA–005 **C. Blondel**
Photodetachment microscopy to an excited state and the electron affinity of phosphorus . . . 188
PPA–006 **T. Carette**
Isotope shifts and hyperfine structures of the $3p^3\ ^4S^o$, $^2D^o$ and $^2P^o$ multiplets of Si^- and $3p^2\ ^3P$ term of Si . . . 189

PPA–007 **A. Costescu**
Anomalous Rayleigh scattering of x rays and photoeffect by inner shell electrons 190
PPA–008 **A. Dimitriou**
Multiphoton excitation and AC-shift of autoionizing states of Mg probed by monitoring the Mg^+ 3p→3s radiative decay 191
PPA–009 **V. Feyer**
Core level spectroscopy and tautomerism of cytosine derivatives in the gas phase 192
PPA–010 **G. F. Gribakin**
Saddle-point "smiles" in electron detachment by few-cycle laser pulses 193
PPA–011 **D. Hanstorp**
Partial photodetachment cross sections in K^- 194
PPA–012 **Y. Kita**
Ab initio quantum Monte Carlo study of the binding of a positron to alkali-metal hydrides 195
PPA–013 **D. Kubala**
Dissociative electron attachment to formic acid: high-resolution absolute scale measurements 196
PPA–014 **B. M. Lagutin**
Four-fold excitation resonances: manifestation in the resonant Auger effect of Kr 197
PPA–015 **M. O. Musa**
Laser-induced free-free transitions in elastic electron scattering from CO_2 198
PPA–016 **A. A. Narits**
Ion-pair formation and resonant quenching in collisions of Rydberg atoms with neutral atoms 199
PPA–017 **G. Purohit**
Electron impact single ionization of noble gas targets in the perpendicular plane geometry 200
PPA–018 **S. D. Stoychev**
Intermolecular Coulombic decay in small, biochemically relevant, hydrogen bonded systems 201
PPA–019 **S. Turchini**
Photoelectron circular dichroism of isopropanolamine 202
PPA–020 **R. V. Tymchyk**
Lowest autoionizing states of beryllium in photoionization problem 203
PPA–021 **S. V. Yalunin**
Surface effect in multiphoton electron emission from metals 204

QOI: Quantum Optics and Information **205**
QOI–001 **D. Aghamalyan**
Generation of photonic time-bin qubit in a tripod atomic media . . 206
QOI–002 **B. Avchyan**
Generation of powerful tunable THz radiation via two-color multiphoton resonance in atomic-molecular systems 207
QOI–003 **B. Avchyan**
Wave-mixing and harmonics generation due to two-color multiphoton resonant excitation of atoms and molecules 208
QOI–004 **O. V. Belyaeva**
Cumulant analysis of entangled multipartite states 209
QOI–005 **T. L. Dimitrova**
Three demonstrations of the wave-particle duality of light and quantum erasing 210
QOI–006 **A. Gogyan**
Efficient generation of Fock states in a single-atom cavity-QED system 211
QOI–007 **S. N. Nikolić**
Propagation of light pulses through medium with electromagnetically induced transparency 212
QOI–008 **Sh. Petrosyan**
Self-induced transparency of probe field in four-level atomic media 213
QOI–009 **N. V. Vitanov**
Smooth composite pulses for high-fidelity quantum information processing 214

UFP: Ultrafast Processes **215**
UFP–001 **T. Carette**
Investigation of the ionization of neon by an attosecond XUV pulse with the time-dependent Schrödinger equation 216
UFP–002 **G. Dridi**
Ultrafast stimulated Raman parallel adiabatic passage by shaped pulses 217
UFP–003 **N. M. Kabachnik**
Angular dependence of the sidebands in photoionization induced by ultrashort x-ray pulses in a strong laser field 218
UFP–004 **G. Karras**
Formation of molecular halide ions from alkyl-halide clusters irradiated by ps and fs laser pulses 219

XDA: Post-Deadline abstracts **220**
FPT–401 **D. A. Glazov**
g factor of few-electron ions: bound-state QED in the presence of magnetic field 221

Index by contribution number **223**

Index by author **225**

Plenary Lectures

PL

Quantum metrology with ultracold atoms — a strongly interacting optical lattice clock

J. Ye[1]

[1] *JILA, National Institute of Standards and Technology and University of Colorado, Department of Physics, University of Colorado, Boulder, CO 80309-0440, USA*

Corresponding Author: Ye@JILA.Colorado.edu

Optical clocks based on atoms confined in optical lattices provide a unique opportunity for precise study and measurement of quantum many-body systems. The state-of-the-art optical lattice clock has reached an overall fractional frequency uncertainty of 1×10^{-16} [1]. One dominant contribution to this uncertainty is clock frequency shift arising from atomic collisions. Collisions between initially identical fermionic Sr atoms can occur when they are subject to slightly inhomogeneous optical excitations during the clock operation [2]. We have recently implemented a seemingly paradoxical solution to the collision shift problem: with a strong atomic confinement in one-dimensional tube-shaped optical traps, we dramatically increase the atomic interactions. Instead of a naively expected increase of collisional frequency shifts, these shifts are suppressed [3]. The large atomic interaction strength creates an effective energy gap in the system such that inhomogeneous excitations can no longer drive fermions into a pseudo-spin anti-symmetric state, and hence their collisions and the corresponding frequency shifts are suppressed. We demonstrate the effectiveness of this approach by reducing the density-related frequency shift to the level of 10^{-17}, representing more than a factor of ten reduction from the previous record [1, 2]. In addition, we have observed well-resolved interaction sidebands separated from the main peak of the clock transition, giving a direct evidence for the removal of the interaction energy from the clock carrier. Control of atomic interactions at the level of 1×10^{-17} removes a fundamental obstacle to accuracy for a many-particle-based optical atomic clock.

References

[1] A. D. Ludlow *et al.*, Science **319**, 1805 (2008).
[2] G. K. Campbell *et al.*, Science **324**, 360 (2009).
[3] M. D. Swallows *et al.*, Science **331**, 1043 (2011).

Observation of Kondo correlations in optical absorption

A. Imamoglu[1]

[1] *Institute of Quantum Electronics, ETH-Zürich, CH-8093 Zürich, Switzerland*
Corresponding Author: imamoglu@phys.ethz.ch

The interaction between a single confined spin and the spins of a Fermionic reservoir leads to one of the most spectacular phenomena of many body physics — the Kondo effect. In this talk, I will describe the first observation of Kondo correlations in optical absorption measurements on a single semiconductor quantum dot tunnel–coupled to a degenerate electron gas. In stark contrast to transport experiments, absorption of a single photon leads to an abrupt change in the system Hamiltonian by turning off the exchange interaction between the quantum dot electron spin and the fermionic reservoir, leading to a quantum quench of Kondo correlations. As a consequence of this quench, the absorption line shape exhibits power law tails, signaling a redistribution of the optical oscillator strength associated with an Anderson orthogonality catastrophe. We find that the power–law exponents characterizing the quench are tunable by an external magnetic field, proving the link to spin physics. This observation, together with the measurement of suppressed magnetization of the quantum dot electron, unequivocally demonstrate that the observed absorption line-shape provides a direct of Kondo correlations. Our experiments arguably provide the first example of many-body physics studied using a single optically active quantum dot.

Quantum sensors on earth and in space

C. Salomon[1]

[1] *Laboratoire Kastler Brossel, CNRS, UPMC, Ecole Normale supérieure, 24 rue Lhomond 75231 Paris, France*

Corresponding Author: christophe.salomon@lkb.ens.fr

Atomic clocks and matter-wave interferometers have made spectacular progress in the last years. Optical clocks have recently reached a frequency stability and accuracy in the 10^{-18} range [1] opening new perspectives for time keeping and fundamental tests. Matter-wave accelerometers and rotation sensors have sensitivities that equal or surpass mechanical devices.

These quantum sensors permit probing space-time properties with a new level of precision both with ground based or space based devices. An improved measurement of Einstein's gravitational red-shift will be made with a precision of two parts per million by the Atomic Clock Ensemble in Space mission (ACES) of the European Space Agency [2]. By comparing clocks of different nature at the 10^{-17}/year level, new limits are obtained for the time variation of fundamental constants of physics such as the fine structure constant alpha and the ratio of electron to proton mass. Matter-wave sensors provide a measurement of the fine structure constant with 6.6×10^{-10} precision [3] and have been proposed to extend the range of gravitational wave detectors towards lower frequencies [4]. Finally we will point out fundamental differences between tests of the gravitational redshift with atomic clocks and tests with atom interferometers through the measurement of acceleration of freely falling atoms [5,6,7].

References

[1] C. W. Chou, D. B. Hume, T. Rosenband, D. J. Wineland, Science **329**, 1630, (2010).
[2] L. Cacciapuotti, and C. Salomon, Eur. Phys. J. Special Topics, **172**, 57 (2009).
[3] R. Bouchendira, P. Cladé, S. Guellati-Khélifa, F. Nez, and F. Biraben, Phys. Rev. Lett. **106**, 080801 (2011).
[4] S. Dimopoulos, P. W. Graham, J. M. Hogan, M. A. Kasevich, and S. Rajendran, Phys. Rev. D **78**, 122002 (2008).
[5] H. Müller, A. Peters, and S. Chu, Nature **463**, 926 (2010).
[6] P. Wolf, L. Blanchet, C. Bordé, S. Reynaud, C. Salomon, and C. Cohen-Tannoudji, Nature **467**, E1 (2010).
[7] P. Wolf, L. Blanchet, C. J. Bordé, S. Reynaud, C. Salomon, and C. Cohen-Tannoudji, arXiv: 1012.1194 submitted to Classical and Quantum Gravity, (2010).

Slow-light and Rydberg polaritons

M. Fleischhauer[1]

[1] *Department of Physics and research center OPTIMAS, University of Kaiserslautern, 67663 Kaiserslautern, Germany*

Corresponding Author: mfleisch@physik.uni-kl.de

Dark-state or slow-light polaritons [1] are quasi-particles generated in the interaction of light with multi-level atoms driven by an external laser close to a Raman resonance. They form the basis of phenomena such as electromagnetically induced transparency, ultra-slow and stationary light, and have interesting applications ranging from quantum information to many-body physics. For example, the dispersion relation of dark-state polaritons can be controlled to a large extend, representing massive Schrödinger particles on the one hand or multi-component objects with a Dirac-like energy-momentum relation on the other. In the latter case the "relativistic" length and energy scales can be widely tuned, making effects such as pair creation and Klein tunneling accessible in the lab. Even exotic systems can be realized and experimentally studied such as the random-mass Dirac model, which shows anomalous localization phenomena. After briefly introducing slow-light polaritons, I will first give an overview of theoretical ideas to study interesting single-particle phenomena. In the second part of the talk I will discuss the prospects to create strong interactions between dark-state polaritons. Particularly promising is here a combination of slow light with Rydberg atoms [2]. The dipole-dipole coupling between atoms in a Rydberg state leads to a strong and long-range interaction between polaritons, as well as a blockade phenomenon [3,4], preventing two excitations to survive within a certain distance from each other. This interaction can give rise to interesting many-body phenomena, such as photons with two-particle correlations of hard spheres [5] or even a crystalization.

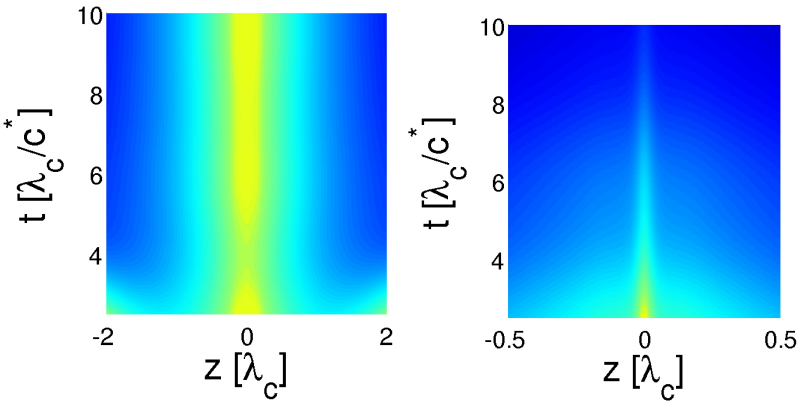

Figure 1: *Klein tunneling of Dirac stationary light. left: Time evolution of density in a box potential with width larger than effective Compton length, $l = 2.5\ \lambda_C$. right: The same in a box with width smaller than effective Compton length $l = 0.2\ \lambda_C$.*

References

[1] M. Fleischhauer, A. Imamoglu, J. P. Marangos, Rev. Mod. Phys. **77**, 633 (2005).
[2] J. D. Pritchard *et al.*, Phys. Rev. Lett. **105**, 193603 (2010).
[3] M. D. Lukin *et al.*, Phys. Rev. Lett. **87**, 037901 (2001).
[4] H. Kübler *et al.*, Nature Photonics **4**, 112 (2010).
[5] A. Gorshkov *et al.*, arXiv:1103.3700.

Raman spectroscopy for exploring cultural heritage

R. R. Ernst[1]

[1] *Laboratorium für Physikalische Chemie, ETH Hönggerberg HCI, 8093 Zürich, Switzerland*
Corresponding Author: richard.ernst@nmr.phys.chem.ethz.ch

The lecture is devoted to the application of non-destructive spectroscopic techniques for pigment analysis in ancient paintings. Pigments have been used since millennia to enhance the appearance of art works. Colors have received symbolic and metaphoric meanings and convey messages to the observer. Their analysis can provide clues for a better understanding of provenience and of age of art works. In this context, spectroscopy becomes of significance for a historic understanding of art in a cultural context.

Raman spectroscopy was found to be particularly revealing. The back scattered light upon laser irradiation of surfaces provides a convenient way of analysis of the pigments used for coloring. The design of a Raman spectrometer for exploring large scale paintings, based on a Bruker Optics SENTERRA Raman Microscope, is described.

The applications described refer to studies of Central Asian Buddhist paintings where a pigment analysis allows insights into the provenience of the paintings and on traditional and non-traditional usage of pigments. Thangka paintings from 13th century Tibet, from Nepal, and from Buriatia, Siberia, will be explored by Raman microscopy.

These studies illustrate also the need of scientists to occasionally change their customary fields of work for exploring new domains that lead to renewed stimulation. Many of our scientific studies have moved far from the interests of society, and the building of bridges has become essential for preventing our isolation in an academic ivory tower. The combination of spectroscopy and art complies with an old dream of the author of bringing together science and culture.

Controlling and imaging quantum gases at the single atom level

I. Bloch[1]

[1] *Ludwig-Maximilians Universität, Fakultät für Physik, 80799 München, Germany*
and
Max-Planck Institut für Quantenoptik, Hans Kopfermann Str. 1,
85748 Garching b. München, Germany

Corresponding Author: immanuel.bloch@mpq.mpg.de

Over the past years, ultracold quantum gases in optical lattices have offered remarkable opportunities to investigate static and dynamic properties of strongly correlated bosonic or fermionic quantum many-body systems. In this talk I will show how it has recently not only become possible to image such quantum gases with single atom sensitivity and single site resolution, but also how it is now possible to coherently control single atoms on individual lattice sites within a strongly correlated quantum gas. Using a tightly focussed laser beam, atoms on selected lattice sites can be addressed and their spin state fully controlled. Magnetic resonance control techniques were employed to achieve sub-lattice period and sub-diffraction limited resolution in our addressing scheme.

The ability to address single atoms on a lattice opens a whole range of novel research opportunities ranging from quantum information processing over the investigation of quantum spin systems to local entropy control, some of which will be discussed in the talk.

PL

Infrared spectrum of H_3^+ from the laboratory to the galactic center

T. Oka[1]

[1] *Department of Astronomy and Astrophysics and Department of Chemistry*
The Enrico Fermi Institute, University of Chicago, USA
Corresponding Author: t-oka@uchicago.edu

Protonated molecular hydrogen, H_3^+, is the simplest polyatomic molecule discovered by J. J. Thomson exactly 100 years ago. It is the most abundant molecular ion in hydrogen dominated plasmas and plays the central role in formation of interstellar molecules. The infrared spectrum of H_3^+ discovered in the laboratory [1] has led to its detection in 1996 toward two young stars deeply embedded in their natal dense clouds [2]. Although it took many years to detect the first signal, once detected, H_3^+, has been observed everywhere. It was detected not only in dense clouds ($n \sim 10^4$ cm^{-3}) as theoretically predicted but, surprisingly, also in diffuse clouds ($n \sim 10^2$ cm^{-3}) where abundant electrons were thought to destroy H_3^+. The most amazing discovery has been the very high abundance of H_3^+ in the Central Molecular Zone (CMZ), a region with radius $\sim$ 200 pc, of the Galactic center. This has revealed a new category of gas with high temperature ($\sim$ 250K) and low density ($\sim$ 100 cm^{-3}) with a high volume filling factor, and high ionization rates (2×10^{-15} s^{-1}) of the environment [3]. Recent extension of this observation to wider regions of the CMZ [4] will be discussed.

References

[1] T. Oka, Phys. Rev. Lett. **45**, 531-534 (1980).
[2] T. R. Geballe and T. Oka, Nature, **384**, 334–335 (1996).
[3] T. Oka, T. R. Geballe, M. Goto, *et al.*, Astrophys. J. **632**, 882–893 (2005).
[4] T. R. Geballe and T. Oka, Astrophys. J. **709**, L70–73 (2010).

Cavity optomechanics: back-action cooling of mechanical oscillators

T. J. Kippenberg[1]

[1] *Ecole Polytechnique Fédérale de Lausanne, CH-1015 Lausanne Switzerland*
Corresponding Author: tobias.kippenberg@epfl.ch

The mutual coupling of optical and mechanical degrees of freedom via radiation pressure has been a subject of interest in the context of quantum limited displacement measurements for gravity wave detection for many decades, however light forces have remained experimentally unexplored in such systems. Recent advances in nano- and micro-mechanical oscillators have, for the first time, allowed the observation of radiation pressure phenomena in an experimental setting and constitute the emerging research field of cavity optomechanics [1].

Using on-chip micro-cavities that combine both optical and mechanical degrees of freedom in one and the same device [2], radiation pressure back-action of photons is shown to lead to effective cooling [3–6] of the mechanical oscillator mode using dynamical backaction, which has been predicted by Braginsky as early as 1969 [4]. This back-action cooling exhibits many close analogies to atomic laser cooling. For instance, it is shown theoretically that only in the resolved sideband regime, cooling to the quantum ground state is possible. With this novel technique the quantum mechanical ground state of a micromechanical oscillator can be reached. Using cryogenic precooling [7] to 600mK the preparation of a micromechanical oscillator to only 2 quanta is shown. Moreover it is possible in this regime to observe strong coupling in which the mechanical and optical mode hybridize. Moreover, the optomechanical interaction allows unprecedented sensitivity of reading out mechanical motion, achieving an imprecision below the level of the zero point motion [8,9].

Optomechanical systems also offer entirely new means to control the light field. Using the recently discovered phenomenon of optomechanically induced transparency [10] it is possible to enable devices that store light in mechanical excitations, or create optical delay lines with unpredecented delay time. Recent highlights of the literature of some of the emerging applications of cavity optomechanics will be reviewed.

References

[1] T. J. Kippenberg, K. J. Vahala, Science **321**, 1172 (2008).
[2] T. J. Kippenberg, H. Rokhsari, T. Carmon, A. Scherer, K. J. Vahala, Phys. Rev. Lett. **95**, 033901 (2005).
[3] V. B. Braginsky, S. P. Vyatchanin, Phys. Lett. A **293**, 228 (2002).
[4] V. B. Braginsky, *Measurement of Weak Forces in Physics Experiments*. (University of Chicago Press, Chicago, 1977).
[5] A. Schliesser, P. Del'Haye, N. Nooshi, K. J. Vahala, J. Kippenberg, Phys. Rev. Lett. **97**, 243905 (2006).
[6] A. Schliesser, R. Riviere, G. Anetsberger, O. Arcizet, T. J. Kippenberg, Nature Physics **4**, 415 (2008).
[7] A. Schliesser, O. Arcizet, R. Riviere, T. J. Kippenberg, Nature Physics 5, 509 (2009).
[8] G. Anetsberger *et al.*, Nature Physics **5**, 909 (2009).
[9] A. Schliesser, O. Arcizet, R. Riviere, G. Anetsberger, T. J. Kippenberg, Nature Physics **5**, 509 (2009).
[10] S. Weis, *et al.*, Science **330**, 1520 (2010).

PL

XUV/x-ray lasers for ultrafast electronic control in simple molecules

F. Martín[1,2]

[1] *Departamento de Química, Módulo 13, Universidad Autónoma de Madrid, 28049 Madrid, Spain*
[2] *Instituto Madrileño de Estudios Avanzados en Nanociencia (IMDEA-Nanociencia), Cantoblanco, 28049 Madrid, Spain*

Corresponding Author: fernando.martin@uam.es

The development of novel XUV/x-ray radiation sources, such as 3rd generation synchrotron radiation devices, free electron lasers and attosecond lasers, in combination with multi-coincidence detection techniques, allows one to probe the inner working of atoms and molecules with unprecedented detail and on a wide range of time scales, from a few attoseconds, the natural scale of electronic motion, to femto and picoseconds, which is the time required for molecular vibrations and dissociation. In most cases, the high energy of the absorbed XUV/x-ray photons leads to ionization and, consequently, theoretical treatments must be aimed at providing an accurate description of both the electronic and dissociative continua.

In molecules, the measurement in coincidence of the momentum of all ejected charged particles produced by absorption of synchrotron radiation provides valuable information on the tiniest details of electron and nuclear dynamics. Also, attosecond pump-probe spectroscopy using femto- and atto-second sources enables investigations of the prompt charge redistribution and localization that accompany photo-excitation processes, where a molecule is lifted from the ground Born-Oppenheimer potential energy surface to one or more excited surfaces, and where subsequent photochemistry evolves on femtosecond timescales. In this talk I will present a few theoretical examples of how theory has been able to disentangle the complex information that arises from sophisticated multicoincidence synchrotron experiments and to provide the basic mechanisms involved in attosecond pump-probe experiments in which H_2 is ionized with a single attosecond pulse (or a train of attosecond pulses) and is subsequently probed by one or several infrared few-cycle pulses. The localization of the electronic charge distribution within the remaining molecular ion is calculated with attosecond time-resolution and is visualized by varying the delay between the pump and probe pulses. The results of these calculations [1,2,3] are compared with recent experimental measurements and provide the different mechanisms that are responsible for the observations.

References

[1] G. Sansone, F. Kelkensberg, J. F. Pérez-Torres, F. Morales, M. F. Kling, W. Siu, O. Ghafur, P. Johnsson, M. Swoboda, E. Benedetti, F. Ferrari, F. Lépine, J. L. Sanz-Vicario, S. Zherebtsov, I. Znakovskaya, A. LHuillier, M. Yu. Ivanov, M. Nisoli, F. Martín, and M. J. J. Vrakking, Nature **465**, 763 (2010).
[2] S. E. Canton, E. Plésiat, J. D. Bozek, B. S. Rude, P. Decleva, and F. Martín, Proc. Nat. Acad. Sci., in press
[3] F. Kelkensberg, W. Siu, J. F. Pérez-Torres, F. Morales, G. Gademann, A. Rouzée, P. Johnsson, M. Lucchini, F. Calegari, J. L. Sanz-Vicario, F. Martín, and M. J. J. Vrakking, Phys. Rev. Lett., to be published.

PL

Half a century of optically pumped magnetometers

E. B. Alexandrov[1]

[1] *Ioffe Physical Technical Institute RAS, 194021 St. Petersburg, Russia*
Corresponding Author: ealexandrov@bk.ru

Optically pumped magnetometers (OPMs) are instruments that allow measurement of a magnetic field, using resonant spectral magnetic features of atoms in both optical and radiofrequency ranges. An initial impetus was given to their evolution in 1950's by invention of magnetic resonance optical detection by F. Bitter [1], and discovery of the principle of optical pumping by A. Kastler [2]. Further development of these ideas resulted in creation of a family of OPMs which allow measuring magnetic fields with extremely high accuracy and sensitivity (i.e., [3,4]). Having no match in absolute accuracy, OPMs can surpass even superconducting quantum interference devices (SQUIDs) in terms of sensitivity.

There are two basic types of OPMs: Mz- and Mx-magnetometers, which correspondingly use Mz resonance signals associated with the constant magnetization of the atoms, and Mx signals associated with transverse component of the magnetic moment, or coherence.

Figure 1 gives a very approximate impression about the metrological characteristics of OPMs as compared to other magnetometric instruments; the arrow shows the generalized vector of development. Among the instruments presented on Fig. 1 are Cs (cesium), K (potassium), ^{3}He (nuclear helium), He-Me (alkaline-helium) Mx- and Mz-magnetometers.

This picture can be noticeably changed with the development of principally new pumping schemes — such as schemes with suppressed spin-exchange broadening [5,6], schemes based on electromagnetically induced transparency [7], the coherent population trapping effect [8], the nonlinear magneto-optical rotation effect [9], and other effects of coherent and non-linear interaction of light with atoms.

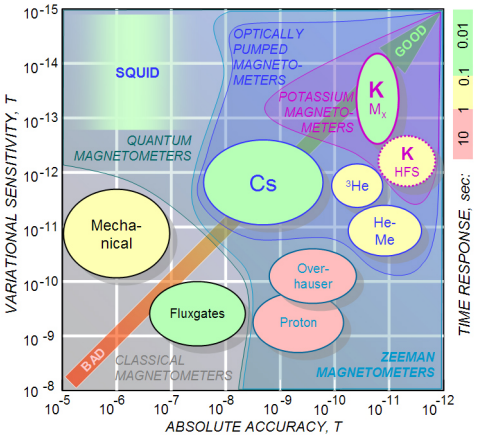

Figure 1: *Approximate classification of magnetometers by their metrological parameters.*

References

[1] F. Bitter, Phys. Rev. **76**, (6), 833 (1949).
[2] A. Kastler, J. Phys. et le Radium **11**, 255 (1950).
[3] D. Budker, M. Romalis, Nature Physics **3**, 227 (2007).
[4] E. Aleksandrov, A. Vershovskii, Advances in Physical Sciences (UFN) **52**, 573 (2009).
[5] J. Allred *et al.*, Phys. Rev. Lett. **89**, 130801 (2002).
[6] I. K. Kominis *et al.*, Nature **422**, 596 (2003).
[7] A. S. Zibrov *et al.*, Phys. Rev. Lett. **76**, 3935 (1996).
[8] J. Kitching *et al.*, IEEE Trans. Instrum. Meas. **49**, 1313 (2000).
[9] D. Budker, V. V. Yashchuk, M. Zolotorev, Phys. Rev. Lett. **81**, 5788 (1998).

PL

Recent progress in high-density alkali-metal magnetometers

M. Romalis[1]

[1] *Department of Physics, Princeton University, Princeton, New Jersey, USA*
Corresponding Author: romalis@princeton.edu

I will describe recent progress of atomic magnetometers based on high-density hot alkali-metal vapor. Careful control of spin-exchange collisions allows such magnetometers to reach sub-femtotesla field sensitivity with a centimeter-sized sensor. A number of practical applications of such magnetometers have been demonstrated, including measurements of magnetoencephalography, paleomagnetism, and NMR signals. In combination with a spin-polarized noble gas (^{3}He or ^{21}Ne), high-density alkali-metal magnetometers have also been used for precision measurements, such as searches for Lorentz-violating CPT-even and CPT-odd spin interactions and for spin-dependent forces. I will also describe two presently ongoing efforts on construction of self-contained fiber-coupled sensors and utilizing spin-squeezing techniques to improve the sensitivity of scalar atomic magnetometers.

Progress Reports

PR

Measuring the gravitational constant G with an atom interferometer

M. Prevedelli[1,5], L. Cacciapuoti[2], Y. H. Lien[4,5], G. Rosi[4,5], F. Sorrentino[3,4,5], and G. M. Tino[3,4,5]

[1] *Dept. of Physics, University of Bologna, 40126 Bologna, Italy*
[2] *Research and Scientific Support Dept., European Space Agency, 2201 AZ Noordwijk, The Netherlands*
[3] *Dept. of Physics and Astronomy, University of Firenze, 50019 Sesto Fiorentino, Italy*
[4] *European Laboratory for Nonlinear Spectroscopy (LENS), 50019 Sesto Fiorentino, Italy*
[5] *Istituto Nazionale di Fisica Nucleare (INFN), 50019 Sesto Fiorentino, Italy*

Corresponding Author: marco.prevedelli@unibo.it

The gravitational constant G is the least precisely measured fundamental constant [1]. Since the first measurement by Cavendish in 1798, accuracy has improved only by two orders of magnitude in more than 200 years and systematic errors have constantly frustrated experimental efforts. As an example the two most recently published experiments [2,3] differ by 5 combined standard deviations.

In this situation even experiments with limited precision but based on different measurement principles can help in identifying systematics and, to this purpose, proof–of–principle determinations of G using atom interferometry have already been published [4,5].

Since 2006 a differential gradiometer based on a ^{87}Rb cold atoms interferometer is operating in Florence aiming at measurement of G at the 100 ppm level. Currently a sensitivity of 500 ppm in one day of continuous measurement has been achieved.

The experiment and the latest results will be presented and possible systematic effects will be discussed.

References

[1] P. J. Mohr, B. N. Taylor, and D. B. Newell, Rev. Mod. Phys. **80**, 633–730 (2008).
[2] H. V. Parks, and J. E. Faller, Phys. Rev. Lett. **105**, 110801 (2010).
[3] J. Luo *et al.*, Phys. Rev. Lett. **102**, 240801 (2009).
[4] J. B. Fixler *et al.*, Science **315**, 74 (2007).
[5] G. Lamporesi *et al.*, Phys. Rev. Lett. **100**, 050801 (2008).

Quantum simulators: the Anderson transition case

J. C. Garreau[1]

[1] *Laboratoire de Physique des Lasers, Atomes et Molécules, Université Lille 1, 59650 Villeneuve d'Ascq, France*

Corresponding Author: jean-claude.garreau@univ-lille1.fr

Condensed matter has been for many decades one of the most fertile fields of physics; yet, some of its most popular models describe only roughly the features of real systems. From the theoretical point of view this is due mainly to the complexity of the interactions among tightly packed electrons and ions forming a real crystal. From the experimental point of view the main difficulty is the measuring of local quantities in a bulk material, where in general only global quantities like the conductivity are accessible. A very good example of that is the very popular Anderson model [1] originally designed to describe the effects of disorder on the quantum dynamics of electrons in a crystal. This model neglects the Coulomb interaction between electrons and predicts an exponential localization of the wave function – in sharp contrast with delocalized Bloch waves in a perfect crystal. The "Anderson localization" is a quantum effect which has never been directly observed in condensed matter.

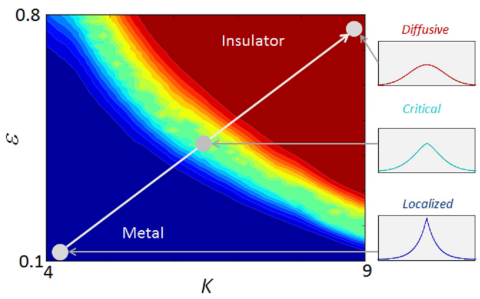

Figure 1: *Phase diagram of the Anderson transition. The plots on the right show the wavefunction at different points across the transition.*

In recent years, the combination of laser and evaporative techniques for cooling atoms allowed to reach very low temperatures in which quantum effects can be observed. Moreover, such atoms can be placed in tailored laser beams that interact with the atoms as a mechanical potential. This provides ways to the realization of almost "ideal" condensed matter systems, in which, atom-atom interactions can not only be made negligible, but even can be externally controlled. And this fine tuning of perturbations is also true concerning decoherence effects! In such low density, highly conservative systems, direct experimental access to quantum probabilities distributions is also granted. This has opened a new and stimulating field of research for both theoreticians and experimentalists. In this progress report we shall discuss the physics of cold-atom systems displaying very cleanly the physics of the Anderson model with adjustable dimensionality. A prominent feature is the famous Anderson metal-insulator transition (Fig. 1) that we have recently observed and characterized [2,3] with a finesse seldom achieved in the study of second-order quantum phase transitions.

References

[1] P. W. Anderson, Phys. Rev. **109**, 1492–1505 (1958).
[2] J. Chabé *et al.*, Phys. Rev. Lett. **101**, 255702 (2008).
[3] G. Lemarié *et al.*, Phys. Rev. Lett. **105**, 090601 (2010).

High precision theoretical spectra of the hydrogen molecule

J. Komasa[1], K. Pachucki[2]

[1] *A. Mickiewicz University, Grunwaldzka 6, 60-780 Poznań, Poland*
[2] *University of Warsaw, Hoża 69, 00-681 Warsaw, Poland*

Corresponding Author: komasa@man.poznan.pl

We present recent advances in theoretical prediction of infrared spectra of the hydrogen molecule and its isotopomers in the $^1\Sigma_g^+$ electronic ground state. The total energy is evaluated from the following expansion in powers of the fine-structure constant $E(\alpha) = \sum_{i=0} E^{(i)}\alpha^i$, in which the coefficients $E^{(i)}$ are expectation values of effective Hamiltonians obtained from the nonrelativistic quantum electrodynamics (NRQED). Subsequent terms of this expansion have clear physical interpretation: $E^{(0)}$ is the nonrelativistic energy, $E^{(1)}\alpha$ is absent, $E^{(2)}\alpha^2$ is the leading relativistic correction, $E^{(3)}\alpha^3$ represents the leading QED effects (and includes $\alpha^3 \ln \alpha$ terms), and so on.

The progress in theory has been made in several directions: (i) implementation of newly developed formulas for exponential molecular wave functions [1]; (ii) development of a new nonadiabatic perturbation theory (NAPT) [2]; (iii) advances in numerical techniques accelerating the convergence of highly singular operators appearing in $E^{(i)}$ as well as techniques of evaluation of multielectron molecular Bethe logarithm.

In the frames of this theory we evaluated the dissociation energy D_0 of all the bound rovibrational states of H_2, HD, and D_2. A sample of the ground rovibrational state D_0 is given in Table 1, where for comparison also the most recent experimental values are shown. The excellent agreement validates the theoretical approach applied to determine the energy levels.

	D_0/cm^{-1}					
	H_2		HD		D_2	
Experiment	36 118.069 62(37)	[3]	36 405.783 66(36)	[4]	36 748.362 86(68)	[3]
Theory	36 118.069 6(10)	[5]	36 405.782 8(10)	[6]	36 748.363 3(9)	[5]
Discrepancy	0.000 0(10)		0.000 9(10)		0.000 4(9)	

Table 1: *The ground state dissociation energy of H_2, HD, and D_2.*

The electric and magnetic moments of allowed transitions observed within the manifold of the rovibrational states have also been evaluated. As far as the electric transition rates are concerned, they are in good agreement with previous theoretical predictions, although more accurate. Our theoretical transition intensities also agree well with the available experimental line intensities. The magnetic dipole transition rates in H_2 were evaluated for the first time. For the lowest rotational states these rates are negligible in comparison with the electric quadrupole transitions, as expected. However, for the highest states they tend to dominate over the quadrupole rates [7].

Perspectives of further increase in accuracy of the theoretical predictions will be discussed. The main challenge involves evaluation of the higher order terms in α and in the electron-to-nuclei mass ratio.

References

[1] K. Pachucki, Phys. Rev. A **82**, 032509 (2010).
[2] K. Pachucki and J. Komasa, J. Chem. Phys. **130**, 164113 (2009).
[3] J. Liu *et al.*, J. Chem. Phys. **130**, 174306 (2009); *ibid.* **132**, 154301 (2010).
[4] D. Sprecher *et al.*, J. Chem. Phys. **133**, 111102 (2010).
[5] K. Piszczatowski *et al.*, J. Chem. Theory and Comput. **5**, 3039 (2009).
[6] K. Pachucki and J. Komasa, Phys. Chem. Chem. Phys., **12**, 9188 (2010).
[7] K. Pachucki and J. Komasa, Phys. Rev. A **83**, 032501 (2011).

New results on Efimov physics and the creation RbCs molecules

F. Ferlaino[1]

[1] *Institute of Experimental Physics, University of Innsbruck, Austria*
Corresponding Author: Francesca.Ferlaino@uibk.ac.at

I will present new results from two different experiments on ultracold gases, both based on scattering length tunability near Feshbach resonances.

In a first experiment, we investigate universal few-body physics with ultracold cesium atoms. We detect various Efimov states in a magnetic field range up to 1 kG by measuring loss resonances in three-body recombination processes [1]. We find in total five distinct Efimov resonances in the same spin channel, all resulting from different Feshbach resonances. Surprisingly, all Efimov resonances occur at the same value of the scattering length, which points to universality across all Feshbach resonances and rules out a significant variation of the three-body parameter.

In a second experiment, we produce a degenerate or near-degenerate ultracold mixture of ^{87}Rb and ^{133}Cs atoms [2]. We investigate the interspecies scattering properties by Feshbach spectroscopy and we determine the background inter-species scattering length to be unusually large and positive. Starting with magneto-associated Feshbach molecules, we perform spectroscopic measurements on the two-photon optical transition that will serve to transfer RbCs molecules to the rovibronic ground state via a STIRAP transfer scheme [3]. This work constitutes a first step towards the production of a quantum gas of ground-state polar molecules.

References

[1] M. Berninger, A. Zenesini, B. Huang, H.-C. Nägerl, F. Ferlaino, R. Grimm, P. Julienne, J. Hutson, to be published.
[2] A. D. Lercher, T. Takekoshi, M. Debatin, B. Schuster, R. Rameshan, F. Ferlaino, R. Grimm, H.-C. Nägerl, arXiv:1101.1409.
[3] M. Debatin, T. Takekoshi, R. Rameshan, L. Reichsöllner, F. Ferlaino, R. Grimm, H.-C. Nägerl, to be published.

PR

Stark-tuned Förster resonance and dipole blockade between few Rydberg atoms: experiment and theory

I. I. Ryabtsev[1], D. B. Tretyakov[1], I. I. Beterov[1], V. M. Entin[1], and E. A. Yakshina[1]

[1] *Institute of Semiconductor Physics, Pr. Lavrentyeva 13, 630090 Novosibirsk, Russia*
Corresponding Author: ryabtsev@isp.nsc.ru

Resonant energy transfer (Förster resonance) between highly excited Rydberg atoms is used in quantum information processing to implement quantum logic gates with neutral atoms [1,2]. Förster resonances take place for two or more atoms in an identical Rydberg state if this state lies midway between two other Rydberg states of the opposite parity. It arises on the distances of several microns due to strong dipole-dipole interaction between Rydberg atoms. Förster resonances can be either accidental for some specific states (quasi-Förster resonance) or precisely Stark-tuned with the electric field. In this report we present our recent experimental and theoretical results on Stark-tuned Förster resonances and dipole blockade in cold Rydberg atoms.

In the experiments we have observed for the first time a Stark-tuned Förster resonance $Rb(37P_{3/2})+Rb(37P_{3/2})\rightarrow Rb(37S)+Rb(38S)$ between two cold Rb Rydberg atoms confined in a small laser excitation volume [3]. The experiments were performed in a magneto-optical trap. A small excitation volume was formed by two tightly focused laser beams in crossed-beam geometry. Single Rydberg atoms were detected with 65% efficiency using selective field ionization and channel electron multiplier that provided the atom-number resolution in combination with the post-selection technique. High-resolution spectra of the Förster resonance have been obtained for 1 to 5 of the detected Rydberg atoms. For precise comparison with theory, we have done the numerical Monte Carlo simulations for 2 to 5 randomly interacting Rydberg atoms. Good agreement between experiment and theory allowed us to identify the numbers of actually interacting Rydberg atoms, taking into account finite detection efficiency.

We have further developed the Monte Carlo theoretical model to investigate spectroscopic features of the Förster resonances and dipole blockade for 2 to 5 interacting Rydberg atoms, which are trapped and localized at finite temperatures in optical dipole traps of various spatial configurations [4]. Effect of the spatial uncertainty on coherence of Förster resonances and dipole blockade has been investigated and analyzed in the context of quantum information processing with Rydberg atoms.

We have also proposed to use adiabatic rapid passage with a chirped laser pulse to deterministically excite only one Rydberg atom from randomly loaded optical dipole traps or optical lattices in the strong dipole blockade regime [5]. The chirped laser excitation has been shown to be insensitive to the random number N of the atoms in the traps. Our method thus overcomes the problem of the $\sqrt{N}$ dependence of the collective Rabi frequency, which was the main obstacle for deterministic single-atom excitation in the ensembles with unknown N. It can be readily applied for single-atom loading of dipole traps and optical lattices.

This work was supported by RFBR (Grant Nos. 10-02-00133 and 10-02-92624), by the Russian Academy of Sciences, by the Presidential Grants No. MK-6386.2010.2 and MK-3727.2011.2, by the Dynasty Foundation, and by the EU FP7 IRSES Project “COLIMA”.

References

[1] M. Saffman *et al.*, Rev. Mod. Phys. **82**, 2313 (2010).
[2] D. Comparat *et al.*, J. Opt. Soc. Am. B **27**, A208 (2010).
[3] I. I. Ryabtsev *et al.*, Phys. Rev. Lett. **104**, 073003 (2010).
[4] I. I. Ryabtsev *et al.*, Phys. Rev. A **82**, 053409 (2010).
[5] I. I. Beterov *et al.*, arXiv:1102.5223.

Direct frequency comb spectroscopy: time and frequency domain approach

T. Ban[1,2], A. Foltynowicz[2], P. Maslowski[2], D. Aumiler[1], G. Pichler[1], and J. Ye[2]

[1] *Institute of Physics, Bijenicka 46, HR-10 000 Zagreb, Croatia*
[2] *JILA, National Institute of Standards and Technology and University of Colorado, Department of Physics, University of Colorado, Boulder, Colorado 80309-0440, USA*
Corresponding Author: ticijana@ifs.hr

Optical frequency comb brings revolutionary advances in frequency metrology and spectroscopy. The comb spectrum consists of a series of equidistant modes, whose frequencies can be described by the simple formula:

$$f_n = nf_{rep} + f_0. \quad (1)$$

Here, f_n is the optical frequency of the n-th comb mode, f_{rep} is the repetition rate of the mode-locked laser and f_0 is the carrier-envelope offset frequency. By measuring and controlling f_{rep} and f_0 it is possible to control the frequencies of all comb modes, providing excellent spectroscopic tool over hundreds of terahertz of the comb bandwidth.

Direct frequency comb spectroscopy (DFCS) employs frequency combs to directly interrogate atoms or molecules. One class of experiments use a frequency comb excitation of an atomic system to study the time-dependent quantum coherence. Unification of the time- and frequency-domain treatments, based on the coherence accumulation effects in systems characterized by the relaxation times longer than the laser repetition period was reported for cold rubidium atoms [1]. In Doppler-broadened rubidium vapor accumulation effects in the time domain lead to a comb-like velocity distribution in the excited state and velocity selective population transfer in the alkali ground-state [2]. We will present the results of the experimental and theoretical investigations of the Doppler-broadened rubidium vapor excited by an optical frequency comb, resulting in novel information about the accumulative effects in multilevel atoms [3].

In one of the most powerful alternative implementations of DFCS, the interaction of the frequency comb with an atomic or molecular sample is enhanced by the use of a high-finesse optical cavity [4]. Precise control of the optical frequency comb allows highly efficient coupling of the individual comb modes to the corresponding cavity resonances, while the long cavity lifetime enhances the effective interaction length between the light field and the intracavity sample. As a result, cavity-enhanced direct frequency comb spectroscopy (CE-DFCS) combines broad spectral bandwidth, high spectral resolution, precise frequency calibration, and ultrahigh detection sensitivity [5]. Here, we will present the results of the CE-DFCS in the near-infrared wavelength region using a scanning Fourier transform spectrometer as a detection system [6,7]. In addition to other CE-DFCS advantages, the newly developed cavity-enhanced frequency comb Fourier transform spectrometer in the mid-IR provides fast acquisition times and further enhanced detection sensitivity, which all together brings it to the frontier of many interesting applications such as trace gas detection, breath analysis and other medical diagnosis, environmental and atmospheric science, etc.

References

[1] A. Marian *et al.*, Science **306**, 2063 (2004).
[2] D. Aumiler *et al.*, Phys. Rev. Lett. **95**, 233001 (2005).
[3] T. Ban *et al.*, Phys. Rev. A **80**, 023425 (2009).
[4] M. J. Thorpe *et al.*, Science **311**, 1595 (2006).
[5] F. Adler *et al.*, Annu. Rev. Anal. Chem. **3**, 175 (2010).
[6] F. Adler *et al.*, Opt. Express **18**, 21861 (2010).
[7] A. Foltynowicz *et al.*, Faraday Disc., DOI:10.1039/C1FD00005E.

PR

Heavy–ion collisions: from formation of quasi–molecules to relativistic regime

A. Surzhykov[1], A. Artemyev[1], Th. Stöhlker[1], and P. Indelicato[2]

[1] *Physikalisches Institut, Universität Heidelberg, D-69120 Heidelberg, Germany and GSI Helmholtzzentrum für Schwerionenforschung GmbH, D-64291 Darmstadt, Germany*
[2] *Laboratoire Kastler Brossel, École Normale Supérieure, CNRS, 75252 Paris, France*
Corresponding Author: surz@physi.uni-heidelberg.de

In this presentation we will review the recent theoretical progress in the study of heavy–ion collisions. Special attention shall be paid to (relatively) slow collisions between two highly–charged projectiles. In such a case, one can observe the formation of quasi–molecules, i.e., short–living systems in which electrons move in the Coulomb field of two nuclei. A novel theoretical approach for the description of the structural properties and dynamical behaviour of these quasi–molecules, recently developed by us [1], will be discussed in detail. Based on this approach, exploiting the B–spline basis sets constructed in Cassini coordinates, we will perform and discuss a systematic analysis of the energy spectra of Th_2^{179+} and U_2^{183+} dimers.

Apart from the low–energy domain, theoretical investigations of the relativistic collisions will be reported. Here, we will focus on the Coulomb excitation of few–electron projectiles interacting with low–Z atomic and molecular targets [2]. Owing to recent experiments performed at the GSI storage ring in Darmstadt, this process has attracted considerable interest. In this contribution, we shall present calculations on the alignment of excited ionic states and discuss the role of relativistic and interelectronic–interaction phenomena.

Work is supported by the Helmholtz Gemeinschaft under Project No. VH–NG–421.

References

[1] A. Artemyev *et al.*, J. Phys. B At. Mol. Opt. Phys. **43** 235207 (2010).
[2] A. Surzhykov *et al.*, Phys. Rev. A **77** 042722 (2008).

Optimal two-qubit gates for trapped neutral atoms at the quantum speed limit

M. M. Müller[1], D. M. Reich[2], M. Murphy[1], T. Calarco[1], H. Yuan[3], K. B. Whaley[4], J. Vala[5], and C. P. Koch[2]

[1] *Institut für Quanteninformationsverarbeitung, Universität Ulm, 89081 Ulm, Germany*
[2] *Theoretische Physik, Universität Kassel, Heinrich-Plett-Str. 40, 34132 Kassel, Germany*
[3] *Research Laboratory of Electronics, Massachusetts Institute of Technology, Cambridge, MA 02139, USA*
[4] *Department of Chemistry and Pitzer Center for Theoretical Chemistry, University of California, Berkeley, California 94720, USA*
[5] *Department of Mathematical Physics, National University of Ireland, Maynooth, Ireland, and School of Theoretical Physics, Dublin Institute for Advanced Studies, 10 Burlington Rd., Dublin, Ireland*

Corresponding Author: christiane.koch@uni-kassel.de

Optimal control is a promising tool for quantum information processing since it allows implementing a desired operation with extremely high fidelity. For quantum optical settings, the implementation of a two-qubit operation such as a CNOT gate typically poses the main difficulty to build a universal quantum computer. In an optimal control approach, implementation of a CNOT gate can be achieved by maximizing the projection of the actual evolution onto CNOT as a functional of a control such as a laser field [1].

However, for a given encoding of qubits in a physical system, it is *a priori* not clear whether CNOT is the two-qubit gate that can best be implemented or whether a gate that is equivalent to CNOT up to local, i.e., single-qubit, operations would be a more suitable choice. Based on the Cartan decomposition and the geometric theory of two-qubit operations [2], we develop a functional to obtain the entangling power of a desired two-qubit gate, i.e., to optimize for a gate that is locally equivalent to the desired two-qubit operation. This functional turns out to be non-convex and we employ a second-order Krotov method to derive a monotonically convergent optimization algorithm [3]. We apply this new functional to the implementation of a fast Rydberg gate [4].

References

[1] J. P. Palao and R. Kosloff, Phys. Rev. A **68**, 062308 (2003).
[2] J. Zhang *et al.*, Phys. Rev. A **67**, 042313 (2003).
[3] D. M. Reich, M. Ndong, and C. P. Koch, arXiv:1008.5126.
[4] D. Jaksch *et al.*, Phys. Rev. Lett. **85**, 2208 (2000).

PR

Test of fundamental symmetries in ^{3}He/^{129}Xe clock comparison experiments

W. Heil[1], C. Gemmel[1], S. Karpuk[1], Yu. Sobolev[1], K. Tullney[1], M. Burghoff[2], W. Kilian[2], S. Knappe–Grüneberg[2], W. Müller[2], A. Schnabel[2], F. Seifert[2], L. Trahms[2], and U. Schmidt[3]

[1] *Institut für Physik, Johannes Gutenberg-Universität, 55099 Mainz, Germany*
[2] *Physikalisch-Technische Bundesanstalt, 10587 Berlin, Germany*
[3] *Physikalisches Institut, University of Heidelberg, 69120 Heidelberg, Germany*
Corresponding Author: Wheil@uni-mainz.de

We discuss the design and performance of a very sensitive low-field magnetometer based on the detection of free spin precession of gaseous, nuclear polarized ^{3}He or ^{129}Xe samples with a SQUID as magnetic flux detector. Characteristic spin precession times T_2^* of up to 60 h were measured in low magnetic fields (about 1 μT) and in the regime of motional narrowing. The achieved signal-to-noise ratio of more than 5000 : 1 leads to an expected sensitivity level (Cramer-Rao Lower Bound) of $\delta B \approx 1$ fT after an integration time of 220 s and of $\delta B \approx 10^{-4}$ fT (100 zeptoTesla) after one day [1].

With the detection of the free precession of co-located ^{3}He/^{129}Xe nuclear spins (clock comparison), the device can be used as ultra-sensitive probe for nonmagnetic spin interactions, since the magnetic dipole interaction (Zeeman-term) drops out in the weighted frequency difference, i.e., $\Delta\omega = \omega_{\mathrm{He}} - (\gamma_{\mathrm{He}}/\gamma_{\mathrm{Xe}})\,\omega_{\mathrm{Xe}}$. We report on searches for a) Lorentz violating signatures by monitoring the Larmor frequencies of co-located ^{3}He/^{129}Xe spin samples as the laboratory reference frame rotates with respect to distant stars (sidereal modulation) [2] and b) spin-dependent short-range interactions induced by light pseudoscalar bosons, such as the axion, invented to solve the strong CP problem [3].

References

[1] C. Gemmel, W. Heil, S. Karpuk, *et al.*, Eur. Phys. J. D **47**, 303–320, (2010).
[2] C. Gemmel, W. Heil, S. Karpuk, *et al.*, Phys. Rev. D **82**, 111901(R) (2010).
[3] M. Burghoff, C. Gemmel, W. Heil, *et al.*, Proc. Workshop on Experimental and Theoretical Approaches to Quantum States of Neutrons in Gravitational Field, Les Houches, France (2010).

Optically pumped magnetometers in life science and fundamental research

G. Bison[1], G. Lembke[1], M. Stumpf[1], S. Afach[1], and M. Petkovic[1]

[1] *Department of Neurology, Friedrich-Schiller-University, Erlanger Allee 101, 07747 Jena, Germany*

Corresponding Author: georg.bison@med.uni-jena.de

Optical pumping magnetometers (OPMs), which were initially developed half a century ago [1], have received a renewed interest over the past decade. Especially their application in life science and in fundamental research has lead to continuing performance improvements to the borders of quantum physics and beyond [2]. Applications in life science include the recording of biomagnetic fields as they are generated by the heart [3] or the brain [4]. Those biomagnetic fields can be mapped by sensor arrays and reveal valuable diagnostic information about the underlying electrophysiological processes. For example, a diagnostic method based on such magnetic recording of the human heart (magneto cardiography, MCG) significantly improves the sensitivity to angina pectoris. A further advantage of MCG is the quick and contact free measurement, but wide spread use of the method is prevented by the high cost of the measurement systems which are usually based on low-temperature SQUIDs. A central goal of our research is to demonstrate the great potential for cost efficient MCG offered by OPMs. For the heart magnetic field, we found that OPMs based on optically detected electron spin resonance in Cs atoms offer the best compromise between cost effectiveness and performance in terms of magnetometric, time, and spatial resolution. Based on a first multichannel OPM sensor [5] we develop a MCG system for clinical tests which will have 57 primary sensors and two times 13 reference sensors. New developments in this field are sensor extensions which allow us to measure all components of the magnetic field and increase the sensor bandwidth significantly.

Another application of OPMs is the search for a permanent electric dipole moment (EDM) of the neutron d_n [6]. This is currently a very active field of fundamental research with the goal to find physics beyond the standard model. Many theoretical predictions of the neutron EDM are about two orders of magnitude smaller than the current experimental limits. The next generation of neutron EDM experiments aim at a direct measurement of the neutron EDM at sensitivities down to $10^{-28}\,\mathrm{e}\cdot\mathrm{cm}$. To measure d_n, ultra cold neutrons are put in a static magnetic field B_0 and are run through a magnetic resonance (Ramsey) cycle. In the presence of d_n and an electric field $E||B_0$ the term in the Hamiltonian which causes the magnetic resonance precession at the Larmor frequency ω_L is given by $\hbar\omega_L = -\mu B_0 - d_n E$. The EDM d_n can be extracted from the linear E dependence of ω_L if the magnetic term does not change between measurements. Satisfying this condition is far from trivial since the relatively large magnetic dipole moment of the neutrons efficiently transfers magnetic field changes of ω_L. The magnetic field has to be controlled at the fT level in order to achieve a resolution of $10^{-28}\,\mathrm{e}\cdot\mathrm{cm}$ under typical conditions. We will report on the development of special OPMs with optimized long term stability to meet those demanding requirements.

References

[1] A. L. Bloom, Appl. Opt. **1**, 61–68 (1962).
[2] E. B. Aleksandrov, A. K. Vershovskii, Physics-Uspekhi **52** (6), 573–601 (2009).
[3] G. Bison, R. Wynands, A. Weis, Opt. Express **11**, 904–909 (2003).
[4] H. Xia, *et al.*, Appl. Phys. Lett. **89**, 211104, (2006).
[5] G. Bison *et al.*, Appl. Phys. Lett. **95** (17), 173701 (2009).
[6] C. A. Baker *et al.*, Phys. Rev. Lett. **97**, 131801 (2006).

CT

Contributed Talks

First observation of spin flips of a single trapped proton

H. Kracke[1], K. Blaum[2,3], A. Mooser[1,4], W. Quint[3,5], C. C. Rodegheri[1,3], S. Ulmer[1,3,5], and J. Walz[1,4]

[1] *Institut für Physik, Johannes Gutenberg-Universität D-55099 Mainz, Germany*
[2] *Max-Planck-Institut für Kernphysik, Saupfercheckweg 1, D-69117 Heidelberg, Germany*
[3] *Ruprecht Karls-Universität Heidelberg, D-69047 Heidelberg, Germany*
[4] *Helmholtz Institut Mainz, D-55099 Mainz, Germany*
[5] *GSI – Helmholtzzentrum für Schwerionenforschung, D-64291 Darmstadt, Germany*
Corresponding Author: kracke@uni-mainz.de

Our experiment aims for the determination of the g-factor or magnetic moment of the (anti)proton with a relative precision of 1 ppb. The comparison of the magnetic moment of the proton and antiproton leads to a stringent test of the matter-antimatter symmetry in the baryon sector [1].

The experiment uses a single proton trapped in a cryogenic double Penning trap stack [2]. Such a double trap setup consists of a precision trap, where the magnetic field is homogeneous and an analysis trap, where a "magnetic bottle" $B(z) = B_0 + B_2 z^2$ is superimposed to the homogeneous field. This setup allows for the spatially separated measurement of the cyclotron frequency ν_c of the proton and the detection of its spin state for the determination of the Larmor frequency ν_L. The g-factor can be calculated as $g = 2\nu_L/\nu_c$. The homogeneous magnetic field in the precision trap allows for a high precision determination of ν_c by application of the invariance theorem $\nu_c^2 = \nu_+^2 + \nu_z^2 + \nu_-^2$ where $\nu_{+,z,-}$ are the respective eigenfrequencies of the proton in the trap. In the analysis trap the continuous Stern-Gerlach effect is applied for the non-destructive determination of the spin eigenstate [3]. The magnetic bottle B_2 couples the spin magnetic moment to the axial frequency $\nu_z = 674$ kHz, thus reducing the determination of the spin direction to the measurement of the axial frequency.

The inhomogeneity is introduced to the trap by a ferromagnetic ring electrode. We measured $B_2 = 3.00(10) \times 10^5\,\mathrm{T{\cdot}m^{-2}}$ which is the largest magnetic field inhomogeneity ever superimposed to a Penning trap. A change of the spin quantum number causes a shift of the axial frequency of $\Delta\nu_{z,SF} = 190$ mHz. However, due to the magnetic inhomogeneity the axial frequency also depends on the angular momentum and thus is sensitive to fluctuations of the energy E_ρ of the radial modes where $\Delta\nu_z/\Delta E_\rho \approx 1\ \mathrm{Hz}/\mu\mathrm{eV}$. Great care has to be taken to avoid spurious changes of the quantum numbers of the radial modes. Having achieved an axial frequency stability in the order of $\Delta\nu_{z,SF}$, spin flips can be resolved in a series of statistical measurements.

In the talk the first observation of spin flips with a single isolated proton is presented. A detailed description of the measurement procedure and data analysis is given yielding the first Larmor resonance curve measured with a single trapped proton. This is the most important breakthrough on the way towards the first direct determination of the magnetic moment of a single free (anti)proton and a new test of the matter-antimatter symmetry in the baryon sector.

References

[1] R. Bluhm *et al.*, Phys. Rev. D **57**, 3932 (1998).
[2] C. C. Rodegheri *et al.*, Hyperfine Interact. **194**, 93 (2009).
[3] W. Quint *et al.*, Nucl. Instr. Meth. B **214**, 207 (2004).

Magnetization dynamics of a dipolar BEC at ultralow magnetic field

E. Maréchal[1], B. Pasquiou[1], G. Bismut[1], P. Pedri[1], L. Vernac[1], O. Gorceix[1], and B. Laburthe–Tolra[1]

[1] *Laboratoire de Physique des Lasers, CNRS, Université Paris Nord, 93430 Villetaneuse, France*

Corresponding Author: etienne.marechal@univ-paris13.fr

One consequence of long-ranged, anisotropic dipole-dipole interactions is that they induce collisions with a change in magnetization. Due to conservation of orbital momentum, they hence also induce a coupling between spin and angular momentum degrees of freedom yielding new interesting physics in the field of dilute quantum gases.

We have studied the spinor properties of S=3 ^{52}Cr atoms at extremely low magnetic field; typically below 1 mG. We have reached a regime where spin dependent contact interactions overwhelm the linear Zeeman effect; the BEC then goes through a phase transition and ceases to be ferromagnetic [1,2]. We evidence a phase transition between a ferromagnetic phase and an unpolarized phase, when the magnetic field is quenched below a critical value Bc (Fig. 1). We also show that the magnetization dynamics is governed by magnetic dipole-dipole interactions. This result [3] opens up the study of spinor physics with free magnetization.

In a second set of experiments [4], we have loaded the Cr BEC in 2D optical lattices. We show that dipolar relaxation is strongly inhibited at low magnetic fields of about 30 mG when the released energy becomes smaller than the vibrational quantum of energy at the bottom of the lattice wells. Just above the threshold, dipolar relaxation populates rotating states in the lattice, in the spirit of Einstein and de Haas effect.

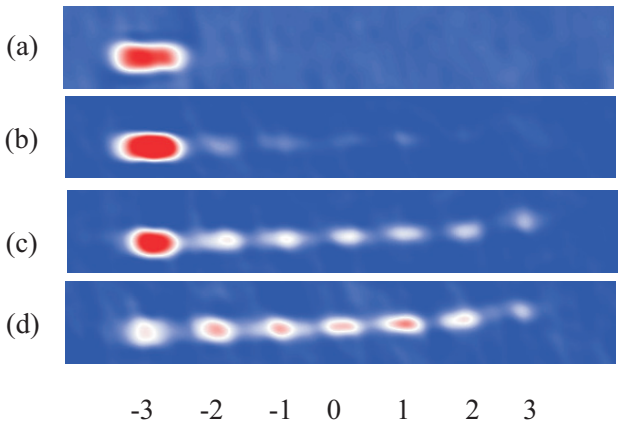

Figure 1: *Stern-Gerlach analysis of the BEC spin composition, after 150 ms of evolution in a given field. The BEC spontaneously depolarizes as the magnetic field is lowered down: a) 1 mG; b) 0.5 mG; c) 0.25 mG; d) 0 mG.*

References

[1] T.-L. Ho, Phys. Rev. Lett. **81**, 742 (1998).
[2] L. Santos and T. Pfau, Phys. Rev. Lett. **96**, 190404 (2006).
[3] B. Pasquiou *et al.*, submitted.
[4] B. Pasquiou *et al.*, Phys. Rev. Lett., **106**, 015301 (2011).

Bound electron *g*-factor measurement by double-resonance spectroscopy on a fine-structure transition

D. Lindenfels[1,2,3], W. Quint[1,2], M. Vogel[1,4], and G. Birkl[4]

[1] *GSI Helmholtzzentrum für Schwerionenforschung, 64291 Darmstadt, Germany*
[2] *Physikalisches Institut, Universität Heidelberg, 69117, Germany*
[3] *MPI für Kernphysik, 69117 Heidelberg, Germany*
[4] *Institut für Angewandte Physik, TU Darmstadt, 64289 Darmstadt, Germany*
Corresponding Author: d.vonLindenfels@gsi.de

Precise determination of bound-electron g-factors in highly charged ions provides stringent tests for state-of-the-art theoretical calculations. The scope reaches from relativistic electron correlation effects on the one hand to bound-state QED terms on the other. Besides, the investigation can contribute to the determination of the fine-structure constant α [1]. In a first approach with boron-like ions with spinless nuclei (e.g., $^{40}Ar^{13+}$ and $^{40}Ca^{15+}$), we will excite the $2\,^2P_{1/2} - 2\,^2P_{3/2}$ fine-structure transition with laser radiation and probe microwave transitions between Zeeman sub-levels in the magnetic field of a Penning trap. From this laser-microwave double-resonance technique the g-factor can be determined on a ppb level of accuracy.

We have prepared a cryogenic trap assembly with a creation trap and a spectroscopy trap—a half-open compensated cylindrical Penning trap. Argon gas will be injected through a remotely controlled valve, working at cryogenic temperature and in the field of a superconducting magnet [2]. Ions are produced by electron impact ionization with electrons from a field emission source. We have developed and tested the electron source, the cryogenic gas valve, and an optical setup to detect the low fluorescence signal of the magnetic dipole transition.

In the future, the trap will be connected to the HITRAP facility at GSI, and the method will be applied to hyperfine-structure transitions of hydrogen-like heavy ions in order to measure electronic and nuclear magnetic moments [3]. The contribution presents techniques and the current status of the experiment.

References

[1] V. M. Shabaev *et al.*, Phys. Rev. Lett. **96**, 253002 (2006).
[2] D. Lindenfels *et al.*, Can. J. Phys. **89**, 79 (2011).
[3] W. Quint *et al.*, Phys. Rev. A **78**, 032517 (2008).

Probing ultracold fermions in optical lattices

J. S. Krauser[1], S. Götze[1], J. Heinze[1], B. Hundt[1], N. Fläschner[1], D.–S. Lühmann[1], C. Becker[1], and K. Sengstock[1]

[1] *Institut für Laserphysik, Universität Hamburg, 22761 Hamburg, Germany*
Corresponding Author: jkrauser@physnet.uni-hamburg.de

CT

The periodic potential in crystals experienced by electrons gives rise to many important phenomena in solid-state physics. Ultracold fermions in optical lattices are particularly well suited to simulate such a system due to fully tunable lattice and atomic interaction parameters: From weak to strong lattices, conductive and insulating phases can be realized.

We present a fully momentum-resolved spectroscopy method which is sensitive to both, form and filling of the different bands. In our setup we prepare an ultracold mixture of ^{87}Rb and ^{40}K in an optical lattice. We modulate the lattice depth thereby creating particle-hole excitations. Subsequently we map the resulting quasimomentum distribution onto real momenta. This gives access to the full band structure, the tunneling energy, and the density of states as shown in Fig. 1. Adding bosons to our system we observe an interaction shift which distorts the single particle band structure depending on the occupation number of bosons. Furthermore, we investigate dynamics of particles in higher orbitals and holes within the first Brillouin zone.

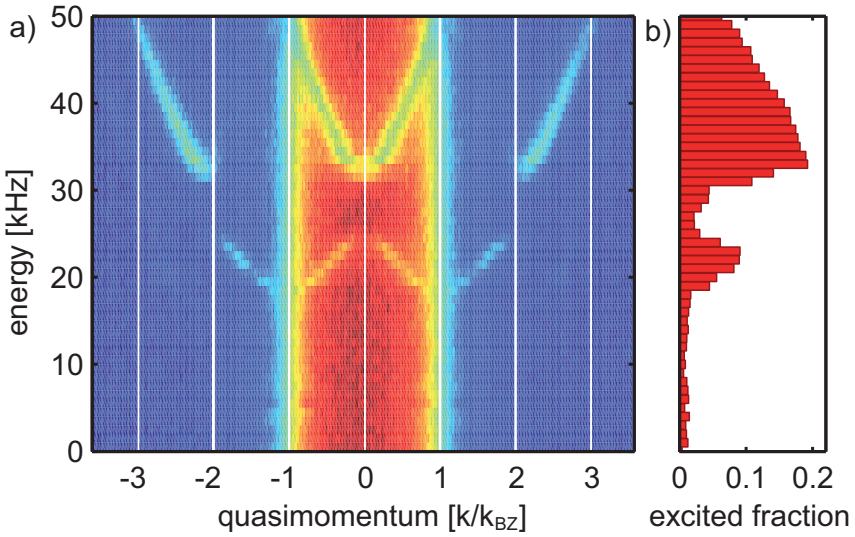

Figure 1: *Spectrum of fermions in an optical lattice: a) The momentum distribution and b) the density of states for different modulation frequencies are shown at a lattice depth of* 8 E_r.

The g-factor of hydrogen-like silicon $^{28}Si^{13+}$

A. Wagner[1], K. Blaum[1], B. Schabinger[1], S. Sturm[1], J. Zatorski[1], Z. Harman[1], C. H. Keitel[1], W. Quint[2], and G. Werth[3]

[1] *MPI für Kernphysik, D-69117 Heidelberg, Germany*
[2] *GSI Darmstadt, D-64291 Darmstadt, Germany*
[3] *Institut für Physik, Johannes Gutenberg-Universität, D-55099 Mainz, Germany*
Corresponding Author: ankewag@uni-mainz.de

The g-factor of the electron bound in hydrogen-like $^{28}Si^{13+}$ has been experimentally determined with a precision of $\delta g/g \approx 5 \times 10^{-10}$, which is the most stringent test of bound-state quantum electrodynamical (BS-QED) calculations in high-electric fields up to date [1]. In comparison to the g-factor measurements of carbon and oxygen [2,3], not only the nuclear charge but also the experimental accuracy have been increased resulting in a higher sensitivity towards the BS-QED corrections.

The measurement has been performed with a single $^{28}Si^{13+}$ ion in a cylindrical Penning trap system [4]. To determine the g-factor, the free cyclotron frequency (ν_c) and the Larmor spin-precession frequency (ν_L) have to be measured. The first one can be obtained by measuring the three eigenfrequencies of the ion and using the invariance theorem [5]. To reach the required precision, a first Penning trap with a very homogeneous magnetic field is required. A second Penning trap is used to determine the spin orientation with the continuous Stern-Gerlach effect [6]. Here a magnetic bottle is produced by a ferromagnetic ring. Due to the interaction of the ion's magnetic moment with the magnetic bottle, a spin-flip can be detected by a very small frequency difference ($\Delta\nu_z = 240\,\mathrm{mHz}$) in the axial frequency ($\nu_z = 420\,\mathrm{kHz}$). Therefore, a very stable axial oscillation frequency is necessary. To induce spin-flips, microwaves near the Larmor frequency are irradiated into the trap. The frequency is scanned and the particular spin-flip rate is measured resulting in a resonance curve from which the Larmor frequency can be extracted. Having measured the frequency ratio $\Gamma = \nu_L/\nu_c$ and knowing the charge-to-mass-ratio of the electron (e/m_e) and the ion (q_{ion}/m_{ion}) from literature the g-factor can be determined via

$$g = 2 \cdot \Gamma \cdot \frac{q_{ion}}{m_{ion}} \cdot \frac{m_e}{e}. \quad (1)$$

The experimentally obtained value with a relative uncertainty on the level of 5×10^{-10}, which is mainly dominated by the uncertainty in the electron mass, is in excellent agreement with the theoretically calculated value [1].

The measurement process and the obtained results are presented.

References

[1] S. Sturm *et al.*, in preparation.
[2] H. Häffner *et al.*, Phys. Rev. Lett **85**, 5308 (2000).
[3] J. Verdu *et al.*, Phys. Rev. Lett. **92**, 093002 (2004).
[4] S. Sturm *et al.*, J. Phys. B **42**, 154021 (2010).
[5] L. Brown, and G. Gabrielse, Phys. Rev. A **25**, 2423 (1982).
[6] H. G. Dehmelt *et al.*, Proc. Natl. Acad. Sci. USA **83**, 2291 (1986).

Scattering of ultracold atoms by an absorbing nanowire

M. Fink[1], J. Eiglsperger[1,2], J. Madroñero[1], and H. Friedrich[1]

[1] *Physik Department, Technische Universität München, D-85747 Garching, Germany*
[2] *Institut für Theoretische Physik, Universität Regensburg, D-93040 Regensburg, Germany*
Corresponding Author: finkm@ph.tum.de

In view of the intense attention currently given to systems involving nanotubes at very low temperatures, we study the fundamental process of scattering an ultracold atom by an infinite cylindrical conducting wire [1]. This is the first calculation of atom-wire scattering, which is based on a theoretically founded potential [2] and on the two-dimensional nature of the problem [3,4].

The near-threshold behavior of all scattering properties can be described with a complex scattering length a. We study the dependence of this scattering length on the properties of the atom-wire system, which can be characterized by a dimensionless ratio R/β where R is the radius of the wire and β is a characteristic length determined only by the properties of the atom. We numerically calculated the scattering length a as a function of the dimensionless ratio R/β. The results of this calculation are shown in Fig. 1 (solid line).

Furthermore we discuss the scattering of atoms by a wire in context of matter-wave diffraction. Therefore we compare our results to the diffraction of electromagnetic waves by a wire.

In Fig. 1 the dashed line shows the scattering length describing the near threshold region for electromagnetic scattering. We can identify an *electromagnetic limit* in atom-wire scattering for $R/\beta \gg 1$, which means large radii or lightweight atoms and an *non-electromagnetic* limit in the case of $R/\beta \ll 1$, which means small radii or heavy atoms.

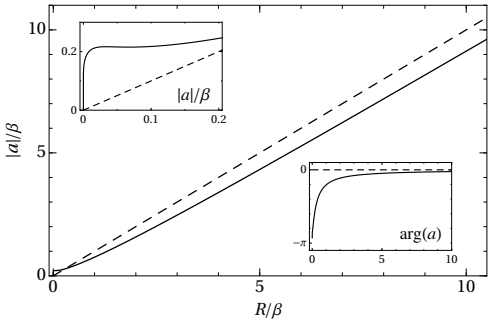

Figure 1: *Scattering length a as a function of the dimensionless ratio R/β for atom-wire scattering (solid line) and for the diffraction of light (dashed line)*

Considering realistic systems, both limits are accessible for experimental setups. For different atoms like H, He, Na or Rb and wire radii ranging form several nanometers up to several micrometers, the ratio R/β varies from 10^{-5} up to 10.

This work contributes to the understanding of fundamental properties of the interaction of atoms with nanostructures and delivers insight into the diffraction of matter-waves in contrast to the well-known diffraction of electromagnetic waves.

References

[1] M. Fink, *et al.*, Phys. Rev. A **81**, 062714 (2010).
[2] C. Eberlein, and R. Zietal, Phys. Rev. A **75**, 032516 (2007).
[3] B. Verhaar, *et al.*, J. Phys. A **17**, 595 (1984).
[4] F. Arnecke, H. Friedrich, and P. Raab, Phys. Rev. A **78**, 052711 (2008).

High-precision mass measurements of stored and cooled highly charged ions for fundamental studies at PENTATRAP

J. Repp[1], Ch. Böhm[1], A. Dörr[1], S. Eliseev[1], M. Goncharov[1], Yu. N. Novikov[2,3], C. Roux[1], S. Sturm[1,4], S. Ulmer[1,4], and K. Blaum[1]

[1] *Max-Planck-Institut für Kernphysik, D-69117 Heidelberg, Germany*
[2] *Petersburg Nuclear Physics Institute, 188300 Gatchina, Russia*
[3] *Extreme Matter Institute, Helmholtz Gemeinschaft, Planckstr.1, 64291 Darmstadt, Germany*
[4] *Johannes Gutenberg-Universität Mainz, Institut für Physik, D-55099 Mainz, Germany*
Corresponding Author: Julia.Repp@mpi-hd.mpg.de

The novel cryogenic mass spectrometer PENTATRAP is being developed at the Max-Planck-Institut für Kernphysik in Heidelberg [1]. Ions of interest are highly charged stable and long-lived nuclides with masses up to uranium. A commercial EBIT and the Heidelberg EBIT [2] will produce the ions of interest. In perspective it is planned to move the PENTATRAP experiment or a duplication to the HITRAP facility to get access to short-lived nuclides [3]. PENTATRAP aims for an accuracy of few parts in 10^{12} for mass ratios of mass doublets. Main features of the five-trap facility are the simultaneous measurements of frequencies, a continuous monitoring of magnetic field fluctuations, a fast ion exchange and highly sensitive cryogenic non-destructive detection systems. The mass of a single highly charged ion with charge-to-mass ratio q/m is determined via the cyclotron frequency $\nu_c = 1/(2\pi) \cdot q/m \cdot B$ of the ion in a magnetic field B.

Mass ratios with this unprecedented accuracy are of interest for tests of fundamental physics. They will contribute to Q-value determinations of relevant β-processes for neutrino physics. Radioactive processes of interest are, e.g., the electron capture process of ^{163}Ho [4] and the β decay of ^{187}Re [5]. Together with cryogenic microcalorimetry the neutrino mass will be probed at a sub-eV level. Furthermore, the mass ratios contribute to stringent tests of quantum electrodynamics in the regime of extreme fields and a test of special relativity [6-8].

This contribution covers the planned fundamental studies with PENTATRAP. Moreover, the experimental setup and the present status of the experiment will be presented.

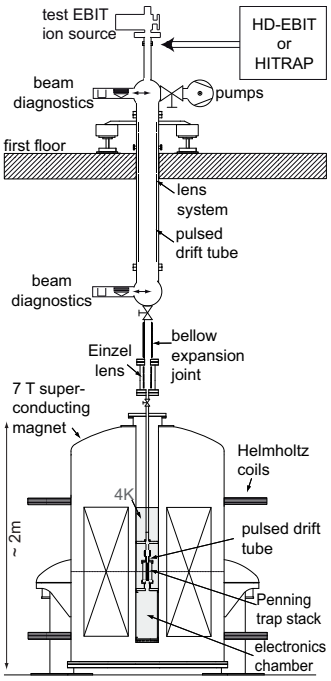

Figure 1: *Experimental setup of the PENTATRAP facility.*

References

[1] K. Blaum, Yu. Novikov, and G. Werth, Cont. Phys. **51**, 149 (2010).
[2] J. R. Crespo López-Urrutia *et al.*, Rev. Sci. Instrum. **75**, 1560 (2004).
[3] J. Kluge *et al.*, Adv. Quantum. Chem. **53**, 83 (2008).
[4] A. De Rújula, M. Lusignoli, Phys. Rev. Lett. B **118**, 429 (1982).
[5] E. Ferri *et al.*, AIP Conference Proceedings **1185** (2009).
[6] V. Shabaev *et al.*, Int. J. Mass Spectrom. **251**, 109 (2006).
[7] T. Stöhlker *et al.*, Hyperfine Int. **172**, 135 (2006).
[8] S. Rainville *et al.*, Nature **438**, 1096 (2005).

Imaging of microwave fields using ultracold atoms

P. Böhi[1], M. F. Riedel[1], and P. Treutlein[1]

[1] *Department of Physics, University of Basel, 4056 Basel, Switzerland*
Corresponding Author: pascal.boehi@unibas.ch

CT

Clouds of ultracold atoms are used as highly sensitive, tunable and non-invasive probes for microwave field imaging with micrometer spatial resolution. The microwave magnetic field drives Rabi oscillations on atomic hyperfine transitions which are read out using state-selective absorption imaging. It is possible to fully reconstruct the microwave magnetic field, including the microwave phase distribution. We use this method to determine the microwave near-field distribution around a coplanar waveguide which is integrated on an atom chip. We compare the extracted microwave field to simulations to deduce the microwave current distribution on the waveguide and induced currents in on-chip wires nearby.

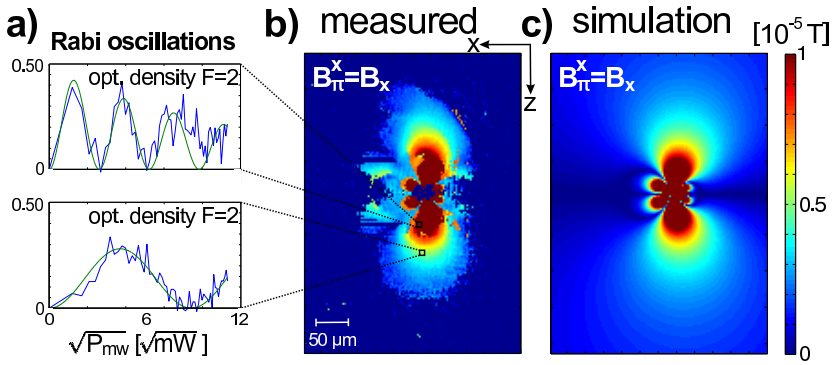

Figure 1: *Comparison of a measured microwave magnetic near-field polarization component to a simulation. The insets show Rabi oscillations at two exemplary pixels.*

References

[1] P. Böhi *et al.*, Appl. Phys. Lett. **97**, 051101 (2010).

First mass measurements with THe-Trap

S. Streubel[1], C. Diehl[1], M. Höcker[1], J. Ketter[1], D. B. Pinegar[1], M. Tremer[1], R. S. Van Dyck, Jr.[2], and K. Blaum[1]

[1] *Max-Planck-Institut für Kernphysik, Saupfercheckweg 1, 69117 Heidelberg, Germany*
[2] *Department of Physics, University of Washington, Seattle, WA 98195-1560, USA*
Corresponding Author: sebastian.streubel@mpi-hd.mpg.de

THe-Trap is a Penning trap mass spectrometer to measure the mass-ratio, and hence the Q-value, of tritium (^{3}H) to its daughter nuclide helium (^{3}He) with an uncertainty of 10^{-11}, which would improve the to date best value by a factor of 40 [1]. This is of relevance for the KArlsruhe TRItium Neutrino experiment (KATRIN) [2], which aims to measure the electron anti-neutrino mass with a sensitivity of 0.2 eV/c^2 (95% c.l.). KATRIN measures the shape of the endpoint region of the β-decay of ^{3}H. The endpoint with a hypothetical zero mass neutrino can be determined by the mass-ratio. This provides an important systematic check for the KATRIN data.

THe-Trap [3] was constructed in Seattle and transferred to Heidelberg in 2008. A major difference compared to its predecessor [4] is the double-Penning trap assembly [5]. This allows storing single ^{3}H and ^{3}He ions simultaneously in separate traps. The mass-ratio measurement has to be carried out in the same magnetic field, so it is planned to exchange the ions between the traps. Compared to a single trap, where reloading of the trap is necessary to switch between the ions, the time between measurements is reduced with the double-trap technique from several hours to minutes. Hence the systematic uncertainty, due to unknown magnetic field fluctuations between the measurements, is decreased. Another new feature is the external loading of the trap by a Penning ion source. This reduces the contamination of the trap surfaces with tritium, which has been observed in a former experiment. The β-decay electrons of tritium ionized the residual gas in the trap, which created undesirable contaminant ions.

At MPIK Heidelberg a dedicated tritium laboratory was installed. In that the ambient temperature is stabilized to 0.2K and the vibration of the cryostat to below 1 μm/s. Beside other environmental parameters, the magnetic field is monitored and stabilized. This is achieved by stabilizing the pressure and the level of the liquid helium surrounding the traps. The result is a stable temperature of the materials and hence, reduced magnetic field fluctuations due to the temperature dependence of the susceptibility. External field fluctuations are measured by a fluxgate magnetometer and a pair of Helmholtz coils surrounding the magnet compensates them [6].

The experiment has been commissioned and first measurements with ions could be performed. A precision of the modified cyclotron frequency of a few parts in 10^{-11} could be reached. The first measurement of a mass-ratio from oxygen to carbon yielded an uncertainty of a few part per billion. The current status of the experiment will be presented.

References

[1] Sz. Nagy *et al.*, Europhys. Lett. **74**, 404–410 (2006).
[2] E. W. Otten, J. Bonn and C. Weinheimer, Int. J. Mass Spectrom. **251** 173–178 (2006).
[3] C. Diehl *et al.*, Hyperf. Interact., accepted (2011).
[4] R. S. Van Dyck, S. L. Zafonte and P. B. Schwinberg, Hyperf. Interact. **132** 163–175 (2001).
[5] D. B. Pinegar, S. L. Zafonte and R. S. Van Dyck, Jr., Hyperf. Interact. **174** 47–53 (2007).
[6] R. S. Van Dyck, Jr. *et al.*, Rev. Sci. Instru. **70**, 1665–1671 (1999).

Sub-Doppler laser cooling and magnetic trapping of thulium atoms

D. Sukachev[1,2], A. Sokolov[1,2], A. Akimov[1,2], N. Kolachevsky[1,2], and V. Sorokin[1,2]

[1] *P. N. Lebedev Physical Institute of the Russian Academy of Sciences, Moscow, Russia*
[2] *Moscow Institute of Physics and Technologies, Moscow Region, Russia*

Corresponding Author: sukachev@gmail.com

We have observed effective sub-Doppler laser cooling of thulium atoms within a magneto-optical trap [1,2]. Generally, sub-Doppler cooling in MOT is prevented by the presence of a magnetic field [3,4]. In case of thulium and other lanthanides the effect of the magnetic field is eliminated due to minimal divergence of Lande-g factors of upper and lower levels of cooling transition [3,4].

The temperature was measured by ballistic expansion of a cold atoms cloud after switching off all laser beams and magnetic fields. The lowest temperature was $25(5)\mu$K with number of atoms of 3×10^6.

Comparing expansion of the atoms cloud in case when magnetic fields were switched off and when they were not (see Fig. 1), we have detected magnetically trapped (MT) atoms. Because of the unfilled $4f$ electron shell the Tm ground state (as well as Dy [5] and Er [6]) possesses a relatively big magnetic momentum of $4\mu_B$ (μ_B is the Bohr magneton) which can interact with gradient magnetic field of the MOT.

About 10^5 atoms were captured in MT. The temperature determined by space profile of the trapped atoms [6] was $40(10)\mu$K. Some evidence of evaporative cooling was observed. The lifetime of MT was about 0.5 s and was limited by inelastic $s-l$ collisions.

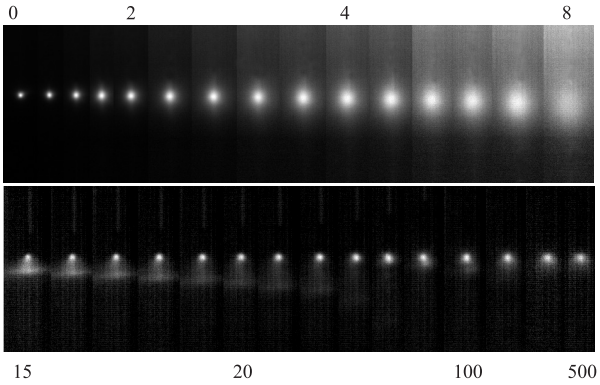

Figure 1: *Upper. The ballistic expansion of the cloud after switching off the laser beams and magnetic field. Numbers denote time of expansion in ms. Lower. Expansion of the atomic cloud after switching off laser beams, magnetic field being on. The bright points are magnetically trapped atoms.*

References

[1] D. Sukachev *et al.*, Phys. Rev. A **82**, 011405 (2010).
[2] D. Sukachev *et al.*, JETP Letters **92**, 772 (2010).
[3] M. Wallhout *et al.*, J. Opt. Soc. Am. B **9**, 1997–2007 (1992).
[4] M. Wallhout, U. Sterr, and S. L. Rolston, Phys. Rev. A **54**, 2275 (1996).
[5] M. Lu, S. H. Youn, and B. L. Lev, Phys. Rev. Lett. **104**, 063001 (2010).
[6] A. J. Berglund, S. A Lee, and J. J. McClelland, Phys. Rev. A **76**, 053418 (2007).

Spectroscopy of alkali metal atoms in dense supercritical helium at low temperature

P. Moroshkin[1], V. Lebedev[1], and A. Weis[1]

[1] *Department of Physics, University of Fribourg, CH-1700 Fribourg, Switzerland*
Corresponding Author: Peter.Moroshkin@unifr.ch

Resonance lines of alkali-metal atoms interacting with rare-gas atoms represent model systems that have been very well studied experimentally and theoretically. Two limiting cases are well known: 1) line broadening due to binary or many-body atomic collisions in the gas phase [1], and 2) a description in terms of the so-called atomic bubble model [2] for metal atoms embedded in superfluid and solid helium cryomatrices. In the gas phase the motion of rare gas atoms is totally uncorrelated even at high densities and their interactions with the alkali atom can be treated independently. On the other hand, in the atomic bubble the motion of the He atoms surrounding the impurity is strongly correlated and is described in terms of collective modes, such as phonons or bubble interface oscillations. Here we address the crossover between these two regimes that has not been studied experimentally nor theoretically so far.

In our experiments, the alkali (Cs, Rb) atoms are introduced into pressurized liquid or solid He (T = 1.5–4K, p = 10–40 bar) by means of laser ablation with a pulsed Nd:YAG laser. The same laser locally heats the helium sample. We monitor the laser-induced fluorescence excited either by the ablation laser pulse, or by a delayed pulse of a much weaker diode laser that does not affect the temperature of the sample and that is resonant with one of the atomic lines.

The fluorescence lineshape of the alkali atom in the undisturbed atomic bubble is nearly Gaussian with a spectral width and shift that increases linearly with helium density [2]. The fast local heating is accompanied by an isobaric expansion of the supercritical fluid in the laser focus and leads to a breakdown of the atomic bubble model. At moderate laser power the lineshape remains Gaussian, although its linewidth increases by ≈20% and the lineshift decreases by ≈50% with respect to undisturbed liquid He matrices. This suggests a quasistatic broadening mechanism due to atomic many-body collisions. At higher laser power the lineshift further decreases and the lineshape transforms into a Lorentzian centered near the free atomic wavelength. This suggests an interpretation in terms of the impact broadening mechanism.

Using alkali-helium interaction potentials from the literature, we calculate the fluorescence lineshapes in the impact and quasistatic approximations for a broad range of helium densities and temperatures and compare them with the experimental spectra. This allows us to estimate the temperature in the laser focus.

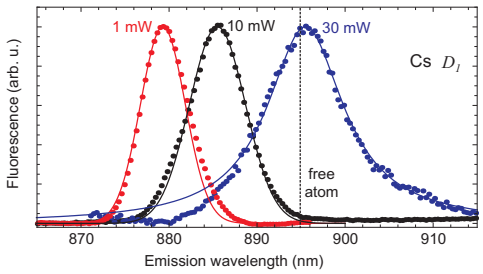

Figure 1: *Typical lineshapes of Cs D_1 transition in dense fluid He at different laser powers. p = 33 bar, local temperature increases with the laser power.*

Work funded by the Swiss National Science Foundation, grant No. 200020–129831.

References

[1] N. Allard, and J. Kielkopf, Rev. Mod. Phys. **54**, 1103–1182 (1982).
[2] T. Kinoshita *et al.*, Phys. Rev. A **52**, 2707–2716. (1995)

Temporal evolution of ultracold polar molecules in a circularly polarized microwave field

A. Avdeenkov[1], T. Kirova[1]

[1] *National Institute for Theoretical Physics (NITheP), Stellenbosch 7600, South Africa*
Corresponding Author: avdeenkov@sun.ac.za

The cooling and trapping of atoms, which is now easily achieved in numerous labs, has recently moved in the direction of the cooling and trapping of polar molecules. Possessing a permanent dipole moment and interacting via long range dipole-dipole (DD) forces, ultracold polar molecules offer new prospects of exciting physics in the fields of controlled ultracold chemistry, quantum computing, and fundamental symmetries tests [1]. A microwave trap for polar molecules was suggested in [2]. It has the advantages of being able to trap molecules in their absolute ground state, as well as having a large enough depth and volume to allow easy loading. In addition, the alignment of molecules by the trapping field, as well as the strong DD interactions between them, leads to a large elastic collisions cross-section which facilitates evaporative cooling [3].

In our work we analyze the temporal evolution of the ultracold molecular population in a microwave (mw) field with a circular polarization. We treat polar molecules as rigid rotors with a permanent dipole moment.The Hamiltonian of two ground state polar molecules in the presence of the mw field is constructed in the basis set of two-molecule bare states. We derive and solve the equation of motion for two-molecule dressed states.

Our aim is to study the effect of different mw field parameters and molecular gas characteristics on the dynamics of all states. As the temperature is very low a molecular gas behaves rather adiabatically. We have tested several ranges of the intermolecular distance R, which correspond to various densities of a molecular gas. Our calculations show that the behavior of populations dynamics is defined by the ratio of the mw field Rabi frequency Ω and the magnitude of the DD interaction V_{DD}. At large enough distances, V_{DD} is too weak and we have the case of two independent molecules dressed by the mw field, which is characterized by the typical Rabi oscillations in the bare states populations and no change in time in the dressed states populations. As the density of the molecular gas increases, the DD interaction becomes significant and causes beatings in the evolution of the bare states, while the dressed states start to slightly oscillate. At a given distance, V_{DD} becomes comparable to Ω and the dressed states oscillate rapidly, while beating and oscillations occur in the bare states time-development.

We further analyze the behavior of the populations as a function of the mw field detuning for different intermolecular distances. A three-peak structure appears in the populations of the bare and dressed states. Upon calculating the eigenvalues of the system, we associate the origin of these peaks with the existence of three avoided crossings in the eigenvalue spectrum. The latter occurs at a certain value of the DD interaction when it becomes equal to the absolute value of the mw field detuning. We found that only the "exchange" channel, which is caused by the exchange of ground and first excited rotational states [4], is responsible for the appearance of these peaks. At small enough distances inelastic processes play a larger role and cause shifts of peaks into the region of positive detunings so that all peaks may only exist at positive detunings. Our analysis demonstrates possible control and manipulation of molecular population in dependence on the gas density and mw field parameters.

References

[1] R. V. Krems, W. C. Stwalley, and B. Friedrich, eds., *Cold Molecules: Theory, Experiment, Application,* (Boca Raton, CRC Press, 2009).
[2] D. DeMille, D. R. Glenn, and J. Petricka, Euro. Phys. J. D **31**, 375–384 (2004).
[3] A. V. Avdeenkov, New J. Phys. **11**, 055016-1–055016-10 (2009).
[4] A. V. Avdeenkov, ICONO 2010: Proceedings of the SPIE–2010; 799314.

The proton radius puzzle

A. Antognini[1,2]
For the CREMA collaboration
[1] *Institute for particle physics, ETH, Zurich, Switzerland*
[2] *Max Planck Institut für Quantenoptik, Garching, Germany*
Corresponding Author: aldo@phys.ethz.ch

At the Paul Scherrer Institute, Switzerland, the CREMA collaboration [1] has measured the $2S - 2P$ transition frequency (Lamb shift) in muonic hydrogen (μp) with 15 ppm precision by means of laser spectroscopy [2]. From this measurement the rms charge radius of the proton was determined.

The new proton radius value $r_p = 0.84184(67)$ fm is 10 times more precise than previously obtained. However, it disagrees by 4 standard deviations from the value extracted from hydrogen spectroscopy and 5 standard deviations from electron-proton scattering data.

The origin of the discrepancies is not yet known. It may come from theory of the muonic hydrogen energy levels (used to deduce our new value), from problems in hydrogen spectroscopy experiments or hydrogen energy level theory (both used to deduce the "H" value), from unexpected proton shape, or may arise from uncalculated or otherwise new effects.

Experimental setup, measurements, results and future perspectives will be presented. Additionally, the key issues and excluded explanations regarding the observed discrepancy will be discussed. The discrepancy simply raises new questions in the muonic sector, in bound-state QED and around the proton structure, holding the potential for new insights.

References

[1] https://muhy.web.psi.ch/wiki/index.php/Main/HomePage
[2] R. Pohl *et al.*, Nature, **466** 213–216 (2010).

Single ion recycling reaction experiments

A. K. Hansen[1], M. A. Sørensen[1], P. F. Staanum[1], and M. Drewsen[1]

[1] *Department of Physics and Astronomy, Aarhus University, 8000 Aarhus, Denmark*
Corresponding Author: anh@phys.au.dk

The interest to experiment with single ions originates partly from a wish to carry out research with well-characterized species, partly from the urge to investigate ions that are extremely difficult to produce. With respect to the first category, single laser cooled atomic ions have, e.g., for more than a decade now been the most successful quantum logic bits in the quest for a practical quantum computer [1], and internal state prepared sympathetically cooled molecular ions have recently become available [2–4] for coherent manipulation with light fields or other molecular physics investigations. In the latter category one finds such exotic entities as transactinide ions. Though transactinide elements, ranging from being Rf ($Z = 104$) to the currently heaviest element $Z = 118$, have been synthesized, their electronic structures and chemistry is still only very rudimentarily understood [5,6], in part due to the extremely low production rates of sometimes only a few detected species per week. However, could the same ion be used repeatedly in, e.g., reaction experiments, quite detailed investigations could be carried out despite these low production rates.

Here, we present what we call a recycling reaction experiment in which the same two laser-cooled and trapped $^{48}Ca^+$ ions were repeatedly made reacting with HD molecules through regeneration by means of UV photodissociation. The two possible reaction products $^{48}CaH^+$ and $^{48}CaD^+$ were identified through non-destructive sympathetically cooled single ion mass spectrometry (SCSI-MS) [7,8]. From a total of 87 recorded reaction events through an 8 hour experimental campaign, the relative formation of $^{48}CaD^+$ was found to be 0.56 ± 0.05, in good agreement with a much longer series of reaction experiments using the most abundant isotope, ^{40}Ca [9]. In the future, we envision the presented method being used in the studies of the chemistry of the transactinides, as well as of rare isotopes of more common elements.

References

[1] D. Leibfried, R. Blatt, C. Monroe, and D. Wineland, Rev. Mod. Phys **75**, 281–324 (2003).
[2] P. F. Staanum *et al.*, Nature Physics **6**, 271–274 (2010).
[3] T. Schneider *et al.*, Nature Physics **6**, 275–278 (2010).
[4] X. Tong, A. H. Winney, and S. Willitsch, Phys. Rev. Lett. **105**, 143001 (2010).
[5] M. Schädel, *The Chemistry of Superheavy Elements* (Kluwers Academic Publishers, Dordrect, The Netherlands, 2003).
[6] R. Eichler *et al.*, Nature **447**, 72–75 (2007).
[7] M. Drewsen *et al.*, Phys. Rev. Lett. **93**, 243201+ (2004).
[8] R. E. March, and J. F. J. Todd, *Practical Aspects of Trapped Ion Mass Spectrometry* (CRC Press, Taylor&Francis Group, Boca Raton, London, New York, 2010).
[9] A. K. Hansen, M. A. Sørensen, P. F. Staanum, and M. Drewsen, unpublished.

QED theory of the nuclear magnetic shielding in hydrogen-like ions

V. A. Yerokhin[1,2,3], Z. Harman[1], and C. H. Keitel[1]

[1] *Max Planck Institute for Nuclear Physics, Saupfercheckweg 1, D-69117 Heidelberg, Germany*
[2] *University of Heidelberg, Philosophenweg 12, D-69120 Heidelberg, Germany*
[3] *Center for Advanced Studies, St. Petersburg State Polytechnical University, Polytekhnicheskaya 29, St. Petersburg 195251, Russia*

Corresponding Author: yerokhin@pcqnt1.phys.spbu.ru

Recent developments in the Penning trap experimental technique greatly improved the accuracy of the determination of the bound-electron g factor in hydrogen-like ions [1] and triggered a number of sophisticated quantum electrodynamics (QED) calculations [2,3]. The comparison between experimental and theoretical results has not only constituted a very precise test of the bound-state QED theory but also led to the most accurate determination of the electron mass [4]. An extension of the measurements to the ions with a non-zero spin nucleus are expected in the near future. This will lead to an accurate test of the magnetic sector of QED as well as to the most precise determination of the nuclear magnetic moments.

Theory of the g factor of an atom with a non-zero spin nucleus can be conveniently parametrized in terms of the nuclear magnetic shielding constant σ, which describes the effective reduction of the coupling of the nuclear magnetic moment $\vec{\mu}$ to an external magnetic field $\vec{B}$, caused by the bound electron(s),

$$H = -\vec{\mu} \cdot \vec{B}\,(1-\sigma)\,.$$

In this work, we present *ab initio* calculations of the nuclear magnetic shielding for the ground state of hydrogen-like ions that include relativistic, finite nuclear size, QED, recoil, and nuclear magnetization distribution effects. The QED self-energy and vacuum-polarization corrections are treated rigorously and calculated to all orders in the binding nuclear strength parameter $Z\alpha$ (where Z is the nuclear charge and α is the finite structure constant). The results obtained significantly improve the theory of the g factor of hydrogen-like ions with a non-zero nuclear spin.

References

[1] H. Häffner *et al.*, Phys. Rev. Lett. **85**, 5308 (2000).
[2] V. A. Yerokhin and P. Indelicato and V. M. Shabaev, Phys. Rev. Lett. **89**, 143001 (2002).
[3] K. Pachucki, U. D. Jentschura, and V. A. Yerokhin, Phys. Rev. Lett. **93**, 150401 (2004).
[4] P. J. Mohr and B. N. Taylor, Rev. Mod. Phys. **7**, 1 (2005).

Quantum simulation of frustrated classical magnetism in triangular optical lattices

R. Le Targat[1], J. Struck[1], C. Ölschläger[1], P. Soltan–Panahi[1], A. Eckardt[2], M. Lewenstein[2], P. Windpassinger[1], and K. Sengstock[1]

[1] *Institute for Laser Physics, University of Hamburg, 22761 Hamburg, Germany*
[2] *ICFO — Institut de Ciències Fotòniques, E-08860 Castelldefels, Spain*
Corresponding Author: rodolphe.letargat@physnet.uni-hamburg.de

Magnetism plays a fundamental role in modern technology, e.g., in storage devices, and rich prospects like spintronics or high temperature superconductors are drawing a considerable attention. Nevertheless, the dynamics of many-body spin systems is still far from being well understood. In the case of geometrically frustrated systems, pairwise interactions are competing and the spins have to compromise. This gives rise to exciting properties but their study is challenging both theoretically and experimentally. As an alternative to condensed matter systems, ultracold atoms in optical lattices have proven to be a very controllable tool to emulate solid state problems.

We present the first realization of a quantum simulator of frustrated classical magnetism with ultracold bosons. By applying a global elliptical forcing [1] to a triangular optical lattice [2], we can tailor the couplings between adjacent sites in different directions. We control in particular the sign of these coefficients, thus allowing for ferromagnetic and antiferromagnetic schemes at will. We therefore faithfully simulate the magnetic interactions of the spin model known as xy model.

We have accessed all possible phases and identified them by means of their distinct quasi-momentum distribution (three of the six relevant cases are shown in Fig. 1). As for the spin frustrated 'spiral' configuration, we successfully observed the spontaneous symmetry breaking between the two ground states of the system. These findings open the route towards highly debated phases like spin liquids [3] and the study of quantum phase transitions.

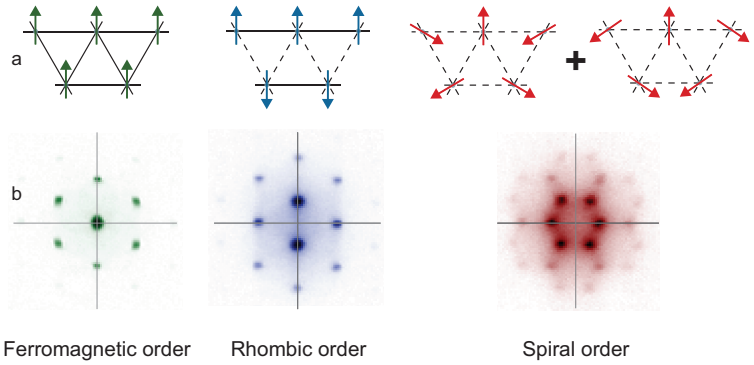

Figure 1: *(a) Three spin configurations with ferromagnetic (solid lines) or antiferromagnetic (dashed lines) couplings. (b) Observed corresponding momentum distributions*

References

[1] A. Eckardt *et al.*, EPL **89**, 10010 (2010).
[2] C. Becker *et al.*, New J. Phys. **12**, 065025 (2010).
[3] L. Balents, Nature **464**, 199–208 (2010).

Using microwave and submillimeter molecular transitions to search for variation of the fundamental constants

M. G. Kozlov[1], S. G. Porsev[1], S. A. Levshakov[2], and A. V. Lapinov[3]

[1] *Petersburg Nuclear Physics Institute, Gatchina, Russia*
[2] *Ioffe Physical-Technical Institute, St. Petersburg, Russia*
[3] *Institute of Applied Physics, Nizhni Novgorod, Russia*

Corresponding Author: mgk@mf1309.spb.edu

The search for the possible variation of fundamental constants is a poor man's way to look for physics beyond the Standard Model. There are two main approaches to such studies. First is to make laboratory measurements with different atomic and molecular clocks in order to look for local variations on the time scale of the order of a year. Second is to compare laboratory measurements with astrophysical observations, where one can study variations on a much bigger space and time scale up to 10 billion years. Here we focus on the second approach.

Molecular spectra depend on two fundamental constants: the fine structure constant α and the electron-to-proton mass ratio μ. In astrophysics all lines are Doppler broadened, $\Gamma/\omega = \Delta V/c$, where ΔV is velocity variance. Because of that, in the search for the possible variations of α and μ, it is desirable to use spectral lines with maximal dimensionless sensitivity coefficients Q_α and Q_μ:

$$\frac{\Delta\omega}{\omega} = Q_\alpha \frac{\Delta\alpha}{\alpha} + Q_\mu \frac{\Delta\mu}{\mu}\,. \tag{1}$$

For optical transitions in astrophysically relevant light atoms and molecules both coefficients are small, $|Q_{\alpha,\mu}| \ll 1$. For microwave and submillimeter transitions, on the contrary, Q_μ is typically of the order of unity. Moreover, for the particular transitions either Q_μ, or Q_α, or both can be much larger.

High sensitivity to μ-variation is characteristic for tunneling transitions in molecules. The best known example is 1.2 cm transition in ammonia (NH_3), where $Q_\mu = 4.5$ [1]. This transition was used to place the most stringent limits on μ-variation at intermediate redshifts $z \sim 1$. It is preferable to observe several lines of one species with different sensitivities. This would give better control on possible systematic effects. Unfortunately, there is only one observed ammonia line and one has to use rotational lines of other molecules as a reference. In partly deuterated ammonia there are several observed mixed tunneling-rotational lines, which have different sensitivities, $0.5 \le Q_\mu \le 1.4$ [2]. Similar situation takes place for hydronium (H_3O^+) [3], but sensitivities are much larger, $-3.5 \le Q_\mu \le 6.4$. Even higher sensitivities of both signs occur for mixed tunneling-rotational transitions in methanol (CH_3OH), where tunneling is associated with hindered rotation of the OH group.

Another class of spectra with high sensitivities corresponds to Λ-doublet transitions in diatomic radicals. These transitions are sensitive to both fundamental constants. It is important that for the most astrophysically relevant molecules OH and CH, the sensitivity coefficients Q_α and Q_μ strongly depend on the rotational quantum number J [4].

References

[1] V. V. Flambaum and M. G. Kozlov, Phys. Rev. Lett. **98**, 240801 (2007).
[2] M. G. Kozlov, A. V. Lapinov, and S. A. Levshakov, J. Phys. B, **43**, 074003 (2010).
[3] M. G. Kozlov and S. A. Levshakov, Astrophys. J. **726**, 65 (2011).
[4] M. G. Kozlov, Phys. Rev. A **80**, 022118 (2009).

Ionization of Rb (Cs) atoms and Rb_n (Cs_n) clusters on He droplets

G. Krois[1], M. Theisen[1], F. Lackner[1], and W. E. Ernst[1]

[1] *Institute of Experimental Physics, Graz University of Technology, Petersgasse 16, A-8010 Graz, Austria*

Corresponding Author: wolfgang.ernst@tugraz.at

He droplets (He_N) are an ideal matrix for preparing and investigating clusters in a superfluid environment. Alkali-metal (Ak) atoms are bound very weakly to their surface by Van-der-Waals forces. Here, we present (i) the ionization of single Rb and Cs atoms on the He_N via a REMPI scheme followed by the subsequent immersion of the Rb^+ (Cs^+) into the He_N[1]. In addition, we present (ii) the observation of stable complexes of Rb_n (Cs_n), which are ionized after their formation on He_N[2].

(i) He_N doped with Rb (Cs) atoms are ionized by applying a resonant two-step ionization scheme. Subsequent immersion of Rb (Cs) ions is observed in time-of-flight (TOF) mass spectra. Rb (Cs) atoms are selectively excited either to the $n^2P_{1/2}$ (Rb: $n = 5$, Cs: $n = 6$), where they can remain on the He_N surface [3,4], or to the $n^2P_{3/2}$ state, where they desorb from the He_N. From there they are ionized by a laser pulse. TOF mass spectra of the ionization products reveal that the intermediate population of the $n^2P_{1/2}$ state does not only make the ionization process Ak-monomer selective, but also gives rise to a very high yield of Ak^+–He_N complexes. Ions with masses of up to several thousand amu have been monitored, which can be explained by an immersion of the single alkali-metal ion into the He_N, where most likely a snowball is formed in the center of the He_N.

(ii) The study of small clusters is intended to fill the knowledge gap between single atoms and bulk material. Due to the energy release in the formation process, which is large for low-spin (LS) states, high-spin (HS) states of Ak clusters on He_N are favorably observed, which is in contrast to the abundance in other preparation processes. Until now the prevailing opinion was that stable clusters of the heavy Ak atoms, Rb and Cs on He_N, are limited to 5 and 3 atoms, respectively [5]. Here, we present stable complexes of Rb_n^+ and Cs_n^+ consisting of up to $n = 30$ atoms, with the detection of large Ak being strongly enhanced by one-photon ionization. Our results also suggest that we monitored both HS and LS state clusters created on He_N. The Van-der-Waals bound high-spin Ak clusters should show strong magnetic behavior, while low-spin states are predicted to exhibit metallic characteristics. Ak clusters prepared in these two configurations appear to be ideal candidates for investigating nanosized particles with ferromagnetic or metallic properties.

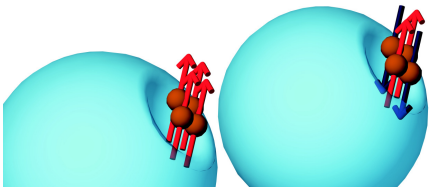

Figure 1: *Schematic of an alkali-metal cluster in high- and low-spin configuration on He_N.*

References

[1] M. Theisen, F. Lackner, W. E. Ernst, Phys. Chem. Chem. Phys. **12**, 14861–14863 (2010).
[2] M. Theisen, F. Lackner, W. E. Ernst, J. Phys. Chem. A (2011) submitted.
[3] G. Auböck *et al.*, Phys. Rev. Lett. **101**, 035301 (2008).
[4] M. Theisen *et al.*, Eur. Phys. J. D **61**, 403–408 (2011).
[5] C. P. Schulz, P. Claas, F. Stienkemeier, Phys. Rev. Lett. **92**, 13401 (2004).

Enhancement of positron annihilation on core electrons

D. G. Green[1], G. F. Gribakin[1]

[1] *Department of Applied Mathematics and Theoretical Physics, Queen's University Belfast, Belfast, BT71NN, Northern Ireland, United Kingdom*

Corresponding Author: dgreen09@qub.ac.uk

Positron annihilation on core electrons is a key process for several experimental techniques (see e.g., [1]). Interpretation of the measured annihilation spectra relies heavily on theoretical input. Specifically, one needs to know the relative probabilities of positron annihilation with inner electrons of various atoms. These are usually calculated using the independent particle model (IPM) with a phenomenological enhancement factor that attempts to account for the important effect of electron-positron correlations.

Starting from a diagrammatic many-body perturbation expansion of the annihilation amplitude [2,3,4], we calculate, *ab initio*, the individual contributions from each electronic subshell to the total γ-spectra and annihilation rate parameter $Z_{\rm eff}$. Figure 1 shows the γ-spectra obtained using both Hartree-Fock and fully correlated (Dyson) incident positron wavefunction, in different orders of the annihilation vertex that includes corrections to the electron-positron attraction at short range.

Overall, the correlation effects are stronger for annihilation on the valence shells. However, the corrections to the IPM vertex also cause significant enhancement for the core electrons, resulting in an increased contribution to the high energy wings of the γ-spectra [4,5].

Subshell	Ar	Kr	Xe
np	4.39	5.20	6.51
ns	2.38	2.55	2.97
$(n-1)d$	...	1.62	1.87
$(n-1)p$	1.42	1.38	1.47
$(n-1)s$	1.34	1.32	1.38

Table 1: *Vertex enhancement factor $\bar{\gamma}_{nl}$ [4].*

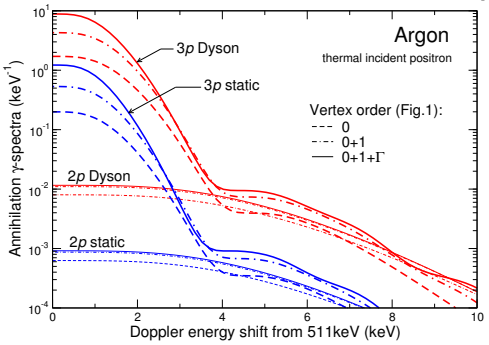

Figure 1: *γ-spectra calculated using HF and Dyson positron wavefunction for different vertex orders.*

To appeal to the predilection of the literature we parametrize the vertex enhancement for a given subshell nl through the quantity $\bar{\gamma}_{nl} \equiv Z^{0+1+\Gamma}_{\rm eff}/Z^{0}_{\rm eff}$, taken at thermal positron momenta, where the superscript denotes the vertex order. Table 1 shows $\bar{\gamma}$ for the valence n and subvalence $(n-1)$ subshells of Ar, Kr, and Xe. For the strongly bound Ar $2s$ subshell, the rate is still enhanced above the IPM by 1.3 times, and can be as much as 1.87 times for the relatively diffuse Xenon $4d$. The vertex enhancement has little dependence on the precise form of the positron wavefunction [4]. Similar vertex enhancements can thus be expected for the (atomic like) core electrons in condensed matter systems.

References

[1] A. Eshed *et al.*, Phys. Rev. Lett. **89** 075503 (2002).
[2] G. F. Gribakin and J. Ludlow, Phys. Rev. A, **70** 032720 (2004).
[3] L. J. M. Dunlop and G. F. Gribakin, J. Phys. B, **39** 1647 (2006).
[4] D. G. Green and G. F. Gribakin 2011 *Manuscript in preparation* (2011).
[5] K. Iwata *et al.*, Phys. Rev. Lett., **79** 39 (1996).

Atomic dark state evolution in the constant laser field

A. J. Krmpot[1], S. M. Ćuk[1], S. N. Nikolić[1], M. Radonjić[1], and B. M. Jelenković[1]

[1] *Institute of Physics, University of Belgrade, Pregrevica 118, 11080 Belgrade, Serbia*
Corresponding Author: krmpot@ipb.ac.rs

In this work the evolution of the dark state of the atom moving through constant resonant laser field was studied by measuring Hanle EIT (electromagnetically induced transparency) resonances in the selected parts of the laser beam which has Π type profile for radial dependence of its intensity. This work was motivated by the fact that the influence of different laser beam profiles on the shape of the Hanle EIT resonances is not thoroughly investigated and that the physical processes during the interaction of atoms with resonant laser light while atom is passing through the laser beam are not explained well enough. The Hanle EIT resonances were studied using $F_g = 2 \rightarrow F_e = 1$ hyperfine transition of ^{87}Rb isotope in the vacuum vapor cell and Π laser beam profile. The Hanle EIT resonances were obtained by detecting transmission of selected segments of the laser beam cross section, after the the entire beam had passed through the Rb cell. The resonances were obtained by moving the small aperture (placed in front of the large area photo-detector) radially across the laser beam. The change of the shape of the Hanle EIT resonances obtained at different radial distances from the laser beam center directly reflects the evolution of the moving atomic system during permanent interaction with resonant laser light of constant intensity. Previous studies of EIT resonances obtained by Π laser beam profile were done mostly theoretically and by detecting the entire laser beam [1,2]. Examination of the EIT resonances in different segments of the Gaussian laser beam cross section was performed in effusive regime in Rb vacuum cell [3] and in diffusive regime in dense He vapor [4]. In the effusive regime the resonances become narrower if detected further from the beam center and in addition two counter-sign peaks of coherent nature appear in the beam wings.

For the Π laser beam profile, in contrast to the Gaussian profile, the narrowing of the Hanle EIT resonances and appearance of two counter-sign peaks occur in the central parts of the laser beam cross section. According to the theoretical model, these counter-sign peaks are not of coherent nature, but appear due to optical pumping to the uncoupled $F_g = 1$ level. The narrowing of the Hanle EIT resonances in the central part of the Π laser beam occurs due to the time of flight. At low laser intensities, due to low efficiency of the optical pumping process, there are neither counter-sign peaks nor line narrowing. When the transition $F_g = 2 \rightarrow F_e = 1$ is artificially closed in the simulation, the counter-sign peaks and line narrowing disappear, regardless of the laser intensity. The analysis of the characteristics of the Hanle EIT resonances obtained in the selected segments of the Π laser beam cross section are of interest because they reveal the details of the evolution of atomic system traversing the constant intensity laser field.

References

[1] M. A. V. Taichenachev *et al.*, Phys. Rev. A **69**, 024501 (2004).
[2] M. Radonjic *et al.*, Phys. Rev. A **79**, 023805 (2009).
[3] A. J. Krmpot *et al.*, Opt. Express **17**, 22491–22498 (2009).
[4] H. Gilles *et al.*, Phys. Rev. Lett. **86**, 1175–1178 (2001).

Strong interference effects in the resonant Auger decay of atoms induced by intense x-ray laser fields

Ph. V. Demekhin[1], L. S. Cederbaum[1]

[1] *Theoretische Chemie, Physikalisch-Chemisches Institut, Universität Heidelberg, Im Neuenheimer Feld 229, D-69120 Heidelberg, Germany*

Corresponding Author: philipp.demekhin@pci.uni-heidelberg.de

The advent of x-ray free electron lasers (XFELs) [1] raises the fundamental question of how the well-studied resonant Auger (RA) decay of atoms will be modified under extreme field conditions. Compared to conventional synchrotron radiation sources, the intensities of the electromagnetic fields generated by XFELs are by several orders of magnitude stronger, and the durations of the light pulses can be made to be similar to the typical lifetimes of highly-excited electronic states. The first theoretical studies of RA decay of atoms exposed to strong x-ray pulses [2,3] showed that the stimulated emission from the resonance back to the ground state starts to compete with the Auger decay. The interplay between the resonant excitation and stimulated emission results in Rabi oscillations between the ground state and the resonance within its Auger decay lifetime and pulse duration [2,3], which leads to spectacular modifications of the RA spectra.

Obviously, a final ionic state is populated coherently by both the direct photoionization and the resonant Auger decay thus naturally inducing interference effects in the electron spectra. On the other hand, as discussed in [3,4], there will be leakages of the populations of the ground state and of the resonant state itself by the direct total photoionization into all possible final ionic states. It has not yet been shown and understood how all these processes evoked by a strong field influence the total electron yield and the spectra and filling this gap is the major goal of this work. The currently operating XFEL, SLAC Linac Coherent Light Source, does not produce so far a monochromatic radiation and its x-ray pulses consist of many spikes with random fluctuations of the frequency, phase and amplitude [1]. The impact of these problems on the RA effect has been studied in [2]. In addition, the x-ray pulse properties are compressed through the propagation in a resonant medium [3,4]. Here, we present the theory of resonant Auger decay of a single atom exposed to a coherent and monochromatic x-ray pulse of a high intensity [5]. This theory is prerequisite for further studies.

The theory includes the coupling between the ground state and the resonance due to an intense x-ray pulse, taking into account the decay of the resonance and the direct photoionization of the ground state, both populating the final ionic states coherently. The theory also considers the impact of the direct photoionization of the resonance state itself which typically populates highly-excited ionic states. The combined action of the resonant decay and of the direct ionization of the ground state in the field induces a non-Hermitian time-dependent coupling between the ground and the 'dressed' resonance stats. The impact of these competing processes on the total electron yield and on the $2s^2 2p^4 (^1D) 3p\ ^2P$ spectator and $2s^1 2p^6\ ^2S$ participator Auger decay spectra of the Ne 1s→3p resonance is investigated. The role of the direct photoionization of the ground state and of the resonance increases dramatically with the field intensity. This results in strong interference effects with distinct patterns in the electron spectra, different for the participator and spectator final states.

References

[1] P. Emma, *et al.*, Nature Photonics **4**, 641–647 (2010).
[2] N. Rohringer and R. Santra, Phys. Rev. A **77**, 053404 (2008).
[3] J.-C. Liu, *et al.*, Phys. Rev. A **81**, 043412 (2010).
[4] Y.-P. Sun, *et al.*, Phys. Rev. A **81**, 013812 (2010).
[5] Ph. V. Demekhin and L. S. Cederbaum, Phys. Rev. A (2011) in press; arXiv:1012.3399v1.

High contrast sub-natural resonance of increased absorption formed in cell filled with Rb and buffer gas

D. Sarkisyan[1], A. Sargsyan[1], R. Mirzoyan[1], Y. Pashayan–Leroy[2], and C. Leroy[2]

[1] *Institute for Physical Research, NAS of Armenia, Ashtarak, 0203, Armenia*
[2] *Laboratoire Interdisciplinaire Carnot de Bourgogne, UMR CNRS 5209 – Université de Bourgogne, F-21078 Dijon Cedex, France*

Corresponding Author: davsark@yahoo.com

It is well known that in Λ-systems when the difference of the probe and coupling laser frequencies is $\nu_p - \nu_{c1} = \Delta_{\rm HFS}$, with $\Delta_{\rm HFS}$ being the hyperfine splitting of the ground level, and also both ν_p and ν_{c1} frequencies are in resonance with the corresponding transition (see Fig. 1), via the electromagnetically induced transparency effect a well-known dark resonance (DR) is observable [1]. We report observation of a sub-natural and high-contrast resonance of increased absorption, i.e., bright resonance (BR) in the Rb 6 mm-long cell filled with an additional 6 Torr Ne buffer gas and under previously unexplored experimental conditions for the coupling and probe radiation configuration. In this case BR is formed for the same probe frequency ν_p, but for another coupling laser frequency ν_{c2} (see Fig. 1), which satisfies the condition $\nu_{c2} - \nu_p = \Delta_{\rm HFS}$. Note, that the nature of the BR is completely different to that presented in [2]. For DR and BR resonances formation two single-frequency extended cavity diode lasers (forming the coupling and probe beams) with $\lambda = 794$ nm and 1 MHz line-width are used. The coupling and the probe lasers power is 1–20 mW and 0.01–1 mW, correspondingly. In Fig. 1 for the comparison both BR and DR are presented for the ^{85}Rb D_1 line for the case where a 3 G longitudinal magnetic field is applied. As it is seen the spectral resolution for DR and BR is similar to each other. The cell temperature is 60°C. The physical explanation will be presented. We believe that from the application point of view the BR resonance could have some benefits compared with the DR.

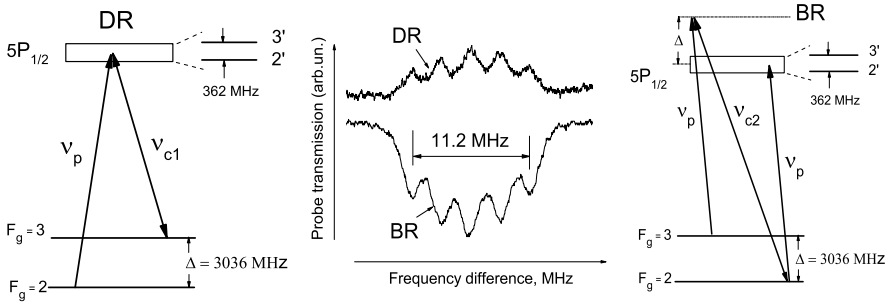

Figure 1: *The splitting of the DR (upper curve, central figure) and BR (lower curve) when a longitudinal magnetic field $B = 3$ G is applied (the both spectrum are combined for comparison). The left diagram shows the configuration of ν_{c1} and ν_p for DR formation, while the right one shows the configuration of ν_{c2} and probe ν_p for BR formation.*

Research conducted in the scope of the International Associated Laboratory IRMAS. Ashtarak team thanks for the ANSEF Opt 2428 support. R. M. acknowledges the support from the NFSAT/CRDF (grant ECSP-10-10GRSP).

References

[1] M. Fleischhauer, A. Imamoglu, J. P. Marangos, Rev. Mod. Phys. **77**, 633 (2005).
[2] A. M. Akulshin, S. Barreiro, and A. Lezama, Phys. Rev. A **57**, 2996 (1998).

A fundamental test of Lorentz invariance using relativistic $^7Li^+$ ion beams

B. Botermann[1,2], D. Bing[3], C. Geppert[1], G. Gwinner[4], T. W. Hänsch[5], G. Huber[6], S. Karpuk[6], T. Kühl[1,2], W. Nörtershäuser[1,2], C. Novotny[1,2], S. Reinhardt[5], G. Saathoff[5], R. Sánchez[2], D. Schwalm[3], Th. Stöhlker[2], and A. Wolf[3]

[1] *Institut für Kernchemie, University of Mainz, 55128 Mainz, Germany*
[2] *GSI Helmholtzzentrum für Schwerionenforschung, 64291 Darmstadt, Germany*
[3] *Max Planck Institut für Kernphysik, 69117 Heidelberg, Germany*
[4] *University of Manitoba, Winnipeg, MB, R3T 2N2, Canada*
[5] *Max Planck Institut für Quantenoptik, 85748 München, Germany*
[6] *Institut für Physik, University of Mainz, 55128 Mainz, Germany*

Corresponding Author: B.Botermann@gsi.de

One of the fundamental principles in modern physics is local Lorentz invariance (LLI), on which the theory of special relativity (SR) is based. Special relativity can be probed by a careful measurement of time dilation. For this, an accelerated ion-beam of $^7Li^+$ ions at a velocity (v) of 33.8% of the speed of light (c) is illuminated by two laser beams to excite the moving ions. The lithium ions are produced by an PIG ion source, accelerated in the SIS18-synchrotron and stored in the experimental storage ring at the GSI Helmholtzzentrum für Schwerionenforschung. The laser beams are aligned parallel and antiparallel to the flight direction of the lithium ions and the frequencies of the lasers are adjusted to drive the 2s $^3S_1 \rightarrow$ 2p $^3P_2$ transition ($\lambda_0 = 548$ nm). Due to the Doppler-shift the laser wavelengths (λ_a, λ_p) have to obey $\lambda_{a,p} = \lambda_0 \cdot \gamma \cdot (1 \pm \beta)$ where $\gamma = (1-\beta)^{-1/2}$ and $\beta = v/c$. The excitation wavelengths are shifted to $\lambda_p = 386$ nm for the parallel and to $\lambda_a = 780$ nm for the antiparallel aligned laser. By performing a simultaneous measurement with both lasers, the Doppler equation for the three wavelengths changes to $\lambda_a \cdot \lambda_p / \lambda_0 = 1 - \varepsilon(\beta)$. Here the additional parameter $\varepsilon(\beta)$ denotes hypothetical deviations from SR and vanishes if SR is valid. It can be parametrized in different frameworks of kinematic [1] and dynamic [2] test thories. In both cases $\varepsilon(\beta)$ is expanded in terms of β, e.g., in the Robertson–Mansouri–Sexl test theory the representation of $\varepsilon(\beta)$ is given as $\varepsilon(\beta) = 2 \cdot \alpha \cdot \beta^2 + \mathcal{O}(\beta^4)$.

The setup used allows a frequency accuracy of $\Delta\nu/\nu = 10^{-9}$. This precision is provided by a laser stabilization scheme using saturation spectroscopy on rubidium and iodine. Considering all other experimental uncertainties, this leads to an upper bound for hypothetical deviations from SR of the order of 10^{-9}. In our recent measurements the results of the so far leading experiment [3] has been improved by roughly a factor of four. By changing the spectroscopy scheme from $\Lambda-$ to saturation spectroscopy it is possible to gain another factor of two in future experiments. Furthermore polarization dependent measurements open the possibility to improve the constraints of several parameters resulting from the standard model extension (SME).

References

[1] R. Mansouri, and R. U. Sexl, General Relativity and Gravitation **8**, 497–513 (1977).
[2] D. Colladay, and V. A. Kostelecký, Phys. Rev. D **58**, 116002 (1998).
[3] S. Reinhardt *et al.*, Nature Physics **3**, 861–864 (2007).

Two-electron one-photon transitions of Mg, Al, and Si in K-shell double photoionization

J. Hoszowska[1], J.–Cl. Dousse[1], J. Szlachetko[2,3], Y. Kayser[1], W. Cao[1], S. H. Nowak[1], P. Jagodziński[3], and M. Kavčič[4]

[1] *Department of Physics, University of Fribourg, CH-1700 Fribourg, Switzerland*
[2] *European Synchrotron Radiation Facility, F-38043 Grenoble, France*
[3] *Institute of Physics, Jan Kochanowski University, 25-406 Kielce, Poland*
[4] *J. Stefan Institute, P.O. Box 3000, SI-1001, Ljubljana, Slovenia*

Corresponding Author: joanna.hoszowska@unifr.ch

The first experimental evidence for the two-electron one-photon (TEOP) transitions following single-photon K-shell double ionization is reported. In the TEOP transition ($1s^{-2}$–$2s^{-1}2p^{-1}$) the two K-shell vacancies are filled simultaneously via a correlated two-electron jump, and one photon is emitted [1]. Compared to the one-electron one-photon (OEOP) transitions ($1s^{-2}$–$1s^{-1}2p^{-1}$)[2,3], the TEOP radiative decay channel is several orders of magnitude weaker and thus experimentally challenging. Results for the branching ratios and energies of the TEOP transitions deduced from charged particle and heavy-ion collision experiments are scarce and show a wide spread of values. Moreover, the change of electronic configuration due to multiple ionization makes comparison with theory often inconclusive. On the theoretical side, depending on how electron correlation effects are taken into account, the calculated TEOP transition rates differ up to a factor of four.

Measurements of the TEOP x-ray spectra of solid Mg, Al, and Si were carried out at the ID21 beamline of the ESRF, Grenoble. Monochromatic synchrotron radiation was used to produce the sample fluorescence which was measured by means of a wavelength dispersive x-ray spectrometer [4]. The TEOP transition energies and the branching ratios were determined and compared to theoretical predictions. A good agreement with the MCDF energies of Martins *et al.* [5] was found. Present branching ratios indicate that most of the existing theoretical predictions overestimate the TEOP radiative transition rates. The obtained results for the OEOP to TEOP branching ratios compare best to perturbation theory calculations [6-8], and fairly well with the most recent relativistic configuration interaction calculations [9]. The latter, yield, however, somewhat smaller TEOP transition rates compared to our experimental values. The present single photon ionization experimental data for the two-electron one-photon transitions provide a stringent test for atomic structure calculations.

References

[1] W. Wölfi *et al.*, Phys. Rev. Lett. **35**, 656–659 (1975).
[2] J. Hoszowska *et al.*, Phys. Rev. Lett. **102**, 073006 (2009).
[3] J. Hoszowska *et al.*, Phys. Rev. A **82**, 063408 (2010).
[4] J. Szlachetko *et al.*, J. Synchrotron Rad. **17**, 400–408 (2010).
[5] M. C. Martins *et al.*, J. Phys. B: At. Mol. Phys. **37**, 3785–3795 (2004).
[6] H. R. Kelly, Phys. Rev. Lett. **37**, 386–388 (1976).
[7] M. Ya. Amusia *et al.*, Phys. Lett. **60A**, 300–302 (1977).
[8] U. I. Safronova and V. S. Senashenko, J. Phys. B: At. Mol. Phys. **10**, L271 (1977).
[9] R. Kadrekar and L. Natarajan, J. Phys. B: At. Mol. Phys. **43**, 155001 (2010).

Dark and light optical nanofibre probes for cold atoms

S. Nic Chormaic[1,2], L. Russell[1,2], M. Daly[1,2], and K. Deasy[2,3]

[1] *Department of Physics, University College Cork, Cork, Ireland*
[2] *Photonics Centre, Tyndall National Institute, Lee Maltings, Cork, Ireland*
[3] *Department of Applied Physics and Instrumentation, Cork Institute of Technology, Cork, Ireland*

Corresponding Author: s.nicchormaic@ucc.ie

Optical nanofibres are narrow cylindrical waveguides fabricated from commercially available optical fibre. Implemented in a cold atom system, they can be used either as 'dark' or 'bright' probes allowing non-destructive access to typical cold cloud characteristics [1] as well as the spectroscopic nature of the trapped atoms.

To utilize the nanofibre as a dark probe (Fig. 1), we position a cloud of approximately 10^8 ^{85}Rb atoms around its waist region, which is approximately 600 nm in diameter. The fluorescence from nearby laser-cooled ^{85}Rb atoms can couple efficiently into the guided modes of the nanofibre. By connecting a suitable low-light level detector to one end of the nanofibre, we can monitor the signal from the cold atomic cloud.

A forced oscillation method [2] is used to measure the average atom temperature above and below the Doppler limit of 140μK for rubidium using a dark nanofibre. Despite the presence of the relatively hot fibre in the cloud of ^{85}Rb atoms, we observe temperatures as low as 90μK.

In a second experiment, a frequency-scanned probe beam is launched through the nanofibre and the resonant light is absorbed at the waist of the nanofibre. The transmitted probe signal is measured using an APD. We present recent single-photon absorption results which demonstrate surface interaction effects and discuss future work on 2-photon absorption in the cold atomic system.

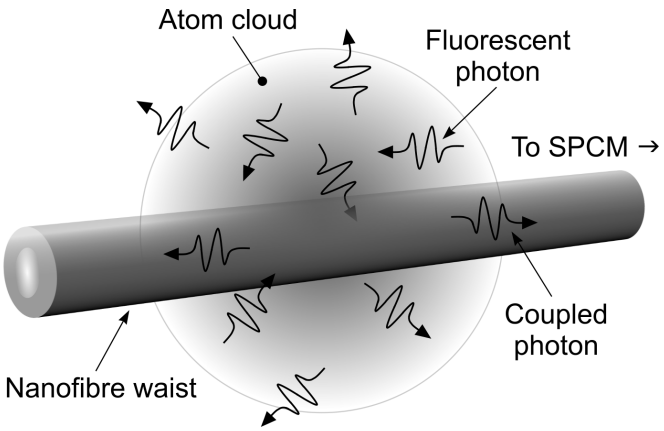

Figure 1: *Schematic illustration of a 'dark' optical nanofibre probe.*

References

[1] M. J. Morrissey *et al.*, Rev. Sci. Instrum. **80**, 053102 (2009).
[2] P. Kohns *et al.*, Europhys. Lett. **22** (7), 517–522 (1993).

Time and frequency metrology with laser cooled atoms: evaluation of the Swiss continuous atomic fountain clock

L. Devenoges[1], G. Di Domenico[1], A. Stefanov[2], A. Joyet[1], and P. Thomann[1]

[1] *Laboratoire Temps-Fréquence, Université de Neuchâtel, 2000 Neuchâtel, Switzerland*
[2] *Federal Office of Metrology, 3003 Bern-Wabern, Switzerland*
Corresponding Author: laurent.devenoges@unine.ch

Atomic fountain clocks presently contributing to TAI (International Atomic Time) are operating in a pulsed mode, i.e., the atoms are successively laser-cooled, launched, and interrogated during their ballistic flight, before the cycle starts over again. This approach has led to important progresses in time and frequency metrology. Nowadays, state-of-the-art fountains provide the best realization of the SI second with relative uncertainties of a few parts in 10^{16}.

Our alternative approach to atomic fountain clocks consists in making use of a continuous beam of laser-cooled cesium atoms. Besides circumventing technical problems such as the Dick effect existing in pulsed fountains, a continuous beam is interesting from the metrological point of view. Indeed, the relative importance of the error budget contributors is quite different in the two types of fountain. As an illustration of the difference, we show in Fig. 1(a) the Ramsey fringes measured with our continuous fountain in a single sweep of 120 s. They were obtained with an atomic flux of 3×10^6 at/s in $F=3, m=0$. The signal to noise ratio ($S/N = 836\ \mathrm{s}^{-1/2}$) is sufficient to reach a relative instability of 6×10^{-14} at 1 s, see Fig. 1(b).

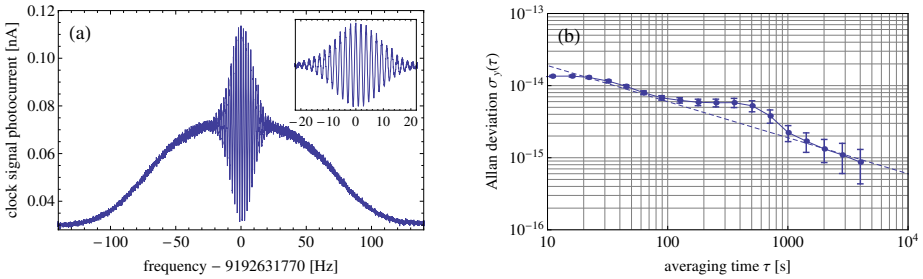

Figure 1: *(a) Ramsey fringes measured with our continuous fountain in a single microwave frequency sweep of* 120 *s around the* $m=0$ *hyperfine transition (b) Allan standard deviation* $\sigma_y(\tau)$ *of our fountain clock measured against an hydrogen maser.*

Evaluation of the frequency shifts specific to the continuous approach are currently underway. Since lasers must remain on at all times, the light shift caused by the atomic beam source, measured to be -1.5×10^{-12}, must be suppressed. This has now been successfully achieved with the help of a light-trap which attenuates the source light by a factor 10^4 and reduces the shift to a negligible level. The second order Zeeman shift is another topic that is dealt with differently in a continuous fountain. A specific method involving Zeeman spectroscopy with low frequency pulses has been developed and combined with Fourier analysis of Ramsey fringes to determine the magnetic field profile. The resulting second order Zeeman shift contribution to the error budget is below 5×10^{-16}. The collisional shift, which appears in pulsed fountain, is also reduced due to the lower atomic density of our continuous beam. Finally, all microwave cavity-related shifts are altered in a continuous fountain since the microwave cavity is substantially different. The latest status of our evaluation will be presented at the conference.

Atomic diffraction to reveal the atomic structure of surfaces, surfaces to construct atomic interferometers

P. Roncin[1], A. Momeni[1], H. Khemliche[1], M. Mulier[1], P. Atkinson[2], M. Eddrief[2], and V. Etgens[2]

[1] *ISMO,UMR8214 CNRS-Université Paris sud-11, 91400 Orsay, France*
[2] *INSP, UMR7588 CNRS-Université Pierre et Marie Curie, Paris 6, France*
Corresponding Author: philippe.roncin@u-psud.fr

We have developed a novel technique based on diffraction of fast atoms at grazing incidence (GIFAD) to image the surface of crystals with an atomic resolution. A well collimated beam of "fast" atoms or molecules in the keV range is sent, close to one degree incidence, onto a single crystal surface oriented along a low index direction. The whole diffracted beam is imaged onto an position sensitive detector. Just as reflection high energy electron diffraction (RHEED) commonly installed on molecular beam epitaxy (MBE) machines, the peak spacing gives the surface lattice parameter. However, with GIFAD the form factor determining the spot intensities is simply the shape of the surface electronic density, i.e., the same information, in the reciprocal space, as the one revealed, in the real space, by an atomic force microscope (AFM). Indeed, the projectile atom, in general, helium, is repelled by the surface electronic density as would be a perfect atomic tip. Since there is no penetration below the surface, GIFAD provides an excellent contrast and well-resolved layer by layer oscillation as needed for ultra thin film applications. The diffraction pattern can be recorded in seconds allowing dynamical applications at almost video rates of surface reconstruction and phase transition taking place very rapidly at the surfaces of semiconductors [1].

Many fundamental aspects are still investigated such as the influence of inelastic processes on decoherence; exciton population, electron-hole pairs excitations at the Fermi level [2], phonons and electron emission [3]. The insight is then focused on electron momentum distribution, phase shift, etc... These will be addressed in detail through various coincidence techniques.

Reversely, it is straightforward to adjust the angle of incidence in such a way that the surface acts like a **beam splitter** or an atomic mirror suitable for applications in atomic interferometry.

Figure 1: *250 eV helium diffracted from a $\beta(2\times4)$ GaAs(001) surface exposed to Ga at 640° C.*

References

[1] H. Khemliche *et al.*, Appl. Phys. Lett. **95** 151901 (2009).
[2] N. Bundaleski *et al.*, Phys. Rev. Lett. **101**, 177601 (2008).
[3] J. Lienemann *et al.*, Phys. Rev. Lett. **106**, 067602 (2011).

Atomic beam measurement of the DC Stark shift of the Cs clock transition frequency

J.–L. Robyr[1], P. Knowles[1], and A. Weis[1]

[1] *Department of Physics, University of Fribourg, 1700 Fribourg, Switzerland*
Corresponding Author: jean-luc.robyr@unifr.ch

The Stark effect describes the shift of atomic energy levels induced by an external electric field. In Cs atomic clocks, the AC Stark shift arising from the blackbody radiation is an important source of systematic frequency shifts. We are currently performing a fully optical Raman-Ramsey pump-probe experiment on a thermal Cs atomic beam to make a precise measurement of the Cs ground state third-order electric polarizabilities which are used to parametrize the Stark shift. We expect accuracy better than 1%. The experimental scheme is similar to that of Cs atomic beam clocks except that the microwave cavities are replaced by a coherent population trapping (CPT) interaction. A CPT coherence is created in a pump interaction (Fig. 1). The atoms then fly through a zone with controlled magnetic and electric fields where no optical interaction occurs, permitting free evolution of the coherence. The fields affect the phase of the evolving CPT coherence, an effect detected in the probe interaction. The dependence of the shift in transition frequency as a function of the applied capacitor voltage has been successfully measured for the seven distinct Δm=0, F=3 $\rightarrow$ F=4 hyperfine ground state transitions. The calibration of the electric field and the calculation of the rms electric field seen by the atoms is a difficult task. Numerical simulation of the field will be compared to direct measurements of the field using the Aharonov-Casher phase shift induced by the motional magnetic field. Work towards a direct measurement of the field using the Cs $D1$ optical Stark shift will also be presented. A measurement of the ratio of the third order tensor and scalar Stark shift $\alpha_2^{(3)}/\alpha_0^{(3)}$ and an absolute value for $\alpha_0^{(3)}$ will be presented and systematic effects will be discussed.

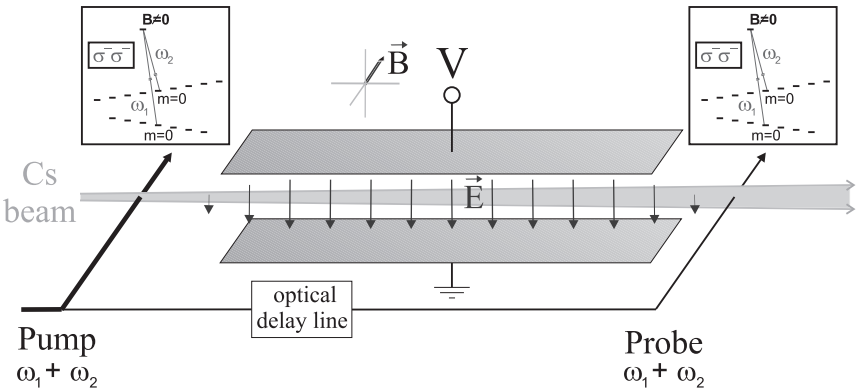

Figure 1: *Raman-Ramsey pump-probe scheme for the Stark shift measurement.*

Work funded by the Swiss National Science Foundation, #200020–126499.

Selective reflection probing of thin film deposition

W. Soares Martins[1], T. Passerat de Silans[1], I. Vidal[1], and M. Chevrollier[1]

[1] *Laboratório de Espectroscopia Ótica, Universidade Federal da Paraíba, Cx Postal 5086, João Pessoa 58051-900,PB, Brazil*

Corresponding Author: martine@otica.ufpb.br

The study of basic mechanisms of interaction between neutral atoms and surfaces is a field of growing interest stimulated by the increasing necessity of dealing with interfaces between gaseous atoms and solid surfaces in nano-engineered devices for fundamental (quantum information, quantum optics, atom optics) as well as applied (nanotechnology) purposes. Controlling the various stages of these processes is a highly motivating quest. A prerequisite for observing the quantum regime, where the atomic center-of-mass has discrete energy states in the confined potential well, is to load the surface well with free atoms. Two mechanisms have so far been proposed for this loading [1,2]. We study the formation of a metallic film, induced by a pump laser beam incident at the interface between a cell window and the atomic cesium vapor it contains. The characterization of the growing film is made through analysis of selective reflection (SR) spectra. SR spectroscopy consists in sending a weak laser beam to the interface between a solid transparent structure and an atomic vapor and detecting the contribution of the laser-excited atoms in the reflected light beam. Around an atomic transition frequency, this contribution can be isolated as a Doppler-free feature, whose shape and spectral shift are particularly sensitive to atomic interactions [3]. SR spectroscopy is thus particularly adapted to studies of atom-surface interactions [4]. For a dielectric substrate/metallic film/atomic vapor structure such as the one we study in this work, SR lineshapes have been shown to exhibit a strong dependence on the film thickness [5] and should therefore allow one to follow the film thickness and the atom-surface interaction strength evolution as the film is being grown. We discuss the achievements and limits of this technique applied to film growth studies.

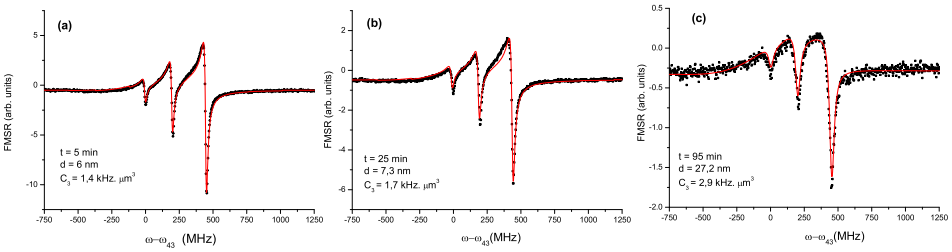

Figure 1: *Experimental FMSR lineshapes (black squares) and their fit (solid red) during formation of a Cs film for window temperature* $214^o C$ *and atomic density* 8.0×10^{14} cm^{-3}. *(a)* $t = 5$ *min, (b)* $t = 25$ *min, (c)* $t = 95$ *min.*

References

[1] T. Passerat de Silans *et al.*, Appl. Phys. B **82**, 367–371 (2006).
[2] A. E. Afanasiev, P. N. Melentiev, and V. I. Balykin, JETP Lett. **86**, 172–177 (2007).
[3] A. M. Akul'shin *et al.*, JETP Lett. **36**, 303–307 (1982).
[4] M. Chevrollier *et al.*, Opt. Lett. **16**, 1879–1881 (1991).
[5] M. Chevrollier *et al.*, Phys. Rev. E **63**, 046610 (2001).

Cs cell Ramsey clock based on coherent population trapping: current status

O. Kozlova[1], J.–M. Danet[1], S. Guérandel[1], and E. De Clercq[1]

[1] *Laboratoire National d'Essai — Systèmes de Référence Temps — Espace, Observatoire de Paris, CNRS, Université Pierre et Marie Curie, Paris, France*

Corresponding Author: olga.kozlova@obspm.fr, emeric.declercq@obspm.fr

A cesium vapour cell atomic clock based on coherent population trapping (CPT) and Ramsey interrogation is described. In the CPT clocks, the alkali atoms are pumped in a non-absorbing dark state by two phase-coherent laser fields whose frequency difference is exactly equal to the ground state hyperfine splitting. Contrary to conventional double resonance clocks, no microwave cavity is needed. The combination of two original techniques [1]: use of crossed linear polarizations allowing a double-lambda excitation scheme of the CPT-resonance, see Fig. 1, and a temporal Ramsey interrogation enables both high contrast and narrow CPT resonances with reduced light shift dependence.

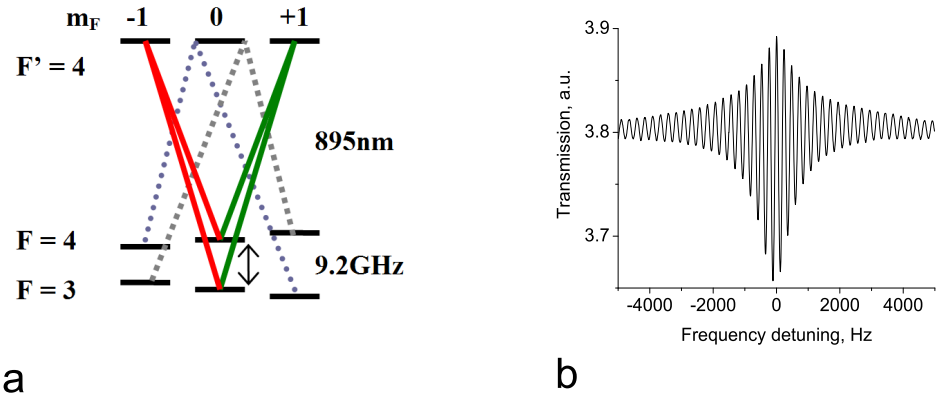

Figure 1: *a. The double Λ scheme in Cs D1 line, only involved levels are shown. b. Raman-Ramsey fringes.*

Our experimental setup uses two extended cavity diode lasers tuned to the Cs D1 line (895 nm), phase-locked 9 GHz apart, and a cm-scale Cs cell. The cell is filled with an additional buffer gas in order to confine the atoms and reduce the Doppler broadening by Dicke effect. The influence of the most relevant parameters on the signal amplitude and on the resonance frequency has been studied. The resonance frequency shift induced by the buffer gas-Cs collisions has been investigated for three gases: Ne, N_2, Ar. The obtained results allowed us to establish the optimal Ar–N_2 buffer gas mixture canceling the shift temperature dependence at the working temperature. Lifetimes of population and coherences have been measured. The double Λ scheme also allows $\Delta m = 2$ transitions which have been observed. Results will be shown at the conference.

This work was supported by DGA.

References

[1] T. Zanon *et al.*, Phys. Rev. Lett., **94**, 193002 (2005).

Nonlinearly-generated atomic signal for robust laser locking

F. Queiroga da Silva[1], W. Soares Martins[1], I. Vidal[1], T. Passerat de Silans[1], and M. Oriá[1]

[1] *Laboratório de Física Atômica e Lasers, Dpto de Física, Universidade Federal da Paraíba, Cx Postal 5086, João Pessoa 58051-900, PB, Brazil*

Corresponding Author: oria@otica.ufpb.br

The use of lasers in atomic physics often demands emission spectral long term stability at an atomic resonance frequency. Locking a laser to the center of an atomic lineshape usually requires a modulation technique with lock-in detection. On the other hand, for many scientific and technical applications, the desired laser frequency is not necessarily at the center of an atomic lineshape, and one only needs to avoid frequency drift, for instance, to build a trap for neutral atoms. For such applications a few simple and reliable techniques have been developed [1-6]. In particular, for techniques using dichroic atomic vapor laser lock (DAVLL) the lock frequency may be tuned around the center of the Doppler-broadened line thanks to a dispersive-like lineshape electronically-generated signal obtained from two lines of magnetically shifted atomic transitions. The large capture range of the error signal makes this stabilization method robust and reliable. In the present work we report on a new method to generate a dispersive signal in a much simpler and direct way. We call this method, ANGELLS, acronym for atomic non-linearly generated laser locking signal. The idea in our configuration is to send a slightly focused laser beam through a vapor cell. The transmitted beam is spatially filtered by an aperture and captured by a photodetector. Positioning the cell around the beam minimum waist we are able to modify the spectral lineshape from an absorptive to a dispersive one, therefore adjusting the symmetry of the error signal. We demonstrate this technique using semiconductor lasers locked to the cesium D_2 optical transition, at 852.1 nm, as well as to rubidium lines, at 780 nm (Fig. 1 (a)). Moreover, saturating the probed atoms with a counter propagating beam we get sharper resonances that increase the accuracy and dynamics of the frequency stabilization (Fig. 1 (b)). The performance of ANGELLS is comparable to magnetically operated techniques, and is a quicker and more reliable way to stabilize a laser on a suitable atomic transition, due to the simplicity of the experimental configuration which avoids magnetic fields. Therefore, we think the ANGELLS technique is nicer than the DAVLL's.

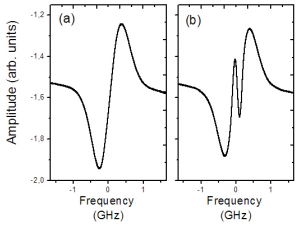

Figure 1: *ANGELLS signal in Rb vapor: (a) nonsaturated, (b) saturated.*

References

[1] G. D. Rovera,G. Santarelli, and A. Clairon, Rev. Sci. Instrum. **65**, 1502–1505 (1994).
[2] B. Cheron *et al.*, J. Phys. III **4**, 401–406 (1994).
[3] K. Corwin *et al.*, Appl. Opt. **37**, 3295–3298 (1998).
[4] G. Wasik *et al.*, Appl. Phys. B **75**, 613–619 (2002).
[5] T. Petelski *et al.*, Eur. Phys. J. D **22**, 279–283 (2003).
[6] N. Beverini *et al.*, Appl. Phys. B **73**, 133–138 (2001).
[7] W. S. Martins *et al.*, Appl. Opt. **49**, 871–874 (2010).

A novel approach to Doppler-width thermometry: Implications for an improved determination of the Boltzmann constant

A. Castrillo[1], M. D. De Vizia[1], E. Fasci[1], L. Moretti[2], G. Casa[1], and L. Gianfrani[1]

[1] *Dipartimento di Scienze Ambientali della Seconda Università di Napoli, Caserta, Italy*
[2] *Dipartimento di Matematica della Seconda Università di Napoli, Caserta, Italy*
Corresponding Author: livio.gianfrani@unina2.it

Doppler-width thermometry is a relatively new method for determining the absolute temperature of a gaseous system at thermodynamic equilibrium. Proposed by Ch. J. Bordé [1], soon after its first implementation [2], this method appeared to be very promising, with the advantage of being conceptually simple, applicable to any gas at any temperature, in whatever spectral region. It consists in retrieving the Doppler width from the highly-accurate observation of the absorption profile corresponding to a given atomic or molecular line. In recent years, there have been a growing interest towards new primary thermometric methods, likely to be employed for highly-accurate determinations of the Boltzmann constant (k_B), in view of a possible new definition of the unit kelvin.

After a proof-of-principle experiment performed on CO_2 in the wavelength window around 2 μm, in which k_B was determined with a relative accuracy of 1.6×10^{-4} [3], we moved to a second generation experiment with the ambitious goal of reaching the target accuracy of 10^{-6} [4]. Performed on water molecules at 1.38 μm, this new experiment is based upon a pair of offset-frequency-locked extended-cavity diode lasers. Such a technique ensures extreme levels of accuracy in controlling and measuring any variation of the laser frequency around a given absolute reference [5]. Apart from the experimental developments, the precise modelling of the line shape is an indispensable prerequisite for an improved determination of k_B. Besides the Doppler effect, other mechanisms can influence the line profile and they all contribute to the overall width. Very recently, speed-dependent effects have been clearly evidenced in the near-IR spectrum of self-colliding $H_2{}^{18}O$ molecules, at pressures between 40 and 500 Pa [6]. This makes more challenging the retrieval of the Doppler width from high-quality absorption spectra with the required accuracy. In fact, a proper treatment of speed-dependence of collisional parameters would require quantum mechanical scattering calculation that are still prohibitively complex for triatomic molecules.

Here, we discuss a radically new strategy for Doppler-width thermometry that results to be much more relaxed with respect to the line-shape problem. Instead of retrieving the Doppler width from the fit of a single spectrum, it results from a set of spectra acquired at different gas pressures with exactly the same temperature, exploiting the relationship between the line-center absorbance and the integrated absorbance. Line fitting is performed by using the semiclassical model known as speed-dependent Voigt profile [6]. This model ensures a refined interpolation of the absorption spectra, thus providing the integrated absorbance and the line-center absorbance with a relative accuracy limited only by the signal-to-noise ratio. First results will be presented and the implications for an improved determination of k_B will be discussed.

References

[1] Ch. J. Bordé, Phil. Trans. Roy. Soc. A **363** (2005) 2177–2201.
[2] C. Daussy *et al.*, Phys. Rev. Lett. **98**, 250801 (2007).
[3] G. Casa, *et al.*, Phys. Rev. Lett. **100**, 200801 (2008).
[4] A. Castrillo, *et al.*, C. R. Phys. **10**, 894–906 (2009).
[5] A. Castrillo, *et al.*, Opt. Expr. **18**, 21851–21860 (2010).
[6] M. D. De Vizia, *et al.*, Phys. Rev. A, in press (2011).

Isotope effects in atomic negative ions: promises and challenges

T. Carette[1], M. R. Godefroid[2]

[1] *Department of Physics, Stockholm University, AlbaNova University Centre, SE-106 91 Stockholm, Sweden*
[2] *Laboratoire de Chimie Quantique et Photophysique, CP160/09, Université Libre de Bruxelles, Brussels, Belgium*

Corresponding Author: thomas.carette@fysik.su.se

Even though the spectroscopic information that we can extract from atomic negative ions (ANI) is limited, photodetachment spectroscopy allows investigating effects that are unique [1]. In the same way, the study of NIs structure by a theoretical approach offers stringent tests of the validity of the picture we have of an atom. Indeed, the balance between the one- and two-body interactions is changed in such system. The possibility of a neutral atom to bind an extra electron has often lead to fundamental interrogations on many-electron systems. Even if we do not have the possibility to explore large arrays of properties of isoelectronic sequences or rich negative ion spectra, the analysis of the periodicity and a-periodicity of electron affinity asks questions that lead to interesting observations [2, 3].

Recent works show that accuracy of the order of 10^{-3} cm^{-1} are achievable in the measurement of detachment thresholds of ANI [4]. It means that the ANIs spectroscopy is tackling an energy domain that was reached some decades ago in bound to bound state spectroscopy, an energy domain typical of isotope effects. Achieving sub-m^{-1} accuracy in traditional spectroscopy lead to many breakthroughs in atomic structure theory as well as in experimental nuclear physics [5]. That this point is being reached by ANIs spectroscopy suggests that we are at the verge of reaching a new understanding of these exotic systems.

It seems straightforward to wonder "what can we learn of the isotope shift on the electron affinity?" as the isotope shift is so much more sensitive to correlation than the energy itself, and in particular much more sensitive to core effects. We present the current status of research on isotope shift on negative ions. By combining experimental data, high accuracy MCHF results and a systematic analysis of the isotope shift on the electron affinity, some patterns can be isolated. We bring into focus the stakes involved in the study of isotope effects in negative ions.

References

[1] T. Andersen, Phys. Rep. **394**, 157–313 (2004).
[2] C. Froese-Fischer *et al.*, Phys. Rev. Lett. **59**, 2263–2266 (1987).
[3] W. Wijesundera and F. A. Parpia, Phys. Rev. A **57**, 3462–3468 (1998).
[4] W. Chaibi *et al.*, Eur. Phys. J. D **58**, 29–37 (2010), and references therein.
[5] J. Bauche and R.-J. Champeau, Adv. At. Mol. Phys. **12**, 39–84 (1976).

Coupling a single quantum bit to an ultra-cold Fermi sea

J. Goold[1,2], M. Fogarty[2], M. Paternostro[3], and Th. Busch[2]

[1] *Clarendon Laboratory, University of Oxford, United Kingdom*
[2] *Physics Department, University College Cork, Cork, Ireland*
[3] *Centre for Theoretical Atomic, Molecular and Optical Physics, Queen's University Belfast, Belfast BT7 1NN, UK*

Corresponding Author: thbusch@phys.ucc.ie

In the past decade ultra-cold quantum gases have emerged as ideal candidates for clean and controllable simulation of condensed matter physics [1]. The versatility of optical potentials combined with the possibility to tune the interparticle interaction strength using Feshbach resonances has already lead to a large number of seminal experimental demonstrations of fundamental quantum mechanical many body phenomena.

Here we demonstrate that another fundamental quantum mechanical many-body effect, the orthogonality catastrophe [2], plays an important role when considering ultracold, coupled systems. For this we consider the behaviour of a single quantum bit which is coupled to a low-dimensional, ultra-cold Fermi gas and show that an initial coherence in the qubit is quickly lost. This is due to the environmental monitoring that occurs in the form of scattering processes between the gas and the atom and we find that the exact dynamics of this process is strongly influenced by the effects of the orthogonality catastrophe within the gas.

We highlight the relationship between the Loschmidt echo and the retarded Green's function — typically used to formulate the dynamical theory of the catastrophe [3]— and demonstrate that the orthogonality catastrophe can be triggered and characterized via local operations on the qubit. Furthermore, we demonstrate how one may observe the expected broadening of the spectral function using Ramsey interferometry on the impurity qubit.

References

[1] I. Bloch, J. Dalibard, and W. Zwerger, Rev. Mod. Phys. **80**, 885 (2008).
[2] P. W. Anderson, Phys. Rev. Lett. **18**, 1049 (1967).
[3] P. Nozières and C. T. Dominicis, Phys. Rev. **178**, 1097 (1969).

Strong laser-induced-coupling between autoionizing states in the vicinity of four-photon excitation of Mg $3p^2\ ^1S_0$ resonance

A. Dimitriou[1], S. Cohen[1], and A. Lyras[1]

[1] *Department of Physics, University of Ioannina, 45110 Ioannina, Greece*
Corresponding Author: tasosdimitriu@yahoo.gr

A fairly recent study on single and double ionization of ground state Mg demonstrated a strong, non-perturbative, light-induced interaction between the $3p^2\ ^1S_0$ state with lower lying (bound) as well as higher lying (autoionizing) states [1]. As a result, that resonance is greatly red-shifted with respect to its zero field position. The latter was revealed by two-photon ionization spectroscopy [2, 3]. Additionally, two photons are absorbed above the 3s threshold, thus populating the Mg^+ 3p level after the system break-up. The above interaction was experimentally probed by recording the produced Mg^+ ions and the fluorescence yield from the ionic 3p→ 3s radiative decay [1]. Although the agreement between experiment and theory was found to be quasi-quantitative, it is evident that the most appropriate tools for shedding more light into the above phenomena are electron spectroscopy and photoelectron angular distribution (PAD) measurements. We shall present experimental data filling a part of that missing piece of information by examining the energy variation of the PADs across the four-photon-excited $3p^2\ ^1S_0$ resonance (Fig. 1). For the purpose of comparison we shall also present the relevant PADs, corresponding to two-photon excitation, for which just a single, on-resonance, measurement exists [3]. These latter measurements are found to be in good agreement with earlier theoretical calculations [4–6].

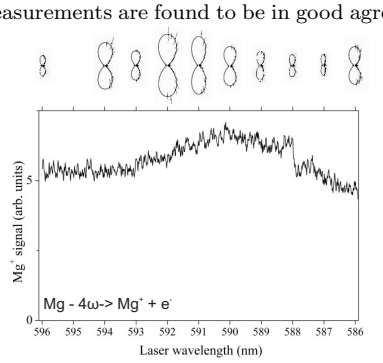

Figure 1: *Mg^+ spectrum recorded in the vicinity of the $3p^2\,^1S_0$ resonance and dependence of PADs drawn as polar plots of the same radial scale.*

Acknowledgments: The experiment was performed at the Central Laser Facility of the University of Ioannina. The research Project is co-funded by the European Union – European Social Fund (ESF) & National Sources, in the framework of the program "HRAKLEITOS II" of the "Operational Program Education and Life Long Learning" of the Hellenic Ministry of Education, Life Long Learning and religious affairs.

References

[1] I. Liontos, A. Bolovinos, S. Cohen, and A. Lyras, Phys. Rev. A **70**, 033403–1 (2004).
[2] R. E. Bonanno, C. W. Clark and T. B. Lucatorto, Phys. Rev. A **34**, 2082 (1986).
[3] Y. L. Shao, C. Fotakis and D. Charalambidis, Phys. Rev. A **48**, 3636 (1993).
[4] R. Moccia and P. Spizzo, J. Phys. B **21**, 1133–1143 (1988).
[5] E. Luc-Koenig, A. Lyras, J-M. Lecomte, M. Aymar. J. Phys B: At. Mol. Opt. Phys **30**, 5213 (1997).
[6] L. L. Nikolopoulos, Phys. Rev. A **71**, 033409–1 (2005).

Cavity electromagnetically induced transparency and all-optical switching with cold ion Coulomb crystals

M. Albert[1], A. Dantan[1], and M. Drewsen[1]

[1] *Danish National Research Foundation Center for Quantum Optics — QUANTOP Department of Physics and Astronomy University of Aarhus, 8000 Aarhus, Denmark*

Corresponding Author: malbert@phys.au.dk

Electromagnetically induced transparency (EIT) is a widely-used quantum interference effect to control the absorption and dispersion properties of a medium [1]. Enclosing an EIT medium in an optical cavity offers an enhanced interaction of the medium with well-defined spatio-temporal cavity field modes. This scenario can be exploited to realize high-efficiency quantum memories [2,3], as well as to enhance the "giant" non-linearities associated with EIT [4], and potentially produce spectacular non-linear effects at the few photon level [5].

Ensembles of ions, laser-cooled to form a Coulomb crystal and enclosed in an optical cavity, represent a near-ideal medium to investigate EIT phenomena, due to their excellent stability and controllable coherent coupling to the cavity field [6,7]. Here, we report on the first observation of cavity EIT with ion Coulomb crystals ($^{40}Ca^{+}$) [8]. We use a novel configuration where both the weak probe field (single photon level) and the more intense control field originate from the same laser and are resonant with the $3d^2D_{3/2} \leftrightarrow 4p^2P_{1/2}$ transition. Both the probe and the control field are injected into the cavity, but with opposite circular polarizations to address separate Zeeman sub-states of the $3d^2D_{3/2}$ level (pump: $m_J = -1/2$, probe: $m_J = +3/2$). In the collective strong coupling regime [6], we observe the predicted normal-mode splitting of the probe reflectivity spectrum, when the cavity and control fields are resonant with the atomic transition [8]. The central EIT feature reaches nearly perfect transparency, while at the same time having a width as low as a few tens of kHz. This is much narrower than the bare cavity linewidth ($\sim$ 2.2 MHz) and two orders of magnitude smaller than observed in previous cavity EIT experiments with neutral atomic ensembles [9,10].

In addition, this allows us to implement a cavity EIT-based, all-optical switching scheme in which the transmission of the probe field is controlled by an additional weak cavity field, close to resonance with the $3d^2D_{3/2} \leftrightarrow 4p^2P_{3/2}$ transition. We show that the EIT-enhanced nonlinear cross-phase modulation between probe (866 nm) and switching (850 nm) fields can be large enough to switch the cavity containing the EIT medium out of resonance for the probe field, thereby blocking its transmission. These results are a milestone for the realization of high-efficiency and long-lived quantum memories [2,3,11] as well as for performing nonlinear optics at low-light levels, e.g., for the realization of single photon quantum gates [12], single-photon transistors [13] or the observation of novel phase transitions for light [14].

References

[1] M. Fleischhauer, A. Imamoglu, and J. P. Marangos, Rev. Mod. Phys. **77**, 633–673 (2005).
[2] M. D. Lukin, S. F. Yelin, and M. Fleischhauer, Phys. Rev. Lett. **84**, 4232 (2000).
[3] A. Dantan and M. Pinard, Phys. Rev. A **69**, 043810 (2004).
[4] H. Schmidt and A. Imamoglu, Opt. Lett. **21**, 1936 (1996).
[5] A. Imamoglu *et al.*, Phys. Rev. Lett. **79**, 1467 (1997).
[6] P. F. Herskind *et al.*, Nature Phys. **5**, 494 (2009).
[7] A. Dantan *et al.*, Phys. Rev. A(R) **80**, 041802 (2009).
[8] M. Albert, A. Dantan, and M. Drewsen, submitted for publication. arXiv:1102.5010v1.
[9] G. Hernandez, J. Zhang, and Y. Zhu, Phys. Rev. A **76**, 053814 (2007).
[10] H. Wu, J. Gea-Banacloche, and M. Xiao, Phys. Rev. Lett. **100**, 173602 (2008).
[11] A. I. Lvovsky, B. C. Sanders, W. Tittel, Nature Photonics **3**, 706 (2009).
[12] C. Ottaviani *et al.*, Phys. Rev. Lett. **90**, 197902 (2003).
[13] K. M. Birnbaum *et al.*, Nature **436**, 87 (2005).
[14] M. J. Hartmann, F. G. S. L. Brandão, and M. B. Plenio, Nature Phys. **2**, 849 (2006).

Photodissociation of HeH^+ in the ground state: comparison with experiment

J. Lecointre[1], X. Urbain[1], J. Loreau[2], and N. Vaeck[3]

[1] *Institute of Condensed Matter and Nanosciences, Université catholique de Louvain, 1348 Louvain-la-Neuve, Belgium*
[2] *Harvard-Smithsonian Center for Astrophysics, Cambridge, USA*
[3] *Laboratoire de Chimie Quantique et Photophysique, Université Libre de Bruxelles, Belgium*
Corresponding Author: Julien.Lecointre@uclouvain.be

The HeH^+ helium-hydride molecular ion has been the subject of numerous works. By investigating the photodissociation process for both hot and cold ions, we will show that there exist significant discrepancies between the theoretical and experimental results. In 1986, van der Zande *et al.* [1] studied the dissociation of HeH molecules produced in the charge exchange between fast HeH^+ ions and an alkali vapor. First direct evidence was reported for hot HeH molecules being formed with large rotational and little vibrational excitation. In 2007, the first experimental data on the photodissociation of HeH^+ were obtained using the free-electron laser in Hamburg FLASH [2]. This experiment revealed the importance of $n \geq 3$ states in the photodissociation, as well as the major role of the Π states during dissociation. In 2010, Pedersen *et al.* [3] produced a source of cold ions by trapping the HeH^+ ions for about 100 ms before studying the photodissociation process so that they can be considered in their $v = 0$ level. For hot and cold ions, the authors measured the branching ratio between the two dissociation pathways as well as the relative contribution of the $^1\Sigma^+$ and $^1\Pi$ states.

In 2009, Sodoga *et al.* [4] computed total and partial photodissociation cross sections and showed the importance of the non-adiabatic couplings, but considered only states up to $n = 3$. Agreement with the experiment was difficult to obtain because the experimental rovibrational distribution of the HeH^+ ions was not known. In the present work, we determine the rovibrational distribution of the ions under experimental conditions of [2] and [3], and use it to compare the theoretical and experimental cross sections.

The vibrational population of a HeH^+ beam was analyzed by dissociative charge exchange, as a function of its trapping time in an electrostatic trap. This procedure allows for a full separation of the contributions of the three predissociated states of HeH* populated in the collision. The vibrational population of the Rydberg excited states of HeH closely reflects the vibrational population of the HeH^+ molecular ions. A predominant population of the $A\ ^2\Sigma^+$ and $B\ ^2\Pi$ states of HeH is expected and the population of the $C\ ^2\Sigma^+$ state should be less probable. The experimental spectra show the overlapping contribution of the rovibrational structure of the $A(v > 0)$ and $B(v - 1)$ states. Varying the trapping conditions, we can estimate the relative importance of the A and B states as well as the lifetimes of interest. We will attempt to find the various factors that could explain the conflicting experimental and theoretical results. In particular, we will argue that states with $n > 3$ should not play a major role in the photodissociation process at the experimental energy.

References

[1] W. J. van der Zande *et al.*, Phys. Rev. Lett. **57**, 1219 (1986).
[2] H. B. Pedersen *et al.*, Phys. Rev. Lett. **98**, 223202 (2007).
[3] H. B. Pedersen *et al.*, Phys. Rev. A **82**, 023415 (2010).
[4] K. Sodoga *et al.*, Phys. Rev. A **80**, 033417 (2009).

New ferroelectric materials studied by cold electron scattering

O. Plekan[1], A. Cassidy[1], R. Balog[1], N. C. Jones[2], and D. Field[2]

[1] *Department of Physics and Astronomy, Aarhus University, DK-8000 Aarhus C, Denmark*
[2] *Department of Physics and Astronomy and Institute for Storage Ring Facilities (ISA), Aarhus University, DK-8000 Aarhus C, Denmark*

Corresponding Author: plekan@phys.au.dk

CT

Recently we have discovered a new and rather remarkable physical phenomenon associated with thin films of material [1]. It has been found that films of nitrous oxide (N_2O) and other species deposited on polycrystalline gold harbour very large electric fields. These fields are a property of the film and appear spontaneously when films of species are laid down on a substrate. The fields point in a direction perpendicular to the surface and may exceed 10^8 V/m for N_2O films laid down at 38K. This finding, which shows itself by the spontaneous generation of a potential at the surface-vacuum interface, was attributed in [1] to dipole alignment between molecules in the film.

The potentials on film surfaces have been measured, as described in [1], by interrogating the surface with electron beams of lowest energy of < 5 meV, resolution $\sim$1.6 meV and maximum current typically of 200 fA, generated through threshold photoionization of Ar at 15.76 eV using synchrotron radiation from the ASTRID storage ring at Aarhus University [2].

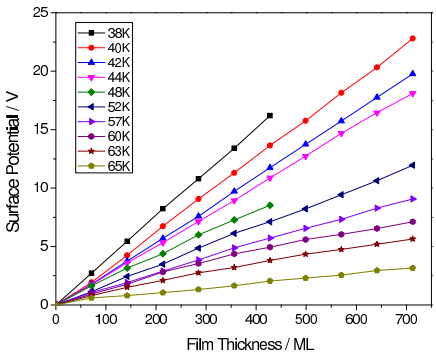

Figure 1: *Surface potentials measured for films of N_2O laid down at ten different deposition temperatures as indicated in the key. Films were accumulated through successive depositions of 71 ML.*

As an example, the variation of measured surface potential for N_2O layer thickness for films laid down at temperatures between 38K and 65K on polycrystalline gold is presented on Fig. 1. The near linear dependence of surface potential with film thickness at any temperature indicates an approximately constant electric field within the medium. Five further dipolar species, propane (0.08D), isopentane (0.13D), isoprene (0.25D), toluene (0.385D), CF_3Cl (0.5D) have been found to show ferroelectric order, establishing a new class of ferroelectric materials. Carbonyl sulphide (0.7D) however behaves in a non-ferroelectric manner and shows no electric field. A Curie temperature can be identified for example for isoprene. A mean field theory has been developed to reproduce the temperature dependence shown in the figure. The success of this approach gives considerable weight to the hypothesis that the mechanism of formation of the ferroelectric state is dipole alignment.

The discovery of this new type of ferroelectric material may have wide ranging applications in device and nano-technology and also influence the electrical nature of dust ice mantles in the interstellar medium.

References

[1] R. Balog *et al.*, Phys. Rev. Lett. **102**, 073003 (2009).
[2] S. V. Hoffmann *et al.*, J. P. Ziesel Rev. Sci. Inst. **73**, 4157 (2002).

Threshold behaviour in photodetachment of K^-

A. O. Lindahl[1], H. Hultgren[1,2], I. Yu. Kiyan[2], J. Rohlén[1], D. J. Pegg[3], C. W. Walter[4], and D. Hanstorp[1]

[1] *University of Gothenburg, SE-412 96 Gothenburg, Sweden*
[2] *Albert-Ludwigs-Universität Freiburg, 79104 Freiburg, Germany*
[3] *University of Tennessee, Knoxville, Tennessee 37996, USA*
[4] *Denison University, Granville, Ohio 43023, USA*

Corresponding Author: dag.hanstorp@physics.gu.se

The Wigner law [1] is a general model that describes the energy dependence of the break up of a system where the long range interactions decrease faster than $1/r^2$. Numerous photodetachment experiments when the residual atom is left in its ground state have been performed where the Wigner law has been successfully applied. The situation is different when the residual atom is left in an excited state. The increased polarizability gives a decreasing range of validity of the Wigner law.

We have investigated the threshold behavior for photodetachment of K^- leaving the residual atom in either K($5f$) or K($5g$). Both states have very large polarizabilities, but with opposite signs. Liu [2] has calculated these to be about 3.9×10^6 a.u. and -3.1×10^6 a.u., respectively.

The threshold in the K($5f$) channel is shown in Fig. 1a. At the threshold the cross section increase is almost like a step function. We attribute this behavior to the large polarizability and thus the strong attraction in the final state. In the K($5g$) channel, shown in Fig. 1b, we see a completely different behavior, with a very slow onset above threshold. In addition, we observe a resonance around 4.325 eV. In order to describe this threshold behavior we have developed a semiclassical model that takes the negative polarizability of the final state into account. This problem can be solved analytically for an induced dipole potential and we will show how the resulting cross section near threshold is given by $\sigma \propto \exp\left[CE^{1/4}\right]$, where E is the energy of the detached electron, and C is a constant proportional to $|\alpha|^{1/4}$ (α is the polarizability).

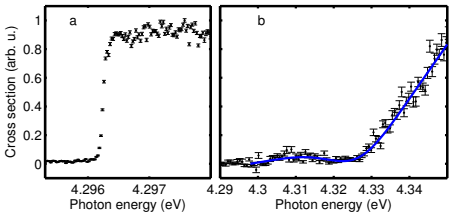

Figure 1: *Cross section at the opening of the K($5f$) (a) and K($5g$) (b) channels. The line is a fit of our proposed threshold model in combination with a resonance.*

The situation with the fast or slow onset depending on whether the interaction is repulsive or attractive is analogous to the situation in nuclear beta decay. In β^- decay the interaction is attractive, and the low end of the energy distribution looks much like the K($5f$) threshold. Similarly, the β^+ decay looks qualitatively like the K($5g$) threshold.

Financial support from the Swedish Research Council is acknowledged. CWW received support from the Wenner-Gren Foundation and from the Andrew W. Mellon Foundation.

References

[1] E. P. Wigner, Phys. Rev., **73**, 1002 (1948).
[2] C.-N. Liu, Phys. Rev. A, **64**, 052715 (2001).

Enhanced radiative recombination of U^{92+} ions with electrons in cold magnetized plasma

M. Pajek[1], D. Banaś[1], M. Czarnota[1], H. F. Beyer[2], F. Bosch[2], C. Brandau[2], S. Chatterjee[2], A. Gumberidze[2], S. Hagmann[2], C. Kozhuharov[2], D. Liesen[2], P. H. Mokler[2], A. Kumar[2], R. Reuschl[2], U. Spillmann[2], Th. Stöhlker[2,4], S. Tashenov[2], S. Trotsenko[2], P. Verma[2], S. Böhm[3], A. Müller[3], E. W. Schmidt[3], A. Surzhykov[4], J.–Cl. Dousse[5], J. Szlachetko[5], D. Sierpowski[6], and A. Warczak[6]

[1] *Institute of Physics, Jan Kochanowski University, 25-406 Kielce, Poland*
[2] *GSI Helmholtzzentrum für Schwerionenforschung, D-64291 Darmstadt, Germany*
[3] *Institut für Kernphysik, Justus-Liebig Universität, D-35392 Giessen, Germany*
[4] *Physikalisches Institut der Universität Heidelberg, D-69117 Heidelberg, Germany*
[5] *Department of Physics, University of Fribourg, CH-1700 Fribourg, Switzerland*
[6] *Institute of Physics, Jagiellonian University, 31-007 Cracow, Poland*

Corresponding Author: m.pajek@ujk.kielce.pl

We have recently proposed [1] new interpretation of the RR enhancement by attributing this effect to the "transverse" distant collisions, characterized by very large impact parameters, in the μm range, occurring in cold magnetized plasma. In the developed theoretical approach called the semiclassical geometrical model (SGM), which adopts the standard quantum mechanical RR cross sections to introduce a simplified concept of fully "absorbing" RR sphere, we demonstrate that the enhancement of RR in a magnetic field is caused by "transverse" distant collisions with large impact parameters, with cut-off value b_{max} depending on a strength of the B-field guiding the electron beam in the electron cooler.

Using this approach, with approximate b_{max} value for the weak B-field regime, we have shown the excess of RR rate due to the "transverse" distant collisions scales as:

$$\Delta\alpha \propto Z^{5/2} B^{1/2} / (T_\perp T_\parallel)^{1/2} / n^{5/4}, \tag{1}$$

which agrees with the RR excess rates scaling found in experiments at the TSR [2]. Moreover, this model predicts strong RR enhancement for low n-states, which was observed in x-ray RR experiment performed at the GSI for the K-shell [4]. It should be noted that for stronger magnetic fields this model predicts rather linear dependence on the B-field, i.e., $\Delta\alpha \propto B$, which was suggested in earlier RR experiment at the GSI [3]. For a better description of the RR enhancement we have performed the Monte Carlo simulations, based on the proposed approach, which predict more realistic B-field dependence and value of impact parameter cut-off. It should be noted that the absolute value of the RR enhancement predicted by the SGM is close to the observed one for the K-shell [4]. However, further Monte Carlo simulations involving the angular distributions of RR photons are needed in order describe in more details the measured RR enhancement for the K-shell.

This work was supported by the Polish Ministry of Science and Higher Education under Grant No. N N202 463539.

References

[1] D. Banaś *et al.*, 15th Int. Conf. on the Phys. of Highly Charged Ions, Shanghai, China, A-b38, (2010).
[2] G. Gwinner *et al.*, Phys. Rev. Lett. **84**, 4822 (2000).
[3] W. Shi *et al.*, Eur. Phys. J. D **15**, 145 (2001).
[4] D. Banaś *et al.*, Eur. Phys. J. ST **169**, 15 (2009).

Contributed Posters

AAP

AMO Physics at Large Facilities

Theoretical investigation of the lithium 2s-2p line broadened by ground hydrogen

N. Lamoudi[1], K. Alioua[2], M. Bouledroua[2], M. Aubert–Frécon[3], and A.–R Allouche[3]

[1] *Department of Physics, Badji Mokhtar University, Annaba, Algeria*
[2] *LPR, Badji Mokhtar University, Annaba, Algeria*
[3] *LASIM, Claude Bernard University, Villeurbanne, France*

Corresponding Author: boulmoncef@netscape.net

This work deals with the pressure broadening phenomenon which undergoes the lithium 2s-2p resonance line when perturbed by hydrogen. It is more concerned with the determination of the photo-absorption spectral profile and the effects of temperature on it. The quantum-mechanical calculations are performed by adopting the most reliable potentials and transition dipole moments. The potential and moment data points, as well as the long-range dispersion coefficients, are adopted from the most recent *ab initio* calculations. The quality of the constructed potentials and moments is assessed by estimating the radiative lifetimes of some excited rovibrational Li(2p)-H levels. The computational results show the sensitivity of the far wings on temperature and the appearance of a satellite structure in the red wing located around the wavelength 1015 nm. Similar theoretical calculations, based on semi-classical models, could find the satellite position close to the wavelength 980 nm.

(v, J)	This work	Ref. [1]
$(2, 3)$	32.6	29.4
$(5, 3)$	36.8	30.5
$(5, 5)$	36.9	
$(7, 12)$	39.0	36.9

Table 1: *Lifetime τ in ns of the molecular $A\ ^1\Sigma^+$ state.*

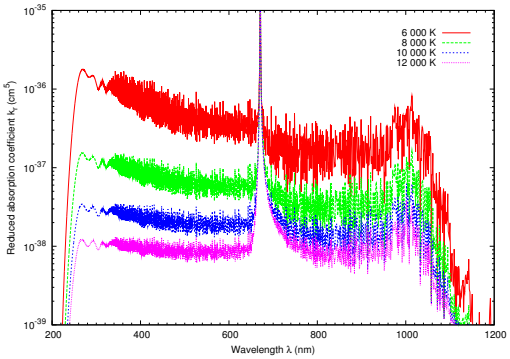

Figure 1: *Blue and red wings of the LiH absorption profiles and their behavior with temperatures.*

References

[1] P. J. Dagdigian, J. Chem. Phys. **64**, 2909 (1976).

Er:Yb:Glass oscillator (ERGO): a low-noise optical frequency comb for frequency metrology

N. Bucalovic[1], S. Schilt[1], V. Dolgovskiy[1], C. Schori[1], L. Tombez[1], G. Di Domenico[1], M. C. Stumpf[1,2], S. Pekarek[2], A. E. H. Oehler[2], T. Südmeyer[2], U. Keller[2], and P. Thomann[1]

[1] *Laboratoire Temps-Fréquence, Institut de Physique, Université de Neuchâtel, Av. de Bellevaux 51, CH-2000 Neuchâtel, Switzerland*
[2] *Department of Physics, Institute of Quantum Electronics, ETH Zürich, CH-8093 Zürich, Switzerland*

Corresponding Author: nikola.bucalovic@unine.ch

Optical frequency combs (OFC) have revolutionized the domain of frequency metrology by enabling a direct link between optical and microwave frequencies. Among the different comb technologies reported to date, Ti:sapphire and fiber lasers are the most established. Ti:sapphire combs are dominant in terms of noise properties, but are also associated with high costs and high complexity. Er-doped fiber lasers emitting in 1.5 μm optical telecommunication region have the advantage of robust diode-pumping as well as easy spectral broadening in novel highly nonlinear fibers. Unfortunately, due to their high gain and low-Q resonator, fiber-lasers come with higher level of quantum noise. In a promising approach, the advantages of mentioned technologies are being combined in SESAM-mode-locked diode-pumped solid state lasers (DPSSL).

Superior noise properties of a fully stabilized OFC generated from a diode-pumped Er:Yb:-glass laser oscillator (ERGO) in the 1.5 μm spectral region are presented alongside a commercial fiber-laser comb stabilized using a similar servo-loop bandwidth. Full stabilization of the ERGO comb is obtained by phase-locking both the carrier-envelope-offset (CEO) beat and the laser repetition rate to the same 10 MHz reference. The ERGO comb has the narrowest reported free-running CEO linewidth (3.6 kHz) at 1.5 μm. Due to the limited phase noise of the free-running CEO-beat, pump current feedback loop of moderate (5 kHz) bandwidth is sufficient to suppress the CEO linewidth. This results in a coherent peak in the CEO RF spectrum with only 0.75 rad-rms residual integrated phase noise and 25 dB SNR at 30 Hz resolution bandwidth [1]. The 20-fold smaller fractional frequency instability of the CEO-beat in the ERGO comb compared to the fiber-comb contributes only 10^{-15} to the optical carrier instability.

In case of comb stabilization to the H-maser, the frequency instability of the comb line is dominated by the contribution of the repetition rate noise. Even higher comb frequency stability can be achieved by locking one comb line directly to an ultra-stable optical reference. In that case, low-noise properties of ERGO comb CEO, compared to the Er-fiber comb in similar CEO locking conditions, is highly beneficial for the overall comb stability.

References

[1] M. C. Stumpf *et al.*, Appl. Phys. B **99**(3), 401–408 (2010).

Spatially resolved magneto-relaxation of magnetic nanoparticles using atomic magnetometry

N. Castagna[1], P. Knowles[1], A. Weis[1], I. Geissbühler[2], A. Petri–Fink[2], and G. Bison[3]

[1] *Department of Physics, University of Fribourg, CH-1700 Fribourg, Switzerland*
[2] *Department of Chemistry, University of Fribourg, CH-1700 Fribourg, Switzerland*
[3] *Department of Neurology, Friedrich–Schiller University, D-07740 Jena, Germany*
Corresponding Author: Natascia.Castagna@unifr.ch

Superparamagnetic iron oxide nanoparticles (SPIONs) that are biocompatible with human tissue are finding many novel diagnostic and therapeutic applications in medical health care. SPION samples have no net equilibrium magnetization. In an external magnetic field, the particles align their individual magnetic moments by physical rotation of the particles, so that a bulk magnetization is created. Once the magnetic field is switched off, the magnetization vanishes with a characteristic time dependence that reflects the particles' environment.

Relaxation times range from nanoseconds in liquids, to seconds, when the particles are bound to a solid surface. The relaxation parameters can be inferred from the time evolution of the magnetization, itself monitored by recording the very-weak associated magnetic field using highly sensitive magnetometers in a technique called magneto-relaxometry. With a single exception [1], magneto-relaxometry relies totally on SQUID magnetometers [2].

Our interest lies in the imaging capabilities of magneto-relaxometry. When functionalized, the SPIONs can be made to bind to specific morphological structures (tumors, organs) in biological tissue. The relaxation signals will thus carry information on the specific particles' macroscopic position and microscopic environment.

We will report on first magneto-relaxometry measurements made by a Cs atomic magnetometer array operated in a second order gradiometer configuration [3]. An extended sample of immobilized nanoparticles is magnetized by a magnetic pulse of several mT. After switching off the magnetizing field, the decay of the SPIONs magnetic field is recorded by the magnetometer array. Two-dimensional relaxation maps can be constructed from the discrete spatial distribution of relaxation times in an off-line analysis. These maps will reveal the structure of the biological entities to which the particles are bound [4].

We acknowledge financial support by the Swiss National Science Foundation (Sinergia grant No. CRSII2-130414-1).

References

[1] S. Knappe, T. H. Sander, O. Kosch, F. Wiekhorst, J. Kitching, and L. Trahms, Applied Physics Letters **97**, 133703-1–133703-3 (2010).
[2] R. Kötitz, P. C. Fannin, and L. Trahms, J. Mag. Magn. Mater. **49**, 42–46 (1995).
[3] G. Bison, N. Castagna, A. Hofer, P. Knowles, J. L. Schenker, M. Kasprzak, H. Saudan, and A. Weis, Applied Physics Letters **95**, 173701-1–173701-3 (2009).
[4] H. Richter, M. Kettering, F. Wiekhorst, U. Steinhoff, I. Hilger, and L. Trahms, Physics in Medicine and Biology **55**, 623–633 (2010).

Laser-induced cesium lithography

W. Soares Martins[1], T. Passerat de Silans[1], I. Vidal[1], M. Oriá[1], and M. Chevrollier[1]

[1] *Laboratório de Espectroscopia Ótica, Universidade Federal da Paraíba, Cx Postal 5086, João Pessoa 58051-900,PB, Brazil*

Corresponding Author: martine@otica.ufpb.br

Interaction processes between atoms and surfaces are increasingly accessible experimentally, due to the development of new investigation tools, and of crucial importance in the development of new material devices, which are now routinely reaching submicron dimensions. Understanding and controlling the process of atom adsorption on surfaces has fundamental appeal and applied value. Neutral-atom sub-micron lithography is one possible application of atom-surface interaction control. Neutral atoms close to a nondispersive surface are attracted to the surface through the van der Waals interaction, and repelled at short range (atomic dimensions) by Pauli repulsion between atomic and surface electrons. The composition of these two terms yields a potential well with a minimum located a few nanometers from the surface. The process of adsorption, whereby free atoms get trapped into the potential well and escape after a mean adsorption time, occurs spontaneously through energy exchanges between free atoms and surface phonons, but systematic loading of the well requires third part intervention, either collisions or light [1,2]. We use such loading of the surface well as a method of nanofabrication to produce patterns on a dielectric surface. The technique consists in illuminating the interface between a dielectric substrate and an atomic vapor with a strong pump laser with a frequency close to an atomic transition frequency. The atoms accumulate in the surface well, forming a film whose local characteristics depend on the surface temperature, atomic vapor density and laser power, allowing the possibility of being modulated with the light spatial profile. We discuss the merits of this lithographic technique and show examples of the patterns obtained.

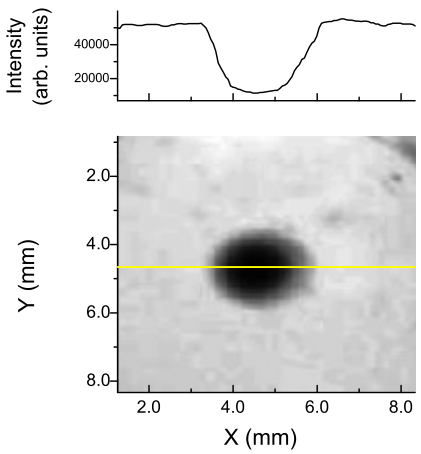

Figure 1: *Typical cesium film formed on a glass window and its thickness profile, reproducing the Gaussian intensity profile of the inducing laser beam.*

References

[1] T. Passerat de Silans *et al.*, Appl. Phys. B **82**, 367–371 (2006).
[2] A. E. Afanasiev, P. N. Melentiev, and V. I. Balykin, JETP Lett. **86**, 172–177 (2007).

All-optical low-noise microwave generation from a 1.5 μm ultra-stable laser

V. Dolgovskiy[1], S. Schilt[1], G. Di Domenico[1], C. Schori[1], and P. Thomann[1]

[1] *Laboratoire Temps-Fréquence, Université de Neuchâtel, 2000 Neuchâtel, Switzerland*
Corresponding Author: vladimir.dolgovskiy@unine.ch

An all-optical ultra-stable microwave oscillator is being developed with a target short-term frequency instability of 10^{-15} at 1 s, with a further $1/\tau$ decrease up to a few hundreds of seconds. We have realized an optical frequency reference by stabilizing an extended cavity diode laser to a high-finesse ($\approx 200\,000$) ultra-low thermal expansion (ULE) Fabry-Perot cavity using the Pound-Drever-Hall locking technique. The horizontally-mounted cavity has a resonance width of 8.1 kHz, experimentally determined from the cavity ring-down time. With a servo loop bandwidth of 1 MHz, the linewidth of the laser relative to the cavity is suppressed, as shown by the frequency noise of the in-loop error signal (Fig. 1). The residual servo loop noise thus contributes only $< 10^{-15}$ (@ 1 s) to the laser instability, which will be limited by the cavity length fluctuation only.

The relative frequency stability of the laser is transferred to the microwave domain using an optical frequency comb. Preliminary attempts of microwave generation using a simple scheme to lock one comb line to the laser have shown a fractional frequency instability of the comb repetition rate at the level of 3×10^{-13} (@ 1 s), limited by the reference used in the stability evaluation.

A detailed characterization of the thermal response of the cavity placed in a vacuum chamber with a dedicated thermally-isolating enclosure will also be presented.

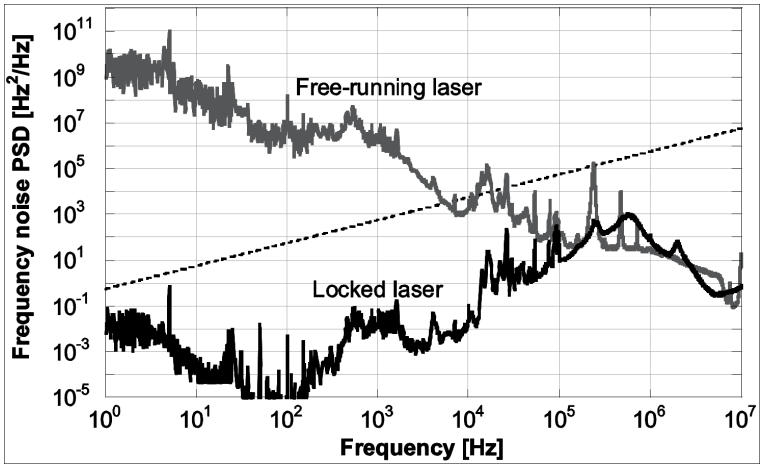

Figure 1: *Frequency noise spectrum of the extended cavity diode laser (free-running and locked to the ULE cavity).*

Investigation on a coupled dark state magnetometer

M. Ellmeier[1], R. Lammegger[1], A. Pollinger[2], W. Magnes[2], and L. Windholz[1]

[1] *Institute of Experimental Physics, Graz University of Technology, 8010 Graz, Austria*
[2] *Space Research Institute, Austrian Academy of Sciences, 8042 Graz, Austria*

Corresponding Author: michaela.ellmeier@tugraz.at

The coupled dark state magnetometer is a new type of magnetometer. Its working principle is based on the coupling of two coherent population trapping (CPT) resonances.

CPT is a quantum interference effect, which in the simplest case is prepared by a coupling of an atomic three level excitation system via a bichromatic laser field. As a consequence of this coupling, the atomic population is trapped in a so called dark state, which is stable against absorption. The benefit of the CPT effect is that the corresponding CPT resonances can have line widths down to 30 Hz in the best case. Hence, they are well suited for precision measurements like magnetometry or CPT atomic clocks.

The required excitation schemes are prepared in the hyperfine structure of the ^{87}Rb D_1 line within a buffered thermal vapor cell. Caused by the coupling of the two CPT resonances the magnetic field measurement is independent of a temperature change. However, the height and width of the CPT resonances are dependent on the cell temperature. Therefore, the choice of a proper cell temperature can increase the signal-to-noise ratio and enhance the sensitivity of the magnetometer.

Improvements of the Hg cohabiting magnetometer for the nEDM experiment at PSI

M. Fertl[1]
For the PSI nEDM collaboration
[1] *Paul Scherrer Institute, 5232 Villigen, Switzerland*
Corresponding Author: martin.fertl@psi.ch

The standard model (SM) of particle physics predicts a static electric dipole moment for the neutron (nEDM), breaking time reversal and parity symmetry. This prediction is several orders of magnitude below the current best experimental limit $d_n < 2.9 \times 10^{-26} e \cdot cm$ (90% CL) [1]. However, several extensions of the SM predict values for the nEDM in the current range of experimental sensitivity. An experiment [2] at the new ultra-cold neutron (UCN) source at the Paul Scherrer Institute (PSI), Switzerland, aims at a factor of five improved sensitivity. Ultimately, the collaboration pursues the goal to improve the sensitivity by another factor of 10. The experiment employs Ramsey's method of separated oscillatory fields to detect a Larmor frequency shift for the UCN in a parallel and an anti-parallel configuration of a magnetic and an electric field. The transmission modulation of a circularly polarized light beam is used to detect the spin precession of a spin polarized ensemble of ^{199}Hg atoms in the same volume as the UCN and thus to measure the applied magnetic field ($\approx 1\ \mu$T). I will present recently achieved improvements of this co-magnetometer. In addition I will present ideas how to further improve this magnetometry technique by using a laser as light source.

References

[1] C. A. Baker *et al.*, Phys. Rev. Lett. **97**, 131801 (2006).
[2] http://nedm.web.psi.ch

High-sensitivity large-area cold atom gyroscope

C. L. Garrido Alzar[1], T. Lévèque[1], M. Meunier[1], F. Pereira Dos Santos[1], and A. Landragin[1]

[1] *LNE-SYRTE, Observatoire de Paris, CNRS, UPMC*
61 avenue de l'Observatoire, 75014 Paris, France

Corresponding Author: carlos.garrido@obspm.fr

The implementation of high precision atomic inertial sensors has made possible applications not only in the field of navigation, but also in areas of fundamental research such as general relativity, geodesy, and metrology. To carry different studies in these fields, we have developed a gyroscope based on cold atom interferometry [1]. In contrast with previous experimental realizations, emphasis was placed on the long term stability and compactness of the device, resulting from the use of laser cooled atoms. Moreover, it has been designed to give access to all six axes of inertia [2] (the three components of acceleration and of that of rotation).

The sensitivity to acceleration is 5.5×10^{-7} m·s^{-2} at one second, limited by residual vibration on our isolation platform. Concerning the rotation, the sensitivity is 2.4×10^{-7} rad $\cdot$ s^{-1} @ 1s, which is at the level of the quantum projection noise due to the finite number of atoms. After 1000 seconds of integration time, we achieve a sensitivity of 1×10^{-8} rad·s^{-1}. We have studied in detail the different sources of systematic effects, which are mainly due to laser-atom interactions [1,3]. The main limitation to the long term performances has been clearly identified to be linked to fluctuations of the atomic trajectories because of Raman laser wave-front distortions. Finally, the accuracy of our gyroscope has been characterized in term of bias and scaling factor.

A new experiment, based on a four pulse configuration [2] is now under study. It enables a huge increase of the enclosed physical area of the interferometer (by a factor 300 compared to the first one ~ 4 mm^2) reaching 11 cm^2 in this new apparatus. Further increase of the area can be obtained by using more efficient Raman beam splitters, a procedure that has been recently demonstrated [4]. This new experiment should push the limits of such gyroscope and open new fields of application, as for instance, the study of the Earth rotation rate short-term fluctuations.

References

[1] A. Gauguet, *et al.*, Phys. Rev. A **80** 063604 (2009).
[2] B. Canuel, *et al.*, Phys. Rev. Lett. **97** 010402 (2006).
[3] A. Gauguet, *et al.*, Phys. Rev. A **78** 043615 (2008).
[4] T. Lévèque, *et al.*, Phys. Rev. Lett. **103** 080405 (2009).

A setup for investigation of VUV transitions of iron group elements for astrophysical applications using synchrotron radiation at MAX-lab, Sweden

H. Hartman[1], H. Nilsson[1], S. Huldt[1], R. Blackwell–Whitehead[1], T. Lennartsson[1], E. Bäckström[2], S. Mannervik[2], and S. Ristinmaa Sörensen[3]

[1] *Lund Observatory, Lund University, Box 43, SE-22100 Lund, Sweden*
[2] *Department of Physics, Stockholm University, SE-106 91 Stockholm, Sweden*
[3] *Department of Physics, Lund University, SE-221 00 Lund, Sweden*

Corresponding Author: Henrik.Hartman@astro.lu.se

We are developing an experimental station at the gas-phase branch line at the 6.65 m normal incidence beam line at I3, MAX-lab, Sweden. It is used to investigate free metal atoms and ions in plasma phase. The sample ions are produced in a hollow cathode discharge lamp, which is illuminated by the synchrotron radiation producing absorption when in resonance with the atomic lines. The synchrotron light is scanned in energy building up an absorption spectrum. Contributions from intrinsic light of the discharge are minimized through geometrical, spectral and temporal filters.

The project's major goal is to measure transition rates (or oscillator strengths) for specific lines in the spectrum of ionized iron, Fe II lines, at vacuum UV wavelengths, 100–130 nm. These transitions are important for many astrophysical applications, e.g., in objects where line fluorescence is prominent, as well as stars observed in the ultraviolet FUSE and HST/STIS region. Level mixing make several of these levels uncertain to calculate. In this wavelength region many other iron-group element ions have important transitions, which will be measured in future projects.

Iron lines are of great importance in analysis of stars and nebulae, not only for abundance studies, but also for diagnostics of the plasma conditions and derivation of physical properties such as temperature, electron density and radiation field.

We describe the experimental setup at the I3 beam line at MAX III, and the early results.

Scalar and vector Cs magnetometer for an nEDM experiment

M. Kasprzak[1], Z. Grujić[1], P. Knowles[1], and A. Weis[1]
For the PSI nEDM collaboration
[1] *Department of Physics, University of Fribourg, CH-1700 Fribourg, Switzerland*
Corresponding Author: Malgorzata.Kasprzak@unifr.ch

The search for a nonzero electric dipole moment (EDM) of the neutron is of primary importance in fundamental particle physics. Experimentally, for neutrons precessing in a small constant magnetic field, the EDM expresses itself as a shift in the precession frequency induced by an electric field which is applied alternately parallel and anti-parallel to the magnetic field. The frequency shift is measured using Ramsey's method of time separated oscillating fields. Any difference in the neutron's Larmor precession frequencies between measurements in the two field alignment geometries indicates the presence of an EDM. To achieve sensitivities to EDM's of a few times 10^{-28} e $\cdot$ cm (the current target needed to advance the field), the primary offset magnetic field, including all its spatial gradients, has to be precisely measured and controlled.

To provide the required sensitivity of magnetic field measurements at the <100 fT/$\sqrt{\text{Hz}}$, a system of sensors based on the optically–pumped atomic Cs magnetometer has been developed at Fribourg University. The Cs sensor itself is based on a spherical, paraffin-coated and evacuated glass cell containing Cs vapour at standard ambient temperature. The magnetometers require laser light of 894 nm to magnetize the atoms in the vapour by orienting their spins, and thus the magnetic moments, via optical pumping. Magnetic resonance via a small applied magnetic field oscillating at the Larmor frequency is used to drive spin precession which has as consequence that the light power transmitted through the sample becomes modulated in a phase-synchronous manner to the applied magnetic field. The modulation and its drive-to-response phase is extracted using phase sensitive detection, from which information on the magnetic field is deduced.

The present magnetometer system consists of eight vacuum compatible and four both vacuum and high voltage compatible sensors. The system is in constant evolution to adapt it to the operating environment of the nEDM experiment at the Paul Scherrer Institut in Villigen, Switzerland. Recently, the sensor geometry has been modified to provide true scalar devices [1], and steps towards extending the device from scalar to vector measurements have been made. In this contribution, results of magnetic field measurements *in situ* as well as the comparative behaviour of different sensor geometries will be presented. The initial results on vector magnetometry (based on the techniques proposed in [2]) will be shown.

References

[1] A. Weis, "rf projection phase error in Cs OPMs", Internal report, University of Fribourg.
[2] E. B. Alexandrov *et al.*, Meas. Sci. Technol. **15**, 918–922 (2004).

Depth profiling of low energy P, In, and Sb implants using synchrotron radiation based high-resolution micro-GEXRF

Y. Kayser[1], D. Banaś[2], W. Cao[1], J.–Cl. Dousse[1], P. Hönicke[3], J. Hoszowska[1], P. Jagodziński[2], A. Kubala–Kukuś[2], S. H. Nowak[1], M. Pajek[2], and R. Unterumsberger[3]

[1] *Department of Physics, University of Fribourg, CH-1700 Fribourg, Switzerland*
[2] *Institute of Physics, Jan Kochanowski University, 25-406 Kielce, Poland*
[3] *Physikalisch-Technische Bundesanstalt, D-10587 Berlin, Germany*

Corresponding Author: yves.kayser@unifr.ch

The characterization of a sample's near-surface properties with x-ray fluorescence (XRF) techniques can be realized by irradiating the latter with a monochromatic x-ray beam at grazing incidence angles (GIXRF) or by observing the emitted x rays at grazing emission angles (GEXRF). The detected XRF signal depends strongly on the incidence, respectively, emission angle, defined relative to the sample surface. Indeed the probed depth region, which extends from the sample surface into the bulk, changes significantly with the angle, varying from a few nm to several hundred nm. The limiting factors to the probed depth region are the surface reflectivity and the absorption of the incident x-ray beam for GIXRF setups, and the surface transmittivity and the self-absorption of the emitted x rays for GEXRF setups. The x-ray absorption is quite pronounced in the sample's depth direction due to the shallow incidence/emission angles.

The variation of the probed depth region with the incidence/emission angle permits nanometer resolution depth-profiling measurements by using GIXRF [1] and GEXRF [2]. Ultra shallow junctions, realized with low implantation energies, decrease the leakage currents in nano-sized semiconductor devices. To support further progress in semiconductor technologies depth-profiling of implanted dopants is needed. Compared to other depth-profiling techniques, x-ray fluorescence based methods offer the advantage to be non-destructive and to permit the quantitative determination of depth profiles located within the first nanometers below the surface or buried deeper inside the wafer.

Besides the geometry, the main difference between GIXRF and GEXRF is the solid angle of detection which is considerably lower for the GEXRF setup due to the requirements on the angular resolution and angular accuracy which should be ideally of the order of 0.01° and 0.005°, respectively [3]. Consequently, wavelength-dispersive detection setups can be used in combination with GEXRF without significant loss of the detection efficiency. High-resolution x-ray detection offers a much better separation of the fluorescence lines, which is very useful in the case of multielemental samples, and is very sensitive to the elemental chemical state. In addition, only GEXRF can profit from focused incident x-ray beams to realize 2D spatial mappings of the sample surface with μm-resolution.

The presented GEXRF depth-profiling measurements were performed at the ESRF, using the Fribourg high-resolution von Hamos bent-crystal spectrometer [4]. The monochromatic x-ray beam delivered by the ID21 beamline was focused by polycapillary optics installed in front of the sample. The depth-profiles of In and Sb ions implanted in Si (fluence 5×10^{14} at./cm^2; implantation energies 1, 2, and 4 keV) and of P ions implanted in Si and Ge (fluence 5×10^{15} at./cm^2; implantation energies 1, 2, 4, 6, 8 keV) could be retrieved and compared to calculations. The lateral homogeneity of the implanted fluence was checked with μm resolution and the transmission efficiency for the employed synchrotron beam energies was experimentally derived.

References

[1] P. Hönicke *et al.*, Anal. Bioanal. Chem. **396(8)**, 2825–2832 (2010).
[2] Y. Kayser *et al.*, Spectrochim. Acta B **65**, 445–449 (2010).
[3] R. Klockenkämper, *Total Reflection X-Ray Fluorescence Analysis*, Wiley, New York, (1997).
[4] J. Hoszowska *et al.*, Nucl. Instrum. Methods Phys. Res. A **376**, 129–138 (1996).

Optical techniques for measuring the nuclear polarization of ^{3}He gas

C. Talbot[1], M. Batz[1,2], P.–J. Nacher[1], and G. Tastevin[1]

[1] *Laboratoire Kastler Brossel, ENS, CNRS, UPMC, 24 rue Lhomond, F-75005 Paris, France*
[2] *Johannes Gutenberg University, Staudingerweg 7, D-55128 Mainz, Germany*

Corresponding Author: nacher@lkb.ens.fr

Metastability exchange optical pumping (ME OP) is an efficient technique capable of producing highly polarized ^{3}He in large volumes for a wide range of applications. A weak rf discharge is sustained in the gas to populate electronically excited states, with a radiative cascade ending as the metastable 2^3S_1 state on which OP is performed (using the 2^3S–2^3P transition at 1083 nm). Due to hyperfine coupling in the 2^3S state, entangled electronic and nuclear orientations are produced when circularly polarized pumping light is absorbed. With the strong coupling to the nuclear orientation of the ground state enforced by ME collisions, the angular momentum of the absorbed light is eventually transferred to the ground state where nuclear polarization is obtained with a high overall photon efficiency. Nuclear polarization in the ground state can be assessed by direct magnetic measurements (using DC magnetometry or NMR), or can be inferred from optical measurements taking advantage of the rf discharge required by ME OP.

Optical measurement techniques include polarimetry of selected spectral lines. From nuclear spin conservation during atom excitation and to hyperfine coupling in all states involved in the radiative cascades, the polarization of the glow light emitted by the plasma reflects the nuclear polarization of the ground state [1–3]. Although easy to implement, its sensitivity depends on gas pressure and on applied magnetic field, and is significantly reduced above 10 mbar or 10 mT.

Another optical technique involves absorption measurements of a weak probe beam tuned to a suitable component of the same 2^3S–2^3P transition that is used for ME OP. It relies on the fact that ME tends to enforce the spin-temperature distribution of populations among the sublevels of the probed 2^3S state that corresponds to the ground state nuclear polarization. The absorption method has been demonstrated by several groups using a He lamp [4–6], then a laser [2], as the probe source. A longitudinal configuration (probe beam along the applied field) [4–6], and a transverse configuration [2,6] have both been used in the early days of ME OP.

With the use of high-power OP lasers that significantly affect the ME-enforced distribution of populations, and with the extension of ME OP experiments to high magnetic fields and high gas pressures (up to several Tesla and several 100 mbar)[7,8], longitudinal and transverse absorption techniques have been systematically revisited. We compare implementations at low and high magnetic fields, and report on dedicated tests performed in small sealed He cells filled with pure ^{3}He gas or isotopic gas mixtures [9]. For a wide range of experimental conditions, we quantitatively discuss the most relevant identified sources of systematic errors in polarization measurements, e.g., the effects of an intense pump beam; of the probe beam power, intensity, or detuning; of traces of ^{4}He in ^{3}He; of absorption line broadening at high pressures; etc. We finally present the pros and cons of these optical techniques and compare them to the other established methods mentioned above.

References

[1] M. Pavlovic and F. Laloë, J. Phys. France **31**, 173–194 (1970).
[2] N. P. Bigelow, P.-J. Nacher and M. Leduc, J. Phys. II France **2**, 2159–2179 (1992).
[3] E. Stoltz *et al.*, Appl. Phys. B **63**, 635–640 (1996).
[4] F. D. Colegrove, L. D. Schearer and G. K. Walters, Phys. Rev. **132**, 2561–2572 (1963).
[5] R. C. Greenhow, Phys. Rev. **136**, A660–A662 (1964).
[6] J. M. Daniels and R. S. Timsit, Can. J. Phys., **49**, 539–544 (1971).
[7] M. Abboud *et al.*, Europhys. Lett. **68**, 480–486 (2004).
[8] A. Nikiel *et al.*, Eur. Phys. J. Special Topics **144**, 255-263 (2007).
[9] C. Talbot *et al.*, *to be published in* Journal of Physics: Conference Series (2011).

Thermo-optical effects on the transduction of mechanical motion of a microspherical pendulum

S. Nic Chormaic[1,2], Y. Wu[1,2], and J. Ward[1,3]

[1] *Physics Department, University College Cork, Cork, Ireland*
[2] *Photonics Centre, Tyndall National Institute, Prospect Row, Cork, Ireland*
[3] *Nano-Optik, Institut für Physik, Humboldt Universität zu Berlin, 10117 Berlin, Germany*
Corresponding Author: s.nicchormaic@ucc.ie

Cavity optomechanics has been of great interest over the past five years due to the promises it offers for studying quantum mechanical effects on macroscopic systems. Dynamical back-action cooling of optomechanical devices makes displacement sensors with a sensitivity approaching the standard quantum limit possible [1]. Cavity-enhanced optical forces are also very promising for building all optical controlled switches and filters in photonic circuits [2]. We have successfully fabricated micropendulums, or cantilevers, made from a microsphere attached to a tapered fibre stem as alternative devices for studying cavity optomechanics.

Silica microspherical pendulums are evanescently coupled to a tapered optical fibre to study thermo-optical effects on their motion. The motion is detected as variations in the transmitted laser power through the tapered fibre. Low frequency (less than 2 kHz) mechanical resonances of the pendulum are observed by taking a fast Fourier transform (FFT) of the transmitted laser power. The thermal damping and amplification of the taper/pendulum coupling noise is investigated and we show how the motion driven thermal feedback affects the mechanical spectrum of the pendulum (Fig. 1). Microspherical pendulums, with low mechanical spring constant, could be used for studying nanoscopic optical and mechanical forces, and optical cooling.

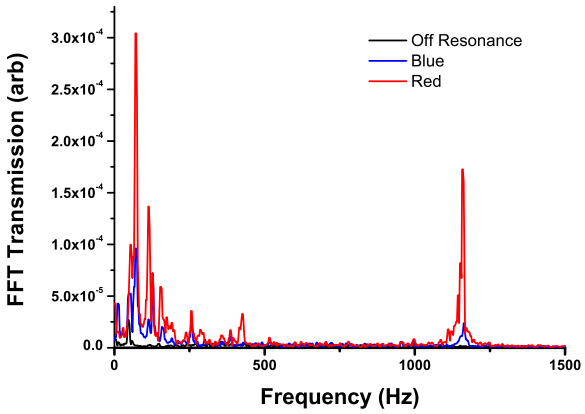

Figure 1: *Mechanical modes of the microsphere pendulum when the light in the fibre is off, blue, and red detuned relative to the sphere resonance.*

References

[1] T. J. Kippenberg, and K. J. Vahala, Opt. Express **15**, 17172–17205 (2007).
[2] J. M. Ward, Y. Wu, V. G. Minogin, and S. Nic Chormaic, Phys. Rev. A **79**, 053839 (2009).

Effects of the sample surface roughness in grazing emission x-ray fluorescence measurements

S. H. Nowak[1], Y. Kayser[1], D. Banaś[2], W. Cao[1], K. Deja[2], J.–Cl. Dousse[1], J. Hoszowska[1], M. Pajek[2], and J. Szlachetko[2,3]

[1] *Department of Physics, University of Fribourg, CH-1700 Fribourg, Switzerland*
[2] *Institute of Physics, Jan Kochanowski University, 25-406 Kielce, Poland*
[3] *European Synchrotron Radiation Facility, F-38043 Grenoble, France*

Corresponding Author: stanislaw.nowak@unifr.ch

We report on the influence of the sample surface roughness on the grazing emission x-ray fluorescence (GEXRF) from thin layers. Samples consisting of 5 nm-thick films of Al, MgO, Fe, and Cr deposited on Si substrates were examined. By varying the growth temperature of the layers and/or applying post-growth annealing, samples with different surface morphologies changing from uniform layers of constant thickness to nm-size islands were obtained. The surface morphology of each sample was first characterized using the atomic force microscopy imaging technique. The sample surfaces were then examined by means of the synchrotron radiation-based high-resolution GEXRF technique, measuring the Kα x-ray lines of Mg, Al, Fe, and Cr with the high-resolution von Hamos Bragg-type bent crystal spectrometer of Fribourg [1] installed at the ESRF beam line ID21 [2]. The measured GEXRF angular profiles were found to exhibit a strong dependence on the surface roughness.

The operational principle of the GEXRF technique [3,4] consists in measuring the intensity evolution of an x-ray fluorescence line around its critical angle for total reflection φ_c. In general, three well described types of GEXRF angular profiles are observed which depend on the sample morphology (bulk-like, layer-like and particle-like) [4]. For samples with a bulk-like structure the emitted radiation is refracted once at the vacuum-bulk interface and the evolution of the GEXRF angular profile follows approximately the variation of the transmission coefficient. For layer-like samples multiple reflections are expected for the emission angles above φ_c, resulting in the occurrence of interference fringes in the detected fluorescence. For samples with a particle-like structure, the angular profile results from the sum of the direct and singly reflected radiation. Thereby, the x-ray intensity is doubled below the critical angle φ_c corresponding to the substrate.

Above mentioned angular profiles assume structures with ideal, flat interfaces. For real samples the roughness of the sample surface should also be considered. In the literature the roughness is taken into consideration as a small perturbation of the interface potential (Nevot-Croce model) [5], as a stack of layers with reduced average densities [5], or as a composition of layers of different thicknesses [6]. These models are reliable for samples characterized by small and moderate roughness. However, they cannot be used for surfaces with large roughness [7], for nonuniform layers with highly correlated height distributions [7], or for particle-like structures, when the fluorescence x rays pass through several successive islands along the sample surface [8]. In the present work the reliability of the above mentioned roughness models was probed with the measured GEXRF angular profiles. In particular, the applicability of these models was tested in their limit; i.e., for the case of nm-size island structures.

References

[1] J. Hoszowska *et al.*, Nucl. Instrum. Methods Phys. Res. A **376**, 129–138 (1996).
[2] J. Szlachetko *et al.*, J. Appl. Phys. **105**, 086101 (2009).
[3] R. S. Becker, J. A. Golovchenko, and J. R. Patel, Phys. Rev. Lett. **50**, 153–156 (1983).
[4] H. P. Urbach and P. K. de Bokx, Phys. Rev. B **53**, 3752–3763 (1996).
[5] L. Nevot, B. Pardo, and J. Corno, Rev. Phys. Appl. **23**, 1675–1686 (1988).
[6] K. Tsuji, S. Sato, and K. Hirokawa, Thin Solid Films **274**, 18–22 (1996).
[7] D. K. G. de Boer, Phys. Rev. B **49**, 5817–5820 (1994).
[8] K. Tsuji *et al.*, J. Appl. Phys. **78**, 969–973 (1995).

Identification of gamma radiation treatment of anticancer drug 5-fluorouracyl by electron paramagnetic resonance

Ş. Osmanoğlu[1], Y. Dicle[2]

[1] *Department of Physics, University of Dicle, 21280 Diyarbakır, Turkey*
[2] *Ziya Gökalp Education Faculty, Department of Physics, University of Dicle, 21280 Diyarbakır, Turkey*

Corresponding Author: sems@dicle.edu.tr

Electron paramagnetic resonance (EPR) measurements proved that paramagnetic species are simultaneously present in powder of anticancer drug 5-Fluorouracyl and these paramagnetic species generated at different absorbed doses (1-25 kGy) obtained through the double integrated of the experimental spectra.

Exponential and bi-exponential functions were used to fit EPR signal/dose curves. It was found that exponential and bi-exponential function provide satisfactory results without correction of absorbed dose depending on EPR signal intensity and decay of free radicals respectively.

The stability of gamma radiation induced EPR signal intensity of gamma irradiated 5-Fluorouracyl was detected over a storage period of six months. The limits of detection of free radicals after irradiation 25 kGy are approximately six months 5-Fluorouracyl. This permitted the discrimination of irradiated 5-Fluorouracyl from nonirradiated.

High-spatial-resolution monitoring of strong magnetic field using Rb nano-thin cell

A. Papoyan[1], D. Sarkisyan[1], G. Hakhumyan[1,2], C. Leroy[2], and Y. Pashayan–Leroy[2]

[1] *Institute for Physical Research, NAS of Armenia, Ashtarak, 0203, Armenia*
[2] *Laboratoire Interdisciplinaire Carnot de Bourgogne, UMR CNRS 5209 – Université de Bourgogne, F-21078 Dijon Cedex, France*

Corresponding Author: aram.papoyan@gmail.com

We report the results of implementation of the so-called λ-Zeeman technique (LZT) to investigate individual hyperfine transitions between Zeeman sublevels (optical domain) of Rb atoms in a strong magnetic field in the range of 10–5000 G. LZT is based on nanometric thin cell (NTC) resonant transmission spectrum of thickness $L = \lambda$, where λ is the resonant wavelength 794 nm for Rb D_1 line [1]. Narrow VSOP resonances (of ∼20 MHz linewidth) in the NTC transmission spectrum (easily obtainable with a diode-laser radiation) are split into several components in a magnetic field; their frequency positions and transition probabilities depend on B field. The examination of the VSOP resonances formed in the NTC allows one to obtain, to identify, and to investigate atomic transitions between the Zeeman sublevels in the transmission spectrum shown in Fig. 1. NTC allows of application of permanent magnets facilitating significantly the creation of strong magnetic fields. The results obtained show that a nano-magnetometer with a local spatial resolution of ∼794 nm can be created basing on a NTC and an atomic transition of ^{87}Rb D_1. The results are important for mapping strongly inhomogeneous magnetic fields. Atomic frequency reference based on NTC and permanent magnets, widely tunable over a range of several gigahertz onto high-frequency wing of transition of ^{87}Rb atom, by a simple displacement of the magnet can be developed, too. Experimental results are in a good agreement with the theoretical values.

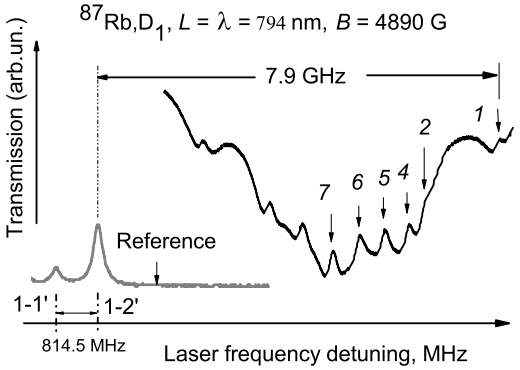

Figure 1: *NTC transmission spectra with $L = \lambda$ for ^{85}Rb D_1 line, $2-3'$ transitions (VSOPs numbered 4,5,6,7) and ^{87}Rb D_1 line, $1-2'$ transitions (VSOPs numbered 1,2) in case of σ^+ excitation at $B = 4890$ G (upper curve). The lower grey curve presents the reference spectrum which is the fluorescence spectrum of NTC at $L = \lambda/2$ for $B = 0$.*

Research conducted in the scope of the International Associated Laboratory IRMAS.

References

[1] A. Sargsyan, G. Hakhumyan, A. Papoyan, D. Sarkisyan *et al.*, Appl. Phys. Lett. **93**, 021119 (2008).

Atomic spectra of high-pressure Cs and Na light sources and their energy applications

G. Pichler[1], M. Rakić[1]

[1] *Institute of Physics, Bijenička cesta 46, 10000 Zagreb, Croatia*
Corresponding Author: pichler@ifs.hr

We compared the visible and the infrared spectra of cesium and sodium high pressure discharge light sources of 70 W, at different voltages from 180 to 240 V. Although the cesium discharge lamp exhibited remarkable white light in the visible spectrum, it suffers from the large infrared radiation intensity, which actually presents losses.

We performed series of measurements on several different cesium high-pressure light sources with the intention to investigate optimal burning conditions for eventual lighting purpose [1]. Cs high pressure discharge lamps with different burner diameter and burner materials were used. The first burner was made of pure sapphire crystal with 5 mm diameter and the second burner was made of alumina with 3 mm diameter. We used a pulsed power supply for both burners. The narrower burner exhibited smooth recombination spectrum with a few atomic lines and a few molecular absorption bands. The relevant plasma had a very high temperature in the burner center and high cesium atom densities at the alumina walls. The spectrum of the 5 mm burner exhibits lower temperature plasma having many atomic emission lines and much lower continuum spectrum from the electron-ion recombination processes. The visible spectra were measured by the digital spectrometer (silicon detector array) and the near infrared spectra were measured by the digital spectrometer (InGaAs detector array). The preliminary results have been published in reference [2].

References

[1] G. Pichler, V. Živčec, R. Beuc, Z. Mrzljak, T. Ban, H. Skenderović, K. Günther, J. Liu, UV, Physica Scripta T105, **98** (2003).
[2] M. Rakić and G. Pichler, Optics Communications **284** 2881–2885 (2011).

Cyclic dipeptide immobilization on Au (111) and Cu (110) surfaces

O. Plekan[1], V. Feyer[2], K. C. Prince[2], S. Ptasinska[3], and N. Tsud[4]

[1] *Department of Physics and Astronomy, Aarhus University, DK-8000 Aarhus C, Denmark*
[2] *Sincrotrone Trieste S.C.p.A., in Area Science Park, Strada Statale 14, km 163.5, I-34012 Basovizza, Trieste, Italy*
[3] *Department of Physics and Radiation Laboratory, University of Notre Dame, 46556 Notre Dame, IN, USA*
[4] *Charles University, Faculty of Mathematics and Physics, Department of Surface and Plasma Science, V Holešovičkách 2, 18000 Prague 8, Czech Republic*

Corresponding Author: plekan@phys.au.dk

Development of metal surface functionalization with biomolecules is one of the essential steps for numerous applications in the field of bio-nano-technology [1]. It has been already shown that organic molecules with suitable functionalities can organize themselves on metal substrates and induce modifications in surface properties [2]. Amino acids consist of three important functional groups, i.e., COOH, NH_2, and a side chain which differentiates the amino acids. For their immobilization on the surface, the number of theoretical and experimental studies concerning interaction of small amino acids and their polymerized forms, (polypeptides and/or proteins), with different metal surfaces are still growing [3].

The present work is focused on the structural configuration of two cyclic peptides (cyclo(Glycyl-Histydyl) and cyclo(Phenylalanyl-Prolyl)), see Fig. 1, which are made up of a ring containing two or more amino acids constrained by peptide bonds. Many cyclic dipeptides can be found in nature and are known to be biologically active [4]. The simplest cyclic peptide, cyclo(glycil-glycil) also called 2,5-diketopiperazine (DKP), is formed by condensation of two glycine molecules. The different functional groups of other amino acids replace the hydrogen attached to the DKP ring, which leads to the formation of a wide range of derivatives with different physical and chemical properties [5].

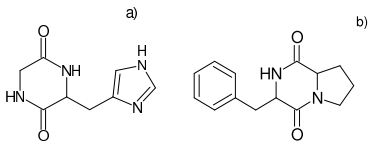

Figure 1: *Schematic structures of the dipeptides: a) cyclo(Glycyl-Histydyl), and b) cyclo(Phenylalanyl-Prolyl).*

Standard synchrotron-based techniques of x-ray photoelectron spectroscopy (XPS) and near edge x-ray absorption fine structure (NEXAFS) have been used to probe the electronic and adsorption properties of cyclo(Glycyl-Histydyl) and cyclo(Phenylalanyl-Prolyl) peptides on Au(111) and Cu(110). The XPS of C, N, and O 1s as well as the absorption spectra at the N and O K-edges were measured for monolayers of both compounds and the nature of the bonding with the two metal surfaces has been determined. On the basis of the XPS and NEXAFS data, the immobilization geometry of these dipeptides will be proposed and discussed.

References

[1] Z. C. Xing, Y. Chang, and I. K. Kang, Sci. Technol. Adv. Mater. **11**, 014101 (2010).
[2] K. C. Barick, D. Bahadur, and J. Nanosci, Nanotech. **10**, 668 (2010).
[3] Y. Zubavichus *et al.*, Nucl. Instr. Methods Phys. Res. A **603**, 111 (2009).
[4] M. P. Sobolevskaya and T. A. Kuznetsoval, Rus. J. Bioorg. Chem **36**, 560 (2010).
[5] J. F. Blake, Biotechniques, Suppl. S. **16** (2003).

Modelling of benchmark x-ray spectra from tungsten ions with charge 44+ to 46+ in the 3.5–8.0 Å range

M. Polasik[1], J. Rzadkiewicz[2,3], K. Słabkowska[1], and K. Kozioł[1]

[1] *Faculty of Chemistry, Nicolaus Copernicus University, 87-100 Toruń, Poland*
[2] *Soltan Institute for Nuclear Studies, 05-400 Otwock-Świerk, Poland*
[3] *Institute of Plasma Physics and Laser Microfusion, Hery 23, 01-497 Warsaw, Poland*
Corresponding Author: mpolasik@uni.torun.pl

Transition energies and transition probabilities have been calculated for electric multipole and magnetic multipole transitions from $3s^2 3p^6 3d^9 4s^x nl$ and $3s^2 3p^5 3d^{10} 4s^x nl$ (x=0, 1, 2; n=4, 5, 6 and l=s,p,d,f) excited-states to $3s^2 3p^6 3d^{10} 4s^x$ ground-state in Zn-like W^{44+} to Ni-like W^{46+} in a wavelength range of 3.5–8.0 Å. In calculations the multiconfiguration Dirac-Fock (MCDF) method [1, 2] including the transverse Breit interaction and quantum electrodynamics corrections has been applied. The MCDF predicted spectrum for various electric multipole and magnetic multipole transitions is illustrated for Ni-like W^{46+} in Fig. 1.

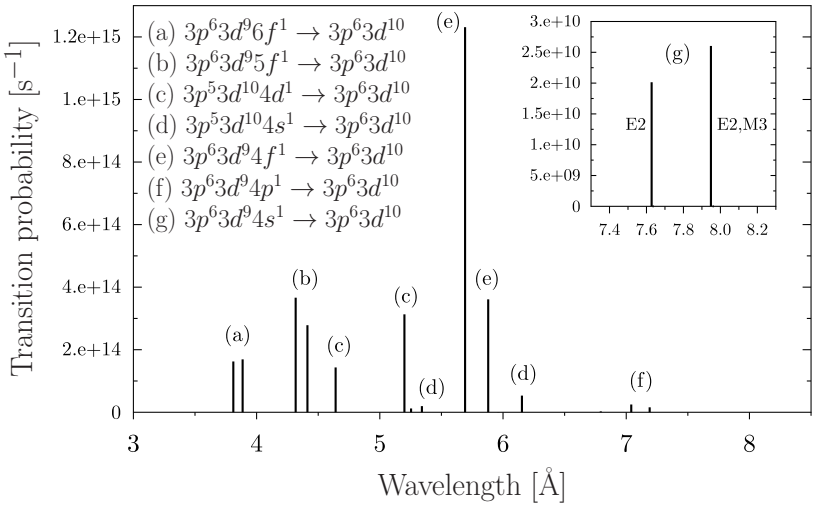

Figure 1: *Calculated theoretical spectrum for various transitions in Ni-like tungsten ion.*

The results of MCDF calculations will be used as the basis for the further benchmark modelling of the radiation emission from tokamak plasmas. In particular, the transitions studied in this work are expected to be constitute the major components of the x-ray radiation emitted by few keV plasma and can be used for the tungsten density and ion temperature diagnostics for JET, JT-60U and ITER tokamak plasmas [3].

References

[1] M. Polasik, Phys. Rev. A **39**, 616 (1989).
[2] M. Polasik, Phys. Rev. A **58**, 1840 (1998).
[3] M. G. O'Mullane, H. P. Summers, A. D. Whiteford *et al.*, Rev. Sci. Instr. **77**, 10F520 (2006).

Spectroscopic parameters for neutral tungsten lines of interest for fusion plasma research

P. Quinet[1,2], É. Biémont[1,2]

[1] *Astrophysics and Spectroscopy, University of Mons – UMONS, B-7000 Mons, Belgium*
[2] *IPNAS, University of Liège, B-4000 Liège, Belgium*

Corresponding Author: quinet@umons.ac.be

Because of its high melting point and thermal conductivity, and its low tritium retention and erosion rate under plasma loading [1,2], tungsten is a very attractive element to be used as a plasma facing material in Tokamak devices. The international thermonuclear experimental reactor ITER will be the next step experimental fusion device which will use tungsten, together with beryllium and carbon-reinforced composite, as plasma facing materials. The main disadvantage of tungsten in these conditions is the large radiative loss due to plasma contamination and its high radiative efficiency. Estimates of the tungsten influx rate to the core plasma will depend on a calculation of transport from the wall surface to the scrape-off layer. Consequently, the identification of emission lines from tungsten will greatly aid modeling of the plasma edge and scrape-off layer transport and facilitate the analysis of the net tungsten influx rates.

A very small number of works have been devoted, in the past, to the determination of radiative parameters in neutral tungsten. To our knowledge, the only available transition rates have been obtained experimentally for a set of 572 lines covering the wavelength range 225 – 1035 nm [3,4]. The aim of the present contribution is to extend these data by performing new calculations of transition probabilities for W I electric dipole lines using a pseudo-relativistic Hartree-Fock model including core-polarization effects [5,6]. The present work is an extension of our previous atomic structure calculations performed in singly ionized (W II) and doubly ionized (W III) tungsten [7,8]. These new results are intended to provide plasma physicists with some of the data they need for spectroscopic diagnostics and modeling of fusion plasmas magnetically confined in reactors.

References

[1] G. Federici *et al.*, Nucl. Fusion **41**, 1967 (2001).
[2] A. Pospieszczyk, *Nuclear Fusion Research* (Springer, Berlin, 2006).
[3] E. A. Den Hartog, D. W. Duquette, and J. E. Lawler, J. Opt. Soc. Am. B **4**, 48 (1987).
[4] R. Kling, and M. Kock, J. Quant. Spectrosc. Rad. Transfer **62**, 129 (1999).
[5] R. D. Cowan, *The Theory of Atomic Structure and Spectra* (University of California Press, Berkeley, 1981).
[6] P. Quinet *et al.*, Mon. Not. R. Astron. Soc. **307**, 934 (1999).
[7] H. Nilsson *et al.*, Eur. Phys. J **49**, 13 (2008).
[8] P. Palmeri *et al.*, Phys. Scr. **78**, 015304 (2008).

Stretched-state optically pumped magnetometer with miniaturized Cs cell

T. Scholtes[1], R. IJsselsteijn[1], S. Woetzel[1], V. Schultze[1], and H.–G. Meyer[1]

[1] *Institute of Photonic Technology, Jena, Germany*

Corresponding Author: Theo.Scholtes@ipht-jena.de

Improving the sensitivity of optically pumped magnetometers by increasing the atomic gas density is limited due to a rapidly growing spin-exchange collision rate between the alkali atoms. One way to suppress relaxation of atomic polarization as a result of this process is pumping all atoms into the ground state Zeeman level with highest angular momentum, the so called stretched state [1,2].

In our experiment this is done by high intensity circularly polarized pumping light resonant with the $D1$ line of cesium. We get rid of power-broadening of the magnetic resonance to a large extent by narrow-band, selective pumping on the N_2 buffer gas broadened and partially overlapping hyperfine structure.

Our miniaturized Cs cell of only 10 mm^3 volume [3] is heated to temperatures between 100–160°C by irradiation with a second, off-resonant laser allowing continuous magnetic measurements. The heating and pumping beams are guided by optical fibers to the vapour cell. The magnetic Zeeman resonance is probed via M_x measurement configuration with an additional radio frequency (rf) magnetic field. Automated measurements with variation of parameters like pump laser power and frequency, rf-field strength and cell temperature were carried out. With optimal parameters, a shot-noise limited sensitivity of 40 $\frac{\mathrm{fT}}{\sqrt{\mathrm{Hz}}}$ in a static magnetic field of 5 μT was achieved.

References

[1] S. Appelt *et al.*, Phys. Rev. A **59**, 2078-2084 (1999).
[2] S. J. Smullin *et al.*, Phys. Rev. A **80**, 033420 (2009).
[3] S. Woetzel *et al.*, Rev. Sci. Instrum. **82**, in press (2011).

Integrated array of optically pumped magnetometers

S. Woetzel[1], R. IJsselsteijn[1], V. Schultze[1], M. Kielpinski[1], T. Scholtes[1], and H.–G. Meyer[1]

[1] *Institute of Photonic Technology, Jena, Germany*

Corresponding Author: Stefan.Woetzel@ipht-jena.de

We present a new design of Cs vapor cell arrays used as optically pumped magnetometer assemblies. The arrays are microfabricated in 4 mm thick silicon wafers. Using supersonic milling, arbitrarily arranged cavities and connecting channels can be created. After closing the assembly by anodic bonding, a central cavity can be used as Cs reservoir, supplying several other cavities with equal vapor densities via canals. Using irradiation of the assembly with well-directed heating laser spots, a temperature distribution can be adjusted. This assures a lower temperature at the reservoir than at the measurement cavities in the setup, thus avoiding Cs deposits in the light path of the measurement cells.

These connected and matched cells can be used for various tasks like the formation of balanced gradiometers, for the reduction of pump light noise, for the compensation of heading errors, or for combinations of these tasks.

Cold Atoms/Molecules, Ions, and Quantum Gases

Vortex lattices in anisotropic traps

N. Lo Gullo[1], S. McEndoo[1], M. Paternostro[2], and Th. Busch[1]

[1] *Physics Department, University College Cork, Cork, Ireland*
[2] *Centre for Theoretical Atomic, Molecular and Optical Physics, Queen's University Belfast, Belfast BT7 1NN, UK*

Corresponding Author: thbusch@phys.ucc.ie

Vortices are topological excitations, which can be observed in rotating, superfluid Bose-Einstein condensates. Due to the single-valuedness condition of the wavefunction they can only carry quantized angular momentum and due to an energetic instability vortices with higher values of angular momentum decay into several vortices with winding number one. These vortices, in turn, arrange themselves into a well ordered lattice structure within the condensate and many beautiful experiments on these structures have been carried out in the recent decade.

The spatial distribution of the vortices in a rotating Bose-Einstein condensate is known to dependent on the strength and shape of the external trapping potential. While for small anisotropies triangular lattices are still the energetically most favourable geometry, strongly anisotropic traps can lead to dramatic deviations from this way of patterning. Here we theoretically explore the lattice structure for the full range of anisotropies and medium rotation speeds. We show that the lattice structure undergoes a rich variety of structural changes, including the formation of stable zig-zag and linear configurations. Each of these spatial re-arrangements can be interpreted in terms of flow patterns in the background gas and is clearly signaled by a change in the behavior of the vortex-lattice eigenmodes.

This new degree of freedom gives a handle to study vortex behaviour and vortex-vortex interactions without being limited to the Abrikosov geometry. Furthermore, the topological nature of the vortices makes our findings applicable to systems beyond atomic Bose-Einstein condensates.

References

[1] S. McEndoo and Th. Busch, Phys. Rev. A **79**, 053616 (2009).
[2] S. McEndoo and Th. Busch, Phys. Rev. A **82**, 013628 (2010).
[3] N. Lo Gullo, Th. Busch, and M. Paternostro, arXiv:1011.2125 (2010).

Observation of resonant 4-body process with cold Rydberg atoms

P. Cheinet[1], J. H. Gurian[1], P. Huillery[1], Y. Bruneau[1], A. Fioretti[1], P. L. Gould[2], J.-M. Zhao[3], D. Comparat[1], and P. Pillet[1]

[1] *Laboratoire Aimé Cotton, CNRS, Bat 505 Campus d'Orsay, 91405 Orsay, France*
[2] *Physics Department, University of Connecticut, Storrs, CT 06269, USA*
[3] *State Key Laboratory of Quantum Optics and Quantum Optics Devices, College of Physics and Electronics Engineering, Shanxi University, Taiyuan 030006, China*

Corresponding Author: patrick.cheinet@u-psud.fr

Cold Rydberg atoms are known for their large interaction properties [1] and constitute a good medium to investigate many body systems. Up to now, many body effects in Rydberg samples have been studied mainly through the broadening of spectral excitation lines [2,3].

We will present new measurements on a 4-body Stark-tuned Förster resonance observed with cesium atoms excited to the n=23 Rydberg level. To detect the Rydberg atoms we use field pulse ionization (FPI) and collect the extracted electrons on a micro-channel plate detector (MCP). Due to different ionization thresholds, the final states are observed with a different time of flight (TOF) signal and can be identified.

Two 2-body resonances, presented in Eqa. 1 and 2, occur respectively at 80.2 V/cm and 80.8 V/cm. Thanks to the proximity of these two resonances, it is possible to see the 4-body energy transfer presented in Fig. 1 which is resonant at 80.3 V/cm. The signature is the $23d$ population which is well separated in the TOF and requires the 4-body process to appear from the $23p_{3/2}$ excitation.

To our knowledge, this constitutes the first direct observation of a 4-body process with Rydberg atoms.

$$23p_{3/2}m_{1/2} + 23p_{3/2}m_{1/2} \rightarrow 23s_{1/2}m_{1/2} + 24s_{1/2}m_{1/2} \quad (1)$$

$$24s_{1/2}m_{1/2} + 24s_{1/2}m_{1/2} \rightarrow 23p_{1/2}m_{1/2} + 23d_{5/2}m_{1/2} \quad (2)$$

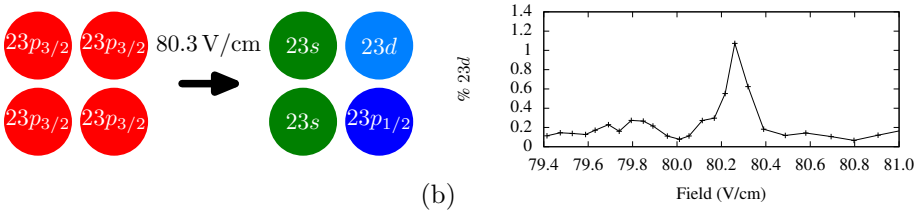

Figure 1: *(a) A four body process is expected at 80.3 V/cm. (b) Percentage of 23d state over the total Rydberg atom number while exciting the* $23p_{3/2}$ *state.*

References

[1] D. Comparat, P. Pillet, JOSA B **27**, A208 (2010).
[2] I. Mourachko *et al.*, Phys. Rev. A **70**, 031401(R) (2004) and references therein.
[3] J. Han, Phys. Rev. A **82**, 052501 (2010).

Microwave spectroscopy and Förster resonance between a few Rydberg atoms reveal an ultracold plasma formation at laser excitation

V. M. Entin[1], D. B. Tretyakov[1], I. I. Beterov[1], E. A. Yakshina[1], and I. I. Ryabtsev[1]

[1] *A.V. Rzhanov Institute of Semiconductor Physics SB RAS, 630090, pr. Lavrenteva 13, Novosibirsk, Russian Federation*

Corresponding Author: ventin@isp.nsc.ru

The experiments on the spectroscopy of various microwave transitions between Rydberg states of cold Rb atoms have been done in a small laser excitation volume in a magneto-optical trap (MOT). A small excitation volume was formed by two tightly focused laser beams in crossed-beam geometry. Independently of the interaction time with the radiation, all microwave transitions exhibited a 1–3 MHz linewidth. An analysis of the experimental conditions has shown that the main source of this line broadening was the inhomogeneous electric field of the photoions that appeared at an excitation of Rb Rydberg atoms by a broadband pulsed laser radiation via three-step scheme 5S→5P→6S→nP.

The cold photoions have a temperature of 100–200μK and they may stay in the excitation region for a long time, if there is no extracting electric field. Their inhomogeneous electric field affects the neighboring Rydberg atoms via the Stark effect, which leads to the shift and broadening of the microwave resonances. A similar phenomenon was observed by us in the experiments on studying a Förster energy-exchange resonance Rb($37P_{3/2}$)+Rb($37P_{3/2}$)→ Rb(37S)+Rb(38S) for the small number of the interacting cold Rb Rydberg atoms. In order to check for the assumption on the photoions' presence at the moment of the laser pulse, we applied an additional pulse of the electric field, which rapidly extracted the ions. This resulted in substantial narrowing of the microwave and Förster resonances.

Overall, it has been shown that presence of even single charged particles in a small excitation volume of Rydberg atoms leads to the broadening and shift of the lines of microwave transitions due to the Stark effect in the inhomogeneous electric field, and that the method of microwave spectroscopy is suitable for non-demolition diagnostics of the ultracold plasma.

This work was supported by RFBR (Grant No. 10-02-00133), by the Russian Academy of Sciences, by the Presidential Grant No. MK-3727.2011.2, and by the Dynasty Foundation.

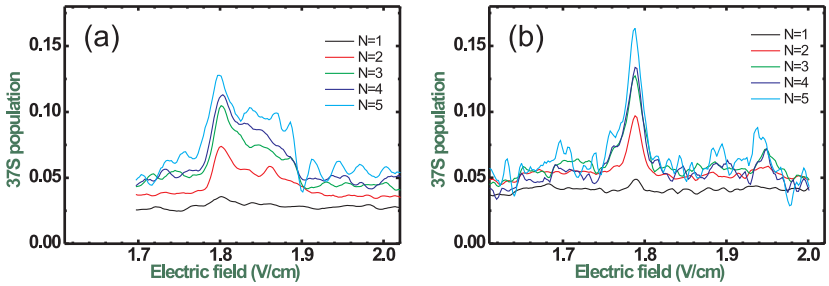

Figure 1: *Experimental records of the Förster resonance in cold Rb Rydberg atoms for various number of the detected Rydberg atoms, N: (a) In the presence of the cold photoions appeared at the laser excitation of the 37P state. The electric field of the photoions shifts and broadens the resonance. (b) An additional electric-field pulse (5 V/cm, 2 μs) rapidly removes photoions. A narrow Förster resonance is observed at 1.79 V/cm.*

Laser assisted Feshbach resonances

E. Gazazyan[1], A. Gazazyan[1], and V. Chaltykyan[1]

[1] *Institute for Physical Research, NAS of Armenia, Ashtarak-2 0203, Armenia*
Corresponding Author: emilgazazyan@gmail.com

Collisions of atoms with formation of Feshbach resonances in the presence of laser field are considered. It is shown that if the energy equals that of the lower stable Stark-shifted level plus the energy of two photons, the resonance is quenched. It is also shown that with the increase in two-photon effective interaction the pattern of resonance scattering changes essentially. Collision of cold atoms in the field of laser radiation has been studied in [1] where the laser-caused decay channel is not taken into account. Influence of non-resonant radiation on the scattering length, as well as formation of molecules, is considered in works [2-4].

In the present work we consider collision of atoms with formation of the Feshbach resonance in the field of laser radiation which couples molecular levels by the two-photon resonance. The two-photon resonance between discrete molecular levels enables, on the one hand, studying the dynamics of levels in dependence on the laser intensity, on the other hand, it makes possible the one-photon transition from the upper level to other (inelastic) channel (Fig. 1) where the molecule decays, under action of laser radiation with the interaction $\Omega_E^{'}$, into two excited atoms flying away from each other. The cross-sections for the elastic and inelastic resonance scattering are obtained.

The appearance of two peaks in the resonance scattering cross section is associated with splitting of the quasi-energy level in the two-level system. This effect is analogous to the Autler-Towns effect for resonance scattering of photons. It is shown that if the energy equals that of the lower stable Stark-shifted level plus the energy of two photons, the resonance is quenched. It is also shown that with the increase in two-photon effective interaction the pattern of resonance scattering changes essentially.

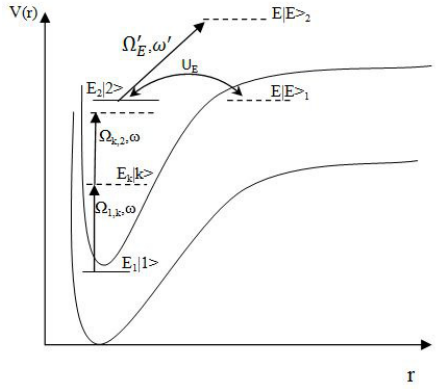

Figure 1: *Diagram of formation of Feshbach resonance in laser field.*

References

[1] S. E. Harris, Phys. Rev. A **66**, 010701(R) (2002).
[2] J. L. Bohn, P. S. Julienne, Phys. Rev. A **56**, 1486 (1997); ibid **54**, R4637 (1996); ibid **60**, 414 (1999).
[3] Y. B. Band, P. S. Julienne, Phys. Rev. A **51**, R4317 (1995).
[4] P. O. Fedichev, Yu. Kagan, G. V. Shlyapnikov, and J. T. M. Walraven, Phys. Rev. Lett. **77**, 2913 (1996).

Production of ultracold, internally state-selected molecular ions in ion traps

M. Germann[1], X. Tong[1], and S. Willitsch[1]

[1] *Department of Chemistry, University of Basel, 4056 Basel, Switzerland*
Corresponding Author: matthias.germann@unibas.ch

Molecular ions represent interesting quantum mechanical system due to their internal degrees of freedom —rotation and vibration— which are absent in atomic ions. Precise selection and control of these degrees of freedom therefore opens up new applications in precision spectroscopy, chemical dynamics studies and quantum-information processing.

We have recently achieved the preparation of rotationally and vibrationally state-selected and translationally cold N_2^+ ions [1]. The ions were generated by threshold photoionization followed by sympathetic cooling of the translational degrees of freedom in a linear Paul trap. Rotational-state lifetimes on the order of 15 minutes were achieved.

For polar ions, the coupling to the ambient blackbody radiation field redistributes the initially prepared single rotational quantum state over a wide range of levels and therefore reduces the state-lifetime considerably. Here we present a way to circumvent this problem using a cryogenic ion trap ($T \approx 10$K) that isolates the ions almost completely from the room-temperature blackbody radiation. Using this setup to investigate polar $BrCl^+$ ions as a test system, we expect to increase the state-life time by several orders of magnitude [2].

References

[1] X. Tong, A. H. Winney, and S. Willitsch, Phys. Rev. Lett., **150**, 143001 (2010).
[2] X. Tong, D. Wild, and S. Willitsch, Phys. Rev. A, **83**, 023415 (2011).

Spectroscopic investigation of the states dissociating to the Li(2s)+Cs(5d) asymptote of LiCs molecule

A. Grochola[1], J. Szczepkowski[2], W. Jastrzębski[2], and P. Kowalczyk[1]

[1] *Institute of Experimental Physics, University of Warsaw, Hoża 69, 00-681 Warsaw, Poland*
[2] *Institute of Physics, Polish Academy of Sciences, Al. Lotników 32/46, 02-668 Warsaw, Poland*

Corresponding Author: Anna.Grochola@fuw.edu.pl

Recently there has been considerable progress in production of cold diatomic molecules. Mixed alkali dimers are of particular interest here because their permanent dipole moments permit manipulating them by external fields, and among them LiCs molecule has the largest dipole moment [1]. As several experimental techniques related to cold molecules involve optical excitation either in the formation or detection stages, a need of precise spectroscopic characterization of molecular states has much increased.

For a number of years we have been involved in investigation of alkali dimers using the polarization labeling method. This double resonance technique surmounts the difficulty of resolving highly congested molecular spectra: with a proper choice of frequencies and polarizations of two laser beams, interacting with a molecular sample, only transitions from few known rovibrational levels in the ground state are observed. This selectivity is particularly useful when studying spectra of molecules which contain heavy species like cesium or rubidium.

In this contribution we present an experimental observation of the $C^1\Sigma^+$ as well as $d^3\Pi$ and $e^3\Sigma^+$ states in LiCs molecule, dissociating to the Li(2s)+Cs(5d) asymptote. Our two-color polarization labeling experiments measuring the C←X system have characterized the $C^1\Sigma^+$ state up to $v' = 8$. Transitions within the d←X and e←X systems are spin-forbidden, but the scheme of angular momentum coupling in the LiCs molecule is sufficiently close to Hund's case (c), to make these transitions partially allowed. Observed triplet states split into several components: $d^3\Pi$ state into $\Omega = 0^+$, 0^-, 1 and 2, $e^3\Sigma^+$ state into $\Omega = 0^-$, 1. Consequently, observed transitions should be labeled rather as $\Omega = 0^+ \leftarrow \Omega = 0^+(X^1\Sigma^+)$ or $\Omega = 1 \leftarrow \Omega = 0^+(X^1\Sigma^+)$, according to selection rules. We were able to experimentally characterize $\Omega = 0^+$, (up to $v' = 8$) and $\Omega = 1$ (up to $v' = 14$) components of $d^3\Pi$ state and $\Omega = 1$ (up to $v' = 11$) component of the $e^3\Sigma^+$ state. The potential curves of all investigated states have been represented by a numerical potential generated with the point-wise inverted perturbation approach (IPA) method [2] and compared with results of theoretical calculations [3].

References

[1] J. Deiglmayr, A. Grochola, M. Repp, O. Dulieu, R. Wester, and M. Weidemüller, Phys. Rev. A **82**, 032503 (2010).
[2] A. Pashov, W. Jastrzębski, P. Kowalczyk, Comput. Phys. Commun. **128**, 622 (2000).
[3] N. Elkork, D. Houalla, and M. Korek, Can. J. Phys. **87**, 1079 (2009).

A new experiment to study cold molecular ion – atom reactions

F. Hall[1], S. Willitsch[1]

[1] *Physical Chemistry Department, University of Basel, Klingelbergstrasse 80, 4056 Basel, Switzerland*

Corresponding Author: felix.hall@unibas.ch

A new experiment for the study of chemical reactions between quantum-state selected atomic and molecular ions and atoms at very low temperatures (T ≈ 10mK) has been conceived and developed, allowing the probing of ion-neutral chemical processes at collision energies two orders of magnitude lower than previously investigated [1]. Previous work on low temperature atomic ion-atom collisions has indicated a rate constant independent of collision energy, as predicted by Langevin theory [2]. The present experiment aims at validating low temperature ion-neutral reaction models [3] and the study of *molecular* effects in cold collisions.

State selected cold molecular ions are produced by sympathetic cooling with a Ca^+ coulomb crystal in a linear rf quadrupole trap [4]. Ultracold ^{87}Rb atoms are generated in a magneto-optical trap. The combination of both traps completely *in vacuo* leads to a highly flexible apparatus, enabling the study of molecular interactions in a regime where quantum mechanical effects may dominate reactions. The design and construction of the experiment are discussed, and results of the test system $^{87}Rb+^{40}Ca^+$ are presented, which itself shows interesting non-Langevin behaviour. Prospects for future investigations in the light of these results are also highlighted.

References

[1] S. Willitsch *et al.*, Phys. Rev. Lett. **100**, 0423203A (2008).
[2] A. Grier *et al.*, Phys. Rev. Lett. **102**, 223201 (2010).
[3] E. Dashevskaya *et al.*, J. Chem. Phys. **118**, 7313 (2003).
[4] X. Tong *et al.*, Phys. Rev. Lett. **105**, 143001 (2010).

Deperturbation of the $3^1\Pi_u$, $4^1\Pi_u$ states in Li_2 and the $c^3\Sigma^+$, $B^1\Pi$ states in NaCs

Z. Jędrzejewski-Szmek[1], P. Kowalczyk[1], A. Grochola[1], and W. Jastrzębski[2]

[1] *Institute of Experimental Physics, University of Warsaw, Warsaw, Poland*
[2] *Institute of Physics, Polish Academy of Sciences, Warsaw, Poland*

Corresponding Author: zbysz@fuw.edu.pl

Absorption spectra of the $3^1\Pi_u$ and $4^1\Pi_u$ states of the lithium dimer have been previously measured. Polarization labelling spectroscopy was used to simplify the excitation spectra, limiting visible transitions to one or more progressions of PQR triplets [1].

Those results were presented at the 41st EGAS conference in 2009. Further analysis revealed that the assignments of quantum numbers reported in earlier publications, e.g., [2], was likely wrong. An improved assignment was made. A deperturbation analysis was performed by extending inverted perturbation approach to simultaneous treatment of two electronic states [3].

This deperturbation framework is also applicable to the $c^3\Sigma^+$ and $B^1\Pi$ states in the sodium–cesium molecule [4,5]. In the language of Hund's case (c) those two states can be described as the third and fourth state with $\Omega = 1$. This means that they are subject to the same electrostatic perturbation as the $^1\Pi$ states in Li_2.

Deperturbation results for the two pairs of states will be presented: unperturbed electronic potential energy curves and perturbation parameters.

References

[1] Z. Jędrzejewski-Szmek *et al.*, Chem. Phys. Lett. **444**, 229–231 (2008).
[2] W. Theiss, H. J. Müschenborn, and W. Demtrôder, Chem. Phys. Lett. **174**, 126–132 (1990).
[3] Z. Jędrzejewski-Szmek *et al.*, Optica Applicata **40**, 577–585 (2010).
[4] A. Grochola, P. Kowalczyk, and W. Jastrzębski, Chem. Phys. Lett. **497**, 22–25 (2010).
[5] A. Grochola *et al.*, (in preparation).

Strong anisotropy in the interaction between ultracold Dy atoms

S. Kotochigova[1], A. Petrov[1]

[1] *Department of Physics, Temple University, Philadelphia, PA 19122-6082, USA*
Corresponding Author: skotoch@temple.edu

In recent years significant efforts have been made to understand the character of interactions between and with submerged-shell atoms. Experimental measurements of the collisional spin-exchange rates between two submerged-shell atoms suggest that these rates are not suppressed and have the same order of magnitude as for nonsubmerged shell atoms [1,2]. Here we discuss the relative strength of the magnetic dipole-dipole, isotropic and anisotropic electrostatic dispersion, and electrostatic quadrupole-quadrupole interactions between submerged-shell Dy atoms at ultracold temperatures. To account for these interactions we calculate the isotropic and anisotropic van der Waals coefficients of the colliding ground state Dy atoms and its quadrupole moment. There are 81 gerade and 72 ungerade potentials that dissociate to the ground state $^5\mathrm{I}_8 + {}^5\mathrm{I}_8$ limit. As a result, the theoretical calculation of the two-body ground state Dy_2 potentials and their dispersion parameters has been challenging. Finally, we show that a substantial part of the loss rate, observed in [1], is due to the anisotropy of the short-ranged dispersion forces.

References

[1] M. Lu, S. Ho Youn, and B. Lev, Phys. Rev. Lett. **104**, 063001 (2010).
[2] C. B. Connolly *et al.*, Phys. Rev. A **81**, 010702(R) (2010).

Excitation and ionization of highly excited Cs atoms on helium nanodroplets

F. Lackner[1], G. Krois[1], M. Theisen[1], M. Koch[1], and W. E. Ernst[1]

[1] *Institute of Experimental Physics, Graz University of Technology, Petersgasse 16, A-8010 Graz, Austria*

Corresponding Author: krois_gu@sbox.tugraz.at

Highly excited states of Cs atoms on the surface of helium nanodroplets are investigated using laser induced fluorescence (LIF) spectroscopy and resonance enhanced multi-photon-ionization time-of-flight (REMPI-TOF) spectroscopy. A two-step excitation scheme via the $6^2P_{1/2}(^2\Pi_{1/2})$ intermediate state using two cw lasers (LIF) or a cw and a pulsed laser (REMPI-TOF) was applied [1]. We show that in addition to Rb [2] also Cs atoms stay bound on the surface of helium nanodroplets when excited into the $n^2P_{1/2}$ (Rb: $n = 5$, Cs: $n = 6$) state. With LIF spectroscopy the highly excited nS ($n = 8 - 11$), nP ($n = 8 - 11$), and nD ($n = 6 - 10$) levels of Cs atoms on helium droplets are investigated by monitoring the $6^2P_{3/2} \rightarrow 6^2S_{1/2}$ transition. REMPI-TOF spectroscopy is used to gain additional information by mass selective ion detection upon ionization of higher excited states. We explain the observed spectrum with the pseudo-diatomic model for helium nanodroplets doped with single alkali-metal atoms. An investigation of spectral trends shows that the $n'^2P(\Pi) \leftarrow 6^2P_{1/2}(^2\Pi_{1/2})$ and $n'^2D(\Delta) \leftarrow 6^2P_{1/2}(^2\Pi_{1/2})$ ($n' > 9$) transitions are lower in energy than the corresponding free-atom transitions. This indicates that the Cs*–He_N potential becomes attractive for these highly excited states.

References

[1] M. Theisen, F. Lackner, F. Ancilotto, C. Callegari, and W. E. Ernst, Eur. Phys. J. D **61**, 403–408 (2011).

[2] G. Auböck, J. Nagl, C. Callegari, and W. E. Ernst, Phys. Rev. Lett. **101**, 035301 (2008).

Chirped optical Stark acceleration and deceleration

C. Maher–McWilliams[1], P. Douglas[1], N. Coppendale[1], A. Gerakis[1], and P. F. Barker[1]

[1] *Department of Physics and Astronomy, University College London, Gower Street, London WC1E 6BT, England*

Corresponding Author: c.maher-mcwilliams@ucl.ac.uk

There is currently considerable interest in controlled cold atomic and molecular collisions which allow high resolution studies of resonant and threshold phenomena and testing of potential energy surfaces (PES's) with high precision [1]. We have developed a technique for producing highly tunable cold atomic and molecular beams using optical Stark acceleration/deceleration. This exploits the interaction between an optical field and the induced dipole moment of a molecule to create a strong optical dipole force [2]. When short pulse, strong laser fields are used, this force is capable of accelerating/decelerating molecules and atoms over nanosecond timescales [3]. This has been accomplished using the strong periodic dipole force created from the interference pattern created by two, near counter propagating intense laser pulses ($\approx 10^{11}$ W $\cdot$ cm^{-2}). The resulting optical potential is called an optical lattice and a frequency difference, $\Delta\omega$, between the two beams creates a moving lattice with a velocity proportional to $\Delta\omega$.

We report on progress towards chirped deceleration and acceleration of a molecular beam, firstly describing the laser system that has been developed to create the decelerating lattice. This system produces two, pulse amplified beams of up to 700 mJ with flat-top temporal profiles. Its frequency and intensity can be well controlled for durations from 20 ns – 10 μs. The two beams are created by amplifying a single, rapidly tunable Nd:YVO_4 microchip type laser at 1064 nm, which can be frequency chirped up to 1 GHz over the duration of the pulse. A 1 GHz chirping range corresponds to a lattice velocity tuning range of 0 to 532 ms^{-1}.

We also describe recent experiments with this laser system to accelerate cold metastable argon (Ar*) produced in a magneto optical trap. Ar* atoms were accelerated from rest to final velocities of 100's of m/s using an accelerating lattice produced by chirping the frequency difference between the two pulses. The accelerated atomic packet maintains a narrow energy distribution and our results show good agreement with simulations.

References

[1] G. Meijer, ChemPhysChem **3**, 495 (2002).
[2] R. Fulton *et al.*, Nature **2**, 465 (2006).
[3] P. F. Barker and M. N. Shneider, Phys. Rev. A **64**, 033408 (2001).

Prospects of the $a^3\Sigma^+ \rightarrow E^1\Sigma^+ \rightarrow X^1\Sigma^+$ optical cycle for ultracold KCs molecule production

E. A. Pazyuk[1], A. V. Stolyarov[1], I. Klincare[2], O. Nikolayeva[2], M. Tamanis[2], and R. Ferber[2]

[1] *Department of Chemistry, Moscow State University, 119991, GSP-2, Moscow, Leninskie gory 1/3, Russia*
[2] *Laser Center, Department of Physics, University of Latvia, 19 Rainis blvd, Riga LV-1586, Latvia*

Corresponding Author: pazuyk@phys.chem.msu.ru

The laser production and manipulation of ultracold molecular assembles are greatly facilitated by accurate knowledge of the structure and dynamic properties of the electronic states involved. In spite of the recent progress in the systematic spectroscopic investigation of the ground and excited states of KCs molecule [1–5], the required reduction of the raw experimental and *ab initio* data to precise interatomic potentials and rovibronic transition probabilities is still challenged and unambiguous procedure.

We report here on branch ratio of the spin-allowed $E^1\Sigma^+ - X^1\Sigma^+$ and spin-forbidden $E^1\Sigma^+ - a^3\Sigma^+$ rovibronic transitions studied experimentally and theoretically in KCs molecule for a wide range of vibrational v and rotational J quantum numbers of the combined electronic states. Relative intensity distributions in rotationally resolved $E \rightarrow X$ and $E \rightarrow a$ laser induced fluorescence (LIF) progressions were simultaneously measured by a Fourier transform spectrometer (FTS) calibrated on the spectral sensitivity of registration system. The *ab initio* quasi-relativistic electronic structure calculations claim that the excited $E^1\Sigma^+$ state is regularly perturbed by the remote triplet $^3\Pi$ states due to spin-orbit coupling effect. The homogeneous perturbation is large enough to induce the pronounced spin-forbidden $E^1\Sigma^+ - a^3\Sigma^+$ transition by borrowing probabilities of the spin-allowed $(2,3)^3\Pi - a^3\Sigma^+$ transitions. The absorption and emission Einstein coefficients were calculated for both singlet-singlet $E - X$ and singlet-triplet $E - a$ rovibronic transitions along with radiative lifetimes of the upper $E^1\Sigma^+$ state and branch ratios of its spontaneous emission to the all possible lower-lying excited states. The calculated $E \rightarrow X$ and $E \rightarrow a$ emission coefficients agree well with the experimental intensity distribution measured from the FTS LIF spectra.

The simulated transition probabilities of the the $a^3\Sigma^+ \rightarrow E^1\Sigma^+ \rightarrow X^1\Sigma^+$ optical cycle elucidate that the ultracold KCs molecules could be efficiently produce in their absolute ground $v_X = 0, J_X = 0$ state in one stimulated Raman step from the high-lying vibrational levels of the singlet X and triplet a states repopulated by spontaneous decay of the photoassociated and translationally cooled colliding atoms.

Moscow team thanks for support the Russian Foundation for Basic Researches by the grant 10-03-00195a. The support from the Latvian Science Council grant Nr 09.1036 is gratefully acknowledged by Riga team.

References

[1] R. Ferber *et al.*, J. Chem. Phys. **128**, 244316 (2008); Phys. Rev. A **80**, 062501 (2009).
[2] J. T. Kim, Y. Lee, and A. V. Stolyarov, J. Mol. Spectrosc. **256**, 57 (2009).
[3] A. Kruzins *et al.*, Phys. Rev. A **81**, 042509 (2010).
[4] M. Tamanis *et al.*, Phys. Rev. A **82**, 032506 (2010).
[5] L. Busevica *et al.*, J. Chem. Phys. **134**, in press (2011).

Ion dynamics in linear RF traps

J. Pedregosa-Gutierrez[1], C. Champenois[1], M. Marciante[1], M. Houssin[1], and M. Knoop[1]

[1] *Physique des Interactions Ioniques et Moléculaires, Université de Provence, Centre Universitaire de St. Jérôme – Case C21, 13397, Marseille, France*

Corresponding Author: j.pedregosa@univ-provence.fr

The quadrupole linear trap is a widespread tool for many fundamental physics experiments (quantum computing, phase transition study, metrology, etc). Compared to quadrupole trap, higher order traps present the interesting feature to generate an almost flat potential well, which induces a small RF-driven motion and a low RF-heating, compared to quadrupole trap. These traps have been widely used in the ultra cold collisions community with buffer gas cooled samples and recently, to produce Coulomb crystals of a new kind thanks to laser cooling [1]. Moreover, multipole traps have been at the heart of a promising microwave ion clock based on a double trap, a quadrupole plus a 16-pole [2].

In this context, we are setting up a novel experimental apparatus to study ion dynamics under laser cooling, in quadrupole and octupole RF traps, aiming at the confinement and transport of a wide panel of ion clouds from small chains to large samples ($N > 10^6$). The setup consists of three trapping regions of different storage potential: quadrupole-quadrupole-octupole. This configuration allows separating the ion creation zone from the laser-cooling zone, in order to avoid perturbations of the potential created by atom deposition on the RF electrodes. The first results produced by this new setup will be presented at the conference.

In the search for the least perturbed harmonic potential for the quadrupole zones, an extensive numerical work has been performed to optimise the geometry of the DC electrodes, which has an important impact on the trapping potential. This trap potential optimization is crucial if large ion clouds are to be trapped. We have found an optimal geometry which presents some advantages with respect to other more complicated configurations [3].

Interpretation of the observed ion dynamics and the stable crystal structures will be carried out by comparing the experimental to the numerical results produced by ion dynamics simulation which can be pursued in different trapping potential using molecular dynamics. Thanks to these simulations, it has been found that few ions stored in an octupole trap and forming a ring crystal structure can be laser cooled to the Doppler limit along the symmetry axis of the trap. We propose the use of this ring for optical frequency metrology [4], in a tight confinement configuration which reduces the frequency sensitivity to the fluctuations of the number of trapped ions. The systematic shifts introduced by the non-null RF electric field are also evaluated for the optical clock transition of calcium ions, showing that a ring of 10 or 20 ions allows reaching a short term stability better than for a single ion without introducing limiting long term fluctuations.

References

[1] K. Okada *et al.*, Phys. Rev. A **80**, 043405 (2009).
[2] J. Prestage and G. Weaver, Proceeding of the IEEE **95**, 2235 (2007).
[3] J. Pedregosa, *et al.*, IJMS **290**, 100–105 (2010), arXiv:1001.1403v1.
[4] C. Champenois, *et al.*, Phys. Rev. A, in print (2010), arXiv:1003.0763v1.

Electron spin resonance of ^{87}Rb monomers on superfluid helium nanodroplets: optical pumping scheme and line shape analysis

J. Poms[1], A. Volk[1], M. Koch[1], and W. E. Ernst[1]

[1] *Institute of Experimental Physics, Graz University of Technology, Petersgasse 16, A-8010 Graz, Austria*

Corresponding Author: markus.koch@tugraz.at

Electron spin resonance (ESR) spectroscopy on superfluid helium nanodroplets (He_N) is a promising tool to study the environment of radicals at very low temperatures, which could recently be demonstrated on ^{85}Rb doped droplets [1]. Electronic perturbation of the alkali-metal atom induced by the He_N leads to an increase of the Fermi contact interaction and hence to a droplet size dependent change of the hyperfine constant a_{HFS}.

This opens the opportunity to use Rb as a spin label for ESR-silent species with high polarizabilities, dipole moments, and/or nuclear spins, which are embedded inside the He_N cryostat. Because of its larger hyperfine coupling, ^{87}Rb is more sensitive for additional influences due to the embedded species, such as a change of van der Waals interaction.

We present the first ESR spectra of single ^{87}Rb atoms on He_N (Fig. 1) [2]. The amplitude of ESR signals, measured by means of optically detected magnetic resonance, turned out to strongly depend on the laser polarization and power. A simple model for optical pumping on He_N has been successfully applied, predicting the most promising ESR peak for the application of spin labeling. Our current work involves modeling of observed line shapes to reveal new information on the droplet size distribution and on the droplet size dependence of a_{HFS}. This is a first step to establish ESR on He_N as a universal diagnostic tool for magnetic properties and spin dynamics of small clusters.

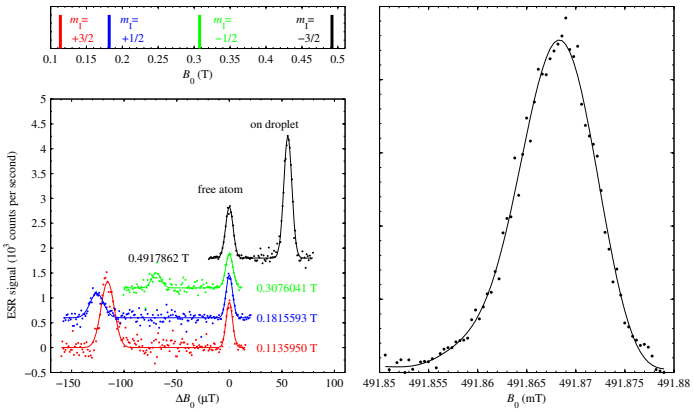

Figure 1: *ESR spectrum of ^{87}Rb on He_N. Left panel top: Calculated ESR spectrum of ^{87}Rb atoms. Left panel bottom: the four on-droplet ESR peaks shifted with respect to the free-atom peaks. Right panel: closeup of the $m_I = -3/2$ on-droplet line, revealing an asymmetry due to the droplet size distribution.*

References

[1] M. Koch, G. Auböck, C. Callegari, and W. E. Ernst, Phys. Rev. Lett. **103**, 035302 (2009).
[2] A. Volk, J. Poms, M. Koch, and W. E. Ernst, J. Phys. Chem. A, in press 2011.

Cold atoms in Laguerre-Gaussian laser beams

L. Pruvost[1], V. Carrat[1], and B. Viaris de Lesegno[1]

[1] *Laboratoire Aimé Cotton, CNRS, Univ Paris-Sud, bat. 505, 91405 Orsay, France*
Corresponding Author: Laurence.Pruvost@lac.u-psud.fr

A Laguerre-Gaussian laser mode, blue-detuned from the atomic resonance, constitutes a power-law trap for cold atoms because its laser intensity profile varies as $r^{2\ell}$, where ℓ is the order of the LG mode.

We have shown that very accurate Laguerre-Gaussian modes (Fig. 1) can be generated starting from a usual Gaussian mode, by applying an holographic method using a spatial light modulator and that they can be used to guide cold atoms [1]. The guiding effect which has been experimentally studied versus the order of the mode and the laser detuning, has been quantitatively interpreted by a 2D-capture model.

Laguerre-Gaussian modes or deformed Laguerre-Gaussian modes [2] could be used for other applications, where specific traps are required. For example, a Bose-Einstein condensate realized in a power-law trap is expected to have different properties than the condensate in a harmonic trap [3]. Condition for condensation is less severe and the condensate would be homogeneous.

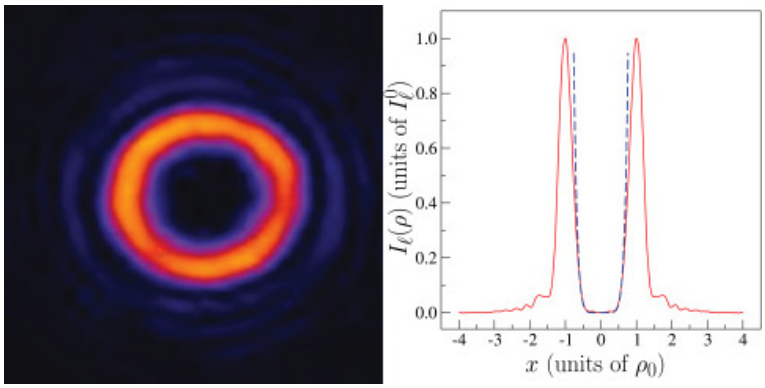

Figure 1: *Holographically-generated Laguerre-Gaussian mode with ℓ=4, and the intensity profile, fitted by a r^8 law near the center.*

References

[1] M. Mestre, F. Diry, B. Viaris de Lesegno, L. Pruvost, Eur. Phys. J. D **57** 1 87–94 (2010).
[2] F. Diry, Ch. Hazera, B. Viaris de Lesegno, L. Pruvost, "Generation and propagation of polygonal-deformed LG modes by using phase-only holograms", in preparation.
[3] A. Jaouadi, N. Gaaloul, B. Viaris de Lesegno, M. Telmini, L. Pruvost, and E. Charron, Phys. Rev. A **82**, 023613 (2010).

Vibrational quantum defect to analyze photoassociation spectra of Rb_2 and Cs_2 and to detect coupled states

L. Pruvost[1], H. Jelassi[2]

[1] *Laboratoire A. Cotton, CNRS, Univ Paris-Sud, bat. 505, 91405 Orsay Cedex, France*
[2] *Centre National des Sciences et Technologies Nucléaires 2020 Sidi Thabet, Tunisia*
Corresponding Author: laurence.pruvost@lac.u-psud.fr

In the context of cold molecule formation, many routes have been discovered, for example using the photo-association process or the magneto-association though a Feshbach resonance.

Starting from cold atoms, the first step is often the photo-association of two cold atoms towards an excited molecule. Such a process creates a long range excited molecule which generally does not decay to a cold molecule in a ground state except if the wavefunction of the excited molecular state presents a non-zero probability at short inter-nuclear distance. This configuration occurs when the excited molecular state is coupled to another one with large probability at short range. The resulting state having two regions of probability, permits both an efficient photo-association and a large Franck-Condon factor, and so the decay to a vibrational ground state.

In many cases the coupling between the two molecular curves is weak, but the wavefunction mixing can become large if the molecular states are nearly resonant. One of the aims of high resolution photo-association spectroscopy near dissociation limit is to find such excited states.

We have developed the method of the vibrational quantum defect. Inferred from experimental measurements of the energy positions, using the Le Roy Bernstein energy law the vibrational quantum defect is plotted versus the energy. This graph shows the deviations from the assumed energy law and any strong variation indicates a perturbation due to a coupling of nearly resonant states. By fitting the graph with a model of coupled series we determine the coupling amplitude and the wavefunction mixing. The method, applied to Rb_2 [1] and Cs_2 [2,3] has permitted us to propose schemes for cold molecule formation, which have been successfully investigated.

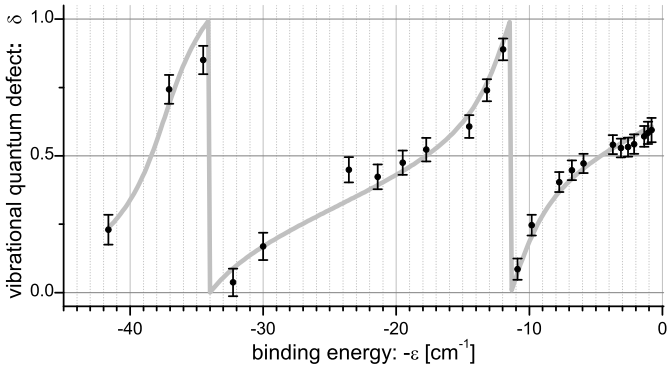

Figure 1: *Analysis of Cs_2 (6s-6p1/2)0g- : vibrational quantum defect versus energy, and the fitting curve using a coupled series model. Figure of reference [3].*

References

[1] H. Jelassi, B. Viaris de Lesegno and L. Pruvost, Phys. Rev. A **74** p012510 (2006).
[2] H. Jelassi, B. Viaris de Lesegno, L. Pruvost, M. Pichler, and W. C. Stwalley, Phys. Rev. A **78**, 022503 (2008).
[3] L. Pruvost and H. Jelassi, J. Phys. B: At. Mol. Opt. Phys. **43**, 125301 (2010).

Counterintuitive behavior of nonsymmetric Penning ionization cross-section for two Rydberg atoms

D. Efimov[1], N. N. Bezuglov[1], K. Michulis[2], A. Ekers[2], I. I. Beterov[3], and I. I. Ryabtsev[3]

[1] *Faculty of Physics, St. Petersburg State University, 198904 St. Petersburg, Russia*
[2] *Laser Centre, University of Latvia, LV-1002 Riga, Latvia*
[3] *Institute of Semiconductor Physics, 630090 Novosibirsk, Russia*

Corresponding Author: ryabtsev@isp.nsc.ru

Penning ionization is one of the key players in the ionization of cold Rydberg gases enabling the bound electrons to escape into the continuum [1]. When two Rydberg atoms with the relative velocity v encounter each other, the ionization occurs at large internuclear separations $R \gg n^2$, where n is the principal quantum number (atomic units are used). We consider a model system of coupling between two hydrogen Rydberg atoms via dipole-dipole interaction leading to the Auger process: one of the atoms undergoes a transition from state $(n_d l_d)$ to a deeper bound state $(n'_d l'_d)$, while the other atom gains the released energy and jumps from state $(n_i l_i)$ to the continuum (state $(\varepsilon_i l'_i)$). If $n_i \gg 1$, it becomes possible in the respective ionization cross section

$$\sigma_{PI} = 3.16 \left[(3/8)\pi\widetilde{\Gamma} v^{-1}\right]^{2/5} \tag{1}$$

to describe the reduced autoionization width $\widetilde{\Gamma}$ [1] of two Rydberg atoms by a simple expression

$$\widetilde{\Gamma} \simeq \frac{1}{4\pi^2}\left[\frac{3^{\frac{1}{6}}}{2^{\frac{1}{3}}}\Gamma(\frac{2}{3})\right]^4 \frac{1}{n_d^3 n_i^3}\left[\frac{3}{17}\left(\frac{1}{2(\tilde{n}_d-1)^2}-\frac{1}{2n_d^2}\right)^{-\frac{17}{3}}+\left(\frac{1}{2\tilde{n}_d^2}-\frac{1}{2n_d^2}\right)^{-\frac{20}{3}}\right] \tag{2}$$

using the asymptotic semiclassical formulae for dipole matrix elements [2]. Here $\tilde{n}_d$ is the principal quantum number of the nearest level below the virtual level with the effective quantum number n_d^* obeying the requirement $n_d^{*-2} = n_i^{-2} + n_d^{-2}$. Figure 1 demonstrates an interesting counter-intuitive phenomenon: decrease of the n_d-value for the bound atom (corresponding to decreasing its size) results in an essential increase of the ionization efficiency.

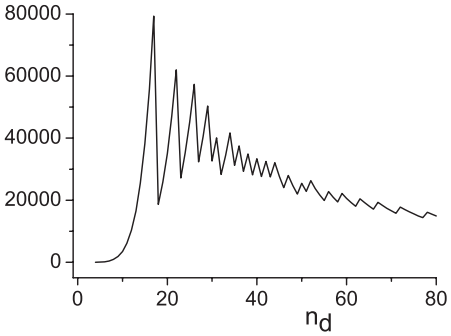

Figure 1: *Reduced cross section $\sigma_{PI} v^{2/5}$ of two Hydrogen Rydberg atoms in p-states ($l_i = l_d = 1$) with the fixed principal quantum number $n_i = 50$ of the ionized atom.*

We acknowledge the support by the EU FP7 IRSES Project COLIMA.

References

[1] T. Amthor *et al.*, Eur. Phys. J. D **53**, 329 (2009).
[2] N. N. Bezuglov, V. M. Borodin, Opt. Spectrosc. **86**, 467 (1999).

Spin domain formation in an expanding anti-ferromagnetic quantum gas

J. Szczepkowski[1,2], M. Witkowski[1,3], R. Gartman[1,4], M. Piotrowski[1,4], M. Zawada[1,4], and W. Gawlik[1,5]

[1] *National Laboratory for Atomic Molecular and Optical Physics, Grudziądzka 5, 87-100 Toruń, Poland*
[2] *Institute of Physics, Polish Academy of Sciences, al. Lotników 32/46, 02-668 Warszwa, Poland*
[3] *Institute of Physics, University of Opole, Oleska 48, 45-052 Opole, Poland,*
[4] *Institute of Physics, Nicolaus Copernicus University, Grudziądzka 5, 87-100 Toruń, Poland*
[5] *Institute of Physics, Jagiellonian University, Reymonta 4, 30-057 Kraków, Poland*
Corresponding Author: jszczep@ifpan.edu.pl

The spontaneous spin-symmetry breaking and spin domain formation have attracted great interest in recent years due to their relation to the theory of quantum phase transitions [1] as well as possible applications in precise measurements [2]. We present an experimental observation of the spontaneous spin-symmetry breaking and generation of spin domains in an anti-ferromagnetic ^{87}Rb F=2 Bose-Einstein condensate. The condensate is formed by up to 10^6 ^{87}Rb atoms in the $|F{=}2, m_F{=}2\rangle$ hfs component of their ground state contained in a magnetic trap. Contrary to all previously published experiments, the spin evolution and spin domain formation occurs during the free-fall expansion in the field of gravity in a presence of a homogeneous magnetic field. In the successive realizations of the identically performed experiment the positions of spin domains vary (Fig. 1). Although after averaging over many realizations the spin domains vanish, they are still present in the averaged power spectra. Additionally collisions between spin domains have been studied experimentally.

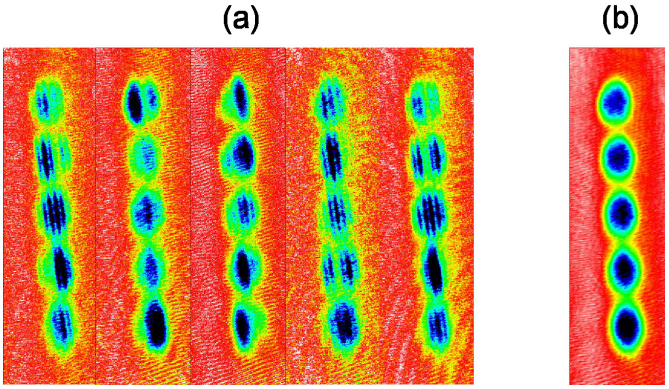

Figure 1: *(a) The successive realizations of the spin domains starting from the same initial experimental conditions. (b) The averaged image of 72 realizations.*

References

[1] A. Lamacraft, Phys. Rev. Lett. **98**, 160404 (2007).
[2] S. R. Leslie *et al.*, Phys. Rev. A **79**, 043631 (2009).

Study of the Bose-Hubbard model by collapse and revival measurements

E. Tiesinga[1], P. R. Johnson[2]

[1] *Joint Quantum Institute, National Institute of Standards and Technology and University of Maryland, 100 Bureau Drive, Stop 8423 Gaithersburg, MD 20899, USA*
[2] *Department of Physics, American University, Washington DC 20016, USA*
Corresponding Author: eite.tiesinga@nist.gov

We show that collapse and revival experiments with interacting atoms trapped in an optical lattice, based on a suggestion by [1], are a sensitive tool for characterizing its many-body ground state. Collapse and revival experiments involve sudden increases of the lattice depth whereby the system transfers from an initial superfluid ground state to a non-stationary state for a lattice depth where tunneling between sites is negligible. The state then evolves independently in each site for a variable amount of time, after which the momentum distribution is measured. The time evolution of momentum states are then sensitive to the amplitude of the initial atom-number Fock states, and, hence, contain information about the superfluid ground state. The frequencies that are present in the time evolution are determined by the two-body interaction strength as well as induced effective three- and higher-body interactions [2]. We show that for superfluid states away from the Mott insulator phase boundary the evolution has many more frequency components than superfluid states close to this boundary.

References

[1] S. Will, T. Best, U. Schneider, L. Hackermuller, D.-S. Luhmann, and I. Bloch, Nature **465**, 7295 (2010).
[2] P. R. Johnson and E. Tiesinga and J. V. Porto and C. J. Williams, New J. Phys. **11**, 093022 (2009).

Fundamental Physics: Experiment

Analysis of the odd parity configurations of tantalum atom–revisited

B. Arcimowicz[1], J. Dembczyński[1], P. Głowacki[1], M. Elantkowska[1], J. Ruczkowski[1], G. H. Guthöhrlein[2], and L. Windholz[2]

[1] *Chair of Quantum Engineering and Metrology, Faculty of Technical Physics, Poznań University of Technology, Nieszawska 13B, PL-60-965 Poznań, Poland*
[2] *Institute of Experimental Physics, Graz University of Technology, Petersgasse 16, A-8010 Graz, Austria*

Corresponding Author: bronislaw.arcimowicz@put.poznan.pl

The attempts of interpretation of the fine and hyperfine structure measurements in tantalum atom, performed so far [1,2], do not allow the prediction of the energy values of unknown levels with sufficient accuracy. On the basis of the results presented in [3,4] one could in principle expect that the appropriate number of odd configurations included in calculations would yield a concise interpretation of the hyperfine structure of all 290 experimentally determined levels. However, in spite of extension of the basis up to 28 configurations, still some substantial differences between the calculated and the measured values occurred, which were hard to explain. Dependent on the assumed theoretical relations between the parameters, the deviations observed suggested either incorrect assignment of the quantum number J or an error in experimental determination of the energy value. Since the calculations included all kinds of interactions predicted in the first and the second order perturbation theory, verification of the experimental data seemed necessary. Experimental energy values for 100 levels were verified. Each spectral line corresponding to the transition involving the level in question was carefully analyzed from the point of view of its hyperfine structure; the results obtained with a Fourier spectrometer [3] were taken into account in this respect. Moreover, in the UV regime the adequate results were obtained with a grating spectrometer PGS-2. The spectra were recorded in higher diffraction orders (3-6) to achieve a sufficient resolution for clear visibility of the hyperfine structure [5].

This work was supported by Politechnika Poznańska under the project DS 63-029/2011

References

[1] B. Arcimowicz, J. Dembczyński, EGAS Conference Graz (2008).
[2] B. Arcimowicz, J. Dembczyński, EGAS Conference Gdańsk (2009).
[3] N. Jaritz, L. Windholz, U. Zaheer, M. Farooq, B. Arcimowicz, R. Engleman Jr, J. C. Pickering, H. Jäger, and G. H. Guthöhrlein, Phys. Scr. **74**, 211–217 (2006).
[4] P. Głowacki, private communication.
[5] B. Arcimowicz, private communication.

The status of the Kielce EBIS facility for the studies of ion-matter interactions

D. Banaś[1], J. Braziewicz[1], M. Pajek[1], J. Semaniak[1], and D. Sobota[1]

[1] *Institute of Physics, Jan Kochanowski University, 25-406 Kielce, Poland*
Corresponding Author: d.banas@ujk.kielce.pl

The status of the new EBIS-A facility constructed by the Dreebit GmbH, Dresden, for the EBIT/x-ray laboratory at the Jan Kochanowski University (UJK) in Kielce designed for the studies of ion-matter interactions is presented. The facility will be used for the interdisciplinary studies involving atoms, molecules, plasmas, surfaces and cells by taking an advantage of low-energy highly charged ions (HCI) and x-ray spectroscopy techniques [1]. The EBIS-A facility, consisting of an EBIT-type ion source, ion beam guiding and diagnostic systems, double focusing analyzing magnet and multipurpose experimental chamber, offers new opportunities for performing the experiments on slow, highly charged ions colliding with matter, including such different phenomena as formation of nanostructures in ion-surface interactions, recombination processes in plasma, fragmentation of biomolecules by electron impact, and radiobiological effects in living cells.

In the EBIS-A facility, low-energy highly charged ions will be produced by the permanent magnet EBIT ion source developed by Dreebit GmbH. The source supplies a wide range of slow highly charged ions from bare ions of light elements to Ne-like and Ar-like ions of high-Z elements. The maximum electron energy and electron current available for ionization of the trapped ions are equal 25 keV and 200 mA, respectively. The produced ions can be extracted both in a pulse mode (pulse width from 2 μs up to 40 μs) and leaky mode (DC) by applying ion acceleration voltage up to 30 kV.

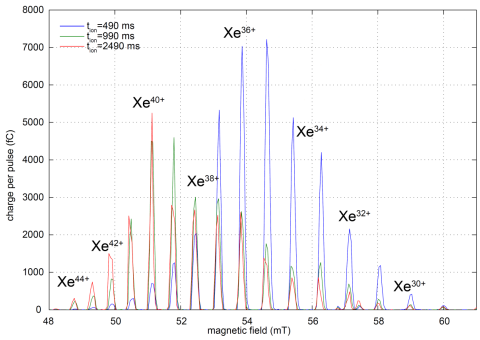

Figure 1: *Results of the first tests of the facility showing the xenon ion beam charge states measured in the experimental chamber for three different trapping times in the EBIT ion source.*

Here, a concept of the laboratory, construction details of the EBIS-A facility, the results of the first tests as well as the research program will be presented.

This work was supported by the Polish Ministry of Science and Higher Education under Grant No. N N202 463539. The equipment was purchased thanks to the financial support of the European Regional Development Fund in the framework of the Polish Innovative Economy Operational Program (contract no. WNP-POIG.02.02.00-26-023/08).

References

[1] D. Banaś *et al.*, Journal of Instrumentation **5**, C09005 (2010).

A versatile setup to study Rydberg atom – surface interactions

D. Barredo[1], R. Daschner[1], H. Kübler[1], R. Löw[1], and T. Pfau[1]

[1] *Physikalisches Institut, Universität Stuttgart, Germany*

Corresponding Author: d.barredo@physik.uni-stuttgart.de

The coherent control of strong interactions between Rydberg atoms hold great promise for the manipulation of quantum information [1]. While to date most exciting results on quantum computation have come from experiments in the ultracold temperature regime, very recently it has been shown that coherent excitations of Rydberg states can also be achieved in thermal ensembles of atoms confined in microcells [2,3]. Compared to ultracold atomic systems, thermal atomic vapor cells offer an attractive alternative in terms of scalability for practical devices, e.g., by making use of current LCD technology. However, for the successful applicability of this approach, decoherence effects with nearby walls need to be minimized.

We aim at studying the surface-Rydberg atom interaction in a UHV environment as a function of surface composition, corrugation, and temperature for different Rydberg states, atomic species and buffer gases. We will further explore to what extent geometric patterned microstructures and electric fields on the surface can be used to tailor the interaction strength with Rydberg atoms, both spatially and temporally. Finally, we plan to investigate and quantitatively measure Casimir forces for dielectrics at finite temperature, which have barely been studied before.

References

[1] M. Saffman, T. G. Walker, and K. Mølmer, Rev. Mod. Phys. **82**, 2313–2363 (2010).
[2] T. Baluktsian *et al.*, Opt. Lett. **35**, 1950–1952 (2010).
[3] H. Kübler *et al.*, Nature Photon. **4**, 112–116 (2010).

Hyperfine structure measurements in the $3d^3 4s4p\ ^6G_J$ levels of atomic vanadium with Fourier transform spectroscopy

Gö. Başar[1], F. Güzelçimen[1], A. Jarmola[2], M. Tamaris[2], R. Ferber[2], and S. Kröger[3]

[1] *Istanbul University, Faculty of Science, Physics Department, 34134 Vezneciler, Istanbul, Turkey*
[2] *Laser Centre, University of Latvia, 19 Rainis Boulevard, 1586 Riga, Latvia*
[3] *Hochschule für Technik und Wirtschaft, Wilhelminenhofstrasse 75A, 12459 Berlin, Germany*
Corresponding Author: gbasar@istanbul.edu.tr

Vanadium is one of the iron-group elements which are important for astrophysics. The spectrum of V is characterized by a broad hyperfine structure caused by the large nuclear magnetic dipole moment of the predominant stable isotope ^{51}V (nuclear spin of $I = 7/2$ and natural abundance more than 99%).

Experimental hyperfine structure analysis of neutral vanadium was performed in the Laser Centre of the University of Latvia with a high-resolution Fourier transform (FT) spectrometer, Bruker IFS 125HR at 0.03 cm^{-1} resolution. A hollow-cathode discharge was used to evaporate vanadium and to excite the free atoms.

The aim of the present study is the determination of magnetic dipole hyperfine structure constants A for the energetically low lying levels belonging to the term $3d^3 4s4p\ ^6G$ of V I. The spectral lines combining the energy levels of this term lie in the wavelength range from 470 nm to 490 nm and, as a rule, have very low intensity. Therefore the spectrum of V I was recorded using an optical bandpass filters in the setup of the high-resolution FT spectrometer to optimize the signal-to-noise ratio.

Nine transitions have been measured and analyzed, the wavelengths of which are listed in the NIST Atomic Spectra Database [1] and the NBS wavelength tables [2]. The measured hyperfine structure patterns were fitted using Voigt profile functions by means of a fit program called FITTER [3]. All hyperfine structures are not completely resolved. Therefore the line profiles were fitted fixing the hyperfine structure constants of the upper levels belonging to the term $3d^3 4s5s\ ^6F$, which are well known from the literature [4]. New results are presented for all six levels belonging to the $3d^3 4s4p\ ^6G$ term.

References

[1] NIST Atomic Spectra Database Version 2.0, online at http://www.nist.gov/pml/data/asd.cfm.
[2] W. F. Meggers, C. H. Corliss, B. F. Scribner, *Tables of Spectral-Line Intensities, Part I - Arranged by Elements*, Natl. Bur. Stand. (U.S.), Monogr. **145** (1975).
[3] G. Guthöhrlein, University of Bundenswehr Hamburg, unpublished (2004).
[4] P. Palmeri *et al.*, Physica Scripta **55**, 586 (1997).

Lifetime measurements and calculations in Y^+ and Y^{2+} ions

É. Biémont[1,2], K. Blagoev[3], L. Engström[4], H. Hartman[5], H. Lundberg[4], G. Malcheva[3], H. Nilsson[5], R. Blackwell–Whitehead[5], P. Palmeri[1], and P. Quinet[1,2]

[1] *Astrophysique et Spectroscopie, Université de Mons–UMONS, 20 Place du Parc, B-7000 Mons, Belgium*
[2] *IPNAS (Bât. B 15), Université de Liège, Sart-Tilman, B-4000 Liège 1, Belgium*
[3] *Institute of Solid State Physics, Bulgarian Academy of Sciences, 72 Tzarigradsko Chaussee, BG-1784 Sofia, Bulgaria*
[4] *Department of Physics, Lund University, PO Box 118, S-221 00, Lund, Sweden*
[5] *Lund Observatory, Lund University, PO Box 43, S-221 00 Lund, Sweden*
Corresponding Author: E.Biemont@ulg.ac.be

Transition probabilities in yttrium ions are needed in astrophysics for the determination of the chemical composition of the sun and of the stars.

In Y II, the available lifetimes are scarce. The only previous measurements are those of Andersen *et al.* [1], Hannaford *et al.* [2], Gorshkov and Komarovskii [3] and Wännström *et al.* [4]. When comparing the different sets of results, it appears that some discrepancies are present and that the different lifetime measurements for the same level do not necessarily agree within the experimental errors. Previous experimental determinations of transition probabilities in Y II include the shock tube measurements by Pitts & Newsom [5] and, more recently, the investigation by Reshetnikova & Skorokhod [6].

Up to now, the measurements of radiative lifetimes in Y III are very limited, the only work being the beam-foil measurements of Maniak *et al.* [7]. In their paper aimed at the determination of elemental abundances in the χ Lupi star from HST/GHRS Echelle spectra, Brage *et al.* [8] emphasized the importance of accurately including the core-valence correlation in the calculations to obtain reliable transition probabilities.

In the present work, we report a new set of theoretical transition probabilities in Y II, obtained using a multi-configuration HFR method including core-polarization effects. The over all quality of the calculations is assessed by comparisons with new and previous lifetime measurements. New measurements of 5 lifetimes in the 4d5p and 5s5p configurations of Y II have been performed using the time-resolved laser-induced fluorescence method. New measurements of two 5p levels in Y III are also reported. The experimental lifetimes are compared to theoretical results and the observed agreement between theory and experiment gives confidence to the oscillator strengths obtained for 84 transitions of Y II in the wavelength range 2243 to 10 605 Å and for 182 transitions of Y III between 643 and 9984 Å.

References

[1] T. Andersen, P. S. Ramanujan, and K. Bahr, Astrophys. J. **223**, 344 (1978).
[2] P. Hannaford *et al.*, Astrophys. J. **261**, 736 (1982).
[3] V. N. Gorshkov, and V. A. Komarovskii, Opt. Spectrosc. **60**, 541 (1986).
[4] A. Wännström *et al.*, Phys. Scr. **38**, 564 (1988).
[5] R. E. Pitts, and G. H. Newsom, J. Quant. Spectrosc. Radiat. Transfer **35**, 383 (1986).
[6] O. F. Reshetnikova, and E. P. Skorokhod, Opt. Spectrosc. **87**, 829 (1999).
[7] S. T. Maniak *et al.*, Astron. Astrophys. **286**, 978 (1994).
[8] T. Brage *et al.*, Astrophys. J. **496**, 1051 (1998).

Experimental verification isotope shift of some levels even parity in neutral Eu

B. Furmann[1]

[1] *Chair of Quantum Engineering and Metrology, Poznań University of Technology, Poznań, Poland*

Corresponding Author: boguslaw.furmann@put.poznan.pl

Isotope shift of electronic levels in neutral europium atom was extensively investigated in the 80's and 90's of the last century [1-7]. Owing to the results of the experimental works, where the sharing rule was applied, as well as the parametrization method for isotope shifts proposed by Bauche [8], the values of the isotope shifts and CSO parameters for the following configurations: $4f^7 5d6s$, $4f^7 6s7s$, $4f^7 6s8s$, $4f^7 6s6d$, $4f^7 6s6p$. The values of one-configuration parameters obtained show good consistency with the results of *ab initio* calculations and with the dependencies observed for other lanthanide elements. These values were obtained predominantly on the basis of the "pure" or "almost pure" electronic levels belonging to the configurations mentioned. In the case of the remaining configurations in europium atom, in particular the following configurations: $4f^6 5d^2 6s$, $4f^7 6s7p$, $4f^7 6s5f$, it is impossible to find pure levels. Thus the interpretation has to account for the configuration mixing. In our newest work (under preparation for publication) [9] we present the results of the new measurements for isotope shifts of the even electronic levels with the energies in the range 30 000–42 000 cm^{-1}, obtained with the method of laser induced fluorescence. The work mentioned contains also an attempt of interpretation of our results and the results known from the literature with the use of the intermediate-coupling from the semiempirical analysis of the fine and the hyperfine structure [10]. For most of the levels analyzed, including the high-lying ones, we obtained a good agreement between our experimental results and the predictions and the *ab initio* results. However, in some cases considerable discrepancies were encountered. It seems astonishing, the more so that the levels which demonstrate such discrepancies, lie relatively low (28 000–32 000 cm^{-1}). These levels were formerly classified in a different way [11]; however, the new assignment does not yield the correct values of isotope shifts (although it provides a good interpretation of the fine and the hyperfine structure). The subject of this contribution are new results of the measurements of isotope shifts for these "controversial" levels.

The work was partially supported by Poznań University of Technology within the frame of the project DS63–029/11.

References

[1] J. R. Kropp, H. D. Kronfeldt, R. Winkler, Z. Phys. A **321**, 365–369 (1985).
[2] H. Bruggemeyer *et al.*, Z. Phys. D **1**, 55-64 (1986).
[3] J. R. Kropp, R. Winkler, J. F. Wyart, Z. Phys. D **2**, 99–103 (1986).
[4] T. Brodzinski, H. D. Kronfeldt, R. Winkler, Z. Phys. D **6**, 363–364 (1987).
[5] H. D. Kronfeldt, P. Seifert, Z. Phys. D **8**, 11–15 (1988).
[6] P. Seifert *et al.*, Z. Phys. D **14**, 99-106 (1989).
[7] H. D. Kronfeldt, D. J. Weber, Phys. Rev. A **43**, 4837–4844 (1991).
[8] J. Bauche, R. J. Champeau, Adv. At. Mol. Phys. **12**, 39–83 (1976).
[9] B. Furmann, D. Stefanska "Isotope shift in mixed even configurations neutral Eu", in preparation.
[10] J. Dembczynski, Private communication.
[11] G. Smith, M. Wilson, JOSA **60**, 1527 (1970).

Hyperfine structure measurements and determination of new energy levels of atomic lanthanum by laser induced fluorescence spectroscopy

F. Güzelçimen[1], Gö. Başar[1], I. Siddiqui[2], L. Windholz[2], and S. Kröger[3]

[1] *Istanbul University, Faculty of Science, Physics Department, 34134 Vezneciler, Istanbul, Turkey*
[2] *Institut für Experimentalphysik, Technische Universität Graz, Petersgasse 16, A-8010 Graz, Austria*
[3] *Hochschule für Technik und Wirtschaft, Wilhelminenhofstraße 75A, 12459 Berlin, Germany*
Corresponding Author: feyza7@gmail.com

In a continuation of previous work done at the TU Graz [1], we have further investigated spectral lines of 5d-shell element lanthanum. In the present work we aimed to determine magnetic dipole hyperfine interaction constant A for higher lying energy levels, to classify new spectral lines as well as to discover new fine structure energy levels of La I.

The measurements have been performed with laser-induced fluorescence spectroscopy using a tunable ring-dye laser pumped by Ar-ion laser. With the dyes Kiton-Red and Rhodamine 6G we cover the spectral range from 560 nm to 625 nm and form 710 nm to 745 nm, respectively. La atoms are produced by sputtering in a hollow cathode discharge.

The hyperfine structure has been analyzed for 73 new spectral lines of La I, which are not listed in Meggers [2] and MIT [3] wavelength tables. The classification program [4] was used to classify the spectral lines. It shows all suggestions of possible transitions for the wavelength of spectral lines taking into account the selection rules for electric dipole radiation. We discovered 10 new fine structure energy levels of even parity. The magnetic dipole hyperfine interaction constants A have been determined for 48 energy levels. They are compared with reference values [5-8], if available. Twelve A constants of even parity levels and one A constants of odd parity level have been measured for the first time.

References

[1] Y. Nighat *et al.*, J. Phys. B **43**, 125001 (2010).
[2] W. F. Meggers, C. H. Corliss, B. F. Scribner, *Tables of Spectral-Line Intensities*, Natl. Bur. Stand. (U.S.), Monogr. **145** (1975).
[3] Harrison G. R. (ed) (1969) *M.I.T. Wavelength Tables*, MIT Press, Cambridge (1969).
[4] L. Windholz, G. H. Guthöhrlein, Physica Scripta **T105**, 55 (2003).
[5] W. J. Childs, U. Nielsen, Phys. Rev. A **37**, 6 (1988).
[6] Gö. Başar *et al.*, Physica Scripta **75**, 572 (2007).
[7] B. Furmann, D. Stefanska, J. Dembczynski, Physica Scripta **76**, 264 (2007).
[8] B. Furmann, D. Stefanska, J. Dembczynski, J. Phys. B **42**, 175005 (2009).

Measurement and evaluation of transitions probabilities of Ar I to III

Ch. Berenguer[1], K. Katsonis[1], P. Tsekeris[2], S. Cohen[2], M. Cornille[3], and R. E. H. Clark[4]

[1] *GAPHYOR, CNRS-LPGP, Université Paris-sud, 91400 Orsay, France*
[2] *Physics Department, University of Ioannina, GR-45110 Ioannina, Greece*
[3] *LUTH, CNRS, Observatoire de Paris, 92190 Meudon, France*
[4] *University of Texas, Sans Antonio, USA*

Corresponding Author: konstantinos.katsonis@u-psud.fr

The subject of this collaborative work is argon spectroscopy, focusing on structure and atomic data evaluation in order to facilitate the diagnostics and modeling of plasmas containing argon. We focus here on transition probability (A_{ij}) measurements and evaluation for Ar I, II, and III. These species are encountered in low temperature argon plasmas, present in many industrial applications, and notably in plasma thrusters. Spectroscopic Ar measurements and data calculation and evaluation have been performed and described previously (see e.g., [1,2]). The experimental spectra presented here (wavelength region of 190 to 940 nm) have been acquired in a Fe-hollow cathode lamp with a low (2 mA) and a high (10 mA) current. The light stemming from the lamp has been guided to a CCD-camera-equipped monochromator via a UV-grade fused silica lens. Background corrections and wavelength calibrations have been made and the grating efficiency has been taken into consideration.

We describe the line identification results and the line intensity and A_{ij} ratios giving experimental A_{ij} values for numerous multiplets. We compare our experimental results with the intensity ratios coming from various experiments and with the A_{ij} ratio results obtained by using our CbA code [3] based on the Coulomb approximation. We obtained theoretical results by calculations with the SST [4] and the CATS codes [5]. We compare our A_{ij} with those evaluated by NIST [6] and with those available in the literature, both theoretical and experimental.

The research leading to these results has received funding from the European Community's Seventh Framework Programme (FP7/2007-2013) under grant agreement N° 218862.

References

[1] Ch. Berenguer, K. Katsonis, S. Danakas, S. Cohen, P. Tsekeris, M. Cornille, ICAMDATA 06 Conference, 28-31 October 2008, Beijing (China).
[2] K. Katsonis, Ch. Berenguer, M. Cornille, IEPC09 Conference, 20–24 September 2009, Ann Arbor (USA) IEPC-2009-**035**.
[3] K. Katsonis, H.-W. Drawin, JQSRT **23**, 1 (1980).
[4] W. Eissner, M. Jones, H. Nussbaumer, Com. Phys. Comm. **8**, 270 (1974).
[5] J. Abdallah Jr., R. E. H. Clark, R. D. Cowan, Report LA-11436-M, Los Alamos, USA (1988). http://aphysics2.lanl.gov/tempweb/.
[6] http://physics.nist.gov/PhysRefData/ASD/index.html

Investigation of the hyperfine structure of Pr I lines involving levels having J= 7/2

S. Khan[1], L. Windholz[1]

[1] *Institute of Experimental Physics, Graz University of Technology, Petersgasse 16, A-8010 Graz, Austria*

Corresponding Author: shamimkhan81@yahoo.com

In this work, we report the discovery of 26 new energy levels of even parity and 12 new energy levels of odd parity having J = 7/2 (this is a selection out of all new levels). The levels were discovered by experimentally investigating their hyperfine structure (hfs) in a hollow cathode discharge lamp (HCL) by the method of laser induced fluorescence (LIF) spectroscopy. High resolution Fourier transform emission spectra for praseodymium [1] are used for extracting the values of investigated wavelengths. The excitation source is a tunable ring-dye laser system, operated with R6G, Kiton Red, DCM and LD700. The laser wavelength is tuned to a strong hyperfine component of the investigated spectral line, and fluorescence signals from excited levels are searched. J-values and hyperfine constants A of the combining levels have been determined from the recorded hyperfine structure. Due to spherical charge distribution inside the nucleus of praseodymium, its electric quadrupole moment is very small and in most cases the electric quadrupole interaction constant B is neglected. The information about the J-values and A-values of the combining levels, together with excitation and fluorescence wavelengths, allows us to determine the energies of the involved levels. The new up to now unknown levels are confirmed by more than one laser excitation. For some of the new levels, beside their wave number, their total angular momentum quantum number J, their parity as well as their magnetic dipole hyperfine interaction constant A are presented in Table 1.

Energy/cm^{-1}	J	parity	A / MHz	Excitation wavelength λ(air)/Å
22 486.816	7/2	even	948.34	7022.178
26 121.376	7/2	even	805(5)	6792.357
27 123.626	7/2	even	684(3)	6255.292, 6070.13
27 231.853	7/2	even	773(2)	7153.26, 7217.149
27 381.792	7/2	even	662(3)	6256.568, 6545.725
27 679.190	7/2	even	654(5)	5802.48, 6045.15
20 012.862	7/2	odd	1133(5)	7045.286
21 975.472	7/2	odd	344(3)	6440.004, 5698.625
22 451.972	7/2	odd	1125(4)	7240.105, 6248.204,7490.283
23 293.356	7/2	odd	759(3)	5936.052, 5965.723, 5722.358
24 443.783	7/2	odd	1046(2)	7016.088, 7496.383
25 350.082	7/2	odd	1074(3)	5984.124, 6478.298
25 788.548	7/2	odd	138(6)	5624.172, 5831.080
26 915.484	7/2	odd	1122(3)	6547.336, 5808.71, 5613.118
27 890.013	7/2	odd	877(5)	5649.664, 6504.24

Table 1: *Data of investigated levels.*

References

[1] B. Gamper, Z. Uddin, M. Jahangir, O. Allard, H. Knockel, E. Tiemann, and L. Windholz, J. Phys. B **44**, 045003 (2011).

Interference between differently localized electrons in N_2O

A. Knie[1], P. Reiss[1], and A. Ehresmann[1]

[1] *Institute of Physics and CINSaT, Universität Kassel, D-34132 Kassel, Germany*
Corresponding Author: knie@physik.uni-kassel.de

For many fundamental processes in nature, quantum mechanical interference leads to dramatic counter-intuitive observations. N_2O is a prototypical linear three-atomic molecule and was investigated with nearly any known experimental technique. For example, in [1] the fluorescence spectrum has been recorded after site selective excitation of the 1s-3π resonance as well as the N_2O $A^2\Sigma$-$X^2\Pi$ transitions are well known [2]. Several resonances of the terminal nitrogen 1s electron are overlapping at exciting-photon energies around 405 eV with the 1s-3π resonance of the central nitrogen atom [3]. It is likely that the overlapping N_t 1s-electron resonances interfere in a similar way as the well known lifetime vibrational interference (LVI) or electronic states interference (ESI). However, it is yet unclear if electrons strongly localized at different molecular sites prior to excitation can interfere. This was investigated via analysis of angularly resolved fluorescence emitted by excited N_2O^+ and NO^+, N_2^+ and N^+ fragments after core-electron resonance excitation by small bandwidth monochromatized synchrotron radiation. One dominantly produced fragment after excitation of the 1s-3π resonances of N_2O is NO^+ [4]. The population of its different excited states has been probed via fluorescence emission from 120 nm–180 nm. Whereas the total fluorescence emission cross section is usually not sensitive to interference a more sensitive probe is the fluorescence angular distribution or a polarization analysis [5]. Experiments have been performed determining the angular distribution of spectrally resolved fluorescence emission after small bandwidth excitation at the UE56/2 PGM 1 beamline at BESSY II, Berlin.

The measured intensities parallel and perpendicular to the electric field vector of the exciting radiation, i.e., horizontally or vertically linear polarized synchrotron radiation, were used to determine the angular distribution parameter β:

$$\beta = 2\frac{I_h - I_v}{I_h + 2I_v} \qquad (1)$$

For a singly ionized N fluorescence line at 174 nm the obtained β-values are given in Fig. 1. Variation of the β-parameter with the exciting-photon energy are observed in the region of overlapping resonances. For an easier comparison the total ion yield is given with the depicted resonances (taken from [3]).

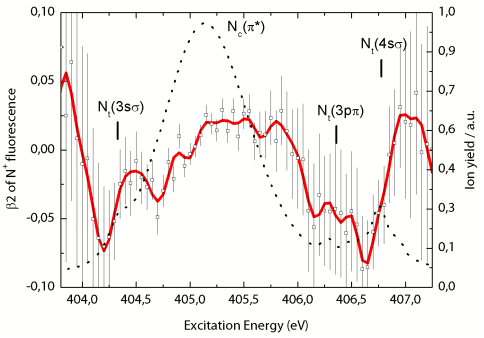

Figure 1: *Angular distribution parameter β of NII fluorescence after excitation of different depicted N_2O resonances. Squares: measured beta values; solid red: FFT filtered guide to the eye; dotted black: total ion yield. Resonances from [3].*

These preliminary results gives evidence for interference effects between electrons of different localizations. The scale of other on ESI based changes of the angular distribution [5] is comparable to the found effect.

References

[1] M. Meyer *et al.*, J. Elec. Spec. **101** 81 (1999).
[2] J. H. Callomon and F. Creutzberg, Phil. Trans. R. Soc. Lond. **A277** 157 (1974).
[3] J. Adachi *et al.*, J. Chem. Phys. **102** 7369 (1995).
[4] J. Murakami *et al.*J. Chem. Phys. **85** 5755 (1986).
[5] Ph. V. Demekhin *et al.*Phys. Rev. Lett. **104** 243001 (2010).

Impurity-phonon coupling in liquid and solid helium

V. Lebedev[1], P. Moroshkin[1], and A. Weis[1]

[1] *Department of Physics, University of Fribourg, CH-1700 Fribourg, Switzerland*
Corresponding Author: Victor.Lebedev@unifr.ch

We present a systematic laser-spectroscopic study of transition-metal (Cu, Au) atoms embedded in liquid and solid ^{4}He cryomatrices. In particular we observe transitions of valence and inner shell electrons. The former yield broad structureless spectral lineshapes (Fig. 1, right), similar to those of the well-studied resonance lines of alkali metal atoms in condensed helium. The latter possess a peculiar structure shown in the left part of Fig. 1. Their spectra consist of a narrow zero-phonon line (ZPL) and a broader redshifted phonon wing (PW). There exists a pronounced difference in the PW spectra observed in superfluid and solid He.

Metal atoms in condensed helium reside in nanoscopic bubbles (topic reviewed in [1]). Electronic transitions in the outer shell induce a sudden change of the bubble size and bubble interface oscillations, which can be understood as strongly localized wavepackets of matrix phonons. The interaction leads to a large homogeneous broadening and a blue shift of the dopant's spectral lines. Electrons in the inner $(n-1)d$-shell of a transition-metal atom are screened by the outer ns-shell and do not interact with the surrounding He atoms. Transitions of the inner shell electrons therefore do not induce large changes of the bubble configuration, and the excitation of the matrix phonons is expected to be strongly suppressed. Nevertheless, the observed phonon wing structure reveals a weak coupling of the d-electrons to phonons.

The experimental laser-induced fluorescence lineshapes provide information on the spectra of the associated phonon wavepackets that can be used to reconstruct their structure and evolution. Our observations suggest a new approach for the investigation of elementary excitations in quantum fluids and solids based on the laser spectroscopy of embedded metal atoms.

This work is supported by the Swiss National Foundation, grant No. 200020–129831.

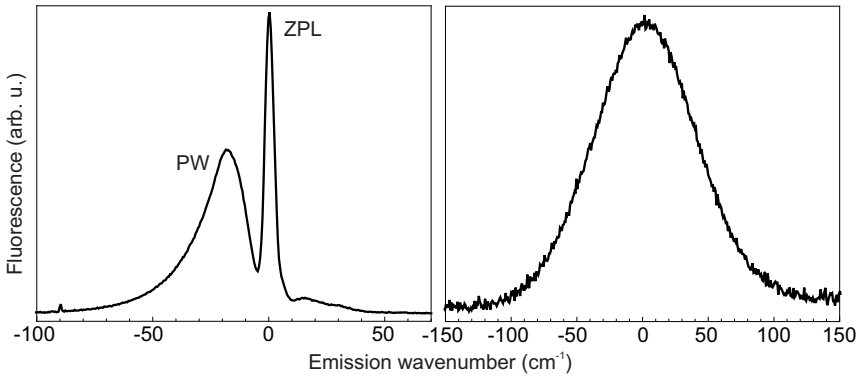

Figure 1: *The lineshapes of the* $3d^9 4s^2\ ^2D_{3/2}$ - $3d^{10}4s\ ^2S_{1/2}$ *(left) and* $3d^{10}5s\ ^2S_{1/2}$ - $3d^{10}4p\ ^2P_{1/2}$ *(right) atomic line of Cu in solid* ^{4}*He.*

References

[1] P. Moroshkin, A. Hofer, and A. Weis, Phys. Rep. **469**, 1–57 (2008).

Electronic structure of semi-core states in $BiFeO_3$ thin films: an experimental and *ab initio* study

Š. Masys[1], S. Mickevičius[2], S. Grebinskij[2], and V. Jonauskas[1]

[1] *Institute of Theoretical Physics and Astronomy, Vilnius University, A. Goštauto Street 12, LT-01108, Lithuania*
[2] *Center for Physical Sciences and Technology, Semiconductor Physics Institute, A. Goštauto Street 11, LT-01108, Lithuania*

Corresponding Author: sarunas.masys@tfai.vu.lt

$BiFeO_3$ (BFO) is a prototypical multiferroic material exhibiting simultaneous coexistence of ferrolectric, ferroelastic, and antiferromagnetic order. As this perovskite also offers room-temperature multifunctionality, it is currently under wide investigation.

Epitaxial thin films of BFO with thickness d ranging from about 150 nm to 200 nm were grown *in situ* at T=1023K by RF magnetron sputtering on lattice-matched $SrTiO_3$ (100) substrate. The XPS data were obtained with the tunable high-energy x-ray photoelectron spectrometer at the x-ray wiggler beam line BW2 of HASYLAB. The photoelectrons were measured using a hemispherical analyzer with parallel detection capability (SCIENTA SES-200). Excitation energy (3000 eV) was chosen and the total energy resolution at this photon energy was 0.6 eV. The binding energy scale was calibrated using the photoemission from gold reference sample.

Theoretical Hartree-Fock (HF) study was performed with DIRAC10 [1] code. Since BFO can be considered as a heavy-element system, in order to properly reproduce the electronic structure of its semi-core states it is necessary to apply relativistic treatment. The influence of spin-orbit interaction was investigated at molecular level by studying BFO unit cell of 10 atoms. HF calculations were carried out using two-component relativistic Hamiltonian [2]. The relativistic all-electron triple-zeta basis set for Bi was taken from [3]. For Fe and O, standard aug-cc-pVDZ and aug-cc-pCVDZ basis sets were adopted, respectively. The comparison between experimental and theoretical results is presented in Fig. 1.

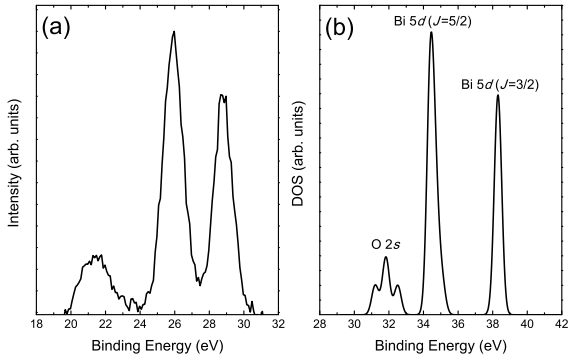

Figure 1: *XPS spectrum of BFO thin film (a) compared to the density of states (DOS) calculated using relativistic Hamiltonian (b).*

References

[1] http://dirac.chem.sdu.dk.
[2] M. Iliaš *et al.*, Chem. Phys. Lett. **408**, 210 (2005).
[3] K. G. Dyall, Theor. Chem. Acc. **115**, 441–447 (2006).

Experimental determination of collisional broadening for the 1083 nm 2^3S–2^3P transition of helium

T. Cantat–Moltrecht[1], P.–J. Nacher[1], and G. Tastevin[1]

[1] *Laboratoire Kastler Brossel, ENS; CNRS; UPMC; 24 rue Lhomond, F-75005 Paris, France*
Corresponding Author: nacher@lkb.ens.fr

Light absorption measurements are routinely performed on the 1083 nm transition of He for plasma diagnosis purpose in helium. They are used, for instance, to map or quantify the density of atoms in the 2^3S metastable state [1,2], or to measure selected populations of Zeeman sublevels and infer the electronic or nuclear polarization of ^{3}He gas in optical pumping experiments [3]. Well-resolved components of the 1083 nm line, such as C_8 and C_9 (2^3S, F=1/2–2^3P_0 and 2^3S, F=3/2–2^3P_0 for ^{3}He), are usually well suited for this purpose. Quantitative analysis of data requires accurate knowledge of absorption lineshapes. Figure 1 displays ^{3}He absorption spectra recorded at low magnetic field and room temperature. For the lowest gas pressure, lines are broadened mostly by the Boltzmann velocity distribution of the atoms (Doppler width: $D \sim 2$ GHz FWHM at 300K). The upper recordings in Fig. 1 demonstrate that the same absorption lines are considerably broadened for gas pressures of a few hundred mbar, and that these components are not resolved any more.

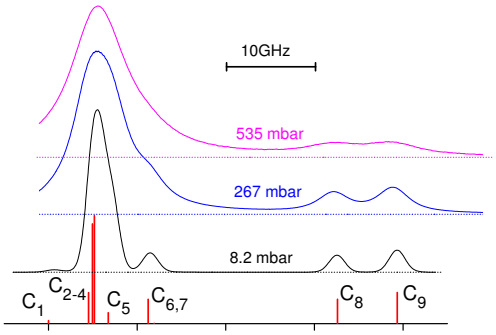

Figure 1: *Examples of absorption spectra recorded at room temperature in sealed cells filled with different amounts of ^{3}He gas. The nine fine and hyperfine structure components C_1–C_9 of the 2^3S–2^3P line at 1083 nm are probed using weak light from a single-frequency DFB laser diode. Their positions and their transition probabilities are displayed at the bottom of the graph.*

To precisely separate the collision-induced and the Doppler broadening in absorption spectra, we have performed series of absorption measurements in sealed glass cells filled (at room temperature) with ^{3}He pressures ranging from 8 to 535 mbar. The experiments were repeated for several cell temperatures between 210 and 370K, and complementary recordings were made using cells filled with ^{3}He-^{4}He mixtures. Data analysis is currently being performed, fitting absorption data with Voigt profiles to extract temperature-dependent FWHM collision and Doppler widths parameters, w and D. Results will be presented and compared to existing experimental [2,4,5] and computed [6] ^{4}He data using mass scaling arguments. The influence of errors in the value of the collision broadening parameter w on nuclear polarization measurements at high pressures and in high magnetic fields [7] will be discussed.

References

[1] M. W. Millard *et al.*, Plasma Sources Sci. Technol. **7**, 389–394 (1998).
[2] K. Tachibana, Y. Kishimoto, and O. Sakai, J. Appl. Phys., **97**, 123301+ (2005).
[3] C. Talbot *et al.*, *to be published in* Journal of Physics: Conference Series (2011), and contribution by C. Talbot *et al.*, this conference.
[4] D. Bloch, G. Trenec, and M. Leduc, J. Phys. B: At. Mol. Phys. **18**, 1093–1100 (1985).
[5] X. Zhao *et al.*, Phys. Rev. A **48**, 4350–4357 (1993).
[6] D. Vrinceanu, S. Kotochigova, and H. R. Sadeghpour, Phys. Rev. A **69**, 022714+ (2004).
[7] K. Suchanek *et al.*, Eur. Phys. J. Special Topics, **144**, 67–74 (2007).

Particularities of Doppler profile for supersonic beams with circular, square, and arbitrary collimating apertures

M. Bruvelis[1], A. Cinins[1], S. Mezinska[1], N. N. Bezuglov[2], I. I. Ryabtsev[3], and A. Ekers[1]

[1] *Laser Centre, University of Latvia, LV-1002 Riga, Latvia*
[2] *Faculty of Physics, St. Petersburg State University, 198904 St. Petersburg, Russia*
[3] *Institute of Semiconductor Physics, 630090 Novosibirsk, Russia*
Corresponding Author: ryabtsev@isp.nsc.ru

Since the collimation angle of particle beams is always finite, the residual Doppler broadening for laser excitation in the direction perpendicular to the particle beam axis is also finite, often comparable with the natural linewidth. Conventionally one involves Gaussian function to describe the Doppler profile $P(\Delta\nu)$ [1]. In an earlier study we have shown that the residual Doppler profile for circular collimating aperture of the supersonic beam can deviate from Gaussian, whereby a convenient analytical representation $P_c(\Delta\nu) = \sqrt{1 - \Delta\nu^2/\Delta\nu_D}$ can be used to describe the most essential core part of the profile [2].

Here, we consider the general case of arbitrary form of collimating aperture, when the Doppler profile is found by double integration over the nozzle exit plane area $\widetilde{A}$ and the aperture plane area A:

$$P_D(\Delta\nu) = \frac{1}{\widetilde{A}A}\int_{\widetilde{A}} d\widetilde{y}d\widetilde{x}\int_A dydx\int_0^\infty dv\frac{v^2}{\sqrt{\pi}v_f^2\Delta v_f}\exp-\frac{(v-v_f)^2}{{\Delta v_f}^2}\delta\left(\Delta\nu - \frac{(x-\widetilde{x})v}{L\lambda}\right), \quad (1)$$

where v is the velocity of an atom in the supersonic beam, v_f is the mean flow velocity of atoms in the beam, Δv_f is the velocity dispersion, L is the distance between the nozzle and the collimating aperture, and λ is the wavelength. The results of numerical calculations for square and circular collimating apertures are shown in Fig. 1. They demonstrate that the Doppler profile can deviate dramatically from the Gaussian shape.

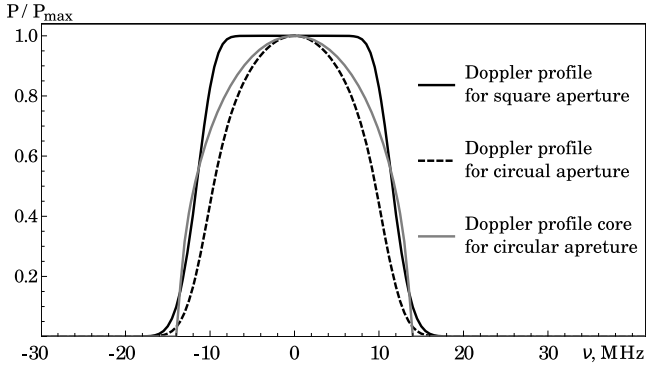

Figure 1: *Doppler profiles obtained by numerical simulations for beams with square and circular collimating apertures, and the core of the Doppler profile for circular collimating aperture.*

Support by the EU FP7 IRSES Project COLIMA is acknowledged.

References

[1] G. Scoles, *Atomic and Molecular Beam Methods*, Oxford, New York, (1998).
[2] N. N. Bezuglov, and M. Yu. Zaharov, *et al.*, Opt. Spectrosc. **102**, 819 (2007).

Hyperfine structure investigations of singly ionized praseodymium and discovery of new Pr II levels

I. Siddiqui[1], S. Khan[1], and L. Windholz[1]

[1] *Institute of Experimental Physics, Graz University of Technology, Petersgasse 16, A-8010 Graz, Austria*

Corresponding Author: imrnsmd@hotmail.com

Hyperfine structure spectra of singly ionized praseodymium have been investigated using laser induced fluorescence (LIF) spectroscopy in a hollow cathode discharge lamp (HCL). In this report we present 4 even parity and 2 odd parity new energy levels of Pr II. A high resolution Fourier transform (FT) spectra for praseodymium [1] is used to extract the values of the investigated wavelengths. Due to discharge conditions inside the HCL working at low pressure, the plasma is weakly ionized and majority of species are neutral atoms most of them in ground states. The others are distributed among all the possible excited states. In most cases the ionic lines have a very weak signal-to-noise ratio as seen in FT-Spectra.

As an example a new level at 33 386.215 cm^{-1}, odd parity, J= 3 and A= 1352(5) MHz is briefly discussed. Laser excitation of the line at 4361.81 Å is performed and a LIF signal is detected at fluorescence lines 3821 Å, 3912 Å, 4156 Å, 4517 Å. The hfs of the investigated line is then recorded digitally and is fitted to obtain spectroscopic parameters of the combining levels. A best fit situation was obtained for values $J_o = 3$, $J_u = 4$, $A_o = 1356$ MHz and $A_u = 1618$ MHz (subscript o refers to 'oben' = upper and u refers to 'unten' = lower) as the parameters for the combining levels. Assuming an unknown upper level a known lower level is searched in the database of known levels. A level at 10 466.41 cm^{-1}, even parity, $J_u = 4$ and $A_u = 1618.9$ MHz is found. The calculated upper level explained all the observed fluorescence wavelengths. Table 1 lists the spectroscopic parameters (level energy, angular momentum J, parity, hfs constant A, excitation and fluorescence wavelength) for the presented levels.

Energy/cm^{-1}	J	parity	A / MHz	Excitation wavelength λ(air)/Å	Fluorescence wavelength λ(air)/Å
9814.860	2	even	-760	4241.26	3821, 3912, 4156, 4517
29 901.053	5	even	1000(3)	5722.61	3773
32 776.991	2	even	1464(7)	4473.84, 4405.12	4405
33 473.726	3	even	998(10)	4399.32, 4273.91	4273
33 386.215	3	odd	1352(5)	4361.81, 4328.40	3821, 3912, 4156, 4517
33 850.957	3	odd	938(4)	4275.15, 4385.45	3841

Table 1: *Data of investigated levels.*

References

[1] B. Gamper, Z. Uddin, M. Jahangir, O. Allard, H. Knockel, E. Tiemann, and L. Windholz, J. Phys. B **44**, 045003 (2011).

New odd-parity energy levels in neutral praseodymium

S. Tanweer I.[1], I. Siddiqui[1], U. Zaheer[1], and L. Windholz[1]

[1] *Institute of Experimental Physics, Graz University of Technology, Petersgasse 16, A-8010 Graz, Austria*

Corresponding Author: imrnsmd@hotmail.com

Discovery of twelve energy levels with odd parity is reported during the systematic investigation of the hyperfine structure of praseodymium spectral lines in a region from 4100 Å to 7800 Å. Laser induced fluorescence in a hollow cathode discharge is used for recording the hyperfine structure of some unclassified lines of neutral praseodymium. In order to investigate the hfs of Pr I, a suitable light source is needed for observing absorption processes. Here then spectroscopy light source is a ring dye laser operated with Rhodamine 6G or Kiton red, Rhodamine 700 (LD700) and Stilbene-3 pumped by a solid state diode-pumped, frequency doubled Nd:Vanadate Nd:YVO4 Verdi V-18 laser system or Ar^+ and Kr^+ laser. From the recorded hyperfine patterns, J-quantum numbers and A-values of the magnetic dipole interaction constant for upper and lower levels have been determined. The energies of new levels have been found by using these constants, excitation and fluorescence wavelengths. The excitation wavelengths have been extracted from Fourier transform (FT) spectra [1]. The new levels have been confirmed by at least one second laser excitation. Parameters of the newly discovered odd levels are shown in Table 1.

Energy/cm^{-1}	J	A/MHz	B/MHz	λ_{exe}/(Å,air)
30 726.768	15/2	1000(3)	0	7271.913, 7102.249
19 011.288	11/2	843(2)	0	7125.974, 7202.521
32 171.524	17/2	474(2)	0	7249.011, 7343.111
32 758.617	13/2	655(10)	0	5665.059, 5750.013
33 212.571	11/2	504(5)	0	5806.283, 6654.468
27 982.305	15/2	680(3)	40(8)	7321.820, 7164.643
26 253.598	7/2	921(5)	0	7279.253, 7490.507
28 658.198	5/2	1230(3)	0	5876.596, 5696.260
28 465.938	3/2	1274(5)	0	5759.353, 5668.341
29 563.391	5/2	875(5)	0	4341.356, 5708.855
32 503.250	11/2	393(4)	0	5748.055, 5890.610
29 855.059	7/2	1080(4)	0	4271.721, 5701.920

Table 1: *Data of investigated levels.*

References

[1] B. Gamper, Z. Uddin, M. Jahangir, O. Allard, H. Knockel, E. Tiemann, and L. Windholz, J. Phys. B **44**, 045003 (2011).

Rotational spectra and time dynamics of metastable He dimers probed by light absorption at 465 nm

B. Glowacz[1,2], G. Tastevin[1], and P.–J. Nacher[1]

[1] *Laboratoire Kastler Brossel, ENS; CNRS; UPMC; 24 rue Lhomond, F-75005 Paris, France*
[2] *M. Smoluchowski Inst. of Phys., Jagiellonian Univ., Reymonta 4, PL-30-059 Krakow, Poland*
Corresponding Author: tastevin@lkb.ens.fr

Metastable He_2^* molecules are weakly bound dimers formed by association of a metastable He^* atom (2^3S) and a ground-state He atom. He_2^* (19 eV energy, 18 s radiative lifetime) is ubiquitous in excited He systems. In contrast with ground-state He_2 ($X^1\Sigma_g{}^+$, observed by mass spectroscopy in 1992) or the doubly excited He_2^{**} ($^5\Sigma_g{}^+$, 40 eV, more recently produced by photoassociation of two laser-cooled He^* atoms), He_2^* can easily be detected optically in its lowest energy state, $a^3\Sigma_u{}^+(v=0)$. We report on absorption measurements in low pressure He gas (1–400 mbar) performed on the $a^3\Sigma_u{}^+(0)$–$e^3\Pi_g(0)$ transition at 465 nm with a homemade laser [1]. Light absorption rates provide direct access to He_2^* number densities, based on quantitative spectroscopic data obtained for the probed rotational branches. The He_2^* density varies for strong laser excitation of He^* at 1083 nm (due to a 100-times higher formation rate from the 2^3P state) and our main goal is to elucidate the potential contribution of He_2^* to the laser-enhanced ^{3}He nuclear relaxation observed in metastability exchange optical pumping (MEOP) experiments [2]. Therefore simultaneous optical monitoring of He^* is implemented and 2^3S–2^3P absorption is probed to measure both He^* densities and ^{3}He nuclear polarization [3].

Measurements mainly involve $^3He_2^*$, but its isotopologues are also studied in isotopic mixtures (relevant for MEOP) and pure ^{4}He gas. Our 465 nm absorption spectra yield rotational temperatures close to the gas temperatures. In addition to the known alternation in line intensities due to spin statistics, we observe in ^{3}He an alternation of line shapes indicative of the underlying structure of the rotational states. When rf excitation is stopped, recorded time decays of absorption signals (strongly influenced by gas pressure, Figs. 1a and b) provide quantitative information about the leading reaction rates for competing formation, ionization, and deexcitation processes, as well as relative abundances of the metastable species. In MEOP experiments, the expected increase of 465 nm light absorption is observed but is so far mild in comparison with the spectacular enhancement of ^{3}He nuclear relaxation rate (Fig. 1c).

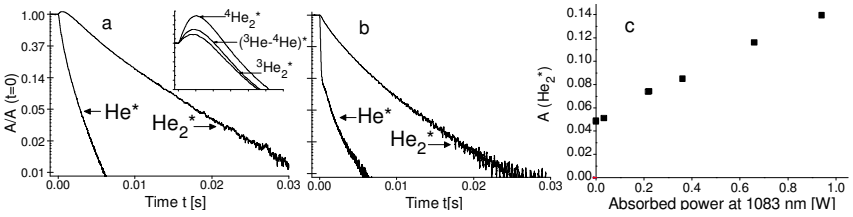

Figure 1: *a, b: Time variation of He_2^* and He^* absorbances $A = -ln(I/I_0)$, normalized to steady-state values; a: 67 mbar (main plot: ^{3}He, inset: 1:1 mixture); b: 267 mbar, ^{3}He. c: He_2^* density versus absorbed pump power in MEOP experiments (32 mbar, ^{3}He). A 3-fold increase is measured at 1 W, where a 340 times faster nuclear relaxation is observed.*

References

[1] G. Tastevin, B. Glowacz, and P.-J. Nacher, J. Low Temp. Phys **158**, 339–345 (2010).
[2] M. Batz, P.-J. Nacher, and G. Tastevin, to appear in J. Phys.: Conf. Series (2011).
[3] C. Talbot *et al.*, *to appear in* J. Phys.: Conf. Series (2011).

New levels of the Pr atom with almost similar energies

U. Zaheer[1,2,3], I. Siddiqui[1], S. Khan[1], E. Hafeez[2], B. Gamper[1], and L. Windholz[1]

[1] *Institute for Experimental Physics, Univ. of Technology Graz, Austria*
[2] *Departement of Physics, Yanbu University College, Yanbu Al Sanaiyah, Saudi Arabia*
[3] *Department of Physics, University of Karachi, Karachi, Pakistan*

Corresponding Author: zaheer103@yahoo.com

A Fourier transform (FT) spectrum of praseodymium [1] extending from UV to IR was investigated. The hyperfine (hf) structures of unclassified lines with sufficient signal to noise ratio were analyzed and some new levels were found (additionally to the new levels in [1]). We present these new levels in this contribution. Some of the new levels have energies almost equal to the energies of already known levels, distinguished either by the difference of J or of parity.

The spectral line 7217.706 Å is a known line [2] but its classification was incorrect, since the hf structure of the line in the FT spectrum did not match with the hf structure predicted assuming the classification as ionic line from [2]. This transition was investigated using laser-induced fluorescence spectroscopy. The recorded hf pattern of the line was fitted and the hyperfine constants were determined. In this way it could be confirmed that the line can be classified as atomic transition between a new upper level of even parity, 25 900.934 cm^{-1}, J = 11/2, to the known lower odd level 12 049.940 cm^{-1}, J = 9/2. The new level has practically the same energy as another already known level of odd parity, 25 900.372 cm^{-1}, and the same angular momentum J = 11/2.

Pr atomic levels with almost similar energy values are observed quite frequently (see Table 1).

J	parity	A / MHz	energy / cm^{-1}	remarks
7/2	odd	400	20 813.430	new level
9/2	odd	1031	20 813.791	known level [2]
9/2	even	572	22 013.711	new level
7/2	odd	975	22 014.123	known level [3]
9/2	odd	761	22 108.630	new level
5/2	odd	1077	22 175.200	new level
11/2	even	494	23 272.372	new level
7/2	odd	562	23 628.233	new level
11/2	even	625	25 900.934	new level
11/2	odd	846	25 900.357	known level [4]
9/2	even	749	27 251.626	new level
5/2	even	330	27 251.239	new level
9/2	odd	889	28 840.138	new level
9/2	even	767	28 840.322	new level
13/2	even	666	28 840.761	new level
11/2	odd	596	29 089.504	new level
11/2	even	593	29 089.490	known level [3]

Table 1: *Data of investigated levels.*

References

[1] B. Gamper, Z. Uddin, M. Jahangir, O. Allard, H. Knöckel, E. Tiemann and L. Windholz, J. Phys. B **44** 045003 (2011).
[2] A. Ginibre-Emery, PhD thesis, Paris, 1988.
[3] G. H. Guthöhrlein, Univ. of Bundeswehr Hamburg, Germany, 2005, private communication,
[4] Zaheer Uddin, PhD thesis, Graz 2006, unpublished,

Fundamental Physics: Theory

Correlation between ionization potential and dipole polarizability of metastable species

P. Bhowmik[1], K. N. Joshipura[1]

[1] *Department of Physics, Sardar Patel University, Vallabh Vidyanagar-388120, Gujarat, India*
Corresponding Author: pujabhowmik@gmail.com

To date, much work has been reported on correlation between electric dipole polarizability and ionization potential [1,2] of atomic systems in the ground state. There are some reports on correlation of polarizability and other parameter also, like atomic radius and volume [2,3].

The systems which we intend to consider presently are metastable atomic species. Normally, an atom in metastable state has larger average radius (and volume). As a result, the corresponding polarizability (being the volume effect) is also quite large compared to the ground state.

To the best of our knowledge, correlation between polarizability and ionization potential for metastable species has not been reported yet. In this paper we present our work on the correlation between polarizability and ionization potential of metastable atoms. Polarizability of many metastable species is not known, while their ionization energies are known. Therefore, using this relation we can roughly estimate the polarizability of these exotic species, and that will be beneficial in field of atomic physics.

The study will be extended to examine the dependence of electron impact ionization cross section with the following quantity, having dimensions of area.

$$\left(\frac{\text{ionization potential}}{\text{polarizability}}\right)^{1/2}$$

Detailed results along with comparisons will be presented in the Conference.

References

[1] B. Fricke, J. Chem. Phys. **84**, 862–866 (1986).
[2] P. Politzer, P. Jin, and J. Murray, J. Chem. Phys. **117**, 8197–8202 (2002).
[3] I. K. Dmitreiva, G. I. Plindov, Physica Scripta **27**, 402–406 (1983).

Higher order effects in the electron impact ionization of water molecule

M. Bouamoud[1], M. Sahlaoui[1], and N. E. H. Benmansour[1]

[1] *Theoretical Physics Laboratory, University Aboubekr Belkaid of Tlemcen, BP 119 Tlemcen 13000, Algeria*

Corresponding Author: m_bouamoud@yahoo.fr

Second Born approximation $(e, 2e)$ calculations are presented for electron-impact ionization of the four outer molecular orbitals of H_2O in its ground state. The first Born term is calculated in the whole analytical way and the second Born term is performed in the closure approximation using semi-analytical calculations.

Triple differential cross sections ($TDCS$) results of electron-impact ionization of $^2A_1$ orbital are compared with the experimental data of Milne-Brownlie [1], which are performed in coplanar asymmetric geometry with the incident energy $E_i = 250$ eV, the ejection energy $E_e = 10$ eV and a scattered angle $\theta_s = 15°$. Cross sections are averaged on the random orientations of the target for accurate comparison with experiments and are compared also with previous theoretical calculations of Champion [2] and Champion *et al.* [3] where the one Coulomb wave model, the (BBK) model [4] and the so-called dynamic screening of the three-body coulomb interactions ($DS3C$) model [5] have been used.

Our results are in better agreement with experiment. Furthermore the second Born approximation gives a reduced binary peak and an enhanced recoil peak in contrast to the results of the first Born approximation, yielding in this way a significant improvement in the recoil region.

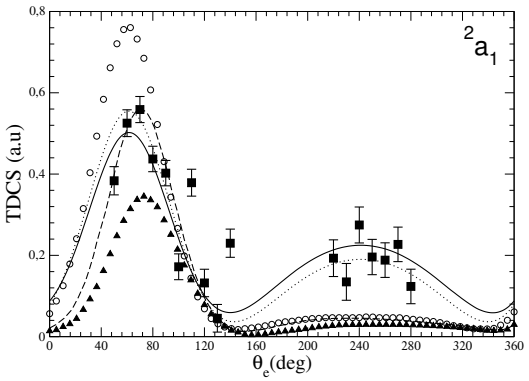

Figure 1: *TDCS for the electron impact ionization of atomic-like orbital $^2A_1$ of water molecule. Experiment [1]: black squares. Present results: solid line for second Born approximation and dotted line for first Born approximation. Results of Champion [2]: open circles. Results of Champion* et al. *[3]: dashed line for DS3C model and triangles up for BBK model.*

References

[1] D. S. Milne-Brownlie *et al.*, Phys. Rev. A **69**, 032701 (2004).
[2] C. Champion, Phys. Med. Biol. **55**, 11–32 (2010).
[3] C. Champion *et al.*, Phys. Rev. A **73**, 012717 (2006).
[4] M. Brauner, J. S. Briggs and H. Klar, J. Phys. B: At. Mol. Opt. Phys.**22**, 2265 (1989).
[5] S. Zhang, J. Phys. B: At. Mol. Opt. Phys. **33**, 3545 (2000).

Optimal trapping wavelengths of Cs_2 and RbCs molecules in an optical lattice

N. Bouloufa[1], R. Vexiau[1], M. Aymar[1], J. G. Danzl[2], M. J. Mark[2], H.-C. Nägerl[2], and O. Dulieu[1]

[1] *Laboratoire Aimé Cotton, CNRS, Université de Paris Sud, Orsay, France*
[2] *Institut für Experimentalphysik und Zentrum für Quantenphysik, Universität Innsbruck Technikerstraße 25, 6020 Innsbruck, Austria*

Corresponding Author: nadia.bouloufa@lac.u-psud.fr

The present work aims at finding optimal parameters for trapping of Cs_2 and RbCs molecules in optical lattices, with the perspective of creating a quantum degenerate gas of ground-state molecules. We have calculated dynamic polarizabilities of Cs_2 and RbCs molecules subject to an oscillating electric field, using accurate potential curves and electronic transition dipole moments. We show that for some particular wavelengths of the optical lattice, called "magic wavelengths", the polarizability of the ground-state molecules is equal to the one of a Feshbach molecule. As the creation of the sample of ground-state molecules relies on an adiabatic population transfer from weakly-bound molecules created on a Feshbach resonance, such a coincidence ensures that both the initial and final states are favorably trapped by the lattice light, allowing optimized transfer in agreement with the experimental observation.

Hyperfine structure of Cs_2 and RbCs excited molecules

N. Bouloufa[1], O. Kriegelsteiner[2], R. Vexiau[1], J. G. Danzl[2], H.-C. Nägerl[2], O. Dulieu[1], and A. Crubellier[1]

[1] *Laboratoire Aimé Cotton, CNRS, Université de Paris Sud, Orsay, France*
[2] *Institut für Experimentalphysik und Zentrum für Quantenphysik, Universität Innsbruck Technikerstraße 25, 6020 Innsbruck, Austria*

Corresponding Author: nadia.bouloufa@lac.u-psud.fr

Unlike ground state alkali-metal diatomics, very little is known about the hyperfine structure of excited electronic states. We present an approach based on an asymptotic model for the hyperfine Hamiltonian to give a first estimate of the expected structure of the rovibrational levels of the Cs_2 and RbCs excited electronic states correlated to the lowest 2S+2P limit. We set up potential curves build on long-range atom-atom interaction connected to short-range *ab initio* results obtained in our group. The hyperfine structure is strongly depending on the projection of the total angular momentum of the molecule, and on the sum of projections of the total angular momentum of the separated atoms. The comparison with the experimental data recorded in Innsbruck will be presented. The possible interaction of electronic states at short distances due to hyperfine coupling is discussed.

Molecular magnets: symmetry constrained manybody theory and the calculation of the parameters of the effective Heisenberg–Van Vleck–Dirac Hamiltonian

D. Ammi[1], M. Atanasov[1,2], and C. Daul[1]

[1] *Department of Chemistry, University of Fribourg, CH-1700 Fribourg, Switzerland*
[2] *Institute of General and Inorganic Chemistry, Bulgarian Academy of Sciences, Bl.11, 1113 Sofia, Bulgaria*

Corresponding Author: claude.daul@unifr.ch

In this communication, we present a study of the electronic structure of A_3 (cf. Fig. 1 where A = H, Li, Na, K, Rb, or Cs) by full CI multi-determinant DFT calculation imposing D_{3h} symmetry. The aim of this study is to probe the adequacy of many-body theory to predict the molecular magnetism of this frustrated triatomic system. If we restrict ourselves to the $|ns\rangle$ valence orbitals, these three atomic orbitals yield three molecular orbitals that are completely determined by symmetry for this simple molecule. That is

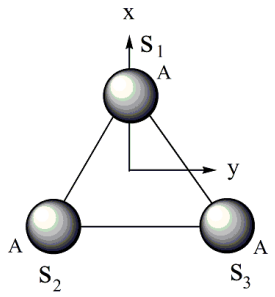

Figure 1: *Coordinate system and identities used in the text.*

$$|a_1'\,\iota\rangle = \frac{\phi_1+\phi_2+\phi_3}{\sqrt{3(1+2S)}}\;;\quad |e'\,\theta\rangle = \frac{2\phi_1-\phi_2-\phi_3}{\sqrt{6(1-S)}}\;;\quad |e'\,\epsilon\rangle = \frac{\phi_2-\phi_3}{\sqrt{2(1-S)}}\;;$$

where

$$S = \langle\phi_i|\phi_j\rangle\;,\; i\neq j\;,$$

and there will be six places to be occupied by the three electrons. This yields $\binom{6}{3} = 20$ possibilities! These twenty microstates, or single determinant, have the following multiplet structure due to the trigonal symmetry:

$$\begin{aligned} a_1^2 e &: {}^2\mathrm{E} \\ a_1 e^2 &: {}^2\mathrm{A}_1 \otimes \left({}^2\mathrm{A}_1 + {}^3\mathrm{A}_2 + {}^1\mathrm{E}\right) = {}^2\mathrm{A}_1 + {}^2\mathrm{A}_2 + {}^4\mathrm{A}_2 + {}^2\mathrm{E} \\ e^3 &: {}^2\mathrm{E} \end{aligned}$$

Thus, the complete CI problem does reduce to the calculation of the interaction matrices for each multiplet in block-diagonal form and we immediately obtain the energy expression for ${}^2\mathrm{A}_1$, ${}^2\mathrm{A}_2$, ${}^4\mathrm{A}_2$, and a 6×6 matrix for the three ${}^2\mathrm{E}$. These elements are easily calculated using Slater's rule. They can be further reduced using the Wigner-Eckart theorem. Thus, we can reduce the calculation of the twenty multiplet energies to the calculation of only seven reduced matrix elements. Results and details are in the poster.

FPT

Critical analysis of the methods of interpretation in the hyperfine structure of free atoms and ions. Case of the extended configuration system of the lanthanum atom

J. Dembczyński[1], M. Elantkowska[1], and J. Ruczkowski[1]

[1] *Chair of Quantum Engineering and Metrology, Faculty of Technical Physics, Poznań University of Technology, Nieszawska 13B, 60-965 Poznań, Poland*

Corresponding Author: Jerzy.Dembczynski@put.poznan.pl

In this work we continue the semiempirical analysis of experimental data, both our own and available in the literature, for the even configurations of lanthanum atom. In the paper [1] the method of quantitative determination of two-body contributions to the fine and the hyperfine structure, resulting from the excitations from electronic closed shells to open shells and from open shells to empty shells, for the model space $(5d+6s)^3$, was described.

The extended configurations system used in this work consists of the following 74 configurations:

$$\begin{aligned}
&5d^3 + \sum_{n'=6}^{12} 5d^2n's + \sum_{n''=6}^{12} 5d^2n''d + \sum_{n'''=5}^{11} 5d^2n'''g + \ 5d6s^2 + \sum_{n'=7}^{12} 5d6sn'\ s \\
&+ \sum_{n''=6}^{12} 5d6sn''d \ + \sum_{n'''=5}^{11} 5d6sn'''g \ + 5d6p^2 + 6s6p^2 + 4f^25d + 4f^26s \\
&+ \sum_{n'=6}^{12} 4f5dn'\ p \ + \sum_{n'=6}^{12} 4f6sn'\ p \ + \sum_{n'=7}^{12} 6s^2n's \ + \sum_{n''=6}^{12} 6s^2n''d
\end{aligned} \tag{1}$$

The main aim of this work is to demonstration that the gradual expansion of the configurations basis, and consequently more precise eigenvector amplitudes, does not change the conclusion of the paper [1], that the operator

$$H_{\mathrm{hfs}} = \sum_{K=1}^{3} T_e^{(\kappa k)K} \cdot T_n^{(K)} \tag{2}$$

describes the partition of the observed hyperfine splittings into the contributions of ranks K=1,2 and 3 within the experimental accuracy, while the operator

$$T_e^{(\kappa k)1} \cdot T_n^{(1)} = \frac{\mu_0 \mu_B}{2\pi} \sum_{i=1}^{N} \left[\widehat{l}_i \left\langle r^{-3} \right\rangle^{01} - \sqrt{10} \left(\widehat{s}_i \widehat{C}_i^2 \right)^{(1)} \left\langle r^{-3} \right\rangle^{12} + \widehat{s}_i \left\langle r^{-3} \right\rangle^{10} \right] \cdot T_n^{(1)} \tag{3}$$

does not fully account for the partition of the interactions of rank K=1 into contributions $\kappa k = 01$, 12 and 10.

This work was supported by The National Centre for Science under project N N519 650740.

References

[1] J. Dembczyński, M. Elantkowska, B. Furmann, J. Ruczkowski, D. Stefańska, J. Phys. B: At. Mol. Opt. Phys. **43**, 065001 (2010).

Resonant Auger decay of the core-excited C*O molecule in intense x-ray laser fields

Ph. V. Demekhin[1], Y.–C. Chiang[1], and L. S. Cederbaum[1]

[1] *Theoretische Chemie, Physikalisch-Chemisches Institut, Universität Heidelberg, Im Neuenheimer Feld 229, D-69120 Heidelberg, Germany*

Corresponding Author: philipp.demekhin@pci.uni-heidelberg.de

Recently [1–3], the resonant Auger (RA) decay of atoms exposed to a coherent and monochromatic x-ray laser pulse of a high intensity has been studied theoretically. It has been demonstrated in these studies that under extreme field conditions (unprecedented high-intensity, 10^{18} W $\cdot$ cm^{-2}, and very short pulse durations, 10–500 fs, [4]) the stimulated emission from the resonance back to the ground state starts to compete with the Auger decay. The interplay between the resonant excitation and stimulated emission results in Rabi oscillations between the ground state and the resonance within its Auger decay lifetime and pulse duration, which leads to spectacular modifications of the RA spectra, like the appearance of multipeak spectra [1,2]. It has also been demonstrated [2,3], that in the presence of such strong fields the total direct photoionizations of the ground state and of the resonant state itself start to play an important role, resulting in additional leakages of the corresponding populations into all possible final ionic states. The role of the direct photoionization of the ground state and of the resonance increases dramatically with the field intensity [3]. In addition, a final ionic state is populated coherently by both direct photoionization from the ground state and resonant Auger decay thus naturally inducing strong interference effects with distinct patterns in the electron spectra [3].

Very recently, the RA effect of molecules in intense x-ray laser fields has been studied theoretically [5]. It has been demonstrated, that not only the vibrational motion plays a role in the decay as in the case of weak fields, but also the rotational motion becomes very important in strong fields. Even for diatomic molecules, light-induced strong non-adiabatic effects dominate the dynamics of the resonant Auger decay which becomes a multidimensional problem in intense fields. In particular, the appearance of the analogue of conical intersections of the complex potential energy surfaces of the ground and 'dressed' resonant states has been predicted in [5]. This phenomenon gives rise to strong coupling between the electronic, vibrational and rotational degrees of freedom of diatomic molecules. The leakages mentioned above were not taken explicitly into account in [5].

In the present work we study theoretically how all the above mentioned processes evoked by a strong field influence the RA effect in molecules. For this purpose we combined the previously developed theoretical approaches for RA in atoms [3] and in molecules [5]. The theory includes conical intersections of the complex potential energy surfaces of the ground and 'dressed' resonant states due to an intense x-ray pulse, taking into account the decay of the resonance and the direct photoionization of the ground state, both populating the final ionic states coherently, as well as the direct photoionization of the resonance state itself. The complete theory is applied to study the dynamics of the Auger decay of the C*O ($1s^{-1}\pi^*$) resonance into the $CO^+(A\ ^2\Pi)$ final ionic state. On this show-case example we illustrate the impact of the aforementioned competing processes on the total electron yield and Auger electron spectra.

References

[1] N. Rohringer and R. Santra, Phys. Rev. A **77**, 053404 (2008).
[2] J.-C. Liu, *et al.*, Phys. Rev. A **81**, 043412 (2010).
[3] Ph. V. Demekhin and L. S. Cederbaum, Phys. Rev. A (2011) in press; arXiv:1012.3399v1.
[4] P. Emma, *et al.*, Nature Photonics **4**, 641–647 (2010).
[5] L. S. Cederbaum, *et al.*, Phys. Rev. Lett. (2010) submitted.

New approach to generation of spin orbitals in relativistic CI calculations for many electron atoms

L. Glowacki[1]

[1] *Pedagogical University, Institute of Physics & Computer Science, ul. Podchorazych 2, 30084, Krakow, Poland*

Corresponding Author: lg@up.krakow.pl

We found that hydrogenic-like wavefunctions used as basis functions in relativistic CI calculations can be very efficient in treating electron correlations. In our calculations we use numerical wavefunctions generated in the hydrogenic-like potential, where atomic number can be non-integer and is unique for each orbital. We believe that such potential accounts for the local screening of the interacting electrons. This approach was tested for electron-electron correlations in helium and lithium. The relativistic configuration-interaction method including Breit interaction and radiative corrections were applied. We obtained several low-lying energy levels in helium with the accuracy (vs. experiment) better than 0.01%. For three electron system the $2s_{1/2} - 2p_{1/2}$, $2s_{1/2} - 2p_{3/2}$ transition energies were computed in lithium, lithium-like neon, lithium-like uranium. Obtained results were in excellent agreement with experimental and the other theoretical data.

In this work we present computational technique and calculations. This approach can be applied to many-electron atoms and allows for uniform treatment of valence-valence and core-valence electron correlations. The calculations of transition energies and oscillator strengths for low-lying $ns_{1/2} - n'p_{1/2}$, $ns_{1/2} - n'p_{3/2}$ transitions in alkali neutral atoms: Na, K, Rb, Cs, Fr have also been performed and will be presented.

Muon-gamma-nuclear spectroscopy of atoms: Cooperative muon-gamma-nuclear processes

A.–V. Glushkov[1,2]

[1] *University of Odessa, P.O.Box 24a, Odessa-9, 65009, Ukraine*
[2] *ISAN, Russian Academy of Sciences, Troitsk, 142090, Russia*
Corresponding Author: glushkov@paco.net

We present a new consistent energy approach to calculation of the cross-section for the negative muon capture by an atom, based on the relativistic many-body perturbation (PT) theory. The calculation results for cross-section of the muon-capture by He atom are listed. It is presented a generalized energy approach in the relativistic theory of discharge of a metastable nucleus with emission of gamma quantum and further muon conversion, which initiates this discharge. The numerical calculation of the corresponding probabilities is firstly carried out for the Sc and Tl nuclei with using the Dirac-Woods-Saxon model. A negative muon captured by a metastable nucleus may accelerate the discharge of the latter by many orders of magnitude [1]. For a certain relation between the energy range of the nuclear and muonic levels a discharge may be followed by muon ejection and muon participates in discharge of other nuclei. The decay probability is linked with imaginary part of the "nucleus core + external nucleon + muon" system energy [1,2]. One should consider 3 channels: 1). radiative purely nuclear 2j-poled transition (probability $P1$; this value can be calculated on the basis of known traditional formula); 2). Non-radiative decay, when a proton transits into the ground state and muon leaves a nucleus with energy $E = E(p-N1J1)-E(i)$, where $E(p-N1J1)$ is an energy of nuclear transition, $E(i)$ is the bond energy of muon in 1s state (P2); 3). A transition of proton to the ground state with muon excitation and emission of gamma quantum with energy E(p-N1J1)-E(nl) (P3). Under condition $E(p-N1J1) > E(i)$ a probability definition reduces to calculation of probability of autoionization decay of 2-particle system. As example, data for Sc, Tl nuclei are presented. The probabilities for some transitions: $P2 = 3.9\times10^{15}$ 1/s (p1/2-p3/2) and $P2 = 3.1\times10^{12}$ 1/s (p1/2-f7/2) [1]. If a muon in an atom is in the initial state p1/2, than the cascade discharge occur with ejection of muon on the first stage and secondly the gamma quantum emission. To consider a case when the second channel is closed and the third one is opened, suppose: $E(p1/2) - E(p3/2) = 0.92$ MeV. Energy of nuclear transition is not sufficient to transit muon to continuum state and it may excite to 2p state. Then, there is the proton transition p1/2-p3/2 with virtual muon excitation to states of nd series and gamma quantum emission. The dipole transition 2p-1s occurs with $P3 = 1.9\times10^{13}$ 1/s. At last, the key features of the possible high-power monochromatic gamma radiation sources on the basis of examined processes are analyzed.

References

[1] A. V. Glushkov *et al.*, In: *Frontiers in Quantum Systems in Chemistry and Physics*, Eds. P. Hoggan, E. Brandas, S. Wilson, G. Delgado-Barrio (Springer, Berlin, 2011) **21**, 331–354.
[2] A. V. Glushkov, O. Khetselius, L. Lovett, In: *Advances in the Theory of Atomic and Molecular Systems,* Eds. P. Piecuch, J. Maruani, G. Delgado-Barrio, S. Wilson (Springer, Berlin, 2009) **20**, 125–172.

Electron-β -nuclear spectroscopy of atoms: bound β-decay and decay of isomeric states for ionized atoms

A.–V. Glushkov[1,2]

[1] *University of Odessa, P.O.Box 24a, Odessa-9, 65009, Ukraine*
[2] *ISAN, Russian Academy of Sciences, Troitsk, 142090, Russia*
Corresponding Author: glushkov@paco.net

Many attempts have been made to influence on the nuclear decay rate by varying chemical environments, or by applying strong electromagnetic fields. It can be expected that the rates of nuclear β decay and electron capture are strongly affected in comparison to those of neutral atoms. In our paper the formalism of the nuclear-QED perturbation theory is used to calculate β decay parameters for a number of transitions. The relativistic calculation method is based on the optimized Dirac-Kohn-Sham formalism with taking into account the nuclear, radiative and exchange-correlation effects and relativistic mean field theory [1,2]. We studied the electronic rearrangement induced by nuclear transmutation in β decay ^{6}He–^{6}Li and calculated the probabilities of excitation to the final discrete states of $^6Li^+$ (including to the doubly excited autoionizing states) as well as the total probabilities for single and double ionization. We present the β decay parameters for transitions: ^{63}Ni–^{63}Cu, ^{241}Pu–^{241}Am etc., and show that the theoretical values agree quite well with some available experimental data. We also studied the chemical environment effect on parameters of the different β transitions, in particular, $^{63}Ni^{(0)}$–$^{63}Cu^{(+1)}$, $Ni^{(+2)}$–$Cu^{(+3)}$, $^{241}Pu^{(0)}$–$^{241}Am^{(+1)}$, $Pu^{(+2)}$–$Am^{(+3)}$. The correct treatment of the chemical environment effect is shown to modify β decay parameters. This is connected with account of a few factors (energy corrections for different substances as well as the possibility of the bound or other decay channels). The half-life period for decay of the tritium atom (ion) has been estimated with taking into account the bound β decay channel correction and some accompanying effects (population of bound states of ^{3}He, population of the continuum states with exchanging the orbital electron by electron, the charge screening effect due to orbital electrons, etc.) [3]. The estimates for a ratio v_b/v_c of bound-state (b) and continuum-state (c) β decay rates for the bare $^{207}Tl^{81+}$ ions and isomeric states of fully ionized ^{144}Tb, ^{149}Dy are given. The effects considered are responsible for creation of elements in the space and astrophysical plasma.

FPT

References

[1] A. B. Glushkov, L. N. Ivanov, Phys.Lett. **A170**, 33-38 (1992).
[2] A. V. Glushkov *et al.*, In: *Frontiers in Quantum Systems in Chemistry and Physics,* Eds. S. Wilson, P. Grout, J. Maruani, G. Delgado-Barrio (Springer, Berlin, 2008) **18**, 505–522.
[3] A. V. Glushkov, O. Khetselius, L. Lovett, In: *Advances in the Theory of Atomic and Molecular Systems,* Eds. P. Piecuch, J. Maruani, G. Delgado-Barrio, S. Wilson (Springer, Berlin, 2009) **20**, 125–172.

Dense spectrum of resonances and capture of particles in the field of a body with near-black-hole metric

V. V. Flambaum[1], G. H. Gossel[1], and G. F. Gribakin[2]

[1] *School of Physics, University of New South Wales, Sydney 2052, Australia*
[2] *School of Mathematics and Physics, Queen's University Belfast, Belfast BT7 1NN, UK*
Corresponding Author: g.gribakin@qub.ac.uk

We consider the problem of scattering of a massless spin-zero particle in the field of a massive body whose radius approaches the black-hole limit, $R \to r_s$, where r_s is the Schwarzschild radius.

For a massive body with $R \leq r_s$ the static Schwarzschild metric has a singularity at $r = r_s$. This may result in an ambiguity in the scattering cross section. Unruh [1] assumed total absorption at $r = r_s$ and obtained the absorption cross section $\sigma_a \simeq 4\pi r_s^2$ at low energy. Kuchiev [2] calculated the gravitational *reflection coefficient* $\mathcal{R}$ at $r = r_s$ by analytically continuing the wavefunction across the event horizon. In Ref. [3] the authors determined the absorption cross section for an arbitrary $\mathcal{R}$. For $\mathcal{R} = 0$ Unruh's result is reproduced, while the use of Kuchiev's reflection coefficient [2] yields σ_a that vanishes at zero energy.

We solve the Klein-Gordon equation $\partial_\mu(\sqrt{-g}g^{\mu\nu}\partial_\nu\Psi) = 0$ with metric $g_{\mu\nu}$, for a body with R only slightly greater than r_s. The s-wave solution outside the body is $\psi \sim e^{-ir_s\epsilon\ln(r-r_s)} + \mathcal{R}e^{ir_s\epsilon\ln(r-r_s)}$ (ϵ is energy), and $\mathcal{R}$ is found by matching with the solution for $r < R$, where the metric of Florides [5] is used. We show that for a massive body such that $\xi = 1 - r_s/R \ll 1$,

$$\mathcal{R} = -\exp[2i\epsilon r_s B(\xi)], \tag{1}$$

where semiclassically, $B(\xi) \simeq A\xi^{-3/4} - \ln\xi$, and $A = \sqrt{\pi}\Gamma(3/4)/[2\Gamma(5/4)] \approx 1.198$. For $\xi \to 0$, $B(\xi) \to \infty$, as the wavefunction oscillates many times in the interior. The short-range phaseshift δ in the asymptotic solution, $\psi(r) \propto \sin[\epsilon r - (Z/\epsilon)\ln 2\epsilon r + \delta_C + \delta]$ (δ_C is the phase for effective charge $Z = -r_s\epsilon^2$) reveals a dense spectrum or resonances (Fig. 1), with energies $\varepsilon_n = n\pi/B(\xi)$ and widths $\gamma_n \sim 2\varepsilon_n^2/B(\xi)$. Particle capture in these resonances describes effective *absorption*, and averaging the S-matrix over the resonances in the $\xi \to 0$ limit is equivalent to setting $\mathcal{R} = 0$.

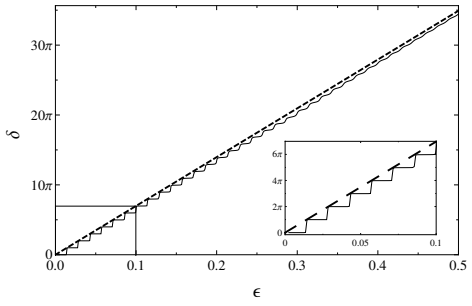

Figure 1: *Solid line shows the short-range phaseshift δ obtained numerically for $r_s = 0.999R$; dashed line is the phase accumulated at $r \leq R$, $\Phi = \epsilon B(\xi)$, see Eq. (1).*

References

[1] W. G. Unruh, Phys. Rev. D **14**, 3251 (1976); Thesis, Princeton Univ., 1971 (unpublished).
[2] M. Yu. Kuchiev, Europhys. Lett. **65**, 445 (2004); Phys. Rev. D **69**, 124031 (2004).
[3] M. Yu. Kuchiev and V. V. Flambaum, Phys. Rev. D **70**, 044022 (2004).
[4] G. H. Gossel, J. C. Berengut, and V. V. Flambaum, arXiv:gr-qc/1006.5541 (2010).
[5] P. S. Florides, Proc. R. Soc. Lond. A **337**, 529 (1974).

Calculated energy levels and lifetimes in Mg-like vanadium

G. P. Gupta[1], A. Z. Msezane[2]

[1] *Department of Physics, S. D. (Postgraduate) College, Muzaffarnagar – 251 001 (Affiliated to Choudhary Charan Singh University, Meerut – 250 004), India*
[2] *Department of Physics and Center for Theoretical Studies of Physical Systems Clark Atlanta University, Atlanta, Georgia 30314, USA*

Corresponding Author: g_p_gupta1@yahoo.co.in

Emission lines from multiply charged Mg-like ions are frequently observed in the spectra of astrophysical plasma and laboratory plasmas. Accurate absorption oscillator strengths for these ions are needed in astrophysical observations and in the study of laboratory plasmas both for diagnostic purposes and for the determination of the effects of impurities on controlled thermonuclear fusion.

We have calculated excitation energies from the ground state for 86 fine-structure levels as well as oscillator strengths and radiative decay rates for all electric-dipole-allowed and intercombination transitions among the fine-structure levels of the terms belonging to the $(1s^2 2s^2 2p^6)3s^2$, 3s3p, 3s3d, 3s4s, 3s4p, 3s4d, 3s4f, $3p^2$, 3p3d, 3p4s, 3p4p, 3p4d, 3p4f and $3d^2$ configuration of Mg-like vanadium. These states are represented by extensive configuration-interaction (CI) wave functions obtained using the CIV3 computer code of Hibbert [1]. The important relativistic effects in intermediate coupling are included through the Breit-Pauli approximation via spin-orbit, spin-other-orbit, spin-spin, Darwin and mass correction terms [2].

Our *ab initio* excitation energies, including their ordering, are in excellent agreement with the compiled energy values of the National Institute for Standards and Technology (NIST), wherever available. The enormous mixing among several fine-structure levels makes it very difficult to identify them uniquely. The mixing among few fine-structure levels is so strong that they are designated by the eigenvector of the second largest magnitude. We identify these strongly mixed levels by their dominant eigenvector [3,4]. From our transition probabilities, we have also calculated radiative lifetimes of fine-structure levels. Our calculated oscillator strengths, radiative rates and the lifetimes are found to be in good agreement with the other available data [5]. In this calculation we also predict new data for several fine-structure levels where no other theoretical and/or experimental results are available.

References

[1] A. Hibbert, Comput. Phys. Commun. **9**, 141 (1975).
[2] R. Glass, A. Hibbert, Comput. Phys. Commun. **16**, 19 (1978).
[3] G. P. Gupta, K. M. Aggarwal, A. Z. Msezane, Phys. Rev. **A70**, 036501 (2004).
[4] K. M. Aggarwal, Vikas Tayal, G. P. Gupta and F. P. Keenan, At. Data Nucl. Data Tables **93**, 615 (2007).
[5] U. I. Safronova, W. R. Johnson and H. G. Berry, Phys. Rev. **A61**, 052503 (2000).

Excitation energies, oscillator strengths and lifetimes in Ni XV

G. P. Gupta[1], A. Z. Msezane[2]

[1] *Department of Physics, S. D. (Postgraduate) College, Muzaffarnagar – 251 001 (Affiliated to Choudhary Charan Singh University, Meerut – 250 004), India*
[2] *Department of Physics and Center for Theoretical Studies of Physical Systems Clark Atlanta University, Atlanta, Georgia 30314, USA*

Corresponding Author: g_p_gupta1@yahoo.co.in

Transitions in multiply ionized Ni are prominent in the spectra of the solar corona and solar flares and Ni is also a dominant impurity in many Tokamaks.

Large scale CIV3 calculations of excitation energies from ground state as well as of oscillator strengths and radiative decay rates for all electric-dipole-allowed and intercombination transitions among the fine-structure levels of the terms belonging to the $(1s^2 2s^2 2p^6)3s^2 3p^2$, $3s3p^3$, $3p^4$, $3s^2 3p3d$, $3p^3 3d$, $3s3p3d^2$, $3s^2 3d^2$, $3s3p^2 3d$, $3s3p^2 4s$, $3s^2 3p4s$, $3s^2 3p4p$, $3s^2 3p4d$ and $3s^2 3p4f$ configurations of Si-like nickel, are performed using very extensive configuration-interaction (CI) wavefunctions [1]. The relativistic effects in intermediate coupling are incorporated by means of the Breit-Pauli Hamiltonian [2]. Small adjustments to the diagonal elements of the Hamiltonian matrices have been made so that the energy splittings are as close as possible to the energy values of the National Institute for Standards and Technology (NIST). In this calculation we have investigated the effects of electron correlations on our calculated data, particularly on the intercombination transitions, by including orbitals with up to $n = 5$ quantum number. We considered up to two electron excitations from the valence electrons of the basic configurations and included very large number of configurations to ensure convergence.

Our calculated excitation energies, including their ordering, are in excellent agreement with the compiled energy values of the National Institute for Standards and Technology, wherever available. The mixing among several fine-structure levels is found to be very strong. These levels are identified by their eigenvector composition [3]. From our radiative rates, we have also calculated the radiative lifetimes of the fine-structure levels. Our calculated lifetimes are found to be in excellent agreement with the experimental values of Trabert *et al.* [4] and the other sophisticated theoretical results. We predict new data for several levels where no other theoretical and/or experimental results are available. We believe that the new oscillator strengths will be useful in many astrophysical applications and in technical plasma modeling.

References

[1] A. Hibbert, Comput. Phys. Commun. **9**, 141 (1975).
[2] R. Glass, A. Hibbert, Comput. Phys. Commun. **16**, 19 (1978).
[3] G. P. Gupta, K. M. Aggarwal, A. Z. Msezane, Phys. Rev. **A70**, 036501 (2004).
[4] E. Trabert *et al.*, Z. Phys. **D11**, 207 (1987).

Transition rates in the B-, C-, N-, O-, and Ne-like sequences from relativistic CI calculations

P. Jönsson[1], S. Gustafsson[1], J. Ekman[1], P. Bengtsson[1], P. Rynkun[2], and G. Gaigalas[2,3]

[1] *School of Engineering, Malmö University, 205-06 Malmö, Sweden*
[2] *Vilnius Pedagogical University, Studenty 39, Vilnius, LT-08106, Lithuania*
[3] *Institute of Theoretical Physics and Astronomy, Vilnius University, A. Goštauto 12, LT-01108, Vilnius, Lithuania*

Corresponding Author: per.jonsson@mah.se

Atomic data are important in astrophysical applications and transition data can be used in the determination of element abundances and plasma diagnostics [1]. To provide for the extensive data needs a number of general computer codes such as SUPERSTRUCTURE, CIV3, and ATSP2K have been developed. As an alternative to these codes, which all rely on the Breit-Pauli approximation, the fully relativistic GRASP2K code [2] can be used. GRASP2K is based on the multiconfiguration Dirac-Hartree-Fock method and implements a bi-orthogonal transformation method that permits initial and final states in a transition array to be optimized separately, which, in many cases, leads to more accurate values of the resulting rates [3]. The GRASP2K package also contains modules to compute diagonal and off-diagonal hyperfine interaction constants, isotope shifts, Landé g_J factors, and splittings of magnetic sub-state in intermediate and strong magnetic fields.

In this work, GRASP2K has been applied to provide highly accurate spectroscopic data for transitions in the B-, C-, N-, O-, and Ne-like sequences [4]. Valence, core-valence, and core-core correlation effects were accounted for through SD-MR expansions to increasing sets of active orbitals. The calculated energy levels generally agree to within a few hundred cm^{-1} with the experimentally compiled results. Babushkin (length) and Coulomb (velocity) forms of transition rates differ with less than 1% for the majority of the allowed transitions.

The perspectives of massive data production on parallel clusters to cover the needs of the astrophysical community is discussed.

References

[1] A. K. Bhatia and G. A. Doschek, At. Data Nucl. Data Tables **55** 315 (1993).
[2] P. Jönsson *et al.*, Comp. Phys. Commun. **177** 597 (2007).
[3] J. Olsen *et al.*, Phys. Rev. E **52** 4499 (1995).
[4] P. Jönsson, P. Rynkun, and G. Gaigalas, At. Data Nucl. Data Tables, accepted (2011).

Nuclear moments and hyperfine structure parameters for heavy atoms within relativistic many-body theory

O. Yu. Khetselius[1]

[1] *Department of Physics, Odessa University, P.O. Box 24a, 65009, Odessa-9, Ukraine*
Corresponding Author: nuclei08@mail.ru

The results of calculating the energies and constants of the hyperfine structure for ^{133}Cs, Cs-like ion of Ba, ^{201}Hg, ^{223}Ra within the relativistic many-body theory [1,2] are presented. The key quantitative factor of the reasonable agreement between theory and experiment, especially in comparison with some versions of the the Dirac-Fock method is connected with more correct accounting the inter-electron correlations, nuclear, radiative effects. The contribution due to inter electron correlations to the hyperfine structure constants is about 120–1200 MHz for different states, contribution due to the finite size of a nucleus and radiative contribution is still $\sim$ 24 MHz (for constant A). For isotope of ^{201}Hg it has been received Q=380.5 barn. It is agreed the best of all with experimental value, received by group Ulm *et al.* (general interval of the experimental values is 300–600 barn). For element of ^{223}Ra our value is Q=1.22 barn. It is in the limits of last experimental measurements values by Wendt group (ISOLDE Collaboration). The role of the nuclear effects contribution (core-polarization ones, which are induced by valence protons of a nucleus), temporal distribution of magnetization in a nucleus (effect of Bohr-Weisskopf) and non-accounted high order QED corrections is analyzed.

References

[1] O. Yu. Khetselius, Phys. Scripta **T34**, 014023 (2009).
[2] O. Yu. Khetselius, Int. J. Quant. Chem. **109**, 3330–3336 (2009).

Parity nonconservation effect in heavy atoms and nuclei: nuclear-relativistic many-body theory

O. Yu. Khetselius[1]

[1] *Department of Mathematics, Odessa University, P.O. Box 24a, 65009, Odessa-9, Ukraine*
Corresponding Author: nuclei08@mail.ru

During the past two decades, the nuclear and atomic-optical experiments to detect parity non-conservation (PNC) have progressed to the point where PNC amplitudes can be measured with accuracy on the level of a few percents in certain heavy atoms and significantly worse in some nuclei (Mössbauer spectroscopy). Nowadays the PNC in atoms has a potential to probe for new physics beyond the standard model. A promising idea (Forston) is to apply the techniques of laser cooling and ion trapping to measurement of the PNC in $6s^2S_{1/2}$-$5d^2D_{3/2}$ transition of Ba^+. In our paper we systematically apply the nuclear-relativistic many-body perturbation theory formalism [1,2] to precise studying PNC effect in heavy atoms with account for nuclear, correlation and QED corrections. There are determined the PNC radiative amplitudes for a set of nuclei (atoms): ^{133}Cs, $^{137}Ba^+$, ^{173}Yb with account of exchange-correlation, Breit, weak e-e interactions, QED and nuclear (magnetic moment distribution, finite size, neutron 'skin') corrections, nuclear-spin dependent corrections due to anapole moment, Z-boson ((A_nV_e) current) exchange, hyperfine -Z exchange ((V_nA_e) current). The weak charge is found for ^{133}Cs, ^{205}Tl and ^{173}Yb and comparison with Standard Model is done. Using the experimental value $E^{PNC}/\beta = 39$ mV/cm (Tsigutkin *et al.*, 2009) and our calculated amplitude value (9.707×10^{-10} ea) one could find for ^{173}Yb (Z=70, N=103) the weak charge value $Q_W = -92.31$ (the SM gives $Q_W = -95.44$). The received data are compared with known earlier and recent results by Flambaun-Dzuba *et al.*, Johnson-Safronova *et al.*, by Johnson-Sapirstein-Blundell *et al.* The role of the nuclear effects contribution (core-polarization ones, which are induced by valence protons of a nucleus), spatial distribution of magnetization in a nucleus (effect of Bohr-Weisskopf) and non-accounted high order QED corrections is analyzed [3,4].

References

[1] O. Yu. Khetselius, Phys. Scripta **T34**, 014023 (2009).
[2] O. Yu. Khetselius, Int. J. Quant. Chem. **109**, 3330–3336 (2009).
[3] W. R. Johnson, M. S. Safronova, U. I. Safronova, Phys. Rev. **A69**, 062106 (2003).
[4] V. V. Flambaum, J. S. Ginges, Phys. Rev. **A72**, 052115 (2005).

Ab-initio multi-configuration Dirac-Hartree-Fock calculation on the lifetimes of levels in $2p^5 3s$ configuration of neutral neon

J. G. Li[1], S. Verdebout[1], and M. R. Godefroid[1]

[1] *Service de Chimie Quantique et Photophysique, Université Libre de Bruxelles, B-1050 Brussels, Belgium*

Corresponding Author: jgli@ulb.ac.be

Accurate determination of the lifetime of levels in the first excited configuration $2p^5 3s$ for neutral neon is important, not only because of their potential applications involving plasma diagnosis, laser techniques, and the interpretation of astrophysical data, but also for testing fundamental many-body theories of atoms.

During the past decades, many experimental measurements on the rate (or corresponding absorption oscillator strength) of the electrical dipole (E1) transition from $^{3,1}P_1^o$ to the ground state have been carried out using different methods. However, these experimental values are not in agreement with each other. In parallel, theoretical calculations were performed through many-body perturbation-theory (MBPT), configuration interaction (CI), multiconfiguration Dirac-Hartree-Fock (MCDHF) and B-spline approaches, attempting to clarify the disagreements in experiments and to give reliable results. Unfortunately, there still exists discrepancies between theory and experiment [1–3]. The principal difficulties in theoretical calculations arise from electron correlation and relativistic effects. The latter give rise to spin-forbidden transition. At present, we performed large-scale calculations using the GRASP2K package [4], taking advantage of the MCDHF method which can deal with the electron correlation and relativistic effects on the same foot. The active space method was adopted, which makes possible to monitor the convergence of the physical quantities concerned. Since the MCDHF method is generally sensitive to the shape of orbital wave functions if the configuration expansion is not complete, a variety of computational models were employed to obtain atomic state wave functions and to evaluate the oscillator strengths for these two E1 lines.

Another appealing subject is the lifetimes of the other two metastable levels $^3P_2^o$ and $^3P_0^o$ in the configuration. For the $^3P_2^o$ level, the magnetic quadrupole transition (M2) probability to the ground state A=0.06790(64) s^{-1} for ^{20}Ne, which is the dominant single-photon decay channel for even isotopes of neon, has been measured recently [5]. This value is different from other theoretical results by about 20%. For the $^3P_0^o$ level however, there is still a lack of experimental and theoretical results. Of particular interest are the odd isotopes of neon for which a new decay channel is opened by hyperfine interactions. Using the computational model mentioned earlier, we calculated the lifetime of metastable levels for even isotopes of neon, and the hyperfine-induced $^3P_{0,2}^o \rightarrow {}^1S_0$ transition probabilities for odd isotopes. We demonstrated that hyperfine interactions drastically quench the lifetime of these two metastable levels.

References

[1] E. N. Avgoustoglou and D. R. Beck, Phys. Rev. A **57**, 4286–4295 (1998).
[2] I. M. Savukov, W. R. Johnson, and H. G. Berry, Phys. Rev. A **66** 052501 (2002).
[3] O. Zatsarinny and K. Bartschat, Phys. Scr. **T134** 014020 (2010).
[4] P. Jönsson, X. He, C. Froese Fischer, and I. P. Grant, Comput. Phys. Comm. **177** 597–622 (2007).
[5] M. Zinner, P. Spoden, T. Kraemer, G. Birkl, and W. Ertmer, Phys. Rev. A **67** 010501(R) (2003).

Universal and specific properties of atomic interactions

T.–O. Müller[1], A. Kaiser[1,2], and H. Friedrich[1]

[1] *Physik Department, Technische Universität München, D-85747 Garching, Germany*
[2] *Johannes Kepler Universität Linz, A-4040 Linz, Austria*

Corresponding Author: tim-oliver.mueller@ph.tum.de

Cold atom interaction has been in the focus of experimental and theoretical research not only since the first realization of a Bose-Einstein condensate. We present a comprehensive approach to understanding all threshold effects occurring in elastic scattering processes. We show that the near-threshold bound state spectrum for interatomic potentials with attractive long-range tails is determined by the same quantities that determine the scattering phases including the occurrence of shape resonances in higher partial waves.

These interatomic potentials support at most a finite number of bound states. A LeRoy-Bernstein type of quantization rule

$$n_{\mathrm{th}} - n = F(E_n) \tag{1}$$

can then be applied [1], where the quantum number n of a bound state is connected to its energy E_n via the *threshold quantum number* n_{th} and the *quantization function* $F(E)$. The integer part of n_{th} coincides with the quantum number of the highest lying bound state. The s-wave scattering length a is related to the threshold quantum number [2] via the relation

$$a = \bar{a} + \frac{b}{\tan(n_{\mathrm{th}}\pi)}\,, \tag{2}$$

where the *mean scattering length* $\bar{a}$ [2] and the *threshold length* b [1] are quantities that depend only on the long-range tail of the potential. So the only short-range information entering the scattering length is contained in n_{th}.

For inverse-power tails $-C_\alpha/r^\alpha$, the threshold quantum number for higher partial waves can easily be approximated from the simple relation

$$n_{\mathrm{th}}(l) = n_{\mathrm{th}}(l=0) - \frac{l}{\alpha - 2} \tag{3}$$

as in [3]. An estimate of the elastic cross section can be given with minimal information, i.e., the dispersion coefficient C_α and the scattering length a (or n_{th}), together with universal tail-dependent functions.

Figure 1 gives an example of results obtained by this principle. It reproduces all significant features of the results obtained by explicit solving the Schrödinger equation for different models for the $^{13}\Sigma_g^+$ potential in Cr_2 [4]. Therefore it is possible to relate the position of shape resonances to the bound state spectrum, and vice versa, with minimum effort and without solving the Schrödinger equation for any certain potential.

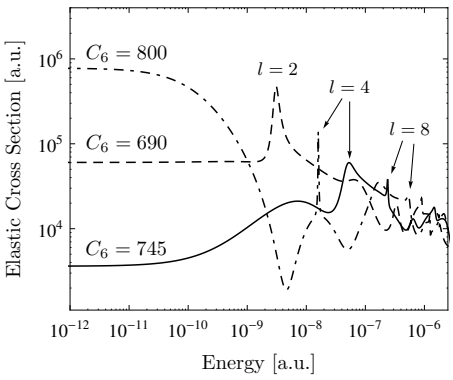

Figure 1: *Elastic cross sections for the scattering of chromium atoms. Each result has been obtained using only the coefficient C_6 and the corresponding scattering length.*

References

[1] P. Raab, and H. Friedrich, Phys. Rev. A **78**, 022707 (2008).
[2] G. F. Gribakin, V. V. Flambaum, Phys. Rev. A **48**, 546 (1993).
[3] M. Lemeshko, and B. Friedrich, Phys. Rev. A **79**, 050501(R) (2009).
[4] Z. Pavlovic, *et al.*, Phys. Rev. A **69**, 030701(R) (2004).

Relativistic calculations on isotope shifts in barium

C. Nazé[1], J. G. Li[1], and M. R. Godefroid[1]

[1] *Service de Chimie Quantique et Photophysique*
Université Libre de Bruxelles, B 1050 Brussels, Belgium
Corresponding Author: cnaze@ulb.ac.be, jgli@ulb.ac.be

Isotope shifts in atomic transition frequencies and energy levels provide valuable insights into atomic structures. It is generally assumed that the shifts are due to differences in nuclear mass (mass shift) and nuclear charge distribution (field shift). For systems with more than one electron, the "*Specific Mass Shift*" appears in the level-mass shift expression. Due to its low ponderation, the responsible mass-polarization operator is usually treated as a perturbation of the infinite-mass Hamiltonian and its estimation requires the calculation of Vinti integrals [1].

Mass and field shifts may provide valuable information about nuclear properties. Measured "modified" isotope shifts for two different transitions are often compared using a King-plot [2] that is expected to exhibit a linear dependence relating the two transition isotope shift pair values. In a recent experiment however [3], surprising deviations from a linear correlation in modified King-plots have been observed for the barium ($Z = 56$) isotopes with nuclear spin $I = 3/2$. The authors suggested that "the nuclear spin could give rise to some additional contribution to the isotope shift for atoms with nuclear spin" and also suggest that these effects might be due to some nuclear spin-dependence of electron correlation.

To investigate theoretically these peculiarities, we perform large-scale calculations of mass and field shifts in the full Dirac-Hartree-Fock scheme using GRASP2K [4] and adopting the active space approach to capture the dominant electron correlation effects. As first tests, we check the quality of the atomic wave functions through a comparison of the available theoretical and experimental excitation energies, fine structure splittings and radiative data.

References

[1] U. Dammalapati *et al.*, Eur. Phys. J. D **53**, 1–8 (2009).
[2] P. Jönsson *et al.*, Comput. Phys. Commun. **177**, 597–622 (2007).
[3] W. H. King, *Isotope Shifts in Atomic Spectra* (Plenum, New York, 1984).
[4] J.P. Vinti, Phys. Rev. **56**, 1120–1132 (1939).

Trigonometric unit circle and the stationary Schrödinger equation

K. Rajchel[1]

[1] *Pedagogical University, Institute of Physics & Computer Science, ul. Podchorazych 2, 30-084, Krakow, Poland*

Corresponding Author: krajchel@up.krakow.pl

A new method resolving the stationary Schrödinger equation has been described. The solution has been obtained by transforming the Schrödinger equation to the Ricatti equation, and next to the form of trigonometric unit circle. Thus, the new analytically solvable potentials and the method to generate them has been demonstrated. The connection between this method and other methods which lead to analytical solutions of the Schrödinger equation has been discussed.

Peculiarities of spectroscopic properties of W^{8+}

P. Rynkun[1], A. Alkauskas[1], G. Gaigalas[2], and Z. R. Rudzikas[2]

[1] *Department of Physics, Vilnius Pedagogical University, Studenty 39, Vilnius LT-08106, Lithuania*
[2] *Vilnius University, Institute of Theoretical Physics and Astronomy, A. Goštauto 12, Vilnius LT-01108, Lithuania*

Corresponding Author: Pavel.Rynkun@gmail.com

Tungsten will be used as a wall material in fusion devices. Therefore, the data on spectral properties of its various ions are of great importance. Such ions, having simple electronic configurations of open shells, are studied widely both experimentally and theoretically, but this is not the case for ions, having open f-shell, due to the large number of energy levels. The use of the second quantization method in coupled tensorial form combined with quasispin technique, described in [1], opens real possibilities to efficiently consider such configurations, as well. Indeed, paper [2] supports this conclusion. Moreover, it revealed an unexpected phenomenon, stating that a large part of electric octopole (E3) transitions may be interpreted as electric dipole (E1) transitions and their probabilities on average are million times higher than those of E1 transitions. The goal of this paper is to further study such ions by performing large-scale multiconfiguration Dirac-Fock calculations for the lowest 30 energy levels of W^{8+} ion. All these levels correspond to

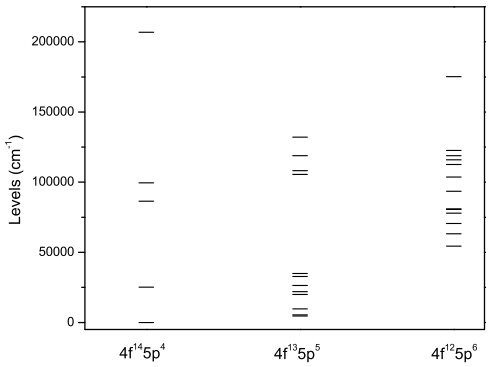

Figure 1: *Configurations of W^{8+} ion in MCDF+B+QED approach.*

$[\mathrm{Kr}]4d^{10}4f^{14}5s^25p^4$, $[\mathrm{Kr}]4d^{10}4f^{13}5s^25p^5$ and $[\mathrm{Kr}]4d^{10}4f^{12}5s^25p^6$ configurations. The relativistic corrections were taken into account in the Breit (with QED corrections) approximation with the help of GRASP2K packages [3,4]. The role of correlation, relativistic and QED corrections is discussed. Analyzing the preliminary results (see Fig. 1) we conclude that, on the one hand, the ground electronic configuration is clearly split into relativistic subconfigurations and, on the other hand, the lowest excited configurations are strongly mixed with the ground one. Therefore, here we have the unique situation when the real electronic configuration is the linear combination of several configurations, having almost equal weights, and, thus, single-configuration approximation is absolutely unfit.

References

[1] Z. Rudzikas, Theoretical Atomic Spectroscopy (Cambridge University Press, 2nd ed. 2007).
[2] G. Gaigalas, *et al.*, Phys. Rev. A (in press) (2011).
[3] P. Jönsson *et al.*, Comput. Phys. Commun. **177**, 597 (2007).
[4] C. F. Fischer, G. Gaigalas, Y. Ralchenko, Comput. Phys. Commun. **175**, 738 (2006).

Nonadiabatic state-independent potential for the hydrogen molecule in ground electronic state

M. Selg[1]

[1] *Institute of Physics, University of Tartu, Riia 142, 51014 Tartu, Estonia*
Corresponding Author: matti@fi.tartu.ee

Nonadiabatic coupling between electronic and nuclear motions cannot be reduced to correcting a single potential energy surface (PES). However, in the case of a simple quantum system, such as H_2 or H_2^+, nonadiabaticity can be adequately described in terms of coordinate-dependent corrections to the nuclear reduced mass. These important characteristics, different for the vibrational ($W_\parallel$) and rotational ($W_\perp$) components, have been recently accurately determined for the H_2 molecule in ground electronic state [1,2]. Thus the very simple and instructive concept of a single PES can still be preserved, and the rovibrational energy levels (E_{vJ}) are found from a modified Schrödinger equation

$$\Phi''_{vJ}(R) = \frac{V_{vJ}(R) - E_{vJ}}{C}\Phi_{vJ}(R) \quad \left(C \equiv \frac{\hbar^2}{2m}\right), \tag{1}$$

where the nonadiabatically corrected effective PES

$$V_{vJ}(R) = V(R) + \frac{C + W_\perp(R) - W_\parallel(R)}{R^2}J(J+1) + \frac{E_{vJ}}{C}W_\parallel(R) \tag{2}$$

depends on both vibrational (v) and rotational (J) quantum numbers. Here $V(R)$ is the state-independent part of the PES, which includes adiabatic, nonadiabatic, relativistic and radiative corrections, while the transformed radial eigenfunctions $\Phi_{vJ}(R)$ are normalized by the condition

$$\int [\Phi_{vJ}(R)]^2 \exp\left(-\frac{W_\parallel(R)}{C}\right) dR = 1. \tag{3}$$

In this report, the full state-independent potential for H_2 has been calculated, combining the nonrelativistic theory of nonadiabaticity [2] with the known relativistic and radiative corrections [3], and applying an inverse perturbational method [4]. Perfect agreement with the high-quality experimental and theoretical data was achieved. Discussion about the correct assignment of the "exotic" level ($J = 4, v = 14$) will be presented. This level is located very close to the dissociation limit, and therefore, one cannot ignore the hyperfine proton-electron spin interaction, which splits the atomic ^{2}S level. As a result, the triplet component of the split molecular level $E_{14,4}$ is located slightly above the zero-point ($E_t = +0.012$ cm^{-1}), while its center of gravity ($E_c = -0.019$ cm^{-1}) as well as the singlet component ($E_s = -0.036$ cm^{-1}) are slightly negative.

The work has been supported by the Estonian Science Foundation through Grant No. 7318.

References

[1] K. L. Bak *et al.*, Phys. Chem. Chem. Phys. **7**, 1747–1757 (2005).
[2] K. Pachucki, J. Komasa, J. Chem. Phys. **130**, 164113/1–11 (2009).
[3] L. Wolniewicz, J. Chem. Phys. **99**, 1851–1868 (2009).
[4] M. Selg, Mol. Phys. **108**, 687–698 (2010).

Spin-orbit coupling effect in the low-lying states of Rb_2, Cs_2 and RbCs molecules

E. A. Pazyuk[1], A. V. Stolyarov[1], and T. Bergeman[2]

[1] *Department of Chemistry, Moscow State University, 119991, GSP-2, Moscow, Leninskie gory 1/3, Russia*
[2] *Department of Physics and Astronomy, SUNY, Stony Brook, NY 11794-3800, USA*
Corresponding Author: avstol@phys.chem.msu.ru

We present the results of *ab initio* calculations on the potential energy curves, transition dipole moments, spin-orbit and angular coupling matrix elements between the electronic states of Rb_2, Cs_2 and RbCs molecules converging to the lowest three dissociation limits. The quasi-relativistic matrix elements have been evaluated for a wide range of internuclear distance in the basis of the spin-averaged wavefunctions corresponding to pure Hund's coupling case (a) by using small (9-electron) effective core pseudopotentials of both atoms. The core-valence correlation has been accounted for a large scale multi-reference configuration interaction method combined with semi-empirical core polarization potentials.

The calculated spin-orbit coupling matrix elements were involved in the deperturbation treatment of the of the fully mixed $A^1\Sigma^+$ and $b^3\Pi$ states as well as to estimate a second order SO effect in the ground singlet $X^1\Sigma^+$ and triplet $a^3\Sigma^+$ states. The resulting transition dipole moments and potentials were used to predict radiative lifetimes and emission branching ratios of excited vibronic states while the calculated angular and spin-orbit coupling matrix elements were transformed to $\Lambda(\Omega)$-doubling constants of the $^{1,3}\Pi$ states. The accuracies of the present results are discussed by comparing with experimental data and preceding calculations.

We also review here physical models and numerical recipes currently developed for the comprehensive deperturbation treatment of the strongly coupled $A^1\Sigma^+$ and $b^3\Pi$ states alkali dimers in a wide range of excitation energy and internuclear distance [1–3]. The interpolation and extrapolation properties of the resulting non-adiabatic models are discussed with respect to accuracy of *ab initio* spin-orbit coupling matrix element required for the adequate reproduction of experimental data sets.

Moscow team thanks for support the Russian Foundation for Basic Researches by the grant 10–03–00195a.

References

[1] H. Salami *et al.*, Phys. Rev. A **80**, 022515 (2009).
[2] O. Docenko *et al.*, Phys. Rev. A **81**, 042511 (2010).
[3] J. Bai *et al.*, Phys. Rev. A, **82**, in press (2011).

Adaptive mapping procedure for scattering length calculation

V. V. Meshkov[1], A. V. Stolyarov[1], and R. J. LeRoy[2]

[1] *Department of Chemistry, Moscow State University, 119991, GSP-2, Moscow, Leninskie gory 1/3, Russia*
[2] *Guelph-Waterloo Center for Graduate Work in Chemistry and Biochemistry, University of Waterloo, Waterloo, Ontario N2L 3G1, Canada*

Corresponding Author: avstol@phys.chem.msu.ru

We have shown that the two-parameter mapping function $r(y;\bar{r},\beta) = \bar{r}\left[1+\frac{1}{\beta}\tan(\pi y/2)\right] \in [0,\infty)$ transforms the conventional radial Schrödinger equation into an equivalent form

$$\frac{d^2\phi(y)}{dy^2} = \left[\frac{\pi^2}{4} + \left(\frac{2\mu}{\hbar^2}\right) g^2(y)\,[E - U(r(y))]\right]\phi(y); \qquad g(y) \equiv \frac{dr(y)}{dy}$$

defined on the finite domain $y(r) \in [(2/\pi)\tan^{-1}(-\beta), 1]$, and allows the s-wave scattering length a_s to be expressed exactly in terms of a logarithmic derivative of the transformed wave function $\phi(y)$ at the outer boundary point $y = 1$ which corresponds to $r = \infty$. In particular for an arbitrary interaction potential that dies faster then $1/r^4$, the modified wave function $\phi(y)$ has no singularities, and

$$a_s = \bar{r}\left[1 + \frac{2}{\pi\beta}\frac{1}{\phi(1)}\frac{d\phi(1)}{dy}\right] .$$

For a well bound potential with equilibrium distance r_e and a long-range tail proportional to $1/r^n$, the optimal mapping parameters are $\bar{r} \approx r_e$ and $\beta \approx (n/2) - 1$. The same mapping function also assures the efficient calculation of all of the bound states [1]. The zero-energy wavefunction $\phi(y)$ may also be combined with wavefunctions for ordinary bound states generated in the same manner [1] to calculate photoassociation absorption matrix elements using any appropriately modified Franck-Condon computer program [2].

An outward integration procedure based on Johnson's log-derivative algorithm [3] combined with a Richardson extrapolation procedure [4] has been successfully implemented for calculating a_s-values for model Lennard-Jones $(2n, n)$ potentials and for realistic potentials that have been reported for the e$^-$-Xe, $Cs_2(a\,^3\Sigma_u^+)$ and $^{3,4}He_2(X\,^1\Sigma_g^+)$ systems.

The Moscow team is grateful to the Russian Foundation for Basic Researches for support through Grant 10–03–00195, while the Waterloo work has been supported by the Natural Sciences and Engineering Research Council of Canada.

References

[1] V. V. Meshkov, A. V. Stolyarov, and R. J. LeRoy, Phys. Rev. A, **78**, 052510–11 (2008).
[2] R. J. LeRoy, *A Computer Program for Solving the Radial Schrödinger Equation for Bound and Quasi-bound Levels and Scattering Lengths*, University of Waterloo Chemical Physics Research Report CP–666 (2011); see http://leroy.uwaterloo.ca/programs/.
[3] B. R. Johnson, J. Comp. Phys. **13**, 445–449 (1973); J. Chem. Phys. **67**, 4086–4093 (1977).
[4] L. F. Richardson, Phil. Trans. Roy. Soc. (London) A **226**, 299 (1927).

Strong polarization of outer electron shells by inner vacancies in Ba

V. L. Sukhorukov[1], I. D. Petrov[1], B. M. Lagutin[1], R. V. Vedrinsky[2], A. V. Nikolsky[2], K. A. Guglev[2], L. A. Demekhina[2], and A. T. Kozakov[2]

[1] *Rostov State Transport University, 344038 Rostov-na-Donu, Russia*
[2] *Southern Federal University, 344082 Rostov-na-Donu, Russia*
Corresponding Author: vls@rgups.ru

Existence of localized virtual space in atoms gives rise to the complex sequence of atomic levels and the strong satellites in corresponding atomic spectra. For rare gases this phenomenon was revealed half a century ago by Minnhagen [1] by optical spectroscopy and confirmed later also using x-ray photoelectron spectroscopy (XPES) [2]. In rare earth elements (REE) the virtual space is extremely localized due to presence of the unoccupied 4f- shell and, therefore, the intense satellites change the x-ray and photoelectron spectra even more drastically than it was revealed in [1,2] for rare gases. Strong dipole polarization of electron shells (DPES) by the 4p- vacancy due to the 4d4d-4p$\{n/\varepsilon\}$ Demekhin *et al.* [3,4] in studying the L$\gamma_{2,3}$ x-ray spectra of REE and was later revisited by Ohno and LaVilla [5,6]. Manifestation of DPES in photoelectron spectra of the 4p- shell of REE was predicted theoretically by Demekhin *et al.* [7] and confirmed by Yarzhemsky *et al.* [8].

In the present paper the influence of DPES on the Ba states with 3p-, 3d-, 4s-, 4p-, 4d-, 5s-, and 5p- vacancies was investigated experimentally and theoretically. In addition to DPES all the single and double electron excitations were taken into account via the technique described by Lagutin *et al.* [9]. Atomic orbitals (AOs) involved in calculation were computed with taking into account relativistic effects within the Pauli-Fock approach [10].

All vacancies mentioned above strongly polarize the higher-lying shells because of the presence of localized virtual space in Ba. The strongest polarization follows the creation of the 4s-, 4p-, and 5s- vacancies. The excitations 4p4d-4s$\{n/\varepsilon\}$f, 4d4d-4p$\{n/\varepsilon\}$f, and 5p5p-5s$\{n/\varepsilon\}\{$s/d$\}$ contribute about 12 eV, 14 eV, and 6 eV to the energy of the center-of-gravity of the 4s-, 4p-, and 5s- vacancies, respectively. These excitations give also rise to the intense satellites in the XPES. Experimental XPES of the 3p-, 3d-, 4s-, 4p-, 4d-, 5s- shells and of the valence band of Ba in solids BaO_2, $BaSO_4$ and $BaTiO_3$ were obtained using ESCALAB 250 photoelectron spectrometer. Spectra were excited by monochromatized Al Kα line having FWHM equal to 0.48 eV. Experimental spectra of solids are in good agreement with the computed spectra if the solid state effects, which broaden the spectral lines up to 0.9 eV in addition to natural width, are taken into account.

References

[1] L. Minnhagen, Ark. Fys. **25**, 203–283 (1963).
[2] U. Gelius, J. Electr. Spectr. **5**, 985–1057 (1974).
[3] V. F. Demekhin *et al.*, Bull. Acad. USSR Ser. Phys. **36**, 352–353 (1972).
[4] V. F. Demekhin *et al.*, Bull. Acad. USSR Ser. Phys. **40**, 352–353 (1976).
[5] M. Ohno, and R. E. LaVilla, Phys. Rev. B **39**, 8845–8851 (1989).
[6] M. Ohno, and R. E. LaVilla, Phys. Rev. B **39**, 8852–8857 (1989).
[7] V. F. Demekhin *et al.*, Metallophysics (Kiev) **60**, 27–39 (1975).
[8] V. G. Yarzhemsky *et al.*, J. Electr. Spectr. **59**, 211–222 (1992).
[9] B. M. Lagutin *et al.*, J. Phys. B **29**, 937–976 (1996).
[10] R. Kau *et al.*, Z. Phys. D **39**, 267–281 (1997).

The $4^1\Sigma^+$ electronic state of LiCs molecule

J. Szczepkowski[1], A. Grochola[2], P. Kowalczyk[2], and W. Jastrzębski[1]

[1] *Institute of Physics, Polish Academy of Sciences, al. Lotników 32/46, 02-668 Warszwa, Poland*
[2] *Institute of Experimental Physics, Warsaw University, ul. Hoża 69, 00-681 Warszawa, Poland*

Corresponding Author: jszczep@ifpan.edu.pl

The $4^1\Sigma^+$ electronic states in heteronuclear alkali dimers are all characterized by exotic shapes of the corresponding potential energy curves. They display either unusually broad potential wells with single minima (KLi, LiCs, KCs, LiRb, NaRb, KRb, RbCs) or double wells (NaLi, NaCs). These specific features result from avoided crossings between the neighboring valence $^1\Sigma^+$ states and the lowest ion-pair potential belonging to the same electronic symmetry. Broad potential wells make the $4^1\Sigma^+$ states attractive candidates for various spectroscopic schemes, allowing for molecular excitation and/or emission both close to the inner turning point of vibrational motion, at low internuclear distances R, and around the outer turning point, at unusually large R. Thus rovibrational levels of the $4^1\Sigma^+$ states may serve as intermediate levels for fluorescence and excitation experiments probing long range parts of interatomic potentials. The $4^1\Sigma^+$ states can be also employed in cold matter experiments as the final states of the photoassociation process or as intermediate states for resonantly enhanced multiphoton ionization (REMPI) of ground state cold molecules. In this contribution we present an experimental observation of the $4^1\Sigma^+$ state in LiCs. Using a highly sensitive technique of polarization labeling spectroscopy [1] we have experimentally observed rovibrational levels of the $4^1\Sigma^+$ state and constructed the corresponding potential curve using the point-wise inverted perturbation approach method [2]. The resulting interatomic potential is compared with the available theoretical prediction [3].

References

[1] W. Jastrzębski, P. Kowalczyk, Phys. Rev. A **51**, 1046 (1995).
[2] A. Pashov, W. Jastrzębski, P. Kowalczyk, Comput. Phys. Commun. **128**, 622 (2000).
[3] N. Elkork *et al.*, Can. J. Phys. **87**, 1079 (2009).

Interaction of variational localized correlation functions for atomic properties

S. Verdebout[1], M. R. Godefroid[1], P. Rynkun[2], P. Jönsson[3], G. Gaigalas[2,4], and C. Froese Fischer[5]

[1] *Service de Chimie Quantique et Photophysique, CP160/09, Université Libre de Bruxelles, Av. F. D. Roosevelt 50, B-1050 Brussels, Belgium*
[2] *Vilnius Pedagogical University, Studenty 39, Vilnius, LT-08106, Lithuania*
[3] *Center for Technology Studies, Malmö University, 205-06 Malmö, Sweden*
[4] *Institute of Theoretical Physics and Astronomy, Vilnius University, A. Goštauto 12, LT-01108, Vilnius, Lithuania*
[5] *National Institute of Standards and Technology, Gaithersburg, USA*

Corresponding Author: sverdebo@ulb.ac.be

Variational methods are used for targeting specific correlation effects by tailoring the configuration space. Independent sets of correlation orbitals, embedded in the localized correlation functions (LCFs), are produced from the multiconfiguration Hartree-Fock (MCHF) or Dirac-Hartree-Fock (MCDHF) calculations [1,2]. These non-orthogonal functions are then coupled to each other by solving the associated generalized eigenproblem. The Hamiltonian and overlap matrix elements are evaluated using the biorthonormal orbital transformations and efficient counter-transformations of the configuration interaction eigenvectors [3]. This method was successfully applied for describing the total energy of the ground state of beryllium [4]. Moreover it has been shown that the energy convergence is faster than with the usual SD-MCHF method for which a single set of orthonormal one-electron orbitals spanning the complete configuration space is optimized.

In the present work, we investigate the interaction of localized correlation functions (LCFI), not only for the $1s^2 2s^2\ ^1S$ state of beryllium but also for the first two excited states: $1s^2 2s2p\ ^3P^o$ and $1s^2 2s2p\ ^1P^o$. For these three states, we evaluate the total energy but also the expectation values of the specific mass shift (SMS) operator, the hyperfine structure (HFS) parameters and the transition probabilities. The comparison between the SMS and HFS results obtained using the LCFI method and the traditional MCHF one stresses the importance of the mixing coefficients contraction within each LCF function. We demonstrate that this unwanted contraction effect can be bypassed by enlarging the associated generalized eigenproblem.

The beryllium atom is a system for which it is still possible to saturate a single orthonormal orbital set through the complete active space MCHF expansions. As such, it constitutes the perfect benchmark for the LCFI method. For larger systems, it becomes hopeless to saturate a single common set of orthonormal orbitals, the LCFI method should be a good alternative for reaching a full-correlated wave function. The present study is a first step in the current development of the extension of both ATSP2K and GRASP2K packages [1,2] that will adopt the biorthonormal treatment for energies, isotope shifts, hyperfine structures and transition probabilities.

References

[1] C. Froese Fischer *et al.*, Comp. Phys. Commun. **176** 559 (2007).
[2] P. Jönsson *et al.*, Comp. Phys. Commun. **177** 597 (2007).
[3] J. Olsen *et al.*, Phys. Rev. E **52** 4499 (1995).
[4] S. Verdebout *et al.*, J. Phys. B: At. Mol. Opt. Phys. **43** 74017 (2010).

Atomic properties of neutral Ne using the LCFI method

S. Verdebout[1], J. G. Li[1], C. Nazé[1], M. R. Godefroid[1], P. Jönsson[2], and G. Gaigalas[3]

[1] *Chimie Quantique et Photophysique, Université Libre de Bruxelles, Brussels, Belgium*
[2] *Center for Technology Studies, Malmö University, 205-06 Malmö, Sweden*
[3] *Institute of Theoretical Physics and Astronomy, Vilnius University, Vilnius, Lithuania*
Corresponding Author: sverdebo@ulb.ac.be

The localised correlation function interaction (LCFI) method, based on the biorthonormal orbital transformations and efficient counter-transformations of the configuration interaction eigenvectors [1], was shown to be efficient for describing the total energy of the beryllium atom [2]. Each localized correlation function (LCF) is dedicated to the description of the electronic correlation associated to a given electron pair. Such functions are produced, using the multiconfiguration Hartree-Fock (MCHF) and Dirac-Hartree-Fock (MCDHF) variational methods, by optimizing the correlation functions and the mixing coefficients on a tailored configuration space. Applying the LCFI method to neon allows us to quantify the contribution of each localized correlation function to different atomic properties [3]. This investigation should turn out to be helpful in the development of efficient correlation models for larger systems.

Neutral neon is a well-known benchmark example for testing many-body approaches. In the present work, we apply the LCFI method to the study of the three lowest terms $2p^6\ ^1S$, $2p^5 3s\ ^3P^o$ and $2p^5 3s\ ^1P^o$ of neutral neon. We investigate the convergence pattern of the total energy, specific mass shift and hyperfine structure parameters for the three considered states. These properties are computed for monitoring the quality of the total polyelectronic wave functions. We present the contribution of each LCF function on the different properties, and additionally discuss the multi-reference models adopted for reaching simultaneously good total and transition energies. A comparison between the results obtained with ATSP2K [4] and GRASP2K [5] should shed some light on the importance of the relativistic effects on each LCF function.

References
[1] J. Olsen *et al.*, Phys. Rev. E **52** 4499 (1995).
[2] S. Verdebout *et al.*, J. Phys. B: At. Mol. Opt. Phys. **43** 74017 (2010).
[3] J. W. Viers *et al.*, Phys. Rev. A **1** 24 (1970).
[4] C. Froese Fischer *et al.*, Comp. Phys. Commun. **176** 559 (2007).
[5] P. Jönsson *et al.*, Comp. Phys. Commun. **177** 597 (2007).

Polarization correlations in radiative recombination and bremsstrahlung

V. A. Yerokhin[1,2], A. Surzhykov[1]

[1] *University of Heidelberg, Philosophenweg 12, D-69120 Heidelberg and Gesellschaft für Schwerionenforschung, Planckstraße 1, D-64291 Darmstadt, Germany*
[2] *Center for Advanced Studies, St. Petersburg State Polytechnical University, Polytekhnicheskaya 29, St. Petersburg 195251, Russia*

Corresponding Author: yerokhin@pcqnt1.phys.spbu.ru

Two fundamental processes are studied that occur in collisions of a heavy atom with an electron, namely the radiative recombination, in which the electron is captured from the continuum into a bound state with emission of a photon, and bremsstrahlung, in which a photon is emitted by an electron scattering from an atom. These two processes are naturally linked at the continuum threshold limit, i.e., the bremsstrahlung at the hard photon end of the spectrum can be shown to be equivalent to the radiative recombination into highly excited atomic states.

In the present work, we investigate the polarization properties of the emitted radiation in these two processes as a function of the polarization of the incoming electrons. In particular, the rotation of the polarization ellipse of the emitted photon induced by the linear polarization of the incoming electron is studied in detail. Fully relativistic approach based on the partial-wave representation of the Dirac wave functions in the external atomic field is used. The results obtained [1] agree with the previous relativistic calculations [2] but extend them into the region of higher impact energies. It is demonstrated that the hard photon end of the bremsstrahlung spectrum is most suitable for experimental studies of the polarization correlations.

The work is supported by the Helmholtz Gemeinschaft (Nachwuchsgruppe VH-NG-421).

References

[1] V. A. Yerokhin and A. Surzhykov, Phys. Rev. A. **82**, 062702 (2010).
[2] H. K. Tseng and R. H. Pratt, Phys. Rev. A **7**, 1502 (1973).

High-Resolution Spectroscopy

Doppler reduced investigation of hyperfine structures of Pr II lines using collinear laser ion beam spectroscopy

N. Akhtar[1,2], N. Anjum[1,2], H. Hühnermann[1,3], and L. Windholz[1]

[1] *Institute of Experimental Physics, Petersgasse 16, TU Graz, Austria*
[2] *Optics Labs P. O. Box 1021, Nilore Islamabad, Pakistan*
[3] *Department of Physics, University of Marburg, Germany*

Corresponding Author: nadeem6676@yahoo.com

In this work, Doppler reduced spectroscopy of selected praseodymium ionic transitions was performed using collinear laser ion beam spectroscopy (CLIBS). CLIBS provides a resolution improved by a factor of 10–20 compared to the Doppler broadened emission lines from a hollow cathode lamp. Using this technique, well resolved hyperfine structures (having FWHM about 60 MHz) are obtained which enables the accurate determination of the hyperfine constants.

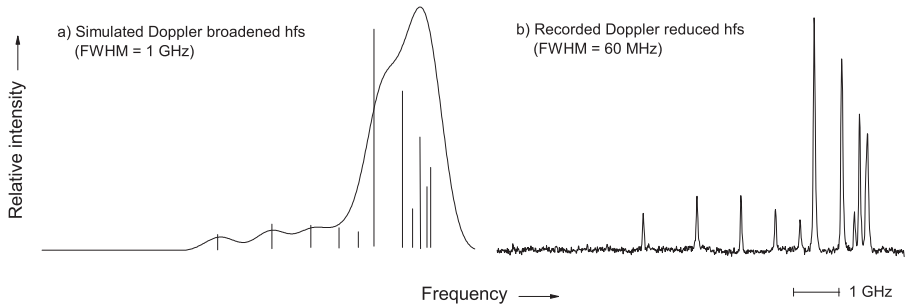

Figure 1: *Hyperfine structure of Pr II line at* 5818.59 *Å illustrating well resolved hyperfine components.*

The praseodymium ions were produced using a surface ion source and accelerated to 20 kV. After passing through an 80° magnet, the ion beam was superposed with the laser in the interaction chambers (light collecting chambers). A ring dye laser operated with Rhodamine 6G, pumped by an argon-ion laser used as light source. In the first light collecting chamber, Doppler tuning was carried out to investigate the hfs. In the second light collecting chamber, the laser was stabilized to one of the hyperfine components to overcome the fluctuations in the accelerating voltage as well as frequency drift of the laser. A photon counting method was used to record the laser induced fluorescence. Transitions in the region 575 nm to 582 nm were investigated and by using a fit program, the magnetic dipole constant A and electric dipole constant B of the involved energy levels were determined. The results are found to be in good agreement with the literature values. Some transitions are investigated for the first time using this technique.

Interference of laser-dressed states in the Autler-Townes effect

J. Ulmanis[1], M. Bruvelis[2], N. N. Bezuglov[3], K. Miculis[2], C. Andreeva[4], T. Kirova[5], A. Ekers[2], and I. I. Ryabtsev[6]

[1] *Physikalisches Institut, Universität Heidelberg, Heidelberg, Germany*
[2] *Laser Centre, University of Latvia, LV-1002 Riga, Latvia*
[3] *Faculty of Physics, St. Petersburg State University, 198904 St. Petersburg, Russia*
[4] *Institute of Electronics, Bulgarian Academy of Sciences, Sofia 1784, Bulgaria*
[5] *National Institute for Theoretical Physics, 7600 Stellenbosch, South Africa*
[6] *Institute of Semiconductor Physics, 630090 Novosibirsk, Russia*

Corresponding Author: christina.andreeva@lu.lv

Interference of laser-dressed states can be observed when light-induced crossings of energy levels enable the population to split between distinct excitation pathways that recombine afterwards. Implications of such interference were discussed in a recent paper describing an experiment with Na_2 molecules [1], but that experiment did not demonstrate resolved interference patterns. Here, we shall demonstrate observation of resolved interference patterns obtained in a Ramsey-type experiment in a supersonic Na/Na_2 atomic/molecular beam. The excitation pathways are generated by applying two laser fields in a three level ladder system $g - e - f$. The lasers are focused in such a way that a strong and short (tightly focused) pump laser couples the two lower levels g and e, and weak and long (less tightly focused) probe laser couples the intermediate e and the upper level f. The energy difference between the dressed states is determined by the pump field Rabi frequency and its detuning off from resonance. Our numerical calculations are based on the density matrix equations of motion using the split propagation technique. A detailed analysis based on both the dressed-state picture and exact numerical experiments show that the spatial distribution and population switching of highly excited atoms can be precisely controlled by varying the frequencies and intensities of both laser fields. We show that such Ramsey-type interferences of dressed states can be used for fast population control and switching.

We acknowledge the support by the EU FP7 IRSES Project COLIMA.

References

[1] N. N. Bezuglov *et al.*, Phys. Rev. A **78** 053804 (2008).

High resolution spectroscopic study of La II by using collinear laser ion beam spectroscopy

N. Anjum[1,2], N. Akhtar[1,2], H. Hühnermann[1,3], and L. Windholz[1]

[1] *Institute of Experimental Physics, Petersgasse 16, TU Graz, Austria*
[2] *Optics Labs P. O. Box 1021, Nilore Islamabad, Pakistan*
[3] *Department of Physics, University of Marburg, Germany*

Corresponding Author: naveedanjum121@yahoo.com

Collinear laser ion beam spectroscopy (CLIBS) is a very powerful and accurate experimental method to resolve extremely narrow hyperfine structure spectra. This kind of high resolution spectroscopy has been used to study several rare earth ions, e.g., Pr II, Nd II, Sm II, Eu II. In this work, the CLIBS technique has been used to investigate hyperfine structure of singly ionized lanthanum (La II). These spectroscopic measurements lead us to determine accurately magnetic dipole and electric quadruple coupling constants A and B respectively.

In our experiment, La ions were produced in an ion source of Johnson type by surface ionization. The ions were accelerated to 20 kV and then passed through an 80 ° magnet. A collimated ion beam was obtained in the interaction chamber where the ions interact with the laser beam. In the interaction chamber the ion velocity and thus its Doppler shifted absorption frequency was tuned by applying an additional voltage (Doppler tuning). In the second interaction chamber the laser was stabilized to one of the hyperfine components of the investigated structure to overcome any drift in laser frequency as well as fluctuations in acceleration voltage. Due to the high density of low lying thermally populated metastable levels in La II, many transitions can be investigated. A ring dye laser, pumped by an Ar^+ laser, was used as the excitation source to obtain the desired laser wavelengths. We have recorded spectral lines in the region of dye Rhodamine 6G. Laser induced fluorescence was recorded by using a photomultiplier tube and a photon counter. Magnetic dipole constants A and electric quadruple constants B of the involved levels have been determined using a fit program.

High-resolution double resonance spectroscopy of the clock transition in ^{87}Rb atomic vapour

T. Bandi[1], C. Affolderbach[1], and G. Mileti[1]

[1] *Institute of Physics, University of Neuchâtel, 2000-Neuchâtel, Switzerland*
Corresponding Author: thejesh.bandi@unine.ch

We present our studies on systematic shifts of the ^{87}Rb clock transition by laser-microwave double-resonance (DR), in view of applications to high-performance vapour-cell atomic clocks [1,2]. In our setup, the ^{87}Rb atoms are held in a cell also filled with a mixture of buffer gases and are optically pumped using a DFB laser emitting on the D2-line (780 nm). Microwave radiation at the ^{87}Rb ground state frequency of 6.835 GHz is applied via a magnetron-type resonator. A static magnetic field is applied to isolate the clock transition ($|F = 1, m_F = 0\rangle \rightarrow |F = 2, m_F = 0\rangle$) of interest here [2].

The DR clock signal has a narrow linewidth of <550 Hz and a contrast > 34%, enabling high-resolution measurement of the transition frequency (10^{-12} fractional resolution). An analysis of the signal-to-noise limit and shot-noise limits for this signal is made, resulting in a limit of $\approx 3 \times 10^{-13}\tau^{-1/2}$ for the clock stability. We have measured the shift of the clock transition frequency as a function of parameters like laser intensity (light-shift), microwave power, and temperature coefficients. A light-shift reduction technique based on precise detuning of the laser frequency is presented (see Fig. 1), which allows controlling the light-shift to a level compatible with a clock instability of $< 10^{-14}$ over one day. The instability contributions of these shifts on the clock frequency stability is estimated and analyzed. Finally, we discuss the impact of temperature gradients present in the cell on the medium- to long-term effects involved in attaining the equilibrium clock frequency [3]. This phenomenon is crucial for understanding the frequency evolution of vapour-cell atomic clocks, including GPS and next generation GALILEO clocks.

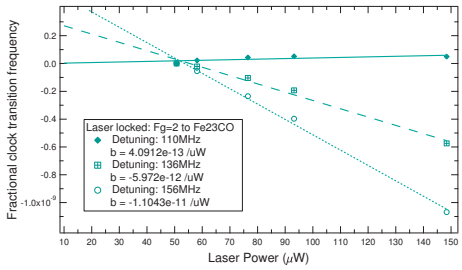

Figure 1: *Light-shift reduction by laser frequency detuning.*

Acknowledgments: We acknowledge the support and funding by European Space Agency (ESA) (contracts 19392/05/NL/CP and 21504/08/NL/GLC), and Swiss National Science Foundation (grant 200020-105624, CRSI20-122693/1).

References

[1] T. Bandi, C. Affolderbach, C. E. Calosso, and G. Mileti, *High-Performance Laser-Pumped Rubidium Frequency Standard for Satellite Navigation*, Submitted to Electronics Letters (Feb 2011).

[2] J. Vanier, C. Audoin, *The Quantum Physics of Atomic Frequency Standards* (Adam Hilger, Bristol, 1989).

[3] J. C. Camparo, C. M. Klimcak, and S. J. Herbulock, IEEE Transactions on instrumentation and measurement **54**, 1873–1880 (2005).

Magneto-optical resonances in D_2 excitation of atomic rubidium vapour confined in an extremely thin cell

A. Berzins[1], M. Auzinsh[1], R. Ferber[1], F. Gahbauer[1], A. Jarmola[1], L. Kalvans[1], A. Papoyan[2], and D. Sarkisyan[2]

[1] *Laser Centre, University of Latvia, Rainis Blvd. 19, LV-1582 Riga, Latvia*
[2] *Institute for Physical Research, NAS of Armenia, Ashtarak-0203, Armenia*
Corresponding Author: andris.beerzinsh@gmail.com

Extremely thin cells (ETCs) [1] confine alkali vapours between two YAG crystal walls separated by only hundreds of nanometers. When the wall separation is equal to the transition wavelength of the rubidium D_2 line, observations of the hyperfine spectrum with a reduced Doppler width on the order of 60 MHz (FWHM) are possible. The reduced Doppler width also makes measurements very sensitive to the laser frequency. We present measurements of the laser induced fluorescence (LIF) of rubidium vapour confined in an ETC as a function of magnetic field for the hyperfine transitions of the rubidium D_2 line. The unpolarized LIF was observed in the direction perpendicular to the linearly polarized exciting radiation's polarization vector as well as to the laser propagation direction, but parallel to the magnetic field, which was scanned. Figure 1 shows an example of the results of measurements on the $F_g = 1 \rightarrow F_e = 1$ transition of ^{87}Rb. The shape of the observed magneto-optical resonances depends sensitively on the detuning Δ of the exciting laser radiation. This dependence provides a sensitive test of the theoretical model, which is based on the optical Bloch equations. This model has been applied successfully to signals from an ETC for excitation of the D_1 line of rubidium [2]. However, the D_2 line presents special challenges because the hyperfine levels are more closely spaced and the influence of neighboring levels is more pronounced. We present experimental signals and theoretical calculations.

HRS

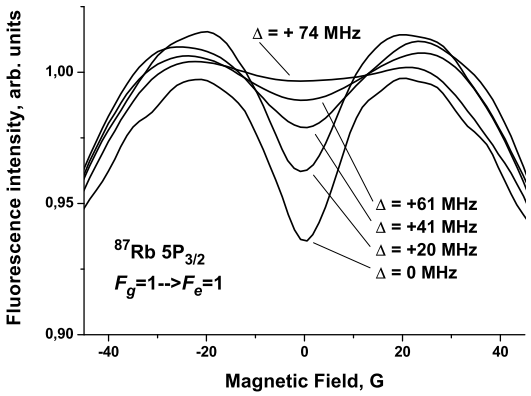

Figure 1: *LIF intensity versus magnetic field in the ETC at the ^{87}Rb $F_g = 1 \rightarrow F_e = 1$ transition for various values of the laser detuning.*

This work was sponsored by the Latvian State Research Programme Grant No. 2010/10-4/VPP-2/1, ERAF project; Nr. 2DP/2.1.1.1.0/10/APIA/VIAA/036, and ESF project; and Nr. 2009/0223/1DP/1.1.1.2.0./09/APIA/VIAA/008.

References

[1] D. Sarkisyan, D. Bloch, A. Papoyan, M. Ducloy, Opt. Commun. **200**, 201 (2001).
[2] M. Auzinsh *et al.*, Phys. Rev. A **81**, 033408 (2010).

Influence of laser power density on bright and dark magneto-optical resonances

A. Berzins[1], M. Auzinsh[1], R. Ferber[1], F. Gahbauer[1], L. Kalvans[1], A. Mozers[1], and D. Opalevs[1]

[1] *Laser Centre. University of Latvia, Rainis Blvd 19, LV-1589 Riga, Latvia*
Corresponding Author: andris.beerzinsh@gmail.com

Magneto-optical resonances observed in alkali metal vapors [1,2] can be dark or bright [3]. In general, when the total angular momentum of the ground state F_g is greater than or equal to the total angular momentum of the excited state F_e, one expects a dark resonance, whereas then $F_g < F_e$ one expects a bright resonance. In practice, however, the observed resonances may not be of the expected variety because of the influence of nearby transitions under Doppler broadening. For example, a resonance may change from dark to bright depending on the laser detuning [4]. Theoretical calculations on the $F_g = 2 \rightarrow F_e = 3$ transition of ^{87}Rb suggest that a dark resonance may be observed at high laser power densities, whereas at lower laser power densities a bright resonance should be observed. Figure 1 shows that when the magnetic field vanishes, a narrow dark resonances is seen for Rabi frequencies Ω above 2 MHz, whereas for lower Rabi frequencies, a bright resonance appears in place of the dark resonance. Experimental measurements are in progress to confirm the effect. The theoretical model is based on the optical Bloch equations, and has been successfully applied to describe magneto-optical resonances in various systems (see, for example, [4]). However, sensitive tests are useful to refine the model, since not all parameters can be determined from the experiment.

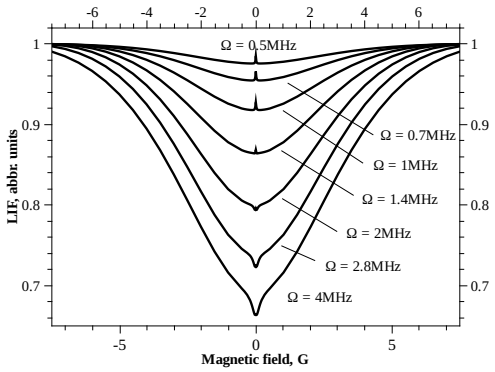

Figure 1: *Theoretical simulations of magneto-optical resonances at ^{87}Rb excitation on the $F_g = 2 \rightarrow F_e = 3$ transition. The exciting laser is detuned by 200 MHz from the exact transition to minimize the influence of the neighboring ($F_g = 2 \rightarrow F_e = 2$) transition.*

This work was sponsored by the Latvian State Research Programme Grant No. 2010/10-4/VPP-2/1, ERAF project; Nr. 2DP/2.1.1.1.0/10/APIA/VIAA/036, and ESF project; and Nr. 2009/0223/1DP/1.1.1.2.0./09/APIA/VIAA/008.

References

[1] J.-C. Lehmann and C. Cohen-Tannoudji, C.R. Acad. Sci. Paris Ser. IV **258**, 4463 (1964).
[2] R. W. Schmieder, A. Lurio, W. Happer, and A. Khadjavi, Phys. Rev. A **2**, 1216 (1970).
[3] G. Alzetta, A. Gozzini, L. Moi, and G. Orriols, Il Nuovo Cimento B **36**, 5 (1976).
[4] M. Auzinsh *et al.*, Phys. Rev. A **79**, 053404 (2009).

Fourier transform spectroscopy and potential construction for low vibrational levels of $B^1\Pi$ state in KCs

I. Birzniece[1], O. Nikolayeva[1], M. Tamanis[1], and R. Ferber[1]

[1] *Department of Physics, University of Latvia, LV-1002 Riga, Latvia*
Corresponding Author: Inese.Birzniece@gmail.com

The lowest $^1\Pi$ state of the KCs molecule, the $B^1\Pi$ state, was studied using a diode lasers for inducing fluorescence that was resolved by a high resolution Fourier-transform spectrometer (FTS) Bruker IFS–125HR. The presence of argon buffer gas yielded rich rotational relaxation spectra enlarging the data set for the $B(1)^1\Pi$ state, to obtain Λ-splitting and to reveal numerous local perturbations. KCs molecules were produced in a linear heat-pipe filled with 10 g of potassium (natural isotope mixture) and 7 g of cesium at temperature about 290°C and were excited in transition $B(1)^1\Pi(v', J') \leftarrow X(v'', J'' = J', J' \pm 1)$. Back-scattered laser induced fluorescence (LIF) was sent onto input aperture of FTS by a pierced mirror. Spectra were recorded by FTS at resolution 0.03 cm^{-1}. A diode laser with 685 nm, 705 nm or 730 nm laser diode installed in a home-made external resonator was used for excitation. Laser frequency used in the experiment varied from 11 992 to 13 760 cm^{-1} for 730 nm diode, from 14 070 to 14 320 cm^{-1} for 705 nm diode and from 14 402 to 14 586 cm^{-1} for 685 nm diode. As a detector mainly silicon photodiode operating at room temperature was used (over 90% of recorded spectra), but in some cases it was replaced by either photomultiplier (Hamamatsu R928) or InGaAs diode operating at room temperature. The assignment of the LIF progressions in the $B \rightarrow X$ spectra was straightforward from measured vibrational and rotational spacings thanks to accurate ground state potential [1]. The term values of the upper rovibronic levels of the $B^1\Pi$ state giving rise to $B \rightarrow X$ LIF were obtained by adding the corresponding ground state level energy to a transition wave number. Uncertainty of measured lines position is 0.1 from spectrum resolution, that is the 0.003 cm^{-1}. Due to the Doppler profile of the absorption transition uncertainty of upper state energy is 0.01 cm^{-1}.

Data covering a large number of adjacent J' were obtained for $v' \in [0; 6]$. Rotational constant $B_{v'}$ has been calculated as dependent on each J'; and $B_{v'}$ values falling out from the smooth behavior indicated the presence of local perturbations. The respective levels were omitted from the fit. Point-wise potential energy curve (PEC) was obtained, describing non-perturbed or weakly perturbed f-levels up to $v' = 4$ with standard deviation (SD) of 0.1 cm^{-1}. Such precision, 10 times worse than experimental uncertainty indicates presence of some perturbations of non-local character. It should be noted that the same PEC describes $v' = 0, 1$ levels included in the fit with SD= 0.005 cm^{-1}. For weakly perturbed levels with $v' = 0$ and 1 included in the fit, the differences between experimental term values and the ones calculated from the PEC does not exceed 0.025 cm^{-1}.

The support from ESF grant Nr. 2009/0223/1DP/1.1.1.2.0/09/APIA/VIAA/008 and the Latvian Science Council grant Nr. 09.1036 is gratefully acknowledged. I. B. is grateful to the ERAF grant Nr. 2010/0202/2DP/2.1.1.2.0/10/APIA/VIAA/013 for support.

References

[1] R. Ferber, I. Klincare, O. Nikolayeva, M. Tamanis, H. Knöckel, E. Tiemann, and A. Pashov, J. Chem. Phys. **128**, 244316 (2008).

Laser spectroscopy of optical transitions in Rb microfabricated-cells

E. Breschi[1], S. Knappe[2], and J. Kitching[2]

[1] *Department of Physics, University of Fribourg, CH-1700 Fribourg, Switzerland*
[2] *Time and Frequency Division, NIST, Boulder Colorado, USA*

Corresponding Author: evelina.breschi@unifr.ch

Precision spectroscopy of microfabricated alkali vapor cells have found applications in compact quantum devices, such as atomic clocks, magnetometers, and gyroscopes [1]. At present, most fabrication techniques for microfabricated-cells rely on the micro-electro-mechanical-systems (MEMS), and in particular on the silicon wafers etching proposed in [2].

In this communication we present an experimental study of the sub-Doppler spectra of the D2 line of Rb confined in microfabricated-cells for application in compact laser stabilization system. We focus our attention on two closely related techniques: saturated absorption spectroscopy (SA) and its variant, based on the detection of the light-induced dichroism, the so-called polarization spectroscopy (PS). We tested the microfabricated SA-spectrometer realized in [3], and we implemented the linear PS-spectrometer proposed in [4], respectively. These experimental configurations are particularly suitable for extreme miniaturization of a device. The microfabricated-cell spectra were compared with a reference glass-cell (cylindrical, diameter and length of 2.5 cm and 8 cm, respectively) at room temperature. Well resolved SA and PS resonances were obtained with a good contrast, and their behaviour as a function of the pump and probe laser intensities, and cell transmission is examined.

The aim of this work is to evaluate the potential of microfabricated-cell for laser stabilization with respect to centimeter-size glass-blown cells. As a comparison we have performed a heterodyne beat of two independently stabilized diode lasers. The reference laser was stabilized to the crossover transition 23-21 of a saturation absorption spectrum in centimeter-size cell. The preliminary measurements of the signal-to-noise ratio and of the Allan deviation for the transition SA22-23 and PS22-23 will be discussed. Further work is in progress to investigate the potentiality of this approach.

References

[1] S. Knappe, MEMS Atomic Clocks (Elsevier 572–605, 2008).
[2] J. Kitching, S. Knappe, L. Hollberg, Appl. Phys. Lett. **81**, 553–553 (2002).
[3] S. Knappe, H. G. Robinson, and L. Hollberg, Optics Express **15**, 6293–6299 (2007).
[4] D. Grosswasser, A. Waxmann, M. Givon, *et al.*, Rev. Scient. Instrum. **80**, 093103 (2009).

High-resolution KMM radiative Auger x-ray spectra of calcium induced by synchrotron radiation

W. Cao[1,2], M. Berset[1], K. Bučar[3], M. Budnar[3], J.–Cl. Dousse[1], K. Fennane[1], J. Hoszowska[1], M. Kavčič[3], Y.–P. Maillard[1], J. Szlachetko[4,5], M. Szlachetko[1], and M. Žitnik[3]

[1] *Department of Physics, University of Fribourg, CH-1700 Fribourg, Switzerland*
[2] *Department of Chemistry, University of Saskatchewan, Saskatoon, S7N 5C9 SK, Canada*
[3] *J. Stefan Institute, P.O. Box 3000, SI-1001 Ljubljana, Slovenia*
[4] *Swiss Light Source SLS, Paul Scherrer Institute, CH-5232 Villigen, Switzerland*
[5] *Institute of Physics, Jan Kochanowski University, 25-406 Kielce, Poland*

Corresponding Author: jean-claude.dousse@unifr.ch

The radiative Auger effect (RAE) is an exotic decay channel of atomic inner-shell vacancies in which a photon and an electron are emitted simultaneously, the transition energy being shared between the two particles. This alternative weak deexcitation channel was predicted already in the 1930s [1] but observed only about 35 years later [2].

Since the RAE transitions are much less intense than their parent diagram x-ray lines and are sitting on the low energy tails of the latter, the RA x-ray spectra are usually measured by means of the wavelength dispersive x-ray spectroscopy technique. To date, experiments based on photoexcitation employing x-ray tubes [3] or charged particle excitation [4] have been carried out. Large discrepancies exist between these few existing experimental data and the available shake-off (up) [5], configuration interaction (CI) [6], DV-X_α [7] and radiative field [8] calculations for the relative intensities as well as for the RA x-ray emission spectral shapes.

In this work, we report on the KMM radiative Auger (RA) x-ray spectra of solid Ca. The target was irradiated with tunable monochromatic synchrotron radiation beams, which allowed us to selectively exclude the contributions to the RA spectral region from other possible processes such as the x-ray resonant Raman scattering or K hypersatellites. Two excitation energies were employed, one in the near K threshold region and the second well above the K absorption edge. The sample x-ray fluorescence was measured by means of high-resolution x-ray spectroscopy using the von Hamos bent crystal spectrometer of Fribourg [9].

The measured overall RA structure of Ca resembles the density of unoccupied s-, p-, and d-states. Due to solid state effects, however, spectral features resulting from the major discrete shake-up transitions could not be resolved. For the total KMM RA to $K\beta_{1,3}$ yield ratio, a value of 0.053(3) was obtained, in fair agreement with the theoretical prediction of 0.056 from [5] but in strong disagreement with the experimental values of 0.016(6) [3] and 0.031(5) [4] obtained in other experiments using for the target excitation the bremsstrahlung of an x-ray tube and a few MeV proton beam, respectively.

References

[1] F. Bloch and P. A. Ross, Phys. Rev. **47**, 884–885 (1935).
[2] T. Åberg and J. Utriainen, Phys. Rev. Lett. **22**, 1346–1348 (1969).
[3] H. R. Verma, J. Phys. B: At. Mol. Opt. Phys. **33**, 3407–3415 (2000).
[4] M. Budnar *et al.*, Nucl. Instrum. Methods Phys. Res. B **63**, 377–383 (1992).
[5] J. H. Scofield, Phys. Rev. A **9**, 1041–1049 (1974).
[6] K. G. Dyall and F. P. Larkins, J. Phys. B **15**, 4103–4112 (1982).
[7] H. Hayashi, N. Watanabe, and Y. Udagawa, J. Phys.: Condens. Matter **8**, 37–46 (2001).
[8] G. B. Baptista, J. Phys. B: At. Mol. Opt. Phys. **34**, 389–404 (2001).
[9] J. Hoszowska *et al.*, Nucl. Instrum. Methods Phys. Res. A **376**, 129–138 (1996).

Laser induced fluorescence spectroscopy of atomic niobium in the wavelength range of 560 nm to 620 nm

A. Er[1], I. K. Öztürk[1], F. Güzelçimen[1], Gö. Başar[1], I. Siddiqui[2], L. Windholz[2], and S. Kröger[3]

[1] *Istanbul University, Faculty of Science, Physics Department, 34134 Vezneciler, Istanbul, Turkey*
[2] *Institut für Experimentalphysik, Techn. Univ. Graz, A-8010 Graz, Petersgasse 16, Austria*
[3] *Hochschule für Technik und Wirtschaft, Wilhelminenhofstraße 75A, 12459 Berlin, Germany*
Corresponding Author: alever82@gmail.com

Laser induced fluorescence spectroscopy was applied to investigate the hyperfine structure of atomic niobium transitions in the wavelength range from 560 nm to 620 nm by using a tunable single-mode cw ring laser with two different dyes, Rhodamine 6G and Kiton Red. Free Nb atoms were produced with a hollow cathode discharge lamp cooled with liquid nitrogen running with a current of about 60 mA in an argon atmosphere of 0.8 mbar.

In total, 48 lines have been investigated. The recorded hyperfine patterns of all lines were fitted with Voigt profile using the program FITTER [1] in order to obtain the magnetic dipole hyperfine constants A of upper and lower levels. For all lines except two, the classification given in [2] was confirmed. A classification program [3] was used to classify the new two lines. The suggested transitions were confirmed by the observed fluorescence wavelengths. At the wavelength 581.9415 nm two lines overlap, which could be recorded separately by use of laser induced fluorescence spectroscopy.

The magnetic dipole hyperfine structure constants A determined in this work are compared with reference values from literature, if available ([4,5] and references therein). Results will be presented for 33 levels of odd parity and five levels of even parity. For eight levels the A constant was determined for the first time.

HRS

References

[1] G. Guthöhrlein, Universität der Bundeswehr Hamburg, unpublished (2004).
[2] C. I. Humphreys, W. F. Meggers, J. Res. Natl Bur. Stand. **34**, 478 (1945).
[3] L. Windholz, G. H. Guthöhrlein, Physica Scripta **T105**, 55 (2003).
[4] S. Kröger *et al.*, Astron. Astrophy. **516**, A70 (2010).
[5] A. Er *et al.*, in preparation.

Creation of dark states in the Autler-Townes spectrum of Na hyperfine levels

T. Kirova[1], N. N. Bezuglov[2], A. Ekers[3], M. Auzinsh[3], K. Blushs[3], and I. I. Ryabtsev[4]

[1] *National Institute for Theoretical Physics, 7600 Stellenbosch, South Africa*
[2] *Faculty of Physics, St. Petersburg State University, 198904 St. Petersburg, Russia*
[3] *Laser Centre, University of Latvia, LV-1002 Riga, Latvia*
[4] *Institute of Semiconductor Physics, 630090 Novosibirsk, Russia*

Corresponding Author: kirova@sun.ac.za

We study the formation of laser-dressed states in a system of atomic levels which include hyperfine structure. Different three-level ladder excitation schemes in Na coupled by a weak probe laser field in the first- and a strong coupling laser field in the second step are considered. Numerical simulations show that the Autler-Townes (AT) [1] spectra are radically different in the two cases, when the number of hyperfine levels of the strongly coupled states is the same or different: in the former case the M_F Zeeman sublevels are fully resolved, while in the latter case some peaks except the outermost ones vanish at strong coupling.

These results are confirmed by applying two theoretical models based on solving Shrödinger's equation for the time evolution of the probability amplitudes in the atomic wavefunction, as well as the optical Bloch equations (OBE's) [2].

Our observations can be explained by the creations of multiple dark states in a multilevel system coupled by a strong field. Experimental study of the above effects is underway.

This work was supported by EU FP6 TOK project LAMOL, European Social Fund, and Latvian Science Council. I. I. R. acknowledges support from RFBR grant No. 08-02-00220 and N. N. Bezuglov thanks the RFBR.

References

[1] S. H. Autler and C. H. Townes, Phys. Rev. **100**, 703–722 (1955).
[2] M. Auzinsh *et al.*, Opt. Commun. **264**, 333–341 (2006).

Precise measurement of the collisional shift of Cs clock frequency in presence of N_2, Ne, and Ar buffer gases

O. Kozlova[1], S. Guérandel[1], and E. De Clercq[1]

[1] *Laboratoire National d'Essai — Systèmes de Référence Temps — Espace, Observatoire de Paris, CNRS, Université Pierre et Marie Curie, Paris, France*

Corresponding Author: olga.kozlova@obspm.fr, emeric.declercq@obspm.fr

For vapour cell clocks it is a usual technique to add buffer gas in the alkali vapor cell in order to increase the interaction time by reducing the effect of wall collisions and in order to reduce the Doppler width by Dicke effect. However the collisions between alkali atoms and the buffer gas can shift the frequency of the resonance by several kHz per torr, and this shift is temperature dependent [1]: $\Delta\nu(T) = P_0\left[\beta + \delta(T - T_0) + \gamma(T - T_0)^2\right]$, where T is the cell temperature, P_0 is the buffer gas pressure in the cell at the reference temperature $T_0 = 273$K, β (Hz/torr), δ (Hz/(torr·K)), γ (Hz/(torr·K)^2) are experimental coefficients.

Using a mixture of gases having opposite signs of the temperature dependence, one can cancel the temperature sensitivity at the working temperature and, thus, improve the clocks stability. Another possibility to cancel the temperature dependence using only one buffer gas is to work around the inversion temperature (for the buffer gases showing strong quadratic temperature dependence).

Here we report on the precise measurement of the coefficients using pulsed CPT clocks [2], which provide a better frequency uncertainty that previous measurement in Cs [3, 4]. For the first time quadratic coefficient γ for N_2 and Ne buffer gases were measured, for Ar this coefficient is too small and we give its upper estimation (Table 1). From the obtained coefficient values we can predict the mixture composition to cancel the temperature dependence near chosen temperature. The inversion temperatures predicted by the mixture compositions were experimentally confirmed for the series of the different N_2-Ar mixture cells (Fig. 1).

The Ne buffer gas shows strong quadratic temperature dependence and the temperature shift vanishes around $(80 \pm 3)\,^\circ$C, which is promising for future miniature atomic clocks with mm-size cell, because it makes possible to use a single buffer gas.

This work was supported by DGA.

Gas	β Hz/torr	δ Hz/torr·K	γ mHz/(torr·K)^2
Ne	721.8 ± 15.0	0.279 ± 0.007	-1.75 ± 0.05
N_2	922.5 ± 4.8	0.824 ± 0.006	-2.51 ± 0.03
Ar	-195.8 ± 1.6	-1.138 ± 0.010	0.0 ± 0.3

Table 1: *Measured pressure and temperature coefficients of collisional shift of Cs clock frequency.*

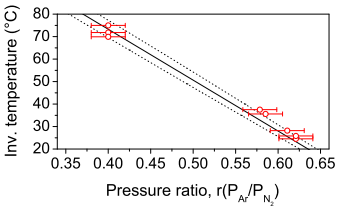

Figure 1: *Inversion temperature versus N_2-Ar mixture composition (black – predicted, red – measured).*

References

[1] J. Vanier and C. Audoin *The quantum physics of atomic frequency standards*, (IOP Publishing, Bristol and Philadelphia, 1989).

[2] T. Zanon *et al.*, Phys. Rev. Lett., **94**, 193002 (2005).

[3] F. Strumia, N. Beverini, A. Moretti, in *Proc. of the 30th Annual Symposium on Frequency Control*, Atlantic City, NJ, 468–472 (1976).

[4] O. Kozlova *et al.*, in *Proc. Of the joint meeting EFTF-IFCS 2009*, Besançon, France (2009).

Laser-induced line narrowing of the coherent population trapping resonance: experiment and theory

O. Kozlova[1], A. Litvinov[2], G. Kazakov[2], B. Matisov[2], R. Boudot[3], S. Guérandel[4], and E. De Clercq[4]

[1] *LNE-SYRTE, Observatoire de Paris, CNRS, UPMC, Paris, France*
[2] *Theoretical physics department, St. Petersburg State Polytechnical University, St. Petersburg, Russia*
[3] *Institut FEMTO-ST, T/F Dept, ENSMM, Besançon, France*
[4] *LNE-SYRTE, Observatoire de Paris, CNRS, UPMC, Paris, France*

Corresponding Author: olga.kozlova@obspm.fr

The coherent population trapping (CPT) phenomenon [1] has been widely investigated in view of application in quantum frequency standards and magnetometers, high-resolution spectroscopy, laser cooling, etc. Owing to very interesting opportunities for application in compact atomic clocks and magnetometers, the shape of CPT resonance and its width in cm- and mm-size cells (containing buffer gas or wall coating) has been studied experimentally and theoretically by several groups [2,3]. In [3] for the first time the idea of a using of laser-induced line narrowing (LILN) effect of the CPT resonance as the base for the development of compact atomic frequency standards was presented. The LILN can be realized only in the case of the CPT excitation of the atomic systems in the sealed cells by "narrow-band" laser. Such quantum frequency standard does not require any antirelaxation wall coating or additional buffer gas in the cell. In this work we theoretically and experimentally study the LILN of the CPT resonance in ^{133}Cs atomic vapors in cm- and mm-size cells without buffer gas and antirelaxation coating.

For the theoretical investigation we take into account both hyperfine and Zeeman structures of the ground and the excited states of ^{133}Cs atoms as well as the probabilities of spontaneous transitions. We theoretically study the dependence of different parameters (such as the length of the cell, the polarization and the intensity of the laser field, the laser linewidth) on the CPT resonance shape. For the case of LILN effect the multifactor optimization for achievement high figure of merit of the CPT resonance was done. We find the optimal parameters for the CPT excitation such as intensity and polarization of the laser fields, magnetic field, and the temperature of the cell.

In the experimental part of the work we present the confirmation of this predicted effect which appears in the case of a narrow-band laser excitation (laser spectral width is less than spontaneous decay of the excited state ~ 5 MHz). The LILN effect was observed in mm-size cell as well in cm-size cell in case of "narrow band" excitation by two different lasers with spectral width 100 kHz and 1 MHz, respectively. In case of mm-size cell the effect LILN is more important, allowing the CPT resonance width of order of several kHz without any buffer gas or coating.

The application of LILN effect in compact atomic clocks will simplify the cell production process (no buffer gas or coating) and thus reduce the cost of the device. We emphasize that the obtained results are of interest for the development of the mm-size magnetometer which allows the accurate measurement of the small magnetic fields with space resolution in some millimeters.

This work was supported by Federal Special-purpose Program "Science and Science-pedagogical personnel of Innovation Russia on 2009-2013" (contract *N°* П2326 from 16.11.2009), by Russian President Grant for Young Candidates of Sciences (project MK-5318.2010.2).

The work of O. K. is supported by DGA. The mm-size cells have been manufactured by FEMTO-ST in the frame of the ANR MHAST contract.

References

[1] G. Alzetta, *et al.*, Nuovo Cimento B, **36B-2-1**, (1976).
[2] S. Brandt, *et al.*, Phys. Rev. A, **56–2** R1063 (1997).
[3] G. Kazakov, B. Matisov, A. Litvinov, I. Mazets, J. Phys. B **40**, 3851 (2007).

Novel study of the $A^1\Sigma^+ \sim b^3\Pi$ complex in KCs and refinement of deperturbation analysis

A. Kruzins[1], I. Klincare[1], O. Nikolayeva[1], M. Tamanis[1], R. Ferber[1], E. A. Pazyuk[2], and A. V. Stolyarov[2]

[1] *Laser Center, Department of Physics, University of Latvia, 19 Rainis blvd, Riga LV-1586, Latvia*
[2] *Department of Chemistry, Moscow State University, 119991, GSP-2, Moscow, Leninskie gory 1/3, Russia*

Corresponding Author: artis.kruzins@fizmati.lv

Experiment-based information on the potential energy curves of the lowest excited $A^1\Sigma^+$ and $b^3\Pi$ states mixed by strong spin-orbit interaction in heavy alkali diatomic molecules is of great importance due to the possibility of their usage as intermediate states for transferring the vibrationally excited cooled molecules into the absolute rovibronic ground state $X^1\Sigma^+(v_X = 0, J_X = 0)$. Recently a high resolution spectroscopy study of the $A^1\Sigma^+ \sim b^3\Pi$ complex in KCs was reported [1,2]. About half of the potential wells of these states was non-uniformly covered by the experiment and powerful deperturbation model was elaborated. The model reproduced observed term values (about 3400) with experimental accuracy. An upper part of potential energy curves coming closer to dissociation limit is most interesting for cold species production. We will present new results obtained exploiting direct excitation of the $A \sim b$ complex aimed to reach higher energy region. Besides it appeared promising to use laser-induced fluorescence (LIF) to $A \sim b$ complex detection in the IR region from higher lying electronic states, among them the $E(4)^1\Sigma^+$ state which was recently studied in details [3]. In doing so, it was necessary to simulate transition probabilities in order to select proper $X \to E \to (A \sim b)$ path.

One of the tasks was to predict and realize transitions to the bottom part of the $b^3\Pi$ state. This was performed both by direct excitations [2] and using LIF from the upper states, such as $(4)^1\Sigma^+$ and $B^1\Pi$ states, which exhibit a considerable mixing with triplet states. As a result of the present study, the $A \sim b$ complex data massive will be considerably enlarged, which will allow us to refine the deperturbation analysis and construct improved deperturbated potential energy curves of $A^1\Sigma^+$ and $b^3\Pi$ states. The work is currently in progress.

Moscow team thanks for support the Russian Foundation for Basic Researches by the grant 10-03-00195a. The support from the Latvian Science Council grant Nr. 09.1036 and from European Social Fund grant 2009/0223/1DP/1.1.1.2.0./09/APIA/VIAA/008 is gratefully acknowledged by Riga team.

References

[1] A. Kruzins *et al.*, Phys. Rev. A **81**, 042509 (2010).
[2] M. Tamanis *et al.*, Phys. Rev. A **82**, 032506 (2010).
[3] L. Busevica *et al.*, J. Chem. Phys. **134**, 104307 (2011).

High resolution spectroscopy of chromium atom

A. Krzykowski[1], P. Głowacki[1], and J. Dembczyński[1]

[1] *Chair of Quantum Engineering and Metrology, Faculty of Technical Physics, Poznań University of Technology, Nieszawska 13B, 60-965 Poznań, Poland*

Corresponding Author: andrzej.krzykowski@put.poznan.pl

Recently Dembczyński *et al.* [1] improved the semi-empirical method of description of atomic structure. It proved to be especially efficient in case of elements with open shell 3d. The quality of such description depends on both the number and the precision of the experimental data regarding the hyperfine splittings of atomic levels. On the other hand, the experimental knowledge of the spectrum of chromium atom is not very extensive. Therefore, our research group undertook a systematic study on this element. Investigations were performed on an atomic beam apparatus by the LIF method (laser induced fluorescence) and ABMR-LIRF method (atomic beam magnetic resonance, detected by laser induced resonance fluorescence). The setup of apparatus is described in [2].

Hyperfine structure intervals for levels in the terms $3d^5$ 4s a^5G and $3d^5$ 4s a^5P of the chromium atom were precisely measured with the use of the ABMR-LIRF method. Magnetic dipole hyperfine interaction constants (A) and electric quadrupole (B) constants for the measured electron levels have been determined with the accuracy of few kHz. The high precision of measurements enabled also estimation of octupole coupling constants (C). Applying LIF method hyperfine structure intervals A and B for several high lying energy levels were determined for the first time.

This work was performed within the framework of DS63-029/11.

HRS

References

[1] J. Dembczyński *et al.*, At. Data Nucl. Data Tables **93**, 149–165 (2007).
[2] A. Jarosz *et al.*, J. Phys. B: At. Mol. Opt. Phys. **40**, 2785–2797 (2007).

AC Stark-shift in double resonance and coherent population trapping in wall-coated cells for compact Rb atomic clocks

D. Miletic[1], T. Bandi[1], C. Affolderbach[1], and G. Mileti[1]

[1] *Laboratoire Temps-Fréquence, Université de Neuchâtel, 2000 Neuchâtel, Switzerland*
Corresponding Author: danijela.miletic@unine.ch

One of the main sources of instability in atomic clocks on medium- to long-term time scales is the frequency shift of the exploited clock reference transition due to the light-shift effect (AC Stark shift). It is therefore critical to carefully stabilize laser parameters, and to find an operational scheme for the clock that minimizes the sensitivity of the clock frequency to fluctuations in the laser parameters.

We have performed a comparative study on double resonance (DR) and coherent population trapping (CPT) clock schemes using the same compact atomic resonator, in view of future high-performance Rb vapour-cell atomic clocks. The rubidium atoms are confined in a 14 mm wall-coated cell placed in a magnetron-type microwave cavity. The volume of the total physics package, including two layers of magnetic shielding, is approximately 1 liter. Light from a DFB laser source is frequency-stabilized to the Rb D1 transition (795 nm) and irradiates the atomic vapour inside the wall-coated cell. DR or CPT signals are obtained by injecting the microwave signal either directly into the microwave cavity or into an electro-optical modulator (EOM) for creating a multi-frequency laser spectrum, respectively.

The AC Stark shift resulting from the monochromatic or multi-frequency optical excitation, in different configurations and clock schemes were precisely measured and studied, as a function of laser intensity and frequency. Under typical operating conditions, the intensity light-shift and the frequency light-shift are $5 \times 10^{-11}/\mu$W and 3×10^{-11}/MHz, respectively, and are of comparable value for both DR and CPT.

Acknowledgments: This work was supported by the Swiss National Science Foundation (project 200020_130381) and the European Space Agency (ESA). We thank F. Gruet for his contribution to this work.

Transition probability determination for some LS-forbidden lines in neutral sulfur by branching ratio measurements

A. Bacławski[1], J. Musielok[1]

[1] *Institute of Physics, Opole University, ul. Oleska 48, 45–052 Opole, Poland*
Corresponding Author: musielok@uni.opole.pl

Transition probabilities (A_{ki}) of spectral lines are important quantities for interpretation of spectra observed from laboratory plasmas as well as astrophysical objects. Since sulfur is an abundant element in the universe, the knowledge of accurate transition probabilities of sulfur lines is of great importance. Results of sophisticated calculations of oscillator strengths for neutral sulfur lines, including intersystem transitions, have been recently published by Zatsarinny and Bartschat [1] and by Deb and Hibbert [2]. Also recently, critically evaluated transition probabilities for sulfur atoms and ions have been reported by Podobedova *et al.* [3]. The agreement between results of the two recent calculations [1,2] for allowed transitions is usually better than for intersystem transition. In this contribution we present branching ratio measurements for SI transitions originating from the upper term 4p' ^{3}D. Three quantum transitions to the lower term 4s' ^{3}D^o (allowed lines) and four transitions to the term 3d ^{5}D^o (LS-forbidden lines) have been studied. The sulfur atoms were excited in a wall-stabilized high-current arc. The radiation emitted from the arc were measured in side-on direction, applying the standard emission spectroscopy method described in detail, e.g., in [4]. Intensities of the selected spectral lines were always measured simultaneously by applying a grating spectrometer with sufficient high spectral resolution and a CCD IR detector. In this way possible uncertainties in relative line intensity measurements are minimized. From directly measured line intensity ratios (forbidden/allowed, I_f/I_a), the corresponding transition probability ratios (A_f/A_a) were evaluated.

In Table 1 the measured data are compared with results of the above mentioned recent calculations [1,2] and with the semiempirical data of Kurucz and Bell [5]. As can be seen the measured A_{ki} ratios agree better with the data of Deb and Hibbert [2].

allowed transition 4s' - 4p'	λ_a (nm)	forbidden transition 3d - 4p'	λ_f (nm)	A_f/A_a this work	Ref. [1]	Ref. [2]	Ref. [5]
$^3D^o_2$–$^3D_3$	963.313	$^5D^o_2$–$^3D_3$	969.160	0.084±0.013	0.078	0.083	0.88
		$^5D^o_3$–$^3D_3$	969.369	6.9±0.4	3.47	3.95	2.78
$^3D^o_3$–$^3D_3$	964.957	$^5D^o_2$–$^3D_3$	969.369	0.23±0.01	0.17	0.23	0.35
$^3D^o_3$–$^3D_2$	969.741	$^5D^o_2$–$^3D_2$	973.987	0.42±0.02	0.36	0.42	1.76
		$^5D^o_3$–$^3D_2$	974.196	0.23±0.01	0.17	0.23	1.11

Table 1: *Experimentally determined transition probability ratios of forbidden and allowed S I lines (A_f/A_a) are compared with ratios taken from calculations.*

HRS

References

[1] O. Zatsarinny and K. Bartschat, J. Phys. B **39**, 2861–2875 (2006).
[2] N. C. Deb and A. Hibbert, At. Data Nucl. Data Tables **94**, 561–602 (2008).
[3] L. I. Podobedova, D. E. Kelleher, and W. L. Wiese, J. Phys. Chem. Ref. Data **38**, 171–439 (2009).
[4] A. Bacławski and J. Musielok, Spectrochim. Acta Part B **63**, 1315–1319 (2008).
[5] R. L. Kurucz and B. Bell, Atomic Line Data Kurucz CD-ROM No. 23 (Cambridge, Mass.: Smithsonian Astrophysical Observatory, 1995).

The x-ray satellites and hypersatellites excited in fast ion-atom collisions

M. Czarnota[1], M. Pajek[1], D. Banaś[1], J.–Cl. Dousse[2], M. Berset[2], O. Mauron[2], Y.–P. Maillard[2], A. Raboud[2], J. Hoszowska[2], M. Polasik[3], K. Słabkowska[3], D. Chmielewska[4], J. Rzadkiewicz[4], and Z. Sujkowski[4]

[1] *Institute of Physics, Jan Kochanowski University, 25-406 Kielce, Poland*
[2] *Department of Physics, University of Fribourg, CH-1700 Fribourg, Switzerland*
[3] *Faculty of Chemistry, Nicholas Copernicus University, 87-100 Toruń, Poland*
[4] *Sołtan Institute for Nuclear Studies, 05-400 Otwock-Świerk, Poland*

Corresponding Author: m.pajek@ujk.kielce.pl

The high-resolution measurements of x-ray satellites and hypersatellites of $L\alpha_{1,2}$ and $L\beta_1$ transitions in multiply ionized atoms give access to study the fine details of a structure of multi-vacancy electronic states. Such measurements are important for testing the atomic structure calculations, in particular, the relativistic multi-configuration Dirac-Fock (MCDF) approach, including the Breit and QED corrections.

The high-resolution measurements of $L\alpha_{1,2}$ and $L\beta_1$ x rays excited by oxygen and neon ions were performed [2] at the Philips cyclotron in the Paul Scherrer Institute (PSI) in Villigen, Switzerland, using O^{6+} and Ne^{6+} ions with energy 278.6 MeV and 177.9 MeV respectively. The excited L-x rays were measured with a high-resolution diffraction von Hamos spectrometer [1] having an instrumental energy resolution and energy calibration of about 0.3 eV.

In order to interpret the observed x-ray satellite and hypersatellite structures the relativistic MCDF calculations [3] were performed for multi-vacancy configurations expected to be excited in collisions with O and Ne ions. To our knowledge, this is the first *systematical* study of the L-shell hypersatellites in ion-atom collisions (see also [4]), which clearly interprets the observed structures in terms of corresponding multi-vacancy configurations.

References

[1] J. Hoszowska *et al.*, Nucl. Instr. and Meth. A **376**, 129 (1996).
[2] M. Czarnota *et al.*, Nucl. Instr. and Meth. B **205**, 133 (2003).
[3] M. Polasik *et al.*, Phys. Rev. A **52**, 227 (1995).
[4] M. Czarnota *et al.*, Phys. Rev. A **81**, 064702 (2010).

High-contrast dark-line atomic resonance of D_1 excitation in nanometric-thin cell filled with rubidium

Y. Pashayan–Leroy[1], C. Leroy[1], A. Sargsyan[2], R. Mirzoyan[2], and D. Sarkisyan[2]

[1] *Laboratoire Interdisciplinaire Carnot de Bourgogne, UMR CNRS 5209 – Université de Bourgogne, F-21078 Dijon Cedex, France*
[2] *Institute for Physical Research, NAS of Armenia, Ashtarak, 0203, Armenia*
Corresponding Author: yevgenya.pashayan-leroy@u-bourgogne.fr

Miniaturization of electromagnetically induced transparency (EIT) setup without loss of resonance characteristics is among the challenges for technological implementation of the EIT. We present the study of EIT on atomic D_1 line of Rb using a nanometric-thin cell (NTC) with atomic vapor column length L in the range of 400–800 nm. It is shown that despite intuitive expectation the reduction of the cell thickness by 4 orders as compared with an ordinary cm-size cell still allows one to form EIT resonance, or so called dark-line atomic resonance (DR) for $L = \lambda = 794$ nm with the contrast of up to 40% (see Fig. 1a), while the best contrast for D_2 line under the same experimental conditions was 5–6% [1]. For DR formation two single-frequency extended cavity diode lasers (forming coupling and probe beams) with $L \approx 794$ nm and 1 MHz linewidth are used. The temperature of the Rb atomic source of the NTC is 140°C. As seen, the velocity selective optical pumping (VSOP) peak demonstrates an increase of the absorption, since the coupling laser transfers a number of atoms from 3 to $2'$, thus increasing the probe absorption for $2 \to 2', 3'$ transitions (also the EIT resonance is superimposed on the VSOP at $2 \to 3'$ transition). The remarkable distinctions of EIT formation in NTC and ordinary cells are demonstrated. Despite the Dicke effect of strong spectral narrowing and increasing of absorption for $L = \lambda/2$, DR is observed both in the absorption and fluorescence spectra. Note, that when the coupling laser is resonant with the corresponding atomic transition DR characteristics weakly depend on L, which allows us to detect DR at the smallest thickness reported up to now, $L = 120$ nm. Figure 1b shows the results of the theory that takes into account the Doppler broadening, non-correlation of the laser fields and the light reflections on the locally highly-parallel NTC's walls behaving as a Fabry-Perot cavity. Note, that although the theoretical model well predicts the high contrast EIT using NTC, however it shows 1.6 times narrower linewidth of the EIT.

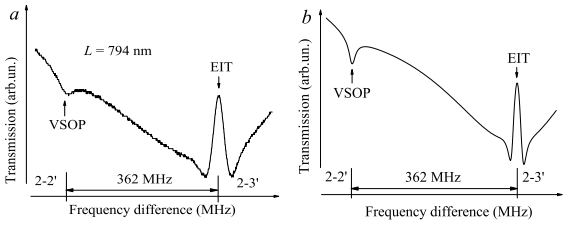

Figure 1: *(a) Experiment:* ^{85}*Rb* D_1 *line, EIT spectrum. The coupling laser is resonant with* $3 \to 3'$ *transition, the probe laser is scanned across* $2 \to 2', 3'$*. NTC thickness is* $L = \lambda = 794$ *nm. (b) Theory: all the parameters are the same as in (a), the Rabi frequencies of the coupling and probe lasers are* 1.5γ *and* 0.1γ*, correspondingly, where* $\gamma = 6$ *MHz.*

Research conducted in the scope of the International Associated Laboratory IRMAS. Ashtarak team thanks for the ANSEF Opt 2428 support. R. M. acknowledges the support from the NF-SAT, NAS RA and CRDF (grant no. ECSP-10-10GRSP).

References

[1] A. Sargsyan, D. Sarkisyan, A. Papoyan, Phys. Rev. A **73**, 033803 (2006).

Theoretical study on the influence of shake process accompanying β^- decay on the structures of x-ray spectra

M. Polasik[1], E. Wiatrowska–Kozioł[1], and K. Kozioł[1]

[1] *Faculty of Chemistry, Nicolaus Copernicus University, 87-100 Toruń, Poland*
Corresponding Author: mpolasik@uni.torun.pl

The structures of the K x-ray spectra originating from the de-excitation of the multi-inner-shell vacancy states created as a result of shake processes accompanying β^- nuclear decay have been studied theoretically for the selected light and medium Z atoms, e.g., boron, carbon, phosphorus, and nickel. Therefore the electron shakeup-plus-shakeoff probabilities as the result of β^- decay have been calculated using multiconfiguration Dirac-Fock wave functions [1] in the sudden approximation model [2]. The diagram and satellites K x-ray transition energies and intensities have been calculated using MCDF-MSAL method [1].

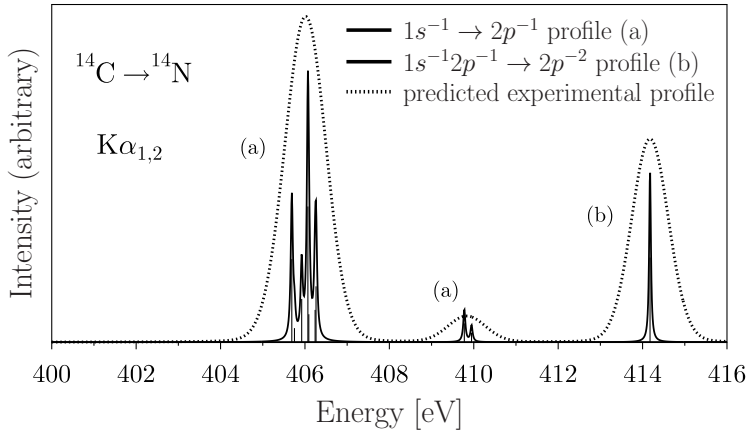

Figure 1: *Predicted $K\alpha_{1,2}$ x-ray diagram and satellites lines shape originating from de-excitation of the K- and L-shell vacancy state in the daughter ^{14}N atom originated from beta-minus decay of ^{14}C. The separation of the satellite line and the diagram line is well visible.*

A comparison of the calculated subshell ionization probabilities for the β^- decay with other theoretical and experimental data available in literature has been also performed. It has been shown that the contributions of the satellite lines are significantly separated from the $K\alpha_{1,2}$ peak for light-Z atoms. In the case of higher-Z atoms the separation of the diagram and satellite lines is not observed and gives no influence on the predicted experimental spectra profile. It is worth to note that the obtained results can be very helpful in interpretation of x-ray spectra accompanying beta-minus decay [3–5].

References

[1] M. Polasik, Phys. Rev. A **58**, 1840 (1998).
[2] T. A. Carlson, C. W. Nestor, T. C. Tucker and F. B. Malik, Phys. Rev. **169**, 27 (1968).
[3] H. H. Hansen, Phys. Rev. C **14**, 281 (1976).
[4] H. H. Hansen and K. Parthasaradhi, Phys. Rev. C **9**, 1143 (1974).
[5] T. A. Carlson, Phys. Rev. **130**, 2361 (1963).

MatLab based modeling of nonlinear interaction of ^{87}Rb atoms with polarized radiation

K. Blagoev[1], G. Todorov[2], V. Domelunksen[3], and V. Polischuk[3]

[1] *Institute of Solid State Physics, Bulgarian Academy of Sciences, 72 Tzarigradsko Chaussee, 1784 Sofia, Bulgaria*
[2] *Institute of Electronics "Acad. Emil Djakov", Bulgarian Academy of Sciences, 72 Tzarigradsko Chaussee, 1784 Sofia, Bulgaria*
[3] *V. A. Fock Physics Institute of University, St. Petersburg State University, 198903, Petergoff, Russia*

Corresponding Author: polisc@vp5233.spb.edu

The ultra-narrow resonances, obtained by means of polarization spectroscopy of alkali atoms, originate from the destruction of the laser-induced coherence in the ground state. In the case of a single frequency, near-resonant excitation and a suitable geometry of irradiation and registration, the well-known ground-state Hanle effect is observed [1]. Coherent population trapping (CPT) [2,3] in Hanle configuration is a nonlinear modification of this effect, observed in the spontaneous emission from the upper level. The ground-state coherence is transmitted from the laser field and as a result higher-rank (k) polarization moments (PMs) are created.

Using the irreducible tensor operator formalism, the basic system of $4(F_f+F_\varphi+1)^2$ equations describing the CPT effect for a chosen transition $F_f \to F_\varphi$ was numerically solved. The numerical calculations take into account the velocity distribution of the atoms, the Gaussian distribution of the laser beam, stray magnetic field and the experimental geometry.

We used Matlab-based programs for numerical modeling of the experimental conditions and the influence of the atomic system parameters on the resonances in the fluorescence. The results of the modeling are compared with the measured ones at different experimental conditions. Conversion of the high rank PMs [4] into observable components is also discussed. Scheme of conversion of the octupole ($k = 3$) and hexadecapole ($k = 4$) PM through the laser and/or magnetic fields into the upper-level quadrupoles f_q^2 is proposed.

HRS

References

[1] E. B. Alexandrov, M. P. Caika, and G. I. Hvostenko, *Interference of atomic states* (Springer-Verlag) (1991).
[2] G. Alzetta, A. Gozzini, L. Moi, G. Orriols, Nuovo Cimento B.**36**, 5–20 (1976).
[3] E. Arimondo, Prog. in Optics, ed. by E. Volf, (Elsevier, Amsterdam) **35**, 257 (1996).
[4] A. I. Okunevich, Optics and Spectroscopy, **91**, 2, 193–204, (2001).

Study of electromagnetically induced transparency in strong magnetic field using Rb nanometric-thin cell

A. Sargsyan[1], R. Mirzoyan[1], A. Papoyan[1], D. Sarkisyan[1], Y. Pashayan–Leroy[2], and C. Leroy[2]

[1] *Institute for Physical Research, NAS of Armenia, Ashtarak, 0203, Armenia*
[2] *Laboratoire Interdisciplinaire Carnot de Bourgogne, UMR CNRS 5209 – Université de Bourgogne, F-21078 Dijon Cedex, France*

Corresponding Author: sarmeno@mail.ru

Electromagnetically induced transparency (EIT) resonance of high 40% contrast obtained with nanometric-thin cell (NTC) of the thickness $L = \lambda$ on the Rb D_1 line allows us to study, for the first time, the EIT splitting in a very wide range of magnetic B-fields of $1 - 1400$ G, as opposed to a small-contrast EIT on D_2 line where it was possible to detect the splitting only for $B < 50$ G [1]. Extremely small thickness of NTC is favorable for the use of permanent magnets, which significantly facilitates application of strong magnetic fields. For EIT formation two extended cavity diode lasers (forming the coupling and probe beams) with $\lambda \approx 794$ nm and 1 MHz line-width are used. The coupling is resonant with ^{87}Rb D_1 line, $2 \to 2'$ transition, while the probe is scanned across $1 \to 1', 2'$ transitions (see the inset in Fig. 1).

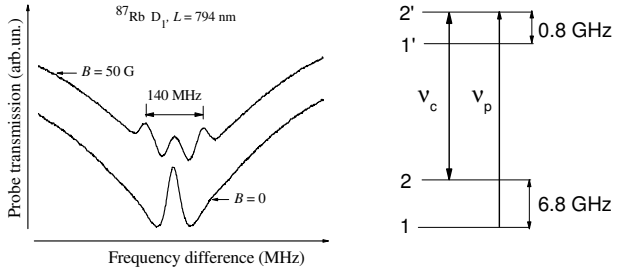

Figure 1: *The upper curve presents three EIT components when a longitudinal magnetic field $B = 50$ G is applied, $L = 794$ nm. The lower curve presents the EIT for $B = 0$. Inset shows the relevant transitions diagram.*

The EIT resonance splitting for $B < 100$ G provides 5-fold better spectral resolution as compared with that obtained in [2]. The case of $B = 50$ G and the NTC temperature 120°C is shown in Fig. 1. The coupling and the probe powers are 5 mW and 0.1 mW, correspondingly. Although in the case of strong B-field 6 EIT components are expected to exist, however for $B > 700$ G only two EIT components are detected. For the first EIT component formation (shifted at $B = 1300$ G by ~ 0.9 GHz to the high-frequency region) two ground states $|2, m_F = 0\rangle$ and $|2', m_F = 0\rangle$ are involved, while for the second EIT component (shifted at $B = 1300$ G by ~ 0.9 GHz to the low-frequency region) the involved ground states are $|2, m_F = -1\rangle$ and $|2', m_F = -1\rangle$. Well resolved EIT components can be used for magnetometry with local nanometric spatial resolution.

Research conducted in the scope of the International Associated Laboratory IRMAS. A. S. thanks ANSEF Opt 2428 support. R. M. thanks the support from the NFSAT/ CRDF (grant ECSP-10-10GRSP).

References

[1] A. Sargsyan, D. Sarkisyan, A. Papoyan, Phys. Rev. A **73**, 033803 (2006).
[2] A. Sargsyan *et al.*, Appl. Phys. Lett. **93**, 021119 (2008).

Theoretical decomposition of the satellite $L\gamma$ x-ray lines spectra of thorium

K. Słabkowska[1], J. Starosta[1], M. Polasik[1], M. Czarnota[2], M. Pajek[2], J.–Cl. Dousse[3], and J. Hoszowska[3]

[1] *Faculty of Chemistry, Nicolaus Copernicus University, 87-100 Toruń, Poland*
[2] *Institute of Physics, Jan Kochanowski University, 25-406 Kielce, Poland*
[3] *Department of Physics, University of Fribourg, CH-1700 Fribourg, Switzerland*
Corresponding Author: katarzyna.slabkowska@uni.torun.pl

The multiple ionization of various shells of target atoms in collisions with heavy ions makes the origin of observed K-, L-, and M-x-ray lines very complex. Therefore, the results of theoretical study [1,2] on the ionization effect of various shells on the positions and shapes of particular x-ray lines are essential for reliable interpretation of the measured x-ray spectra. The profound importance of such theoretical research has been revealed in numerous cases of the thorough analysis of observed K-, L-, and M-x-ray lines [3,4].

In this study, the line shapes of the $L\gamma_1$ (L_2N_4), $L\gamma_2$ (L_1N_2), $L\gamma_3$ (L_1N_3) and $L\gamma_6$ (L_2O_4) diagram and satellite x-ray transitions of thorium have been calculated using the extensive multiconfiguration Dirac-Fock (MCDF) method [1]. In Fig. 1 we have presented the preliminary results of the decomposition of experimental $L\gamma$ x-ray spectrum of thorium [5] on the contributions corresponding to the MCDF predictions for particular hole configurations. As already shown for thorium, these x-ray spectra are indeed very complex and their reliable analysis is only tractable if MCDF calculations as the ones presented here are available.

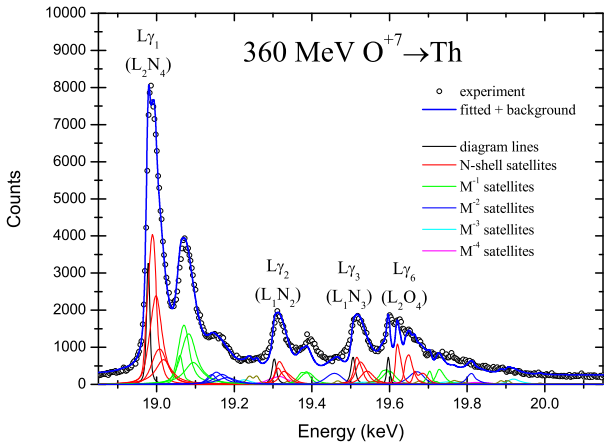

Figure 1: *The decomposition of experimental $L\gamma$ x-ray spectrum of thorium on the MCDF contributions for particular hole configurations.*

HRS

References

[1] M. Polasik, Phys. Rev. A **52**, 227 (1995).
[2] M. Polasik, K. Słabkowska, Radiat. Phys. Chem. **75**, 1497 (2006).
[3] M. Czarnota *et al.*, Nucl. Instr. and Meth. in Phys. Res. B **205**, 133 (2003).
[4] M. Czarnota *et al.*, Radiat. Phys. Chem. **68**, 121 (2003).
[5] M. Pajek *et al.*, Phys. Scripta T**92**, 382–384 (2001).

Influence of open-shell effect on double K-shell hole states radiative de-excitation parameters

K. Słabkowska[1], K. Kozioł[1], M. Polasik[1], and E. Wiatrowska–Kozioł[1]

[1] *Faculty of Chemistry, Nicolaus Copernicus University, 87-100 Toruń, Poland*
Corresponding Author: katarzyna.slabkowska@uni.torun.pl

In order to explanation of $K^h\alpha_{1,2}$ x-ray hypersatellite lines parameters and radiative natural widths of K^{-2} levels the multiconfiguration Dirac-Fock calculations [1, 2] have been carried out. It is important to note that in case of open-shell atoms (when deexcitation concerns many states) every state has a specific lifetime and width, and, in consequence, the shapes and natural width of x-ray line strongly depends on open-shell or closed-shell configurations type (see Fig. 1).

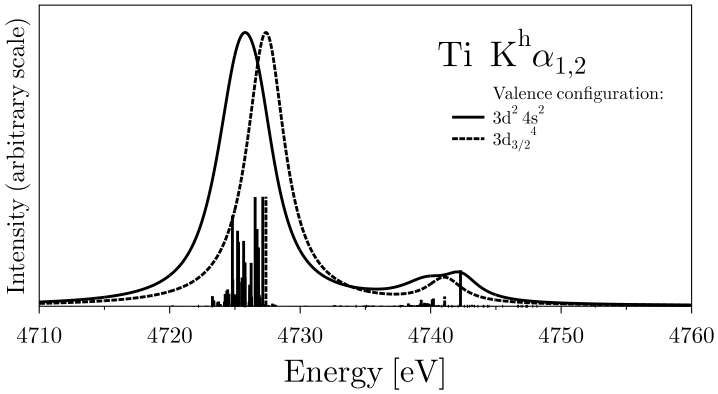

Figure 1: *Predicted $K^h\alpha_{1,2}$ shapes for two different Ti configurations: $3d^24s^2$ (open shell) and $3d^4_{3/2}$ (closed shell).*

Moreover, the influence of Breit and QED corrections on parameters of $K^h\alpha_{1,2}$ x-ray radiative transitions and K^{-2} levels have been considered. It has been found that the Breit and QED corrections cause the differences in particular radiative natural widths of K^{-2} levels for open-shell atomic systems (see Table 1).

Atomic level	Sum of radiative transition rates [$\times 10^{17}$s^{-1}]		Radiative level width [eV]	
	with B+Q	without B+Q	with B+Q	without B+Q
$\|6p^1\rangle_{J=1/2}$	1.722	1.659	113.37	109.19
$\|6p^1\rangle_{J=3/2}$	1.528	1.659	100.56	109.19
average	1.625	1.659	106.97	109.19

Table 1: *The sum of radiative transition rates for de-excited K^{-2} states and radiative width for KK levels calculated with (marked as 'with B+Q') and without (marked as 'without B+Q') Breit and QED corrections.*

References

[1] M. Polasik, Phys. Rev. A **39**, 616 (1989).
[2] M. Polasik, Phys. Rev. A **58**, 1840 (1998).

Photoionization, Photodetachment, Anions

Electron scattering from krypton: high-resolution electron scattering experiments and *B*-spline *R*-matrix calculations

M. Allan[1], O. Zatsarinny[2], and K. Bartschat[2]

[1] *Department of Chemistry, University of Fribourg, CH-1700 Fribourg, Switzerland*
[2] *Department of Physics and Astronomy, Drake University, Des Moines, IA 50311, USA*
Corresponding Author: Michael.Allan@unifr.ch

In a joint experimental and theoretical effort, we carried out a detailed study of elastic scattering and electron impact excitation of the $4p^5 5s$ states in Kr [1]. The incident electron energy resolution was about 13 meV at a current of about 400 pA. A specially designed magnetic angle changer allowed for measurements up to 180° scattering angle. The calculations were performed in a fully relativistic Dirac *B*-spline *R*-matrix (DBSR) framework [2]. We present independently normalized, absolute angle-differential cross sections over the entire angular range ($0° - 180°$) for a number of energies in the near-threshold region, as well as energy scans for selected angles. An example of the latter, for the $5s[3/2]_2$ state measured at 135°, is shown in the figure. The experimental results are seen to be in very satisfactory agreement with predictions from the DBSR model [2,3].

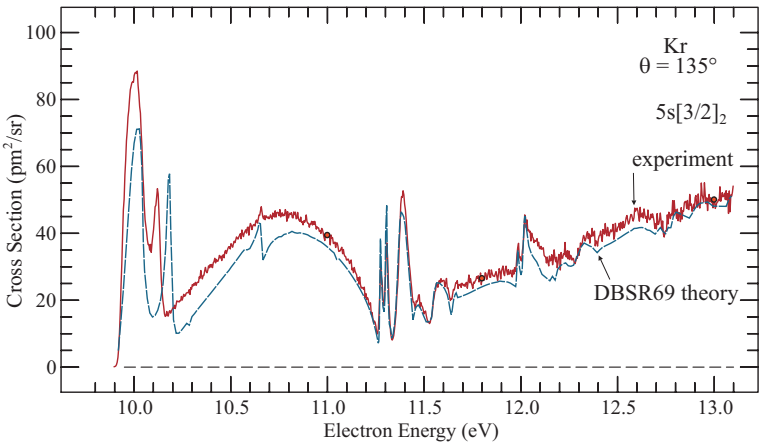

Figure 1: *Cross section for electron-impact excitation of Kr.*

It should be emphasized that the test is very stringent since we compare the absolute values of the cross sections, *i.e.*, the heights of the curves, *and* the many sharp resonances, their energies, widths and heights in the spectrum. The latter indicate that the branching ratios, with which the individual resonances decay into the accessible final excited states, are also correctly described by the theory. The new data also clearly improve the agreement between experiment and theory relative to our earlier comparison [3] with the experimental data of Phillips [4].

References

[1] M. Allan, O. Zatsarinny, and K. Bartschat, J. Phys. B **44**, 065201 (2011).
[2] O. Zatsarinny and K. Bartschat, Phys. Rev. A **77**, 062701 (2008).
[3] T. H. Hoffmann *et al.*, J. Phys. B **43**, 085206 (2010).
[4] J. M. Phillips, J. Phys. B **15**, 4259 (1982).

Electron scattering in $Pt(PF_3)_4$: elastic scattering, vibrational and electronic excitation

M. Allan[1]

[1] *Department of Chemistry, University of Fribourg, CH-1700 Fribourg, Switzerland*
Corresponding Author: Michael.Allan@unifr.ch

The interest in electron interactions with $Pt(PF_3)_4$ is motivated by its use as a platinum precursor for the deposition of nano-sized wires in the method of focused electron beam induced processing (FEBIP) [1]. It has the advantage, over precursors with carbon-containing ligands, of not causing carbon deposits. It is a very remarkable compound, volatile despite its high mass (547 amu!).

Experimental absolute differential cross sections for elastic scattering, vibrational and electronic excitation by low-energy electrons from $Pt(PF_3)_4$ are presented. The electronically excited states are characterized by electron energy-loss spectroscopy. Figure 1 shows a sample energy-loss spectrum with vibrational excitation. Remarkable is the very low frequency Pt−P stretch vibration which can be used to monitor the purity of the sample.

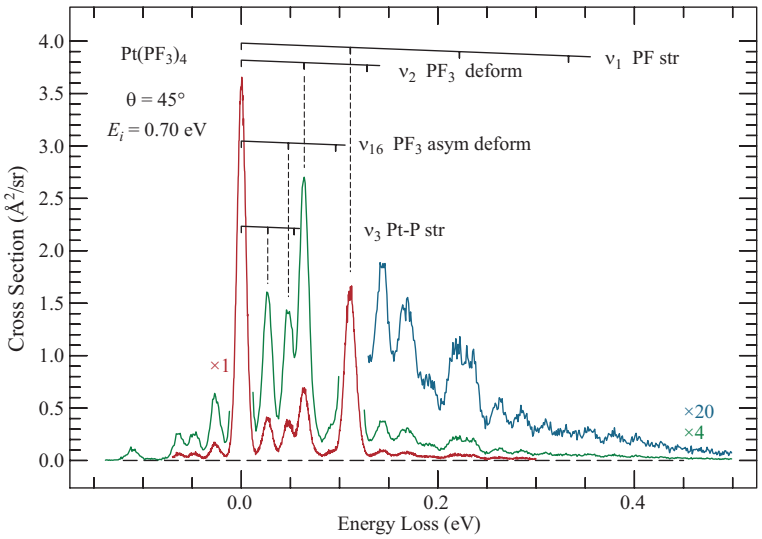

Figure 1: *Electron energy-loss spectrum.*

Vibrational excitation cross sections revealed five shape resonances at 0.84, 1.75, 3.3, 6.6, and 8.5 eV. The elastic cross section has a deep Ramsauer-Townsend minimum around 0.25 eV (at $\theta = 135°$). The angular distributions of the elastic cross section above 6.5 eV show an unusually narrow peak at an angle which decreases with increasing energy (it is at 40° at 20 eV), related to the high (tetrahedral) symmetry.

References

[1] I. Utke, P. Hoffmann, and J. Melngailis, J. Vac. Sci. Technol. B **26**, 1197 (2008).

Absolute angle-differential vibrational excitation cross sections for electron collisions with diacetylene

M. Allan[1], O. May[1], J. Fedor[1], B. C. Ibănescu[1], and L. Andrić[2]

[1] *Department of Chemistry, University of Fribourg, CH-1700 Fribourg, Switzerland*
[2] *CNRS et Laboratoire de Chimie Physique–Matière et Rayonnement, Université Pierre et Marie Curie, F-75231 Paris Cedex 05, France*

Corresponding Author: Michael.Allan@unifr.ch

Electron collisions with diacetylene (1,3-butadiyne, H−C≡C−C≡C−H) are of special interest to astronomers due to the recent discovery of the H−C≡C−C≡C$^-$ anion in interstellar space [1]. We measured absolute cross sections for vibrational excitation by electron impact and for dissociative electron attachment. The selectivity of vibrational excitation reveals detailed information about shape resonances. Excitation of the C≡C stretch and of double quanta of the C−H bend vibrations reveal a $^2\Pi_u$ resonance at 1 eV (autodetachment width about 30 meV) and a $^2\Pi_g$ resonance at 6.2 eV (autodetachment width 1–2 eV). There is a strong preference for excitation of even quanta of the bending vibration. The excitation of the odd and even quanta of the bending vibration have very different angular distributions: the former have a maximum at 90°, the latter a minimum. Excitation of the C−H stretch vibration reveals σ^* resonances at 4.3, 6.8, and 9.8 eV, with autodetachment widths of about 2 eV. The detailed information about resonances permits conclusions about mechanism of dissociative electron attachment [2].

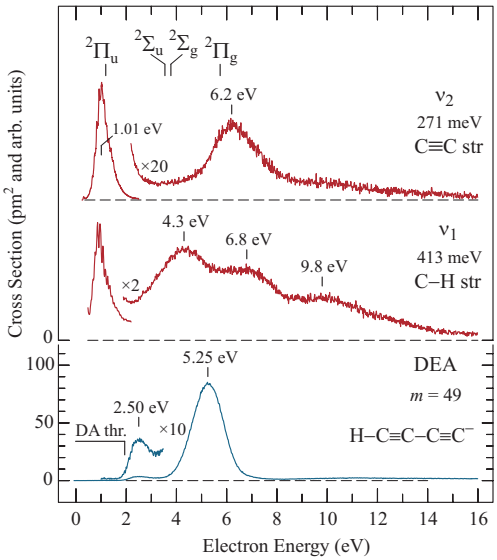

Figure 1: *The top two curves show cross sections for exciting the C−H and C≡C stretch vibrations. The DEA spectrum (loss of H) is shown at the bottom.*

References

[1] J. Cernicharo *et al.*, Astronomy and Astrophysics **467**, L37 (2007).
[2] O. May, J. Fedor, B. C. Ibănescu, and M. Allan, Phys. Rev. A **77**, 040701(R) (2008).

Effects of laser light in a negative ion sputter ion source — sulphur vs. chlorine production

P. Andersson[1], M. Martschini[1], J. Rohlén[2], A. O. Lindahl[2], O. Forstner[1], P. Steier[1], D. Hanstorp[2], and R. Golser[1]

[1] *Fakultät für Physik, Universität Wien, AT-1090 Wien, Austria*
[2] *Department of Physics, University of Gothenburg, SE-412 96 Gothenburg, Sweden*
Corresponding Author: pontus.andersson@univie.ac.at

Accelerated mass spectroscopy (AMS) investigations of ^{36}Cl ($t_{1/2}$ = 0.30 Ma) at natural isotopic concentrations requires high particle energies for the separation from the stable isobar ^{36}S. These energies are usually provided by tandem accelerators with terminal voltages > 5 MV. In recent measurements we have at VERA reached a ^{36}S suppression factor of above 10^4, primary due to the inclusion of a split-anode ionization chamber in combination with a silicon strip detector. In these measurements we have demonstrated that ^{36}Cl analyze at 3 MV terminal voltages can now be competitive to measurements at larger tandems [1,2].

In an effort to further suppress the ^{36}S production during ^{36}Cl measurements, a new method involving optical filtering through a cw high power laser, aimed directly at the cathode in the cesium sputter negative ion source, has been investigated.

The experimental setup implemented on the VERA tandem accelerator is shown and the resulting change in ^{36}S/^{36}Cl detection as an effect of, up to 0.5 W of cw 445 nm light focused on to a ^{36}Cl standard sample during sputtering, is presented.

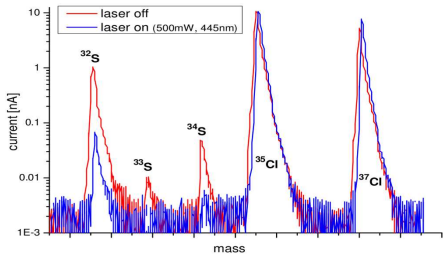

Figure 1: *Mass-spectrum showing the reduction in the sulphur output when the 445 nm laser is applied directly into the source.*

Results from a preceding experiment performed at the negative ion accelerator at the University of Gothenburg are also shown. Figure 1 demonstrates how the mass-spectrum is changed under the influence of the 445 nm laser. With the light present, there is a suppression in the sulphur production and an increase in the chlorine production, resulting in change of more than a factor of 10 in the Cl/S production ratio. A similar change in the Cl/S production ratio was found when light of 1064 nm wavelength was used, ruling out the effect of sulphur photo-detachment. A time constant in the production ratio change after the extinction of the light was also observed.

Some possible mechanisms for explaining these effects are proposed.

Financial support from the Swedish Research Council is acknowledged.

References

[1] P. Steier, O. Forstner, R. Golser, W. Kutschera, M. Martschini, S. Merchel, T. Orlowski, A. Priller, C. Vockenhuber, A. Wallner, Nucl. Instr. and Meas. B, **268** 744–747 (2010).
[2] M. Martschini, O. Forstner, R. Golser, W. Kutschera, S. Pavetich, A. Priller, P. Steier, M. Suter, A. Wallner, *Recent advances in AMS of 36Cl with a 3-MV-tandem*, Accepted for publication in Nucl. Instr. and Meas. B (2011).

Photodetachment microscopy to an excited state and the electron affinity of phosphorus

C. Blondel[1], C. Delsart[1], C. Drag[1], R. J. Peláez[1,2], and M. Vandevraye[1]

[1] *Laboratoire Aimé-Cotton, Centre national de la recherche scientifique, bâtiment 505 Université Paris-sud, F-91405 Orsay cedex, France*

[2] *Present address: Laser Processing Group, Instituto de Optica. CSIC, Madrid, Spain*

Corresponding Author: christophe.blondel@u-psud.fr

Implementation, on the photodetachment microscope, of a cesium sputtering ion source made it possible to study detachment of $^{31}P^-$ ions, just above every accessible fine-structure threshold corresponding to the excitation of the $3s^2 3p^3\ ^2D^o$ doublet. This is about 11 370 cm^{-1} above the $3s^2 3p^3\ ^4S^o_{3/2}$ ground state of atomic phosphorus.

Photodetachment microscopy, however, produces free electron interferograms that can still be analyzed so as to provide a measure of the photoelectron energy with interferometric accuracy. From the five measured thresholds, we have extracted with a good consistency the four independent atomic parameters of the problem, namely the two fine-structure intervals of P^-, the $^2D_{5/2}-^2D_{3/2}$ interval of the neutral, and, e.g., the $^3P_2 \rightarrow ^2D_{3/2}$ (^3P lowest level to ^2D lower level) detachment energy. Photodetachment microscopy, as already noticed for sulfur [1], does not only make it possible to improve the fine-structure spectroscopy of the studied negative ion, it can also give a new insight in the spectroscopy of the parent neutral atom.

Though photodetaching to an excited state obviously gives new possibilities to study anions the binding energy of which lies in the far infrared, electron affinities determined in this way have their accuracy limited by the accuracy of the excited atomic levels. This is exactly what happens with phosphorus, the electron affinity of which appears now limited by the present-state accuracy of the $3s^2 3p^3\ ^2D^o$ excited levels [2]. The result obtained, with a preliminary value of 6 021.8(1) cm^{-1} or 0.74661(2) eV, nevertheless offers a 1/5 reduction of the uncertainty of the electron affinity of P, with respect to the previous measurement at 6 022.35(51) cm^{-1} or 0.74668(6) eV [3]. Final values, with optimized uncertainties, will be given at the conference.

PPA

References

[1] C. Blondel *et al.*, J. Phys. B: At. Mol. Opt. Phys. **39**, 1409–1416 (2006).
[2] N. Svendenius, Physica Scripta **22**, 240–287 (1980).
[3] P. Andersson *et al.*, J. Phys. B: At. Mol. Opt. Phys. **40**, 4097–4107 (2007).

Isotope shifts and hyperfine structures of the $3p^3\ {}^4S^o$, $^2D^o$ and $^2P^o$ multiplets of Si^- and $3p^2\ {}^3P$ term of Si

T. Carette[1], M. R. Godefroid[2]

[1] *Department of Physics, Stockholm University, AlbaNova University Centre, SE-106 91 Stockholm, Sweden*
[2] *Laboratoire de Chimie Quantique et Photophysique, CP160/09, Université Libre de Bruxelles, Brussels, Belgium*

Corresponding Author: thomas.carette@fysik.su.se

Thanks to advances in experimental techniques during the last two decades, the achievable accuracy of negative ion photodetachment threshold measurements allows now to differentiate isotopes [1]. The accessibility of such small effects in negative ions bears promises for new stringent tests of theoretical models. Indeed, the negative ions are not only highly correlated systems, but most of their properties are only known relatively to their counterparts in the neutral system (e.g., the electron affinity is the difference between the total energies of the two systems). Getting reliable isotope shifts (IS) on electron affinities (EA) requires a well-balanced description between the neutral and its negative ion of both valence and core-valence correlation effects. In this regard, the multi-configuration Hartree-Fock (MCHF) variational approach proved to be a valuable tool for characterizing the main contributions to the IS on the EA [2].

Recently, the MCHF method has also been successfully used for obtaining highly accurate wave functions for the bound states arising from the ground configurations of C and C^- [2], the latter being the lightest negative ion with two bound terms ($2p^3\ {}^4S^o$ and $^2D^o$). This study shows, in particular, that up to 99.6% of the correlation energy can be obtained for seven-electron systems using a standard MCHF approach and moderate computer resources. Silicon, the next carbon-group element ($3p^2$), allows three bound terms in its negative ion ($3p^3\ {}^4S^o$, $^2D^o$ and $^2P^o$). Having a relatively large core ($1s^2 2s^2 2p^6$) and few valence electrons (4 and 5), it is a good candidate for testing different core-valence correlation models saturating the (non-trivial) valence correlation.

We perform large scale MCHF calculations on all bound terms of Si^- and on the $3p^2\ {}^3P$ multiplet of Si, testing various ways of including the correlation involving core electrons. We predict an anomalous isotope shift on the electron affinity of $-0.66(6)$ m^{-1} for the $(30-28)$ isotope pair. We calculate the hyperfine structures of the considered multiplets for the isotope 29 of silicon. Our theoretical value for the $A_2(^3P)$ hyperfine constant of ^{29}Si is in good agreement with the only available observation [4]. We also report the b_q electric field gradients at the nucleus that could be of interest in a study of the unstable silicon isotopes.

References

[1] W. Chaibi *et al.*, Eur. Phys. J. D **58**, 29–37 (2010), and references therein.
[2] T. Carette *et al.*, Phys. Rev. A **81**, 042522 (2010).
[3] T. Carette and M. R. Godefroid, arXiv:1101.5318v1 (2011), Phys. Rev. A (in press).
[4] S. A. Lee and W. M. Fairbank, Phys. Rev. A **82**, 042515 (2010).

Anomalous Rayleigh scattering of x rays and photoeffect by inner shell electrons

A. Costescu[1], K. Karim[2], M. Moldovan[2], S. Spanulescu[3], and C. Stoica[1]

[1] *Department of Physics, University of Bucharest, 077125 Bucharest, Romania*
[2] *Department of Physics, UMF Targu Mures, 540142 Targu Mures, Romania*
[3] *Department of Physics, Hyperion University of Bucharest, 030629 Bucharest, Romania*
Corresponding Author: a_costescu@hotmail.com

Rayleigh scattering by 2s bound electrons in neutral and partially ionized atoms is studied using the Green function method, including retardation, multipoles, relativistic kinematics, and screening effects. The aim of the paper is to obtain simple formulas for the anomalous scattering coefficients, valid in a large energy range, from few hundred eV up to the x-ray and gamma-ray regime. As in the case of 1s electrons, the spurious singularities introduced by the retardation in a nonrelativistic approach are canceled by the relativistic kinematics terms [1]. However, for energies under the photoionization threshold, special care has to be taken for obtaining convenient analytical expressions by properly handling the Appell functions involved, in order to get a higher numerical precision. For the neutral and ionized atoms case, a screening model based on a nonrelativistic Hartree-Fock central field method has been used [3]. Starting from the S-matrix element for the elastic scattering photons by 2s electrons we finally get the useful formula for the total photoeffect cross-section in the right nonrelativistic limit:

$$\sigma_{2s}^{ph} = \frac{4}{3}\pi^2 r_0^2 \alpha^5 Z^6 \frac{m^3}{\omega^3}\frac{\Omega_1}{\omega}\left(1+\frac{3}{8}\alpha^2 Z^2\frac{m}{\omega}\right)\left(1-\frac{32}{5}\frac{\omega_{2s}}{\omega}\frac{\omega_{2s}}{m}\right)\frac{e^{-|\tau_1|[\pi+\chi_{2s}(\omega)]}}{1-e^{-2\pi|\tau_1|}} \quad (1)$$

A comparison of the numerical results generated by these formulas with the results of full relativistic calculus [4,5] has been made and in most cases a very good agreement (within few percents) has been found. This allowed us to obtain the total photoeffect cross section and direct radiative recombination cross section for the 2s electrons with a good precision also. For a given hot plasma velocity distribution, fairly good results may be obtained for average recombination rate and average power loss due to direct radiative recombination.

PPA

References

[1] A. Costescu, S. Spanulescu, Phys. Rev. A **73**, 022702 (2006).
[2] A. Costescu, S. Spanulescu and C. Stoica, J. Phys. B: At. Mol. Opt. Phys **40**, 2995 (2007).
[3] A. Costescu, S. Spanulescu and C. Stoica, J. Phys. B: At. Mol. Opt. Phys **44**, 045204 (2011).
[4] L. Kissell http://adg.llnl.gov/Research/scattering.
[5] J. H. Scofield, Lawrence Radiation Laboratory Report No. CRL 51326 (Livermore, CA) (1973, unpublished).

Multiphoton excitation and AC-shift of autoionizing states of Mg probed by monitoring the Mg^+ 3p→3s radiative decay

A. Dimitriou[1], I. Liontos[2], S. Cohen[1], and A. Lyras[1]

[1] *Department of Physics, University of Ioannina, 45110 Ioannina, Greece*
[2] *LENS Institute, via Nello Carrara 1, I-50019, Sesto Fiorentino, Florence, Italy*
Corresponding Author: tasosdimitriu@yahoo.gr

Recently, experiments on single and double ionization of ground state alkaline earth atoms in the proximity of four-photon excitation of the $mp^2\ ^1S_0$ autoionizing states (Mg–m= 3 [1], Ca–m= 4 [2], Sr–m= 5 [3]) were performed with laser pulses of ns duration and low laser intensity ($I<10^{12}$ W/cm^2). Those studies showed the unexpected absorption of a number of photons in excess of the minimum one required for ionization above the first ms threshold. This fact was attributed to the strong light-induced interaction between $mp^2\ ^1S_0$ states with other bound and autoionizing states resulting to the production of singly charged ions in excited states. The populations of the latter were then probed by detecting the fluorescence emitted during their radiative decay. Particularly for Mg, fluorescence ($\sim$ 280 nm) emitted from the Mg^+ 3p→3s transition was observed. Theoretical calculations explained the large red shift of the $3p^2\ ^1S_0$ state to a non-perturbative AC-Stark interaction with the bound 3s4p $^1P_1$ level (third photon from the ground state) and the 3p3d $^1P_1$ autoionizing state (fifth photon)[1]. In the present study we use the same method (see Fig. 1) for characterizing that interaction in more detail and we largely extend the examined wavelength range towards the blue side of the $3p^2\ ^1S_0$ resonance. Specifically, the new data cover the (zero-field) direct five-photon excitation of the ground state to the 3p3d $^1P_1$ level as well as to the even higher lying 3p5s $^1P_1$ one (that has not been included within the previous [2] theoretical model). The pronounced (blue) shifts exhibited by those resonances as well as of an additional (presently unidentified) one with increasing laser intensity will be presented and discussed.

PPA

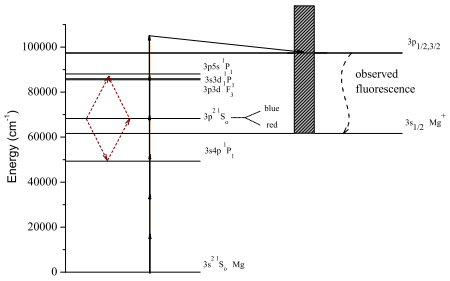

Figure 1: *Energy level diagram of Mg.*

Acknowledgments: The experiment was performed at the Central Laser Facility of the University of Ioannina. The research Project is co-funded by the European Union – European Social Fund (ESF) & National Sources, in the framework of the program "HRAKLEITOS II" of the "Operational Program Education and Life Long Learning" of the Hellenic Ministry of Education, Life Long Learning and religious affairs.

References

[1] I. Liontos, A. Bolovinos, S. Cohen, and A. Lyras, Phys. Rev. A **70**, 033403 (2004).
[2] I. Liontos, S. Cohen and A. Lyras, J. Phys. B: At. Mol. Opt. Phys **43**, 095606 (2010).
[3] I. Liontos, S. Cohen, and A. Bolovinos, J. Phys. B **41**, 2693 (2008).

Core level spectroscopy and tautomerism of cytosine derivatives in the gas phase

V. Feyer[1], O. Plekan[2], A. Kivimaki[3], K. C. Prince[1], T. E. Moskovskaya[4], I. L. Zaytseva[4], D. Yu. Soshnikov[4], and A. B. Trofimov[4]

[1] *Sincrotrone Trieste, in Area Science Park, I-34149 Basovizza (Trieste), Italy*
[2] *Department of Physics and Astronomy, Aarhus University, Ny Munkegade 120, 8000, Aarhus C, Denmark*
[3] *Laboratorio TASC, IOM-CNR, Basovizza (Trieste), I-34149, Italy*
[4] *Laboratory of Quantum Chemistry, Irkutsk State University, 664003 Irkutsk, Russia*
Corresponding Author: vitaliy.feyer@elettra.trieste.it

Tautomers of DNA bases can cause genetic mutations by pairing incorrectly with wrong complementary bases, and these mutations can be the precursors to some molecular based diseases. Therefore, the tautomerism of cytosine and its biologically active modifications has been the subject of a great number of theoretical and experimental investigations due to their biochemical significance. Low energy spectroscopies such as microwave, laser and infrared techniques are commonly used as methods to investigate the conformational and tautomeric equilibria of biomolecules, while the high energy technique of x-ray photoemission spectroscopy has yielded a smaller amount of significant structural information about biomolecules in the gas phase. In the present studies we successfully apply x-ray photoemission spectroscopy to the study of tautomers of cytosine derivatives see Fig. 1.

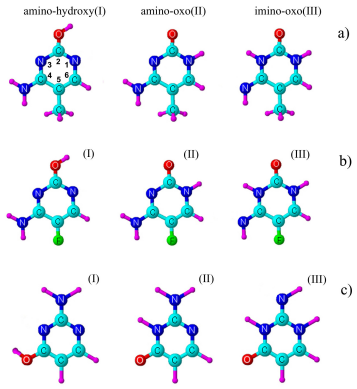

Figure 1: *Chemical structures of the a) 5-methylcytosine, b) 5-fluorocytosine and c) isocytosine.*

The effects of the methylation, halogenation and isomerism on the relative stabilities of cytosine tautomers can be clearly seen in the spectroscopic results and they are further confirmed by the calculations. By comparison with cytosine data [1] we may conclude that the methylation of C5 carbon atoms changes significantly the imino-oxo versus amino-oxo tautomeric equilibrium. In 5-methylcytosine these tautomers are present with nearly the same population, while in the case of cytosine the concentration of the amino-oxo form was higher by a factor two. The substitution of hydrogen by fluorine on the C5 position leads to a strong dominance of the hydroxy tautomer. The spectra of isocytosine show the co-existence of the two tautomeric forms amino-oxo and amino-hydroxy, with the amino-oxo form less stable by 2.07 kcal/mol at 425K. The advantage of Y photoemission spectroscopy compared with low energy spectroscopy for thermally evaporated compounds is that the core level photoemission intensities well above threshold are directly proportional to the population of the corresponding chemical state, and in addition the sample is in thermal equilibrium.

References

[1] V. Feyer, O. Plekan, R. Richter, M. Coreno, *et al.*, J. Phys. Chem. A. **113**, 5736 (2009).

Saddle-point "smiles" in electron detachment by few-cycle laser pulses

M. C. Smyth[1], S. F. Shearer[1], and G. F. Gribakin[1]

[1] *School of Mathematics and Physics, Queen's University Belfast, Belfast BT7 1NN, UK*
Corresponding Author: g.gribakin@qub.ac.uk

In this work we examine the positions of the saddle points in the complex time plane and their contributions to the photoelectron spectra for different intensities and carrier-envelope phases.

Strong-field ionization by few-cycle laser pulses is a powerful tool for studying laser-matter interaction with unprecedented time resolution. Analytical approaches such as the Keldysh-type theory of Gribakin and Kuchiev [1] have proved to be very useful in providing insights and describing quantitatively the effects of multiphoton detachment from negative ions.

The aim of the present work is to extend the approach of [1] to electron detachment from negative ions by few-cycle linearly polarized laser pulses. For a long periodic pulse of frequency ω, the transition amplitude is calculated over one period $T = 2\pi/\omega$ and is given by two saddle points in the complex time plane. Application of the saddle-point method to the amplitude for a laser pulse with N optical cycles [e.g., of the form $\mathbf{A}(t) \propto \sin^2(\omega t/2N)\sin(\omega t + \alpha)$] produces $2(N+1)$ saddle points in complex time, which form a characteristic "smile" (see Fig. 1). Numerical calculations are performed for H^- in a 5-cycle pulse with frequency 0.0043 a.u. and intensities of 10^{10}, 5×10^{10}, and 10^{11} W/cm^2, and varying the carrier-envelope phase α.

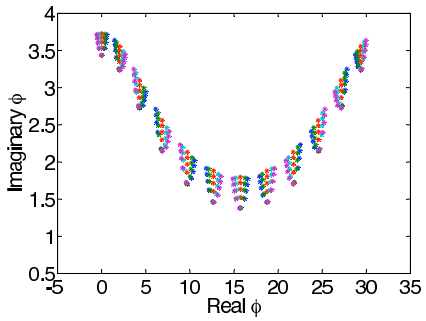

Figure 1: *Saddle points for a 5-cycle laser pulse with intensity $I = 10^{10}$ W/cm^2, $\alpha = 0$, $\theta = 0$–180 degrees, and photoelectron energy $0 \le \varepsilon \le 10\omega$.*

In Fig. 1 each of the 12 groups of asterisks shows the complex saddle-point phases $\phi = \omega t$ for five photoelectron energies between $\varepsilon = 0$ and 10ω and five angles $\theta = 0$, 45, 90, 135, and 180 between the photoelectron momentum and laser polarization. In the adiabatic approach, the twelve saddle points correspond to the instants at which electron detachment takes place. The points near the centre of the pulse, where the field is strongest, are closer to the real axis. In each group the points closest to the real axis correspond to the smallest photoelectron energy. In general, the closer the saddle point to the real axis, the larger its contribution to the amplitude.

Using this approach we determine the spectrum of the photoelectrons as a function of ε and θ, as well as the angle-integrated energy spectra and total detachment probabilities. The dominant contribution to the transition amplitude is given by 5–6 saddle points near the pulse centre. We also examine the dependence of the photoelectron angular distributions on the carrier-envelope phase, and show that measuring such distributions can provide a way of determining this phase.

References

[1] G. F. Gribakin and M. Yu. Kuchiev, Phys. Rev. A **55** 3760 (1997).

Partial photodetachment cross sections in K^-

A. O. Lindahl[1], H. Hultgren[1,2], I. Yu. Kiyan[2], J. Rohlén[1], D. J. Pegg[3], C. W. Walter[4], and D. Hanstorp[1]

[1] *University of Gothenburg, SE-412 96 Gothenburg, Sweden*
[2] *Albert-Ludwigs-Universität Freiburg, 79104 Freiburg, Germany*
[3] *University of Tennessee, Knoxville, Tennessee 37996, USA*
[4] *Denison University, Granville, Ohio 43023, USA*

Corresponding Author: dag.hanstorp@physics.gu.se

Atomic negative ions are ideal systems to test electron-electron correlation models, since the effects are more pronounced than in neutral systems. Doubly excited states are formed in the attachment process when one electron is captured and an electron in the parent atom is simultaneously excited. Such states decay via autodetachment and are manifested as resonances in the photodetachment cross section. By detecting the produced excited atoms it is possible to measure the partial photodetachment cross sections for different reaction paths.

We have built an experimental setup in which it is possible to perform high resolution photodetachment experiments detecting highly excited atoms. The detection is based on resonance ionization using a two-step process. First, the excited residual atom is further excited to a Rydberg state using an IR laser and then the Rydberg state is ionized in an electric field. The positive ion thus produced is detected with a position sensitive detector.

The setup has been used to study photodetachment from K^-. Partial cross sections for the K($7s$), K($5f$) and K($5g$) channels were measured in the photon energy range 4.25–4.36 eV. A number of resonances were observed in the K($7s$) partial cross section, below the opening of the K($5f$) channel. The same resonances have previously been investigated by Kiyan *et al.* [1] in the K($5s$) channel.

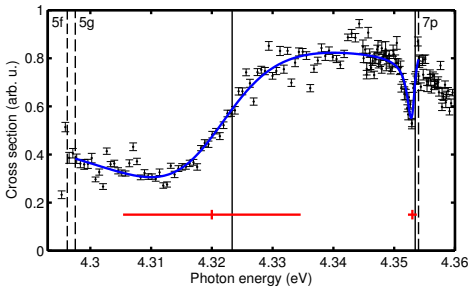

Figure 1: *Cross section for the K(7s) photodetachment channel. The line is a fit containing a constant background and two Shore profiles for the resonances.*

In the region between the thresholds of the K($5g$) and K($7p$) channels the measured cross sections show resonance structures (Fig. 1). These observed resonances are in agreement with the calculations by Liu [2], who attributed them to doubly excited states.

Financial support from the Swedish Research Council is acknowledged. CWW received support from the Wenner-Gren Foundation and from the Andrew W. Mellon Foundation.

References

[1] I. Y. Kiyan, *et al.*, Phys. Rev. Lett., **84**, 5979 (2000).
[2] C. -N. Liu, Phys. Rev. A, **64**, 052715 (2001).

Ab initio quantum Monte Carlo study of the binding of a positron to alkali-metal hydrides

Y. Kita[1], M. Tachikawa[1]

[1] *Quantum Chemistry Division, Yokohama-city University, 22-2 Seto, Kanazawa-ku, Yokohama 236-0027 Japan*

Corresponding Author: ykita@yokohama-cu.ac.jp

The positron (e^+) is the anti-particle of the electron (e^-) and has the same mass and spin, but opposite charge. Positrons injected into a liquid or solid induce processes such as ionization or electronic excitation of atoms/molecules, formation of a metastable bound state of a positron and an electron, that of positronic molecular complexes (positronic compound), etc., before the positron undergoes pair-annihilation with an electron. Properties such as the electronic/positronic structures and the stable geometry of the positronic compounds are, however, not revealed in detail by experiments due to the very short life-time of such compounds (10^{-7}–10^{-10} s).

Theoretical work by Crawford [1] suggests that any molecule having a dipole moment larger than a critical value of 1.625 D is able to bind either one e^- or e^+ in its electrostatic field. Since alkali-metal hydrides, such as LiH, NaH, and KH, have the dipole moment larger than this critical value, it is strongly expected that these molecules can bind a positron.

In this study, we have theoretically analyzed the positron affinity (PA), which is a binding energy of a positron, of alkali metal hydrides (XH, X=Li, Na, and K) with the quantum Monte Carlo (QMC) method [2]. The QMC method, especially diffusion Monte Carlo (DMC) technique, is one of the most accurate *ab initio* techniques for atoms, molecules, and solids. Using DMC technique, we can accurately evaluate the positron affinity (PA), which is the binding energy of a positron to atoms or molecules [3]. Figure 1 shows the PAs obtained with DMC calculations and dipole moments of LiH, NaH, and KH. This figure clearly shows that a polar molecule with a larger dipole moment binds a positron more strongly.

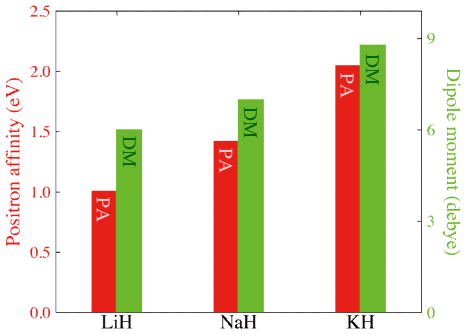

Figure 1: *The positron affinity (PA) and the molecular dipole moment (DM) of alkali-metal hydrides XH (X= Li, Na, and K).*

References

[1] O. H. Crawford, Proc. Phys. Soc. **91**, 279 (1967).

[2] B. L. Hammond, W. A. Lester Jr., and P. J. Reynolds, *Monte Carlo Methods in Ab Initio Quantum Chemistry* (World Scientific, 1994).

[3] Y. Kita, R. Maezono, M. Tachikawa, M. Towler, and R. J. Needs, J. Chem. Phys. **131**, 134310 (2009).

Dissociative electron attachment to formic acid: high-resolution absolute scale measurements

D. Kubala[1], O. May[1], and M. Allan[1]

[1] *Department of Chemistry, University of Fribourg, CH-1700 Fribourg, Switzerland*
Corresponding Author: Dusan.Kubala@unifr.ch

We carried out a study of dissociative electron attachment (DEA) to formic acid (HCOOH). We focused on absolute, high resolution/low noise measurements of the dissociative channel leading to production of $HCOO^-$ anion

$$e^- + HCOOH \longrightarrow HCOO^- \longrightarrow H + HCOO^-. \quad (1)$$

The study was motivated by current interest of theory in the process and, according to astrophysical observations, by the role the DEA to HCOOH could play in formation of more complex molecules in the interstellar media [1]. An older relative measurement was presented by Pelc *et al.* in [2].

Relative yields of $HCOO^-$ were recorded under the resolution of approximately 60 meV with a standard trochoidal electron monochromator (TEM)/ quadrupole instrument and subsequently normalized to absolute data measured with recently constructed time-of-flight mass spectrometer/TEM apparatus [3] working with energetically broader beam. Final cross-section is displayed in Fig. 1. The shape of our spectrum is in excellent agreement with the one dimensional R-matrix model of Gallup *et al.* [4], who propose that the rotation of the O-H bond out of plane, caused by σ^*/π^* coupling is not essential for the description of DEA to the formic acid — contrary to the conclusion of [5].

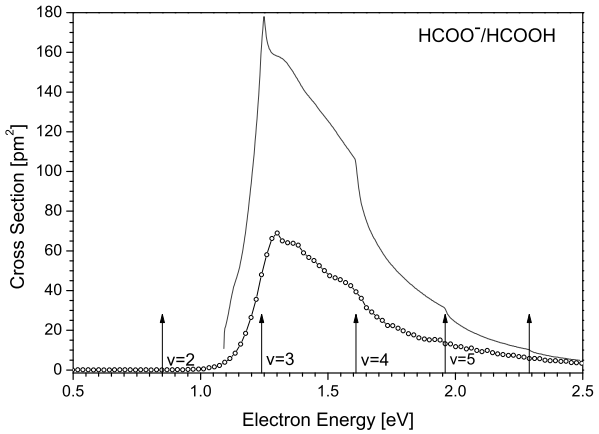

Figure 1: *DEA cross section for $HCOO^-/HCOOH$. Line with circles – experimental data; solid line – theory of Gallup* et al.*[4]; arrows – thresholds for excitation of the O-H vibrational mode.*

References

[1] S. D. Rodgers, S. Charnley, Mon. Not. R. Astron. Soc. **320**, L61 (2001).
[2] A. Pelc *et al.*, Chem. Phys. Lett. **361**, 277 (2002).
[3] J. Fedor, O. May, M. Allan, Phys. Rev. A, **78**, 032701 (2008).
[4] G. A. Gallup, P. D. Burrow, I. I. Fabrikant, Phys. Rev. A **79**, 042701 (2009).
[5] T. N. Rescigno, C. S. Trevisan, A. E. Orel, Phys. Rev. Lett. **96**, 213201 (2006).

Four-fold excitation resonances: manifestation in the resonant Auger effect of Kr

B. M. Lagutin[1], Ph. V. Demekhin[1], V. L. Sukhorukov[1], I. D. Petrov[1], H. Schmoranzer[2], K.–H. Schartner[3], and A. Ehresmann[4]

[1] *Rostov State Transport University, 344038, Rostov-on-Don, Russia*
[2] *Fachbereich Physik, TU Kaiserslautern, D-67653, Kaiserslautern, Germany*
[3] *I. Physikalisches Institut, Justus-Liebig-Universität, D-35392, Giessen, Germany*
[4] *Institut für Physik, Universität Kassel, D-34132, Kassel, Germany*

Corresponding Author: bml@rgups.ru

It is an established fact that the resonant Auger effect (RAE) in atomic Kr is strongly influenced by interference of the direct non-resonant [0] $\rightarrow 4p^4 5p\varepsilon\ell$ and resonant [0] $\rightarrow 3d^9 np \rightarrow 4p^4 5p\varepsilon\ell$ pathways which causes an energy dependence of the angular distribution parameters of photoelectrons (β_{el}) or fluorescence (see e.g., [1-4]). Large differences between the calculated and measured $\beta_{el}(\omega)$ remain in some cases and stimulate a search of new possible mechanisms of RAE.

In this work we have studied the $4p^4 \rightarrow n_1\ell_1 n_2\ell_2 n_3\ell_3 n_4\ell_4$ four-fold excitations (4ex) of the $4p^6$ Kr ground state and their manifestation in RAE. The $4s^2 4p^2 5d^1 5p^1 8d^2$ state was considered as an example. It provides a Coulomb interaction between the $3d^9 np$ single-resonant and the $4p^4 5p\varepsilon\ell$ final states via the "bridge" $4s^1 4p^4 5d^0 5p^1 8d^2$ state. The strength of the interaction is substantial because of the large value of the 4p4p–4s5d Coulomb matrix element.

The results of the model calculation presented in Fig. 1 illustrate the significant manifestation of the 4ex state in RAE. Possible influences of the 4ex states on other than RAE spectra were also analyzed theoretically.

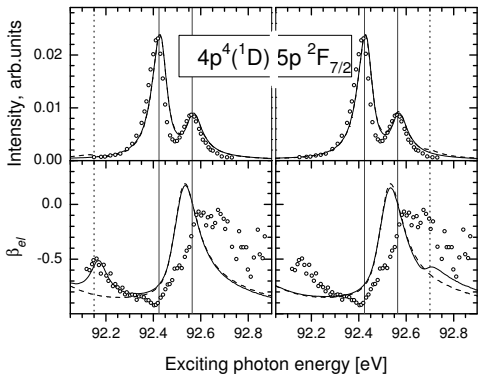

Figure 1: *Line intensities and the β_{el} parameters computed with (solid lines) and without (dashed lines) inclusion of one selected 4ex states. Experiment [3,4] – open circles. Vertical lines: positions of the 3d–np resonances (solid); position of the 4ex resonance (dotted).*

PPA

References

[1] B. M. Lagutin *et al.*, Phys. Rev. Lett. **90**, 073001–4 (2003).
[2] K. H. Schartner *et al.*, J. Phys. B **38**(22), 4155–4170 (2005).
[3] A. Sankari *et al.*, Phys. Rev. A **76**(2), 022702 (8pp) (2007).
[4] A. Sankari *et al.*, Phys. Rev. A **77**(3), 032720 (7pp) (2008).

Laser-induced free-free transitions in elastic electron scattering from CO_2

M. O. Musa[1], A. MacDonald[2], L. Tidswell[2], J. Holmes[2], and B. Wallbank[2]

[1] *Gulf University for Science and Technology, PO Box 7207, Hawally, 32093, Kuwait*
[2] *St. Francis Xavier University, Antigonish, NS, Canada*

Corresponding Author: musa.m@gust.edu.kw

We present measurements of laser-induced free-free transitions of electrons scattered from CO_2 molecules in the ground electronic state at incident electron energies of 3.8 and 5.8 eV under pulsed CO_2 laser field. The differential cross section of free-free transitions involving absorption and emission of up to two photons were measured at various scattering angles with the polarization of the laser either parallel with or perpendicular to the the momentum change vector of the scattered electrons. The results of the parallel geometry are found to be in qualitative agreement with the predictions of the Kroll-Watson approximation within the experimental uncertainty whereas those of the perpendicular geometry show marked discrepancy with the Kroll-Watson predictions.

References

[1] N. M. Kroll and K. M. Watson, Phys. Rev. A **8**, 804 (1973).
[2] A. Weingartshofer, J. K. Holmes, G. Caudle, E. M. Clarke and H. Kruger Phys. Rev. Lett. **39**, 269 (1977).
[3] M. O. Musa, A. MacDonald, L. Tidswell, J. Holmes and B. Wallbank, J. Phys. B **43**, 175201 (2010).

Ion-pair formation and resonant quenching in collisions of Rydberg atoms with neutral atoms

A. A. Narits[1,2], V. S. Lebedev[1,2]

[1] *P. N. Lebedev Physical Institute of the Russian Academy of Sciences, 53 Leninskiy prospect, 119991 Moscow, Russian Federation*
[2] *Moscow Institute of Physics and Technology, 9 Instituskiy per., 141700 Dolgoprudniy, Moscow Region, Russian Federation*

Corresponding Author: narits@sci.lebedev.ru

The work is devoted to studies of ion-pair formation and resonant quenching processes in slow collisions between highly excited atoms and ground-state atoms with small electron affinities. We elaborate a general approach for the calculation of transition matrix elements between the ionic and Rydberg-covalent states of a diatomic quasimolecular system by using the momentum representation for the highly excited electron wave function and a technique of nonreduced tensor operators. The key point of the theory is that it allows one to exactly evaluate the matrix elements of ion-covalent coupling by taking into account both the short-range and the long-range parts of the electron-atom interaction. In particular, it correctly describes the variation of the Rydberg atom wave function in the range of electron coordinates, which is responsible for transition between ionic and covalent terms. This plays an important role in collisions involving strongly polarizable atoms with small electron affinities. It is shown that the general expression of the present theory for the ionic-covalent coupling parameter contains some available analytical results of previous works as special cases. Particular attention is paid to the investigation of the effects associated with the long range part of electron-perturber interaction in the charge transfer processes involving strongly polarizable perturbing atoms with small electron affinities.

The theory developed was applied to the investigation of the ion-pair formation and resonance quenching processes

$$A(nl) + B \to A^+ + B_t^- \to \begin{cases} A^+ + B^-, \\ A(n'l') + B. \end{cases} \quad (1)$$

in collisions of the Rydberg atoms $Ne(ns, nd)$ with alkaline-earth atoms Ba, Sr, and Ca (electron affinities are equal to 144, 52, and 24 meV, respectively) in the range of relative internuclear velocities of 10^{-4}–10^{-3} a.u. Transition matrix elements, probabilities, and cross sections of the processes under consideration have been calculated. The cross sections have been obtained in the framework of the semiclassical theory of nonadiabatic transitions. It was shown that the exact evaluation of the ionic-covalent matrix elements becomes essential for high principal quantum numbers when the ion-pair formation occurs at particularly large internuclear distances. In a wide range of principal quantum numbers the cross sections obtained in the dipole approximation using the Taylor expansion of the Rydberg electron wave function [1,2] in the vicinity of the anion center differ from those calculated using the exact matrix elements by an order of magnitude. For sufficiently low n the results calculated using the dipole approximation agree well with the developed theory. It was shown that the influence of the long-range polarization interaction increases with the decrease of relative velocity.

The work was partially supported by the Russian Foundation for Basic Research (Grant Nos. 09-02-01024, 11-08-00879) and Ministry of Education and Science of Russian Federation (programme Development of the Scientific Potential of Higher Education Institutions, Project No. 2.1.1/4294).

References

[1] I. I. Fabrikant, V. S. Lebedev, J. Phys. B **33**, 1521–1531 (2000).
[2] I. I. Fabrikant, M. I. Chibisov, Phys. Rev. A **61**, 022718-1–022718-7 (2000).

Electron impact single ionization of noble gas targets in the perpendicular plane geometry

G. Purohit[1], P. Singh[1], V. Patidar[1], and K. K. Sud[1]

[1] *Department of Physics, School of Engineering, Sir Padampat Singhania University, Bhatewar, Udaipur-313601, India*

Corresponding Author: g_vpurohit@yahoo.com

There has been remarkable progress in the theoretical description of electron impact single ionization (i.e., (e, 2e) processes) of atoms in recent years. Electron impact ionization is a fundamental process in atomic physics and kinematically complete studies of electron-impact ionization can be obtained using (e, 2e) technique. Fundamentally an (e, 2e) process is one where an electron of well defined energy and momentum is incident on a target, ionizes it and the outgoing electrons are detected in coincidence with their energies and angles resolved. This process plays a key role in many natural and technological processes. The (e, 2e) technique can be used to probe the structure of ionized targets and to understand the delicate collision dynamics. Through the careful choice of geometrical arrangement and the energies of incoming and exiting electrons one can predict the physics which will dominate the shape and magnitude of the triple differential cross section. The calculation of triple differential cross section opens up a whole new area of theoretical study and offers a direct insight into the subtleties of spin-dependence and other purely relativistic effects etc. Since the first coincident measurement of (e, 2e) process on atoms by Erhardt *et al.* [1] and Amaldi *et al.* [2] extensive theoretical and experimental investigations have been done to measure the TDCS. Extensive data are available for the ionization of simple targets like hydrogen and helium and even for more complex atomic and molecular targets, clusters and surfaces.

Recently, there have been several attempts to explain the features of TDCS for the (e, 2e) processes on inert targets like Ne, Ar, and Xe [3-6] but there are still certain discrepancies in theoretical results and measurements, which requires more theoretical efforts to understand the collision dynamics of these targets. We present in this communication the results of our calculation of TDCS for the Ne, Ar, and Xe atoms in perpendicular geometry from near threshold to intermediate energies. The two outgoing electrons emerge perpendicular to the direction of incident electrons so this geometry provides a test of the most sophisticated scattering theories. We compare our results with the recent measurements of Nixon *et al.* [7]. We discuss the dependence of TDCS on incident electron energy, nuclear charge of the target and post collision interaction.

References

[1] H. Ehrhardt *et al.*, Phys. Rev. Lett. **22**, 89 (1969).
[2] U. Amaldi *et al.*, Rev. Sci. Instrum. **40**, 1001 (1969).
[3] M. A. Stevenson *et al.*, Phys. Rev. A **79**, 012709 (2009).
[4] M. A. Stevenson and B. Lohmann, Phys. Rev. A **77**, 032708 (2008).
[5] G. Purohit, V. Patidar and K. K. Sud, J. Electron Spectroscopy and Related Phenomena **175**, 1 (2009).
[6] G. Purohit, V. Patidar and K. K. Sud, J. Physics: Conference Series **235**, 012013 (2010).
[7] K. L. Nixon, A. J. Murray and C. Kaiser, J. Phys. B: At. Mol. Opt. Phys. **43**, 085202 (2010).

Intermolecular Coulombic decay in small, biochemically relevant, hydrogen bonded systems

S. D. Stoychev[1], A. I. Kuleff[1], and L. S. Cederbaum[1]

[1] *Theoretische Chemie, Physikalisch-Chemisches Institut, Universität Heidelberg, Im Neuenheimer Feld 229, D-69120 Heidelberg, Germany*

Corresponding Author: spas.stoychev@pci.uni-heidelberg.de

Intermolecular (interatomic) Coulombic decay (ICD) [1] is an extremely efficient electronic decay mode, initiated by removal of an electron from the inner-valence shell of atomic and molecular clusters. The ICD process is characterized by the relaxation of an initially ionized state on one site of the system that results in the emission of a low energy electron from a neighboring site. The two positively charged ions that are formed in the decay repel each other which typically leads to a Coulomb explosion of the system. As a consequence, ICD does not only break the bond in the complex and produces highly reactive radicals, but it is also a source of low energy electrons [2,3] known to be responsible for irreversible damage of biological systems. In the last decade, ICD was extensively studied both theoretically and experimentally in a large variety of systems (see the up-to-date ICD bibliography list [4]).

An important aspect of the ICD process is that it is extremely fast, transpiring typically on a femtosecond scale, thus being orders of magnitude faster than the other possible relaxation modes of the system (like radiative decay or nuclear dynamics). In principle, ICD can be outperformed by the autoionization of the initially ionized subsystem when the latter is energetically allowed. Therefore, if an inner-valence ionized atom or molecule cannot autoionize, but has neighbors, like in a van der Waals cluster or in a hydrogen bonded counterpart, the system is a prime candidate for ICD. Weak interactions of these kind are typical in biochemistry and the ICD process is likely to happen in systems containing the hydrogen bonded macromolecules common in living tissues.

The present work is devoted to the theoretical study of ICD and related phenomena initiated by inner-valence ionization of small bimolecular systems that contain an oxygen atom as a proton donor or as a proton acceptor: H_2O–HCHO, H_2O–H_2CNH, H_2O–NH_3, NH_3–H_2O, H_2O–H_2S, H_2S–H_2O and H_2O–H_2O. This bimolecular set contains seven types of hydrogen bonding which are typical for biochemistry and thus gives a clue to the processes that can take place in living tissues. In particular, a qualitative estimate of the ICD of biosystems interacting with water (their usual medium) is made: the ionization of the inner-valence shell of H_2O triggers ICD in all of the studied species. For the purpose of our study we have used high-precision *ab initio* methods in optimizing the geometries and computing the single- and double-ionization spectra of the studied systems, as reported in [5]. The energy range of the emitted ICD electrons, as well as the kinetic energy of the dissociating ions produced by ICD is also shown.

PPA

References

[1] L. S. Cederbaum, J. Zobeley, and F. Tarantelli, Phys. Rev. Lett. **79**, 4778 (1997).
[2] T. Jahnke, *et al.*, Nature Phys. **6**, 139 (2010).
[3] M. Mucke, *et al.*, Nature Phys. **6**, 143 (2010).
[4] http://www.pci.uni-heidelberg.de/tc/usr/icd/ICD.refbase.html.
[5] S. D. Stoychev, A. I. Kuleff, and L. S. Cederbaum, J. Chem. Phys. **133**, 154307 (2010).

Photoelectron circular dichroism of isopropanolamine

S. Turchini[1], D. Catone[1], G. Contini[1], N. Zema[1], M. Stener[2], P. Decleva[2], and T. Prosperi[1]

[1] *ISM-CNR, via del fosso del Cavaliere, 00133, Roma, Italy*
[2] *Dipartimento di Scienze Chimiche, Università di Trieste, Via L. Giorgieri 1, I-34127 Trieste, Italy and Consorzio Interuniversitario Nazionale per la Scienza e Tecnologia dei Materiali, INSTM, Unità di Trieste and DEMOCRITOS CNR-IOM National Simulation Center, Trieste, Italy*

Corresponding Author: stefano.turchini@ism.cnr.it

Asymmetry in the interaction of circularly polarized light with chiral molecules has been studied since Pasteur's pioneering experiments on optical activity. As originally pointed out by Ritchie [1], helicity-dependent effects should be observed in photoelectron emission from chiral molecules even if randomly oriented. The circular dichroism in photoelectron spectroscopy (PECD) is due to the dipole interaction term, while in the absorption process it is related to the second order interference terms, the electric dipole-electric quadrupole, and electric dipole-magnetic dipole. The strong intensity of the dipole dis-symmetry was exploited in gas phase experiment where it is possible to take advantage from the highly developed experimental methods of photoelectron spectroscopy. In the present studies we successfully apply PECD spectroscopy to the study of 1-amino-2-propanol (isopropanolamine) in the gas phase. Isopropanolamine is a linear saturated bifunctional molecule amenable to intra-molecular interactions and different conformations (Fig. 1). The isopropanolamine is a worthy test experiment because it is a structural isomer of 2-amino-1-propanol (alaninol), with an exchanged position of the two functional groups (-OH,-NH_2) at the chiral carbon on a similar skeleton structure. As a matter of fact the study of molecules which share well definite electronic and structural properties can shed light on features of the electronic and structural properties, which match some characteristic of the experimental dispersion of the dichroism. The considerations developed in this work are directly related to a previous PECD investigation on the valence band of alaninol [2]. The experimental dispersion of the dichroism of valence electronic states and C 1s core level of isopropanolamine, as a function of the photoelectron kinetic energy, is compared with its theoretical value calculated employing a multicentric basis set of B-spline functions and a Kohn-Sham Hamiltonian [3]. To compare experimental and theoretical dichroism dispersion a Boltzmann average on the conformers population was performed, having as guideline in composing the sum the ground state ionization energy sequence to assign conformer character to the features of the photoelectron spectra.

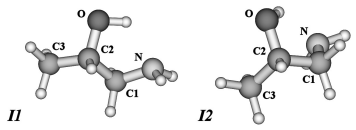

Figure 1: *Sketch of the calculated structures of the two conformers of S-(+)-isopropanolamine (I1 and I2).*

Comparing the experimental HOMO and HOMO-1 dichroism dispersion of isopropanolamine and alaninol an important resemblance was found. Classical spectroscopic techniques as absorption and standard photoelectron spectroscopy cannot reach the same sensitivity of PECD because the characteristic features in the spectra slightly changes or are not clearly related upon tiny difference in the electronic structure.

References

[1] B. Ritchie, Phys. Rev. A, **13**, 1411 (1976).
[2] S. Turchini, D. Catone, G. Contini, N. Zema, S. Irrera, M. Stener, D. Di Tommaso, P. Decleva, and T. Prosperi, ChemPhysChem 10 (11), **10**, 1839 (2009).
[3] M. Stener, G. Fronzoni, D. D. Tommaso, and P. Decleva, J. Chem. Phys., **120**, 1411 (2004).

Lowest autoionizing states of beryllium in photoionization problem

A. I. Opachko[1], V. M. Simulik[2], R. V. Tymchyk[2], and T. M. Zajac[3]

[1] *Department of Electronic Systems, Uzhgorod National University, Uzhgorod, Ukraine*
[2] *Institute of Electron Physics, National Academy of Sciences, Uzhgorod, Ukraine*
[3] *Department of Electronic Systems, Uzhgorod National University, Uzhgorod, Ukraine*
Corresponding Author: romannetmail@gmail.com

The method of interacting configurations in complex number representation (MICCNR) [1] is applied to the investigations of the autoionizing levels of beryllium (the photoionization problem). The positions of the lowest ^1P autoionizing states (AIS) of Be atom are presented in the table. The results are compared with the experimental data [2,3] and the theoretical calculations by the other methods [4-7].

^1P	MICCNR	[2]	[3]	[4]
$2p3s$	10.71	10.71	10.93	10.77
$2p3d$	11.84	11.86	11.86	11.86
$2p4s$	12.03	11.97	12.10	12.07
$2p4d$	12.42	12.47	12.50	12.49

^1P	MICCNR	[5]	[6]	[7]
$2p3s$	10.71	10.73	10.63	10.91
$2p3d$	11.84	11.85	12.03	11.83
$2p4s$	12.03	12.09	12.09	12.09
$2p4d$	12.42	12.49	12.61	12.44

Table 1: *Lowest AIS of Be atom in eV.*

PPA

References

[1] S. M. Burkov *et al.*, J. Phys. B **21**, 1995–1208 (1988).
[2] G. Mehlman-Ballofet and J. M. Esteva, Astrophys. Journal **157**, 945–956 (1942).
[3] J. M. Esteva, G. Mehlman-Ballofet, and J. Romand, Journal Quant. Spectrosc. Radiat. Transfer **12**, 1291 (1972).
[4] P. L. Altic, Phys. Rev. **169**, 21–26 (1968).
[5] V. I. Lengyel, V. T. Navrotsky, and E. P. Sabad, J. Phys. B **23**, 2847–2867 (1990).
[6] Hsin-Chang Chi, Keh-Ning Huang, and K. T. Cheng, Phys. Rev. A **43**, 2542–2545 (1991).
[7] Dae-Soung Kim *et al.*, Phys. Rev. A **61**, 062701(1–9) (2000).

Surface effect in multiphoton electron emission from metals

S. V. Yalunin[1,2], M. Gulde[2], and C. Ropers[2]

[1] *Department of Physics, I. Kant State University of Russia, 236041 Kaliningrad, Russia*
[2] *Courant Research Center Nano-Spectroscopy and X-Ray Imaging, University of Göttingen, 37077 Göttingen, Germany*

Corresponding Author: yalunin@bk.ru

First nonperturbative consideration of multiphoton electron emission was done by Keldysh [1] in the context of ionization of atoms. The Keldysh approach requires, however, that the frequency of the laser field be much lower than the electron binding energy and, therefore, the minimum number of absorbed photons be large. This limitation was overcome by Reiss [2] where he applied the generalized Bessel functions initially proposed in the context of electron-positron pair creation. We present a comprehensive nonperturbative treatment of weak-field and strong-field photoemission from metal surfaces and the transition between the two regimes, focusing on several key aspects that differ from their gas phase counterparts. This includes surface effects, such as electron reflection and back scattering as well as the use of delocalized initial states. Several theoretical methods which require varying degrees of analytical and numerical effort are compared. Figure 1 shows the wavefunction obtained within Crank-Nicolson computations at F=30 V/nm. The special feature of our Crank-Nicolson implementation is the use of transparent boundary conditions and an incoming plane wave in the metal. The classical trajectories were computed according to [3]. Figure 2 illustrates the transition between the weak-field (F<18 V/nm) and strong-field (F>18 V/nm) regimes as well as shows comparisons between our modified perturbation theory, Crank-Nicolson method, and Floquet approach (we show only 4-photon contribution). We find that our analytical approach produces very accurate results both in the weak and strong laser field regimes. The results were obtained for λ = 800 nm, Fermi energy E_F = 4.5 eV and work function W = 5.5 eV.

PPA

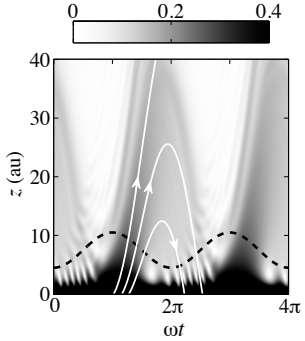

Figure 1: *Absolute value of the wavefunction $|\psi(z,t)|$ (metal surface $z = 0$). Dashed black line shows schematically electric force. Solid white lines show classical trajectories.*

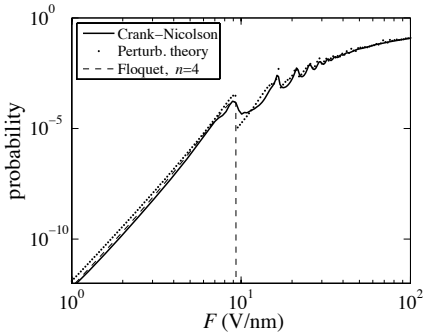

Figure 2: *Photoemission probability (the ratio of time-averaged outgoing and incoming current densities) as a function of peak electric field of incident light.*

References

[1] L. V. Keldysh, Sov. Phys. JETP **20**, 1307 (1965).
[2] H. R. Reiss, Phys. Rev. A **22**, 1786 (1980).
[3] P. B. Corkum, Phys. Rev. Lett. **71**, 1994 (1993).

Quantum Optics and Information

Generation of photonic time-bin qubit in a tripod atomic media

D. Aghamalyan[1], Yu. Malakyan[1]

[1] *Institute for Physical Research of Armenian National Academy of Sciences, Ashtarak 2, 0203, Armenia*

Corresponding Author: davagham@gmail.com

A new method of preparing a single photon in temporally delocalized entangled modes is proposed and analyzed. We show that in a medium of four-level atoms with tripod-level configuration a strong parametric interaction between two one-photon pulses emerges, if the medium was initially prepared in a coherent superposition of the two ground states, while a strong classical field drives the neighbor transition from the third ground state. The analytical solution of Maxwell equations reveals that under electromagnetically induced transparency (EIT), the quantum fields propagate with significantly small absorption and with different group velocities that leads to their temporal split into well-separated pulses, the amplitudes of which are well controlled by the driving field. The proposed scheme can serve as a robust source of narrow-band one-photon qubits with an entanglement between two temporal modes, not sensitive to losses in atmosphere and in telecommunication waveguides. We show also that in our scheme a controllable degree of temporal entanglement can be achieved.

Contribution withdraw by author request.

Generation of powerful tunable THz radiation via two-color multiphoton resonance in atomic-molecular systems

H. Avetissian[1], B. Avchyan[1], and G. Mkrtchian[1]

[1] *Centre of Strong Field Physics, Yerevan State University, 0025 Yerevan, Armenia*
Corresponding Author: avchyan@ysu.am

Tunable, compact high-power terahertz sources are of great interest due to the important properties of terahertz radiation and its significant applications [1]. There are several promising mechanisms for developing coherent terahertz sources: difference-frequency generation; plasma based via laser-induced wakefields, femtosecond electron bunches, ultrashort laser pulses; and accelerator based via synchrotron and transition radiation of ultrashort electron beams.

In the present work, we propose a scheme for tunable high-power terahertz radiation generation in three-level systems of Γ-configuration. Typical examples of such configuration are hydrogen-like atomic-ionic systems or evenly charged homonuclear diatomic molecular ions. Since for these systems the first excited electronic state usually lies in the UV–VUV domain, the excitation of such systems by optical lasers is possible via multiphoton channels. The coherent scattering spectrum of a three-level system by multiphoton resonant excitation has been considered in the paper [2]. Because of inversion symmetry, the minimal radiation frequency is near the incident laser frequency. For generation of low frequency radiation corresponding to slow oscillations of level populations, one should break the inversion symmetry of quantum system. Here, it is realized by means of second laser action. We investigate coherent radiation generation process in the low frequency range of the spectrum due to the multiphoton-resonant excitation of a three-level system by two laser beams of multiple frequencies.

We also consider the superradiation of atomic ensemble and show that one can obtain coherent THz radiation with the power of a watt level. Hence, the considered scheme may serve as a promising compact source of coherent, tunable high-power THz radiation.

This work was supported by SCS of RA under Project No. 10-3E-17 and CRDF/NFSAT/SCS -ECSP-09-72.

References

[1] M. Tonouchi, Nature Photonics **1**, 97–105 (2007).
[2] H. K. Avetissian, B. R. Avchyan, and G. F. Mkrtchian, Phys. Rev. A **77**, 023409 (2008).

Wave-mixing and harmonics generation due to two-color multiphoton resonant excitation of atoms and molecules

H. Avetissian[1], B. Avchyan[1], and G. Mkrtchian[1]

[1] *Centre of Strong Field Physics, Yerevan State University, 0025 Yerevan, Armenia*
Corresponding Author: avchyan@ysu.am

Harmonics generation and wave-mixing are fundamental processes of traditional nonlinear optics which have been extensively studied with the appearance of lasers. Unprecedented progress of last decade in this field with advent of superintense laser sources has allowed of higher-order harmonics generation at the laser-atom interaction through the continuum spectrum. Depending on the laser-atom interaction parameters harmonics generation may also occur via bound-bound transitions [1]. In this case the high-power light resonant scattering at which only a few resonant levels of an atom are involved in the interaction process is of certain interest as it can provide high efficiency of high-order harmonics generation and wave-mixing. As it has been shown for some atomic-molecular systems, one can achieve efficient multiphoton excitation when the system has a mean dipole moment in the stationary states. For this goal, as practically convenient examples of such systems we can use hydrogen-like atomic/ionic systems, molecules with permanent dipole moments, or evenly charged homonuclear diatomic molecular ions [2–4].

In the present work, we investigate wave-mixing and harmonics generation by two-color multiphoton resonant excitation of atoms-molecules possessing permanent dipole moments in strong laser fields under the such circumstances when only the bound states are involved in the interaction process. The spectra corresponding to harmonics generation and wave-mixing at the multiphoton induced transitions are investigated both analytically and numerically.

This work was supported by SCS of RA under Project No. 10-3E-17 and CRDF/NFSAT/SCS -ECSP-09-72.

References

[1] H. K. Avetissian, B. R. Avchyan, and G. F. Mkrtchian, Phys. Rev. A**77**, 023409 (2008)
[2] H. K. Avetissian and G. F. Mkrtchian, Phys. Rev. A **66**, 033403 (2002).
[3] G. N. Gibson, Phys. Rev. Lett. **89**, 263001 (2002).
[4] H. K. Avetissian, B. R. Avchyan, and G. F. Mkrtchian, Phys. Rev. A **74**, 063413 (2006).

Cumulant analysis of entangled multipartite states

O. V. Belyaeva[1], A. S. Chirkin[1]

[1] *Faculty of Physics, M. V. Lomonosov Moscow State University, Moscow, Russia*
Corresponding Author: lisenok.msu@mail.ru

Cumulant analysis is a powerful technique to study entangled quantum fields, especially multimode ones. For single mode squeezed fields this analysis was applied in paper [1]. It is well known that all cumulants, which have the order higher than second, are equal to zero for fields with Gaussian statistics, and all cumulants possess the same values for states with the Poissonian statistic. Thus the cumulant analysis simplifies the determination of statistics of random parameters.

Joint cumulants for multimode random fields take into account more complicated statistical relationships than correlation functions of the same orders [2]. The third order joint cumulant takes into account a statistical relation of the second order, and the fourth order joint cumulant a statistical relation of the third order and so on. We have applied the cumulant analysis to three- and four-mode entangled quantum states formed in coupled optical parametrical processes studied by us earlier [3,4]. The joint cumulants of the third and the fourth orders and their dependency on nonlinear processes' parameters are calculated. Joint cumulants for GHZ, W and Dicke states are also analyzed. As a result, we have revealed that the joint cumulants provides sensitive technique of entangled multipartite states.

References

[1] V. V. Dodonov, I. M. Dremin, P. G. Polynkin, V. I. Man'ko, Phys. Lett. A **193**, 209 (1994).
[2] A. N. Malakhov, Cumulant analysis of stochastic non-Gaussian processes, Moscow, 1978 (in Russian).
[3] O. V. Belyaeva, A. S. Chirkin, J. Russ. Laser Res. **30**, 499 (2009).
[4] A. S. Chirkin, M. Yu. Saigin, Phys. Scr. **T135**, 014029, (2009).

Three demonstrations of the wave-particle duality of light and quantum erasing

T. L. Dimitrova[1,2], N. Castagna[2], and A. Weis[2]

[1] *Faculty of Physics, Plovdiv University, 4000 Plovdiv, Bulgaria*
[2] *Department of Physics, University of Fribourg, CH-1700 Fribourg, Switzerland*
Corresponding Author: tldimitrova@abv.bg

One century after establishing quantum mechanics on the basis of the wave-particle duality of quantum objects, the concept of duality still presents a great fascination for students, as for the general public. Often, the mysterious features of the quantum world are described in terms of Gedankenexperiments, or are explained to occur in invisible nanostructures or complex physical devices. This makes it difficult to illustrate the weird features of quantum physics by hands-on demonstration experiments which are educational tools of undisputed value.

The dual nature of light offers beautiful ways for demonstrating quantum features on a macroscopic scale. Over the past years, we have developed in Fribourg several demonstration experiments that show, using the same device, the wave and the particle nature of light, and the transition from one aspect to the other [1–5]. We profit from the fact that EGAS-43 is held in Fribourg to present the following three experiments as live demonstrations during poster sessions:

- We display **double slit interference** with individual photons [1,2] from a strongly attenuated green laser pointer which ensures that there is only a single photon in the apparatus at each moment. Interference patterns are registered by a CCD camera equipped with an image intensifier and displayed on a computer monitor. By integrating a large number of camera frames, one sees how the seemingly random dot patterns representing individual photons gradually evolve into the smooth classical interference pattern.
- A **Michelson interferometer** (a variant of the apparatus described in [1,2]) is operated either with strong light, or with individual photons. The path length difference in the interferometer is periodically scanned by a piezo-driven mirror which moves the interference pattern across a small aperture, after which the light is detected either by a photodiode or a photomultiplier. Signals are displayed by an oscilloscope and a loudspeaker. With individual photons, the oscilloscope shows photomultiplier pulses, which, after signal averaging, add up to the smooth classical interference pattern. The large spatial separation of the interfering beams allows us to demonstrate that "*the photon interferes with itself*". Indeed, after adjusting the path length difference to see/hear an interference minimum, the photon rate increases significantly, when one of the beams is blocked by hand [2].
- Our most recent development [3] is a compact (portable) device that illustrates the phenomenon of **quantum erasing** with individual photons [4,5]. It uses a double slit interferometer, in which a photomultiplier is moved across the fringe pattern, so that the spatial intensity modulation is rendered acoustically. When inserting orthogonal polarizers after the two slits, the photons' paths become labeled and interference disappears. Interference can be made to reappear by inserting, before the detector, a suitably oriented polarizer (the "eraser"), which destroys the which-way information. The disappearance and reappearance of interference can be well heard in the loudspeaker signals.

Project financed in parts by SNF Scopes program (grant No. IZ73Z0–127942–1).

References

[1] T. L. Dimitrova and A. Weis, Am. J. Phys. **76**, 137–142 (2008).
[2] http://www.sps.ch/artikel/progresses/wave_particle_duality_of_light_for_the_classroom_13/.
[3] T. L. Dimitrova and A. Weis, submitted to Eur. Phys. J.
[4] T. L. Dimitrova and A. Weis, Eur. J. Phys. **31**, 625–637 (2010).
[5] T. L. Dimitrova and A. Weis, Phys. Scr. **T135**, 014003 (2009).

Efficient generation of Fock states in a single-atom cavity-QED system

A. Gogyan[1], S. Guérin[2], and Yu. Malakyan[1,3]

[1] *Institute for Physical Research of Armenian National Academy of Sciences, Ashtarak 2, 0203, Armenia*
[2] *Laboratoire Interdisciplinaire Carnot de Bourgogne, UMR CNRS 5209, BP 47870, F-21078 Dijon, France*
[3] *Centre of Strong Field Physics, Yerevan State University, 1 A. Manukian St., Yerevan 0025, Armenia*

Corresponding Author: agogyan@gmail.com

Pure photon Fock states are useful for many quantum-optical applications, including quantum information processing, quantum computing, and quantum cryptography.

We have suggested and analyzed a simple and highly effective scheme to produce Fock states with arbitrary given number of photons. The essence of the mechanism is the following. A four-level atom with double Raman transitions is trapped in a cavity QED (e.g., ^{6}Li atoms or $^{40}Ca^+$). Two ground states, 1 and 2, and two upper states, 3 and 4, of the atom are Zeeman sublevels (Fig. 1). The atom (ion) interacts with two pumping fields at transitions 1–4 and 2–3, while the cavity is coherently coupled to the atom on both transitions 4–2 and 3–1. While interacting with the classical fields, linearly polarized cavity photons at transitions 4–2 and 3–1 are generated. Moreover, the number of photons is easily controlled by changing the intensity and duration of the classical fields. We have shown that the generated many-photon Fock state wavefunction is the sum of single-photon wavepackets, which is due to the absence of correlation between photons. We have also proposed a scheme for generation of Fock states in an atom with many Zeeman sublevels. The scheme for experimental realization of the process is elaborated.

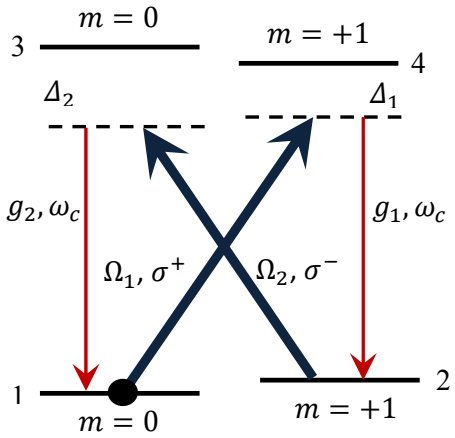

Figure 1: *Relevant atomic level structure in an external magnetic field. Shown is the case when the Landé g_L factors of the ground and excited states have opposite signs.*

QOI

Propagation of light pulses through medium with electromagnetically induced transparency

S. N. Nikolić[1], V. Djokic[1], A. J. Krmpot[1], S. M. Ćuk[1], and B. M. Jelenković[1]

[1] *Institute of Physics, University of Belgrade, Pregrevica 118, 11080 Belgrade, Serbia*
Corresponding Author: stankon@ipb.ac.rs

We investigated propagation of light pulses through hot Rb vapor, when the light pulse is slowed due to induced coherences between Zeeman sublevels of the hyperfine level of Rb electronic ground state.

In our experiment, pump and probe light fields are derived from the single external cavity diode laser beam. We employed $5^2S_{1/2}, F_g = 2 \rightarrow 5^2P_{1/2}, F_e = 1$ transition in ^{87}Rb. Pump field is σ^+ circularly polarized light while the σ^- pulse of the weak probe field is generated by the Pockels cell [1]. Thus, two fields make Lambda scheme and lead to electromagnetically induced transparency (EIT) between Zeeman sublevels of the ground hyperfine $F = 2$ level [2]. Both fields copropagate through Rb cell filled with 30 torr of Ne buffer gas. Rb cell is placed inside triple layer of MuMetal. Axial magnetic field is generated by the solenoid around the cell in order to investigate dependence of EIT features on two-photon detuning. Delays of probe field pulses with respect to reference pulses were measured using identical fast photodiodes and oscilloscope.

Influence of laser intensity and cell temperature on delays of σ^- pulses is investigated. Delays were measured for different pulse lengths and shapes. Transient behavior of the EIT, after square pulse of σ^- light is applied, were also studied. Dependence of the pulse delay on the pulse length as well as EIT waveforms obtained at different time instants after sudden generation of probe field, could be explained by the Ramsey effect of multiple interaction of atomic coherence with the coherent laser light. This Ramsey effect is induced by atomic motion out and then back to the laser beam due to the diffusion of Rb atoms in the buffer gas cell [3].

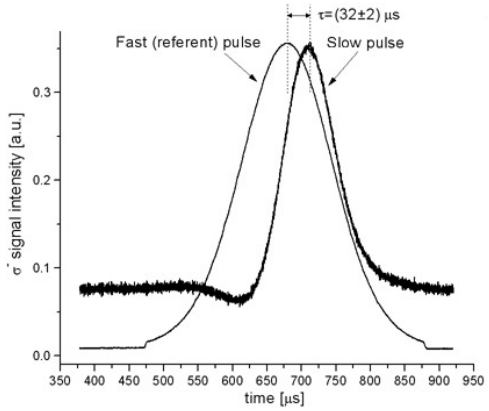

Figure 1: *Pulse of σ^- polarization traveling through EIT medium was delayed 32 μs compared to referent pulse propagating in vacuum. Input peak power for σ^- component was 15% of overall laser power. Total intensity was 32 mW/cm^2 and length of the cell was 8 cm. Corresponding group velocity was about 2.5 km/s.*

References

[1] D. F. Phillips *et al.*, Phys. Rev. Lett. **86**, 783–786 (2001).
[2] M. Fleischhauer, A. Imamoglu, and J. P. Marangos, Rev. Mod. Phys. **77**, 633–673 (2005).
[3] Y. Xiao *et al.*, Opt. Express **16**, 14128–14141 (2008).

Self-induced transparency of probe field in four-level atomic media

Sh. Petrosyan[1], Yu. Malakyan[2,1]

[1] *Institute for Physical Research of Armenian National Academy of Sciences, Ashtarak 2, 0203, Armenia*
[2] *Centre of Strong Field Physics, Yerevan State University, 1 A. Manukian St., Yerevan 0025, Armenia*

Corresponding Author: shushanpet@gmail.com

The effect of self-induced transparency (SIT) for probe field in the N-type atoms is predicted. The two ground states of atoms are coupled via two-photon Raman transitions by means of probe and driving fields, which are strongly detuned from one photon resonance, while the probe field is also resonantly connected to third optical transition from the second ground state (Fig. 1). It is found that the probe absorption features the Doppler profile in dependence on Raman detuning δ with a narrow deep for small values of δ. However, in the vicinity of $\delta = 0$, an ultra-narrow EIT resonance with subnatural width is observed caused by the probe field itself. The effect is based on the suppression of two-photon Raman transition between the two ground states induced by the probe field acting on the third optical transition and creating the EIT conditions in the created ladder system. As a result, a new narrow probe-transparency resonance arises with linewidth smaller than natural width despite the Doppler broadening. The effect is explored analytically and numerically. A scheme is elaborated to demonstrate the SIT experimentally in alkali vapors at room temperatures.

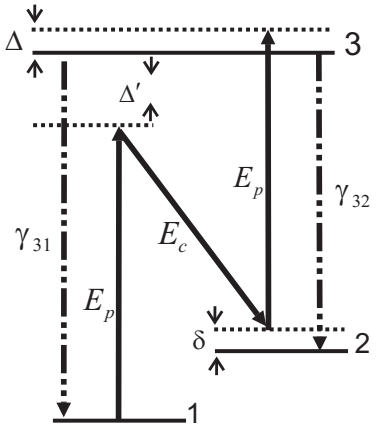

Figure 1: *N-type interaction of three-level atom with probe E_p and coupling E_c fields.*

QOI

Smooth composite pulses for high-fidelity quantum information processing

B. T. Torosov[1], S. I. Ivanov[1], and N. V. Vitanov[1]

[1] *Department of Physics, Sofia University, 5 James Bourchier blvd, 1164 Sofia, Bulgaria*
Corresponding Author: vitanov@phys.uni-sofia.bg

The composite pulse technique developed originally in nuclear magnetic resonance (NMR) [1] is a powerful tool for quantum state manipulation. This technique replaces the single pulse used traditionally for driving a two-state transition in a quantum system by a sequence of pulses with suitably chosen phases, which are used as a control tool for shaping the excitation profile in a desired manner. This technique combines the accuracy of resonant excitation with a robustness similar to adiabatic techniques. Composite pulses have therefore enjoyed increasing attention in the field of quantum computation, wherein ultrahigh fidelity of gate operations is required [2].

The existing methods for design of composite pulses are developed for pulses of rectangular temporal shapes, which are suited for NMR experiments [1], and atomic excitation with microsecond pulses [2]. However, rectangular pulse shapes are hard to implement on shorter time scales, for instance, with femtosecond pulses. Ultrashort pulses hold a great promise for quantum computation because of the absence of decoherence and the emergence of techniques for selective and efficient control of qubits. The theory of composite sequences of pulses with smooth envelopes, however, is largely missing, which has limited hitherto the use of this powerful control technique on short and ultrashort time scales.

We have developed a simple systematic approach, which allows the construction of composite sequences of pulses with smooth shapes that can create ultrahigh-fidelity excitation profiles [3]. Our method is based upon the SU(2) representation of the propagator of the two-state system, instead of the commonly used intuitive SO(3) rotations in the Bloch vector picture [1]. This makes possible the application of composite pulses to quantum control and quantum information processing with short and ultrashort laser pulses. We have derived an exact analytic formula for the composite phases for arbitrarily accurate broadband pulses, examples of narrowband, passband, and fractional-π pulses, as well as composite pulses with detuning compensation [3].

We have used this method to design composite sequences which reduce dramatically the addressing error in a lattice of closely spaced atoms or ions, and at the same time significantly enhance the robustness of qubit manipulations [4]. In this manner one can beat the diffraction limit, for only atoms situated in a small spatial region around the center of the laser beam are excited, well within the laser beam waist.

We have used the same SU(2) approach for optimization of the technique of adiabatic passage between two quantum states by composite sequences of chirped pulses: composite adiabatic passage (CAP) [5]. The nonadiabatic losses can be canceled to any desired order with sufficiently long sequences, regardless of the nonadiabatic coupling. The values of the composite phases are universal for they do not depend on the pulse shapes and the chirp. The accuracy and robustness of the CAP technique greatly exceed those for a single chirped pulse, which makes CAP suitable for ultrahigh-fidelity quantum information processing.

References

[1] R. Freeman, *Spin Choreography* (Spektrum, Oxford, 1997).
[2] H. Häffner, C. F. Roos, R. Blatt, Phys. Rep. **469**, 155 (2008).
[3] B. T. Torosov and N. V. Vitanov, Phys. Rev. A, in press (2011).
[4] S. S. Ivanov and N. V. Vitanov, Opt. Lett., in press (2011).
[5] B. T. Torosov, S. Guérin, and N. V. Vitanov, to be published.

Ultrafast Processes

Investigation of the ionization of neon by an attosecond XUV pulse with the time-dependent Schrödinger equation

T. Carette[1], L. Argenti[2], and E. Lindroth[1]

[1] *Department of Physics, Stockholm University, AlbaNova University Centre, SE-106 91 Stockholm, Sweden*
[2] *Departamento de Química, Módulo 13, Universidad Autónoma de Madrid, 28049 Madrid, Spain*

Corresponding Author: thomas.carette@fysik.su.se

Recent advances in attosecond XUV pulse generation pave the way for time-resolved investigation and control of electron wave-packets [1].

Fairly inert and simple, rare-gases offer good opportunities for exploring the new experimental techniques. A good example is the study of photo-electron spectra of rare-gases in streaking experiments where the effective asymptotic delay between the absorption of an XUV photon and the release of an electron by the atom is revealed [2]. The interpretation of this as well as of similar experiments often relies on single-particle models where the interaction of the photoelectron with the remaining electrons in the atom is approximated by a local static potential. The assumptions at the basis of these models, however, come with two major limitations: they do not account for the underlying many-electron processes which unfold on the same time-scale as the photoelectron emission, and they do not properly enforce the exclusion principle.

With the present contribution we tackle those issues. We investigate theoretically the single ionization of neon by an attosecond XUV pulse, aiming at a better understanding of the outgoing electron wave-packet in the early stages of its detachment. To do so, we integrate the one-electron time-dependent Schrödinger equation numerically where the interaction between the electron and external field, considered as classical, is treated at the level of the dipole approximation and where the non-local interaction with the spectator electrons in the time-dependent Hamiltonian is accounted for with a configuration-averaged effective Hartree-Fock potential.

References

[1] F. Krausz and M. Ivanov, Rev. Mod. Phys. **81**, 163–234 (2009).
[2] M. Schultze *et al.*, Science **328**, 1658–1662 (2010).

Ultrafast stimulated Raman parallel adiabatic passage by shaped pulses

G. Dridi[1], S. Guérin[1], and H. R. Jauslin[1]

[1] *Institut Carnot de Bourgogne, UMR 5209 CNRS, Université de Bourgogne, BP 47870, 21078 Dijon, France*

Corresponding Author: ghassen.dridi@u-bourgogne.fr

We present a general and versatile technique of population transfer based on *parallel adiabatic passage* [1] by femtosecond shaped pulses. Their amplitude and phase are specifically designed to optimize the adiabatic passage corresponding to parallel eigenvalues at all times. We show that this technique allows robust adiabatic population transfer in a Raman system with the total pulse area as low as 3π, corresponding to a fluence of one order of magnitude below the conventional stimulated Raman adiabatic process. This process of short duration, typically picosecond and subpicosecond, is easily implementable with modern pulse shaper technology and opens the possibility of ultrafast robust population transfer with interesting applications in quantum information processing.

References

[1] G. Dridi, S. Guérin, and H. R. Jauslin, Phys. Rev. A **80**, 043408 (2009).

Angular dependence of the sidebands in photoionization induced by ultrashort x-ray pulses in a strong laser field

A. K. Kazansky[1,2], N. M. Kabachnik[3,4]

[1] *Ikerbasque Foundation, Alameda Urquijo, 36, Bilbao 48011, Spain*
[2] *Departamento de Fisica de Materiales – CFM, Centro Mixto CSIC-UPV/EHU, Apto 1078, 20080, San Sebastian/Donostia, Basque Country, Spain*
[3] *Institute of Nuclear Physics, Moscow State University, 119991 Moscow, Russia*
[4] *Donostia International Physica Center (DIPC), E-20018 San Sebastian/Donostia, Basque Country, Spain*

Corresponding Author: nkabach@gmail.com

When a photoelectron is produced by an XUV pulse in the presence of a laser pulse, the electron energy can be changed due to interaction with the electromagnetic field of the laser. Depending on the characteristics of the pulses, there are different scenarios of the process. The basic parameters which determine the character of the process are the durations of the XUV and the IR pulses, τ_X and τ_L, respectively, and the period of the laser field T_L. If $\tau_X \ll T_L$, the created pulse of photoelectrons (replica of the XUV pulse) is extremely short and all electrons appear in the laser field practically at the same phase. This is a typical case of the conventional streaking effect.

In another limiting case of the laser assisted photoelectric effect when $\tau_L > \tau_X \gg T_L$, specific structures at the wings of a photoline, the so-called sidebands, appear. The sidebands consist of a regular sequence of lines with the interval between lines equal to the laser photon energy.

In this work the angular distribution of photoelectrons produced by a few-femtosecond x-ray pulse from Ne atoms in a strong laser field is theoretically considered. At large energy of the photoelectrons, the photoline in the spectrum is accompanied by numerous sidebands. The number of the sidebands and their intensity strongly vary with the emission angle, revealing the gross-structure. We have shown that while the sidebands themselves appear due to interference of electrons emitted at the same phase but at different periods of the laser wave, the gross-structure is determined by the interference of electrons emitted during one period [1]. Similar effects have been recently considered for the sidebands in laser assisted Auger decay [2,3].

Special attention is paid to the transition regime from streaking to the sideband formation. The effect of light polarization and dichroism for the sidebands is discussed.

UFP

References

[1] A. K. Kazansky, I. P. Sazhina, and N. M. Kabachnik, Phys. Rev. A **82**, 033420 (2010).
[2] A. K. Kazansky and N. M. Kabachnik, J. Phys. B **42**, 121002 (2009).
[3] A. K. Kazansky and N. M. Kabachnik, J. Phys. B **43**, 035601 (2010).

Formation of molecular halide ions from alkyl-halide clusters irradiated by ps and fs laser pulses

G. Karras[1], S. Danakas[2], and C. Kosmidis[1]

[1] *Department of Physics, University of Ioannina, 45110 Ioannina, Greece*
[2] *Central Laser Facility, University of Ioannina, 45110 Ioannina, Greece*
Corresponding Author: gkarras@cc.uoi.gr

The interaction of molecular clusters with laser radiation has attracted considerable interest in the last decade, especially with the advent of strong and ultra-short laser pulses [1-3]. Their interaction with strong electromagnetic fields created by lasers led to the observation of highly charged, energetic ions and electrons, and emission of x rays and neutrons. Furthermore, high order harmonic generation has been observed from laser-cluster interaction and, as reported recently, with larger efficiency compared to bulk matter.

The intra-cluster photochemical processes are the subject of the present work and more specifically the formation of molecular halogen ions from the interaction of alkyl halide clusters with laser irradiation. Our study is focused on methyl iodide clusters, which is a benchmark system, and on ethyl halide clusters $(C_2H_5X)_n$ (where X=I, Br, Cl). In the current work we present experimental results acquired from the irradiation of alkyl-halide clusters with picosecond and femtosecond laser pulses. Neutral clusters are formed in a supersonic molecular beam and their ionization is induced by a 35 ps Nd:YAG laser and a 20 fs Ti:Sapphire laser. The ionic signal is investigated under various experimental conditions, such as wavelength (266, 532, and 1064 nm for ps pulses, 400 and 800 nm for fs pulses), polarization (linear and circular) and laser intensity by means of a linear time-of-flight mass spectrometer.

For both pulse durations the formation of molecular halogen ions was verified. The efficiency of molecular halogen ion formation is found to depend strongly on the laser wavelength and pulse duration. The ionization/excitation schemes involve in both cases the multiphoton absorption by the clusters and the combined action of the laser and the intracluster electric field. Energy transfer through 'trivial' mechanisms and/or inter-molecular Coulombic decay process seem to have a significant contribution to the molecular halogen ion formation in the ps domain, while in the fs region this is probably facilitated by a rescattering process and/or by photon absorption. A physical mechanism for the interpretation of our experimental results is proposed. For fs pulses this is depicted in Fig. 1.

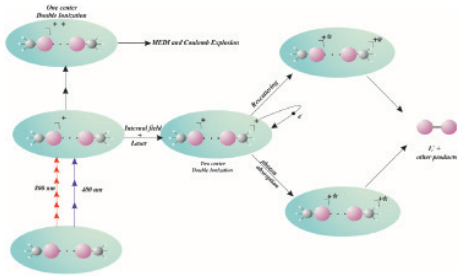

Figure 1: *Physical mechanism for the molecular halogen formation.*

References
[1] Th. Fennel, *et al.*, Rev. Mod. Phys. **82**, 1793–1842, (2010).
[2] I. V. Hertel, W. Radloff, Rep. Prog. Phys. **69**, 1897–2003, (2006).
[3] T. E. Dermota, Q. Zhong, A. W. Jr. Castleman, Chem. Rev. **104**, 1861–1886, (2004).

Post-Deadline abstracts

g factor of few-electron ions: bound-state QED in the presence of magnetic field

D. A. Glazov[1,2], A. V. Volotka[1,2], A. A. Schepetnov[1], M. M. Sokolov[1], V. M. Shabaev[1], I. I. Tupitsyn[1], and G. Plunien[2]

[1] *Department of Physics, St. Petersburg State University, St. Petersburg, Russia*
[2] *Institut für Theoretische Physik, Technische Universität Dresden, Dresden, Germany*

Corresponding Author: glazov.d.a@gmail.com

The bound-electron g factor has been the subject of intense experimental and theoretical investigations over the past decade. In particular, recent high-precision measurements for low-Z hydrogen-like ions, together with corresponding theoretical studies, have lead to the new value of the electron mass. The experiments with middle-Z ions, in particular, with boron-like argon, are presently in preparation [1]. An extension of these studies to high-Z H-like, Li-like, and B-like systems planned in the framework of the HITRAP project will provide a stringent test of bound-state QED in the strong electric field of the nucleus. Moreover, investigations of the heavy boron-like ions can lead to an independent determination of the fine-structure constant α [2].

We present the evaluation of the g factor values for lithium-like and boron-like ions in the wide range of the nuclear charge number $Z = 12$–92. The rigorous QED approach together with the large-scale configuration-interaction Dirac–Fock–Sturm method are employed for the evaluation of the contributions of the interelectronic interaction (IIC) of first and higher orders in $1/Z$. First-order radiative corrections are calculated with an effective screening potential in order to take into account partly the interelectronic interaction. In case of the heavy lithium-like ions the diagrams of the two-electron self-energy and vacuum polarization are evaluated rigorously [4]. The one-electron (NMS) and many-electron (SMS) nuclear recoil effects are taken into account. The nonlinear effects in magnetic field are estimated and found to be significant in case of the middle-Z boron-like ions due to the relatively small fine-structure splitting.

Dirac	0.663 775 447
IIC $1/Z$	0.000 657 525
IIC $1/Z^{2+}$	−0.000 007 5
QED α	−0.000 768 9
QED α^2	0.000 001 2
Screened QED	−0.000 001 0
Recoil NMS	−0.000 018 2
Recoil SMS	0.000 008 4
Total	0.663 647 (1)

Table 1: *Contributions to the g factor of boronlike argon.*

References

[1] D. von Lindenfels, W. Quint, M. Vogel, private communication
[2] V. M. Shabaev *et al.*, Phys. Rev. Lett. **96**, 253002 (2006)
[3] V. A. Yerokhin and U. D. Jentschura, Phys. Rev. A **81**, 012502 (2010)
[4] A. V. Volotka *et al.*, Phys. Rev. Lett. **103**, 033005 (2009); D. A. Glazov *et al.*, Phys. Rev. A **81**, 062112 (2010)

Index by contribution number

AAP–001 . . . 67
AAP–002 . . . 68
AAP–003 . . . 69
AAP–004 . . . 70
AAP–005 . . . 71
AAP–006 . . . 72
AAP–007 . . . 73
AAP–008 . . . 74
AAP–009 . . . 75
AAP–010 . . . 76
AAP–011 . . . 77
AAP–012 . . . 78
AAP–013 . . . 79
AAP–014 . . . 80
AAP–015 . . . 81
AAP–016 . . . 82
AAP–017 . . . 83
AAP–018 . . . 84
AAP–019 . . . 85
AAP–020 . . . 86
AAP–021 . . . 87
AAP–022 . . . 88

CAM–001 . . . 90
CAM–002 . . . 91
CAM–003 . . . 92
CAM–004 . . . 93
CAM–005 . . . 94
CAM–006 . . . 95
CAM–007 . . . 96
CAM–008 . . . 97
CAM–009 . . . 98
CAM–010 . . . 99
CAM–011 . . . 100
CAM–012 . . . 101
CAM–013 . . . 102
CAM–014 . . . 103
CAM–015 . . . 104
CAM–016 . . . 105
CAM–017 . . . 106
CAM–018 . . . 107
CAM–019 . . . 108
CT–001 . . . 25
CT–002 . . . 26
CT–003 . . . 27
CT–004 . . . 28
CT–005 . . . 29
CT–006 . . . 30
CT–007 . . . 31
CT–008 . . . 32
CT–009 . . . 33
CT–010 . . . 34
CT–011 . . . 35
CT–012 . . . 36
CT–013 . . . 37
CT–014 . . . 38
CT–015 . . . 39
CT–016 . . . 40
CT–017 . . . 41
CT–018 . . . 42
CT–019 . . . 43
CT–020 . . . 44
CT–021 . . . 45
CT–022 . . . 46
CT–023 . . . 47
CT–024 . . . 48
CT–025 . . . 49
CT–026 . . . 50
CT–027 . . . 51
CT–028 . . . 52
CT–029 . . . 53
CT–030 . . . 54
CT–031 . . . 55
CT–032 . . . 56
CT–033 . . . 57
CT–034 . . . 58
CT–035 . . . 59
CT–036 . . . 60
CT–037 . . . 61
CT–038 . . . 62
CT–039 . . . 63
CT–040 . . . 64

FPE–001 . . . 110
FPE–002 . . . 111
FPE–003 . . . 112
FPE–004 . . . 113
FPE–005 . . . 114
FPE–006 . . . 115
FPE–007 . . . 116
FPE–008 . . . 117
FPE–009 . . . 118
FPE–010 . . . 119
FPE–011 . . . 120
FPE–012 . . . 121
FPE–013 . . . 122
FPE–014 . . . 123
FPE–015 . . . 124
FPE–016 . . . 125
FPE–017 . . . 126
FPE–018 . . . 127
FPT–001 . . . 129
FPT–002 . . . 130
FPT–003 . . . 131
FPT–004 . . . 132
FPT–005 . . . 133
FPT–006 . . . 134
FPT–007 . . . 135
FPT–008 . . . 136
FPT–009 . . . 137
FPT–010 . . . 138
FPT–011 . . . 139
FPT–012 . . . 140
FPT–013 . . . 141
FPT–014 . . . 142
FPT–015 . . . 143
FPT–016 . . . 144
FPT–017 . . . 145
FPT–018 . . . 146
FPT–019 . . . 147
FPT–020 . . . 148
FPT–021 . . . 149
FPT–022 . . . 150
FPT–023 . . . 151
FPT–024 . . . 152
FPT–025 . . . 153
FPT–026 . . . 154
FPT–027 . . . 155
FPT–028 . . . 156
FPT–029 . . . 157
FPT–401 . . . 221

HRS–001 . . . 159
HRS–002 . . . 160
HRS–003 . . . 161
HRS–004 . . . 162
HRS–005 . . . 163
HRS–006 . . . 164
HRS–007 . . . 165
HRS–008 . . . 166
HRS–009 . . . 167
HRS–010 . . . 168
HRS–011 . . . 169
HRS–012 . . . 170

HRS–013 171
HRS–014 172
HRS–015 173
HRS–016 174
HRS–017 175
HRS–018 176
HRS–019 177
HRS–020 178
HRS–021 179
HRS–022 180
HRS–023 181
HRS–024 182

PEL–005 6
PL–001 2
PL–002 3
PL–003 4
PL–004 5
PL–006 7
PL–007 8
PL–008 9
PL–009 10
PL–010 11
PL–011 12

PPA–001 184
PPA–002 185
PPA–003 186
PPA–004 187
PPA–005 188
PPA–006 189
PPA–007 190
PPA–008 191
PPA–009 192
PPA–010 193
PPA–011 194
PPA–012 195
PPA–013 196
PPA–014 197
PPA–015 198
PPA–016 199
PPA–017 200
PPA–018 201
PPA–019 202
PPA–020 203
PPA–021 204
PR–001 14
PR–002 15

PR–003 16
PR–004 17
PR–005 18
PR–006 19
PR–007 20
PR–008 21
PR–009 22
PR–010 23

QOI–001 206
QOI–002 207
QOI–003 208
QOI–004 209
QOI–005 210
QOI–006 211
QOI–007 212
QOI–008 213
QOI–009 214

UFP–001 216
UFP–002 217
UFP–003 218
UFP–004 219

Index by author

— A —

Afach, S. . . . 23
Affolderbach, C. . . . 162, 174
Aghamalyan, D. . . . **206**
Akhtar, N. . . . **159**, 161
Akimov, A. . . . 34
Albert, M. . . . **60**
Alexandrov, E. B. . . . **11**
Alioua, K. . . . 67
Alkauskas, A. . . . 149
Allan, M. . . . **184–186**, 196
Allouche, A.–R . . . 67
Ammi, D. . . . *133*
Andersson, P. . . . **187**
Andreeva, C. . . . **160**
Andrić, L. . . . 186
Anjum, N. . . . 159, **161**
Antognini, A. . . . **37**
Arcimowicz, B. . . . **110**
Argenti, L. . . . 216
Artemyev, A. . . . 20
Atanasov, M. . . . 133
Atkinson, P. . . . 51
Aubert–Frécon, M. . . . 67
Aumiler, D. . . . 19
Auzinsh, M. . . . 163, 164, 169
Avchyan, B. . . . **207, 208**
Avdeenkov, A. . . . **36**
Avetissian, H. . . . 207, 208
Aymar, M. . . . 131

— B —

Bäckström, E. . . . 75
Bacławski, A. . . . 175
Balog, R. . . . 62
Ban, T. . . . **19**
Banaś, D. . . . 64, 77, 80, **111**, 176
Bandi, T. . . . **162**, 174
Barker, P. F. . . . 100
Barredo, D. . . . **112**
Bartschat, K. . . . 184
Başar, Gö. . . . **113**, 116, 168
Batz, M. . . . 78
Becker, C. . . . 28
Belyaeva, O. V. . . . **209**
Bengtsson, P. . . . 142
Benmansour, N. E. H. . . . 130
Berenguer, Ch. . . . 117
Bergeman, T. . . . 151
Berset, M. . . . 167, 176
Berzins, A. . . . **163, 164**
Beterov, I. I. . . . 18, 92, 106
Beyer, H. F. . . . 64
Bezuglov, N. N. . . . 106, 123, 160, 169
Bhowmik, P. . . . **129**
Biémont, É. . . . 86, **114**
Bing, D. . . . 47
Birkl, G. . . . 27
Birzniece, I. . . . **165**
Bismut, G. . . . 26
Bison, G. . . . **23**, 69
Blackwell–Whitehead, R. . . . 75, 114
Blagoev, K. . . . 114, *179*
Blaum, K. . . . 25, 29, 31, 33
Bloch, I. . . . **7**
Blondel, C. . . . **188**
Blushs, K. . . . 169
Böhi, P. . . . **32**
Böhm, Ch. . . . 31
Böhm, S. . . . 64
Bosch, F. . . . 64
Botermann, B. . . . **47**
Bouamoud, M. . . . **130**
Boudot, R. . . . 171
Bouledroua, M. . . . **67**
Bouloufa, N. . . . **131, 132**
Brandau, C. . . . 64
Braziewicz, J. . . . 111
Breschi, E. . . . **166**
Bruneau, Y. . . . 91
Bruvelis, M. . . . 123, 160
Bucalovic, N. . . . **68**
Bučar, K. . . . 167
Budnar, M. . . . 167
Burghoff, M. . . . 22
Busch, Th. . . . **58**, **90**

— C —

Cacciapuoti, L. . . . 14
Calarco, T. . . . 21
Cantat–Moltrecht, T. . . . 122
Cao, W. . . . 48, 77, 80, 167
Carette, T. . . . **57**, **189**, **216**
Carrat, V. . . . 104
Casa, G. . . . 56
Cassidy, A. . . . 62

Castagna, N. **69**, 210
Castrillo, A. 56
Catone, D. 202
Cederbaum, L. S. 45, 135, 201
Chaltykyan, V. 93
Champenois, C. 102
Chatterjee, S. 64
Cheinet, P. **91**
Chevrollier, M. **53**, **70**
Chiang, Y.–C. 135
Chirkin, A. S. 209
Chmielewska, D. 176
Cinins, A. 123
Clark, R. E. H. 117
Cohen, S. 59, 117, 191
Comparat, D. 91
Contini, G. 202
Coppendale, N. 100
Cornille, M. 117
Costescu, A. **190**
Crubellier, A. 132
Czarnota, M. 64, 176, 181
Ćuk, S. M. 44, 212

— **D** —

Daly, M. 49
Danakas, S. 219
Danet, J.–M. 54
Dantan, A. 60
Danzl, J. G. 131, 132
Daschner, R. 112
Daul, C. **133**
Deasy, K. 49
De Clercq, E. 54, 170, 171
Decleva, P. 202
Deja, K. 80
Delsart, C. 188
Dembczyński, J. 110, **134**, 173
Demekhin, Ph. V. **45**, **135**, *197*
Demekhina, L. A. 153
Devenoges, L. **50**
De Vizia, M. D. *56*
Dicle, Y. 81
Di Domenico, G. 50, 68, 71
Diehl, C. 33
Dimitriou, A. **59**, **191**
Dimitrova, T. L. **210**
Djokic, V. 212
Dolgovskiy, V. 68, **71**
Domelunksen, V. 179
Dörr, A. 31
Douglas, P. 100
Dousse, J.–Cl. . . . 48, 64, 77, 80, **167**, 176, 181
Drag, C. 188
Drewsen, M. 38, 60
Dridi, G. **217**
Dulieu, O. 131, 132

— **E** —

Eckardt, A. 40
Eddrief, M. 51
Efimov, D. 106
Ehresmann, A. 119, 197
Eiglsperger, J. 30
Ekers, A. 106, 123, 160, 169
Ekman, J. 142
Elantkowska, M. 110, 134
Eliseev, S. 31
Ellmeier, M. **72**
Engström, L. 114
Entin, V. M. 18, **92**
Er, A. **168**
Ernst, R. R. **6**
Ernst, W. E. **42**, 99, 103
Etgens, V. 51

— **F** —

Fasci, E. 56
Fedor, J. 186
Fennane, K. 167
Ferber, R. 101, 113, 163–165, 172
Ferlaino, F. **17**
Fertl, M. **73**
Feyer, V. 84, **192**
Field, D. 62
Fink, M. **30**
Fioretti, A. 91
Flambaum, V. V. 139
Fläschner, N. 28
Fleischhauer, M. **5**
Fogarty, M. 58
Foltynowicz, A. 19
Forstner, O. 187
Friedrich, H. 30, 146
Froese Fischer, C. 155
Furmann, B. **115**

— **G** —

Gahbauer, F. 163, 164
Gaigalas, G. 142, 149, 155, 156
Gamper, B. 127
Garreau, J. C. **15**
Garrido Alzar, C. L. **74**
Gartman, R. 107
Gawlik, W. 107
Gazazyan, A. 93

Gazazyan, E. **93**
Geissbühler, I. 69
Gemmel, C. 22
Geppert, C. 47
Gerakis, A. 100
Germann, M. **94**
Gianfrani, L. **56**
Glazov, D. A. **221**
Głowacki, P. 110, 173
Glowacki, L. **136**
Glowacz, B. 126
Glushkov, A.–V. **137, 138**
Godefroid, M. R. . . . 57, 145, 147, 155, 156, 189
Gogyan, A. **211**
Golser, R. 187
Goncharov, M. 31
Goold, J. 58
Gorceix, O. 26
Gossel, G. H. 139
Götze, S. 28
Gould, P. L. 91
Grebinskij, S. 121
Green, D. G. **43**
Gribakin, G. F. 43, **139**, **193**
Grochola, A. **95**, 97, 154
Grujić, Z. 76
Guérandel, S. 54, 170, 171
Guérin, S. 211, 217
Guglev, K. A. 153
Gulde, M. 204
Gumberidze, A. 64
Gupta, G. P. **140, 141**
Gurian, J. H. 91
Gustafsson, S. 142
Guthöhrlein, G. H. 110
Güzelçimen, F. 113, **116**, 168
Gwinner, G. 47

— H —

Hafeez, E. 127
Hagmann, S. 64
Hakhumyan, G. 82
Hall, F. **96**
Hänsch, T. W. 47
Hansen, A. K. **38**
Hanstorp, D. **63**, 187, **194**
Harman, Z. 29, 39
Hartman, H. **75**, 114
Heil, W. **22**
Heinze, J. 28
Höcker, M. 33
Holmes, J. 198
Hönicke, P. 77
Hoszowska, J. **48**, 77, 80, 167, 176, 181
Houssin, M. 102
Huber, G. 47
Hühnermann, H. 159, 161
Huillery, P. 91
Huldt, S. 75
Hultgren, H. 63, 194
Hundt, B. 28

— I —

Ibănescu, B. C. 186
IJsselsteijn, R. 87, 88
Imamoglu, A. **3**
Indelicato, P. 20
Ivanov, S. I. 214

— J —

Jagodziński, P. 48, 77
Jarmola, A. 113, 163
Jastrzębski, W. 95, 154
Jastrzębski, W. 97
Jauslin, H. R. 217
Jędrzejewski-Szmek, Z. **97**
Jelassi, H. 105
Jelenković, B. M. 44, 212
Johnson, P. R. 108
Jonauskas, V. 121
Jones, N. C. 62
Jönsson, P. **142**, 155, 156
Joshipura, K. N. 129
Joyet, A. 50

— K —

Kabachnik, N. M. **218**
Kaiser, A. 146
Kalvans, L. 163, 164
Karim, K. 190
Karpuk, S. 22, 47
Karras, G. **219**
Kasprzak, M. **76**
Katsonis, K. **117**
Kavčič, M. 48, 167
Kayser, Y. 48, **77**, 80
Kazakov, G. 171
Kazansky, A. K. 218
Keitel, C. H. 29, 39
Keller, U. 68
Ketter, J. 33
Khan, S. **118**, 124, 127
Khemliche, H. 51
Khetselius, O. Yu. **143, 144**
Kielpinski, M. 88
Kilian, W. 22

Kippenberg, T. J. **9**
Kirova, T. *36*, 160, **169**
Kita, Y. **195**
Kitching, J. 166
Kivimaki, A. 192
Kiyan, I. Yu. 63, 194
Klincare, I. 101, 172
Knappe, S. 166
Knappe–Grüneberg, S. 22
Knie, A. **119**
Knoop, M. 102
Knowles, P. 52, 69, 76
Koch, C. P. **21**
Koch, M. 99, 103
Kolachevsky, N. 34
Komasa, J. **16**
Kosmidis, C. 219
Kotochigova, S. **98**
Kowalczyk, P. 95, 97, 154
Kozakov, A. T. 153
Kozhuharov, C. 64
Kozioł, K. 85, 178, 182
Kozlov, M. G. **41**
Kozlova, O. **54**, **170**, **171**
Kracke, H. **25**
Krauser, J. S. **28**
Kriegelsteiner, O. 132
Krmpot, A. J. **44**, 212
Kröger, S. 113, 116, 168
Krois, G. *42*, **99**
Kruzins, A. **172**
Krzykowski, A. **173**
Kubala, D. **196**
Kubala–Kukuś, A. 77
Kübler, H. 112
Kühl, T. 47
Kuleff, A. I. 201
Kumar, A. 64

— L —

Laburthe–Tolra, B. 26
Lackner, F. 42, 99
Lagutin, B. M. 153, **197**
Lammegger, R. 72
Lamoudi, N. 67
Landragin, A. 74
Lapinov, A. V. 41
Lebedev, V. 35, **120**
Lebedev, V. S. 199
Lecointre, J. **61**
Lembke, G. 23
Lennartsson, T. 75
Leroy, C. 46, 82, 177, 180
LeRoy, R. J. 152
Le Targat, R. **40**
Lévèque, T. 74
Levshakov, S. A. 41
Lewenstein, M. 40
Li, J. G. **145**, 147, 156
Lien, Y. H. 14
Liesen, D. 64
Lindahl, A. O. *63*, 187, 194
Lindenfels, D. **27**
Lindroth, E. 216
Liontos, I. 191
Litvinov, A. 171
Lo Gullo, N. 90
Loreau, J. 61
Löw, R. 112
Lühmann, D.–S. 28
Lundberg, H. 114
Lyras, A. 59, 191

— M —

MacDonald, A. 198
Madroñero, J. 30
Magnes, W. 72
Maher–McWilliams, C. **100**
Maillard, Y.–P. 167, 176
Malakyan, Yu. 206, 211, 213
Malcheva, G. 114
Mannervik, S. 75
Maréchal, E. **26**
Marciante, M. 102
Mark, M. J. 131
Martín, F. **10**
Martschini, M. 187
Maslowski, P. 19
Masys, Š. **121**
Matisov, B. 171
Mauron, O. 176
May, O. 186, 196
McEndoo, S. 90
Meshkov, V. V. 152
Meunier, M. 74
Meyer, H.–G. 87, 88
Mezinska, S. 123
Michulis, K. 106
Mickevičius, S. 121
Miculis, K. 160
Mileti, G. 162, 174
Miletic, D. **174**
Mirzoyan, R. 46, 177, 180
Mkrtchian, G. 207, 208
Mokler, P. H. 64
Moldovan, M. 190

Momeni, A. . . . 51
Mooser, A. . . . 25
Moretti, L. . . . 56
Moroshkin, P. . . . **35**, 120
Moskovskaya, T. E. . . . 192
Mozers, A. . . . 164
Msezane, A. Z. . . . 140, 141
Mulier, M. . . . 51
Müller, A. . . . 64
Müller, M. M. . . . 21
Müller, T.–O. . . . **146**
Müller, W. . . . 22
Murphy, M. . . . 21
Musa, M. O. . . . **198**
Musielok, J. . . . **175**

— **N** —

Nacher, P.–J. . . . **78**, **122**, 126
Nägerl, H.-C. . . . 131, 132
Narits, A. A. . . . **199**
Nazé, C. . . . **147**, 156
Nic Chormaic, S. . . . **49**, **79**
Nikolayeva, O. . . . 101, 165, 172
Nikolić, S. N. . . . 44, **212**
Nikolsky, A. V. . . . 153
Nilsson, H. . . . 75, 114
Nörtershäuser, W. . . . 47
Novikov, Yu. N. . . . 31
Novotny, C. . . . 47
Nowak, S. H. . . . 48, 77, **80**

— **O** —

Oehler, A. E. H. . . . 68
Oka, T. . . . **8**
Ölschläger, C. . . . 40
Opachko, A. I. . . . 203
Opalevs, D. . . . 164
Oriá, M. . . . **55**, 70
Osmanoğlu, Ş. . . . **81**
Öztürk, I. K. . . . 168

— **P** —

Pachucki, K. . . . 16
Pajek, M. . . . **64**, 77, 80, 111, **176**, 181
Palmeri, P. . . . 114
Papoyan, A. . . . **82**, 163, 180
Pashayan–Leroy, Y. . . . 46, 82, **177**, 180
Pasquiou, B. . . . 26
Passerat de Silans, T. . . . 53, 55, 70
Paternostro, M. . . . 58, 90
Patidar, V. . . . 200
Pazyuk, E. A. . . . **101**, 151, 172
Pedregosa-Gutierrez, J. . . . **102**
Pedri, P. . . . 26
Pegg, D. J. . . . 63, 194
Pekarek, S. . . . 68
Peláez, R. J. . . . 188
Pereira Dos Santos, F. . . . 74
Petkovic, M. . . . 23
Petri–Fink, A. . . . 69
Petrosyan, Sh. . . . **213**
Petrov, A. . . . 98
Petrov, I. D. . . . 153, 197
Pfau, T. . . . 112
Pichler, G. . . . 19, **83**
Pillet, P. . . . 91
Pinegar, D. B. . . . 33
Piotrowski, M. . . . 107
Plekan, O. . . . **62**, **84**, 192
Plunien, G. . . . 221
Polasik, M. . . . **85**, 176, **178**, 181, 182
Polischuk, V. . . . **179**
Pollinger, A. . . . 72
Poms, J. . . . **103**
Porsev, S. G. . . . 41
Prevedelli, M. . . . **14**
Prince, K. C. . . . 84, 192
Prosperi, T. . . . 202
Pruvost, L. . . . **104**, **105**
Ptasinska, S. . . . 84
Purohit, G. . . . **200**

— **Q** —

Queiroga da Silva, F. . . . 55
Quinet, P. . . . **86**, 114
Quint, W. . . . 25, 27, 29

— **R** —

Raboud, A. . . . 176
Radonjić, M. . . . 44
Rajchel, K. . . . **148**
Rakić, M. . . . 83
Reich, D. M. . . . 21
Reinhardt, S. . . . 47
Reiss, P. . . . 119
Repp, J. . . . **31**
Reuschl, R. . . . 64
Riedel, M. F. . . . 32
Ristinmaa Sörensen, S. . . . 75
Robyr, J.–L. . . . **52**
Rodegheri, C. C. . . . 25
Rohlén, J. . . . 63, 187, 194
Romalis, M. . . . **12**
Roncin, P. . . . **51**
Ropers, C. . . . 204
Rosi, G. . . . 14

Roux, C. 31
Ruczkowski, J. 110, 134
Rudzikas, Z. R. 149
Russell, L. 49
Ryabtsev, I. I. **18**, *92*, **106**, **123**, 160, 169
Rynkun, P. 142, **149**, 155
Rzadkiewicz, J. 85, 176

— S —

Saathoff, G. 47
Sahlaoui, M. 130
Salomon, C. **4**
Sánchez, R. 47
Sargsyan, A. 46, 177, **180**
Sarkisyan, D. **46**, *82*, 163, 177, 180
Schabinger, B. 29
Schartner, K.–H. 197
Schepetnov, A. A. 221
Schilt, S. 68, 71
Schmidt, E. W. 64
Schmidt, U. 22
Schmoranzer, H. 197
Schnabel, A. 22
Scholtes, T. **87**, 88
Schori, C. 68, 71
Schultze, V. 87, 88
Schwalm, D. 47
Seifert, F. 22
Selg, M. **150**
Semaniak, J. 111
Sengstock, K. 28, 40
Shabaev, V. M. 221
Shearer, S. F. 193
Siddiqui, I. 116, **124**, 125, 127, 168
Sierpowski, D. 64
Simulik, V. M. 203
Singh, P. 200
Słabkowska, K. 85, 176, **181**, **182**
Smyth, M. C. 193
Soares Martins, W. 53, 55, 70
Sobolev, Yu. 22
Sobota, D. 111
Sokolov, A. 34
Sokolov, M. M. 221
Soltan–Panahi, P. 40
Sørensen, M. A. 38
Sorokin, V. 34
Sorrentino, F. 14
Soshnikov, D. Yu. 192
Spanulescu, S. 190
Spillmann, U. 64
Staanum, P. F. 38
Starosta, J. 181
Stefanov, A. 50
Steier, P. 187
Stener, M. 202
Stöhlker, Th. 20, 47, 64
Stoica, C. 190
Stolyarov, A. V. 101, **151**, **152**, 172
Stoychev, S. D. **201**
Streubel, S. **33**
Struck, J. 40
Stumpf, M. 23
Stumpf, M. C. 68
Sturm, S. 29, 31
Sud, K. K. 200
Südmeyer, T. 68
Sujkowski, Z. 176
Sukachev, D. **34**
Sukhorukov, V. L. **153**, 197
Surzhykov, A. **20**, 64, 157
Szczepkowski, J. 95, **107**, **154**
Szlachetko, J. 48, 64, 80, 167
Szlachetko, M. 167

— T —

Tachikawa, M. 195
Talbot, C. 78
Tamanis, M. 101, 165, 172
Tamaris, M. 113
Tanweer I., S. **125**
Tashenov, S. 64
Tastevin, G. 78, 122, **126**
Theisen, M. 42, 99
Thomann, P. 50, 68, 71
Tidswell, L. 198
Tiesinga, E. **108**
Tino, G. M. 14
Todorov, G. 179
Tombez, L. 68
Tong, X. 94
Torosov, B. T. 214
Trahms, L. 22
Tremer, M. 33
Tretyakov, D. B. 18, 92
Treutlein, P. 32
Trofimov, A. B. 192
Trotsenko, S. 64
Tsekeris, P. 117
Tsud, N. 84
Tullney, K. 22
Tupitsyn, I. I. 221
Turchini, S. **202**
Tymchyk, R. V. **203**

— U —

Ulmanis, J. . . . 160
Ulmer, S. . . . 25, 31
Unterumsberger, R. . . . 77
Urbain, X. . . . 61

— V —

Vaeck, N. . . . 61
Vala, J. . . . 21
Vandevraye, M. . . . 188
Van Dyck, Jr., R. S. . . . 33
Vedrinsky, R. V. . . . 153
Verdebout, S. . . . 145, **155, 156**
Verma, P. . . . 64
Vernac, L. . . . 26
Vexiau, R. . . . 131, 132
Viaris de Lesegno, B. . . . 104
Vidal, I. . . . 53, 55, 70
Vitanov, N. V. . . . **214**
Vogel, M. . . . 27
Volk, A. . . . 103
Volotka, A. V. . . . 221

— W —

Wagner, A. . . . **29**
Wallbank, B. . . . 198
Walter, C. W. . . . 63, 194
Walz, J. . . . 25
Warczak, A. . . . 64
Ward, J. . . . 79
Weis, A. . . . 35, 52, 69, 76, 120, 210
Werth, G. . . . 29
Whaley, K. B. . . . 21
Wiatrowska–Kozioł, E. . . . 178, 182
Willitsch, S. . . . 94, *96*
Windholz, L. . . *72*, 110, 116, 118, *124*, *125*, *127*, 159, *161*, 168
Windpassinger, P. . . . 40
Witkowski, M. . . . 107
Woetzel, S. . . . 87, **88**
Wolf, A. . . . 47
Wu, Y. . . . 79

— Y —

Yakshina, E. A. . . . 18, 92
Yalunin, S. V. . . . **204**
Ye, J. . . . **2**, 19
Yerokhin, V. A. . . . **39**, **157**
Yuan, H. . . . 21

— Z —

Zaheer, U. . . . 125, **127**
Zajac, T. M. . . . 203
Zatorski, J. . . . 29
Zatsarinny, O. . . . 184
Zawada, M. . . . 107
Zaytseva, I. L. . . . 192
Zema, N. . . . 202
Zhao, J.-M. . . . 91
Žitnik, M. . . . 167